

**Identification of genes involved in suppression of
growth- and stress- related defects associated with
wall hypoacetylation**

Dissertation

Rajesh Kumar Natarajan

September 2024

**Identification of genes involved in suppression of
growth- and stress- related defects associated with
wall hypoacetylation.**

Inaugural Dissertation

for the attainment of the title of doctor
in the Faculty of Mathematics and Natural Sciences
at the Heinrich Heine University Düsseldorf

Presented by

Rajesh Kumar Natarajan

From Chennai, Tamil Nadu, India



Düsseldorf, September 2024

From the Institute for Plant Cell Biology and Biotechnology
at the Heinrich-Heine-University Düsseldorf

Published with the permission of the
Faculty of Mathematics and Natural Sciences at
Heinrich-Heine-University Düsseldorf

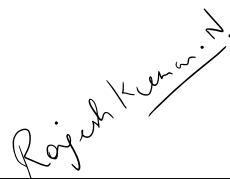
Supervisor: Prof. Dr. Markus Pauly

Co-Supervisor: Prof. Dr. Björn Usadel

Date of oral examination: 24.02.2025

Statutory declaration

This dissertation is the result of my research, considering the “Rules and principles for safeguarding and good scientific practice at the Heinrich Heine University Düsseldorf”. No other person’s work has been used without due acknowledgement. I did not use literature other than the ones cited in the text and listed in the reference section. This dissertation has not been submitted or published in the same or similar form elsewhere. I have not failed a doctoral examination procedure previously.



City: Düsseldorf

Date: 11.09.2024

Rajesh Kumar Natarajan

Matriculation number: 3039748

The research detailed in this dissertation was conducted from August 2020 until December 2023 at the Heinrich Heine University Düsseldorf in the Institute for Plant Cell Biology and Biotechnology under Prof. Dr. Markus Pauly.

Summary

Plant cell walls are composed of intricately structured polymers, including polysaccharides that are often modified with *O*-linked acetate groups. These modifications are crucial for plant growth, development, and stress responses. However, understanding the biological significance of cell wall acetylation has been challenging due to the pleiotropic phenotypes exhibited by mutants with altered acetylation levels. A key focus of this study is the *ALTERED XYLOGLUCAN9 (AXY9)* gene, which plays a significant role in the *O*-acetylation of multiple wall polysaccharides. The loss of function of *AXY9* results in severe developmental defects, including extreme dwarfism and male sterility. To overcome the technical challenges associated with studying this mutant, a conditionally complemented *axy9* line (*pAXY*) was developed. Through a forward genetic screen on *pAXY* mutants, novel genes involved in the suppression of the phenotype associated with hypoacetylation were identified. These findings reveal that the recovery of growth in these suppressor mutants is not directly linked to the hypoacetylation. Instead, the study uncovers alternative compensatory pathways that contribute to growth recovery, such as the involvement of brassinosteroid (BR) signaling. Specifically, the suppression of a *WD40* and *PHOX3* genes appears to enhance BR signaling, promoting growth despite reduced wall acetylation. The interaction between cell wall integrity and hormone signaling pathways highlights a complex regulatory network that compensates for defects in wall structure. In addition to these genetic insights, this thesis also utilizes synthetic biology approach to reconstruct the xyloglucan (XyG) backbone *O*-acetylation pathway in *Yarrowia lipolytica*, a non-conventional yeast species. While significant strides have been made in identifying the molecular components involved in plant cell wall polymer synthesis, how these components interact to control the length and decoration patterns of polysaccharides remains largely unknown. By co-expressing the *CSLC4*, *XXT2*, and *XyBAT1* genes, an *O*-acetylated β -1,4-glucan backbone was produced, providing valuable insights into the biosynthesis of plant cell wall polysaccharides. This approach not only advances our understanding of the mechanisms of *O*-acetylation but also demonstrates the potential of *Y. lipolytica* as a versatile platform for synthetic biology and metabolic engineering. Overall, this research sheds light on the genetic and molecular mechanisms that regulate cell wall *O*-acetylation in plants.

List of Abbreviations

<i>A. thaliana</i>	<i>Arabidopsis thaliana</i>
<i>A. tumefaciens</i>	<i>Agrobacterium tumefaciens</i>
ADP	adenosine triphosphate
Ac	acetyl
acetyl-CoA	acetyl-coenzyme A
AIR	alcohol insoluble residue
Amp	ampicillin
Api	apiose
<i>Araf</i>	arabinofuranose
<i>Arap</i>	arabinopyranose
AXS	UDP-apiose synthase
AXY	altered xyloglucan
BLAST	basic local alignment search tool
BMGY	buffered complex media containing glycerol
BMMY	buffered complex media containing methanol
bp	base pair
C	deoxycytosine monophosphate
cDNA	complementary deoxyribonucleic acid
CMT	cortical microtubules
Col0	<i>Arabidopsis thaliana</i> ecotype Columbia 0
CSC	cellulose synthase complex
CSLA	cellulose synthase like class A
CSLC	cellulose synthase like class C
CTAB	cetyltrimethylammonium bromide
D2O	deuterium oxide
DHB	2,5-dihydroxybenzoic acid
DMSO	dimethyl sulfoxide
DNA	deoxyribonucleic acid
dNTPs	deoxyribonucleic triphosphates
DSS	3-(Trimethylsilyl) -1-propanesulfonic acid
E-CELBA	<i>endo</i> -1,4- β -D-glucanase
<i>E. coli</i>	<i>Escherichia coli</i>
EDTA	Ethylenediaminetetraacetic acid
EI	electron impact ionization
EMS	ethyl methanesulfonate
Frc	fructose
Fuc	fucose

g	gram
<i>g</i>	gravity
G	deoxyguanosine monophosphate
GAE	UDP-glucuronic acid epimerase
Gal	galactose
GalA	galacturonic acid
GC-MS	gas chromatography mass spectrometry
GDP	guanosine diphosphate.
Gen	gentamycin
GFP	green fluorescent protein
GH	glycosyl hydrolase
Glc	glucose
GlcA	glucuronic acid
GMD	GDP-mannose dehydratase
GME	GDP-mannose epimerase
GMP	GDP-mannose pyrophosphorylase
GT	glycosyltransferase
H ₂ O	water
H ₂ SO ₄	Sulphuric acid
HCl	hydrochloric acid
HPAEC-PAD	high-performane anion exchange chromatograph with pulsed amperometric detection
IRX	irregular xylem
Kan	kanamycin
kb	kilobase pairs
kDa	kilodalton
KOH	potassium hydroxide
LB	lysogeny broth
LC-MS	liquid chromatography mass spectrometry
<i>m / z</i>	mass to charge ratio
MALDI-TOF	matrix assisted laser desorption ionization time of flight
Man	mannose
ManS	mannan synthase
Mb	megabase pairs
MES	4-Morpholineethanesulfonic acid
mg	milligram
min	minute
mL	millilitre
MLG	mixed linkage glucan
MM	minimal media containing methanol

MS	Murashige and Skoog
n	number of replicates / sample size
N/A	not applicable
Nat	nourseothricin
<i>N. benthamiana</i>	<i>Nicotiana benthamiana</i>
n.d.	not determined
NaOH	sodium hydroxide
<i>nasturtium</i>	<i>Tropaeolum majus</i>
NCBI	national center for biotechnology information
nd	not detected
ng	nanogram
NMR	nuclear magnetic resonance
NST	nucleotide sugar transporter
<i>O. sativa</i>	<i>Oryza sativa</i>
OD	optical density
OLIMP	oligosaccharide mass profiling
P	phosphate
<i>P. pastoris</i>	<i>Pichia pastoris</i>
PCR	polymerase chain reaction
PGI	phosphoglucose isomerase
PGM	phosphoglucomutase
PM	plasma membrane
PMI	phosphomannose isomerase
PMM	phosphomannomutase
qRT-PCR	quantitative reverse transcription polymerase chain reaction
RG	rhamnogalacturonan
Rha	rhamnose
RHM	rhamnose synthase
RNA	ribonucleic acid
Rnase	ribonuclease
SNP	single nucleotide polymorphism
Spc	spectinomycin
TAE	tris, acetic acid and EDTA
TAIR	the Arabidopsis information resource
T-DNA	transfer DNA
TE	tris EDTA
TFA	trifluoro acetic acid
tris	2-Amino-2-(hydroxymethyl)-1,3-propanediol
U	unit
UDP	uridine diphosphate

UGD	UDP-glucose dehydrogenase
UGE	UDP-glucose epimerase
UGP	UDP-glucose pyrophosphorylase
UXE	UDP-xylose epimerase
UXS	UDP-xylose synthase
WT	wild type
XEG	xyloglucan endoglucanase
XG	xylogalacturonan
XLT	xyloglucan L-side-chain glycosyltransferase
XST	xyloglucan S-sidechain glycosyl transferase
XTH	xyloglucan transglycosylase / hydrolase
XXT	xyloglucan xylosyl transferase
XyBAT	Xyloglucan backbone acetyl transferase
XyG	xyloglucan
Xyl	xylose
<i>Y. lipolytica</i>	<i>Yarrowia lipolytica</i>
YNB	yeast nitrogen base
YPD	yeast extract, peptone and dextrose
µg	microgram

Table of contents

Summary	<i>i</i>
List of Abbreviations	<i>ii</i>
List of Figures	<i>ix</i>
List of Tables	<i>xi</i>
1. Introduction	<i>1</i>
1.1 Plant cell wall polysaccharides	<i>1</i>
1.1.1 Structures	<i>1</i>
1.1.2 Biosynthesis	<i>4</i>
1.1.2.1 Cellulose	<i>5</i>
1.1.2.2 Hemicellulose	<i>6</i>
1.1.2.2.1 Xylan	<i>7</i>
1.1.2.2.2 Heteromannan	<i>9</i>
1.1.2.2.3 Mixed-linkage glucan	<i>10</i>
1.1.2.2.4 Xyloglucan	<i>12</i>
1.1.2.3 Pectin	<i>17</i>
1.2 Lignin	<i>20</i>
1.3 O-acetylation mechanism and its biological significance in plant cell wall	<i>21</i>
1.4 Thesis objectives	<i>25</i>
2 Materials and methods	<i>27</i>
2.1 Materials	<i>27</i>
2.1.1 Plant lines	<i>27</i>
2.1.2 Microbial strains	<i>29</i>
2.1.3 Plasmids	<i>30</i>
2.1.4 Primers	<i>31</i>
2.1.5 Cultivation media	<i>34</i>
2.1.6 Chemicals	<i>35</i>
2.1.7 Kits	<i>37</i>
2.1.8 Equipment	<i>37</i>
2.1.9 Software/tools	<i>40</i>
2.2 Methods	<i>40</i>
2.2.1 Media and growth conditions	<i>40</i>
2.2.1.1 Soil grown <i>Arabidopsis thaliana</i>	<i>40</i>
2.2.1.2 Soil grown <i>Nicotiana benthamiana</i>	<i>41</i>
2.2.1.3 Bacterial growth conditions	<i>41</i>
2.2.1.4 <i>Yarrowia lipolytica</i> growth conditions	<i>41</i>
2.2.2 Molecular biology methods	<i>42</i>
2.2.2.1 Plant nucleic acid extraction	<i>42</i>
2.2.2.1.1 DNA extraction from leaf tissues for genotyping	<i>42</i>
2.2.2.1.2 DNA extraction from leaf tissues for Whole Genome Sequencing	<i>42</i>
2.2.2.1.3 RNA extraction from stem tissues	<i>43</i>
2.2.2.2 Genomic DNA extraction from <i>Y. lipolytica</i>	<i>43</i>
2.2.2.3 Plasmid DNA extraction	<i>43</i>
2.2.2.4 Gel DNA extraction	<i>44</i>
2.2.2.5 DNA clean and concentration	<i>44</i>

2.2.2.6	DNA/RNA concentration measurement	44
2.2.2.7	Genotyping PCR and Gel electrophoresis	44
2.2.2.8	Transcriptional analysis using qRT-PCR	45
2.2.2.9	DNA amplification for cloning	45
2.2.2.10	Plasmid linearisation	46
2.2.2.11	Cloning methods	46
2.2.2.11.1	Gibson Assembly	46
2.2.2.11.2	Gateway Cloning	47
2.2.2.11.3	Blunt-End cloning	47
2.2.2.12	Sequencing methods	48
2.2.2.12.1	Sample prep from BSA and Whole Genome Sequencing of <i>A. thaliana</i>	48
2.2.2.12.2	Whole plasmid sequencing	48
2.2.2.12.3	Sanger sequencing	49
2.2.2.13	Transformation of <i>E. coli</i>	49
2.2.2.14	Preparation of <i>Y. lipolytica</i> competent cells and transformation	50
2.2.2.15	Transformation of <i>Agrobacterium tumefaciens</i>	51
2.2.2.16	Infiltration in <i>Nicotiana benthamiana</i>	51
2.2.2.17	Mammalian 2-hybrid assay for protein-protein interaction	51
2.2.3	Subcellular localization using confocal microscopy	52
2.2.4	Bioinformatic methods	53
2.2.4.1	Analysis of Whole Genome Sequencing data	53
2.2.4.2	Protein structural analysis and interaction prediction	53
2.2.5	Analytical methods	54
2.2.5.1	Preparation of alcohol insoluble residue (AIR) from <i>A. thaliana</i> stem material	54
2.2.5.2	Preparation of alcohol insoluble residue (AIR) from <i>Y. lipolytica</i> cell wall material	55
2.2.5.3	Measurement of acetic acid content in <i>A. thaliana</i> AIR material	56
2.2.5.4	Oligosaccharide Mass Profiling (OLIMP) by MALDI-TOF	56
2.2.5.5	Separation of oligosaccharides using Size Exclusion Chromatography (SEC)	57
2.2.5.6	Monosaccharide compositional analysis using HPAEC-PAD	57
2.2.5.7	Glycosidic Linkage Analysis	58
2.2.5.8	Crystalline cellulose measurement	59
2.2.6	Statistical analysis methods	59
2.2.6.1	Chi-squared test	59
2.2.6.2	Tukey HSD and ANOVA	60
3.	<i>A forward genetic screen to identify genes involved in suppression of growth and stress related defects associated with wall hypoacetylation</i>	61
3.1	Background	61
3.1.1	Potential and challenges of forward genetic approach in uncovering genetic pathways	62
3.2	Results	65
3.2.1	Identification, growth characterization, and <i>O</i> -acetate content of suppressor mutants	65
3.2.2	Inheritance pattern of suppressor mutations	68
3.2.3	Bulk segregant analysis and whole genome sequencing on <i>saxy</i> mutants	69
3.2.4	Validation of SNPs identified by BSA and NGS	78

3.2.5	Validation of suppressor mutations by second allele approach	87
3.2.5.1	Gene expression analysis of suppressor genes	91
3.2.5.2	Cell wall characterization of <i>pAXY</i> suppressor mutants	92
3.2.6	Functional implications of <i>pAXY</i> suppressor mutations	99
3.2.6.1	Localization and interaction profiling of <i>AtWD40</i>	99
3.2.6.2	Localization and interaction profiling of <i>AtKH26</i>	108
3.2.6.3	Localization and interaction profiling of PHOX3	111
3.3	Discussion	114
3.3.1	Genetic basis of growth recovery in <i>O</i> -acetylation mutants	114
3.3.2	Correlation between cell wall composition and growth recovery	115
3.3.3	Proposed regulatory interactions in BR signaling and their role in <i>pAXY</i> growth phenotype suppression	116
3.3.4	Loss of ORRM2 repression in <i>pAXY atkh26</i> mutants may rescue <i>pAXY</i> growth phenotype	120
4.	<i>Heterologous production of O-acetylated xyloglucan backbone in Yarrowia lipolytica</i>	122
4.1	Background	122
4.1.1	Advantages of heterologous expression over other conventional methods	122
4.1.2	Advantages of <i>Yarrowia lipolytica</i> for <i>O</i> -acetylation studies over <i>Pichia pastoris</i>	125
4.1.3	Considerations for reconstruction of glucan <i>O</i> -acetylation pathway in <i>Y. lipolytica</i>	126
4.2	Results	127
4.2.1	Engineering <i>Y. lipolytica</i> strains for xyloglucan backbone <i>O</i> -acetylation pathway integration	127
4.2.2	Oligosaccharide mass profiling (OLIMP) analysis of <i>O</i> -acetylated glucan synthesis in engineered <i>Y. lipolytica</i> strains	129
4.2.3	Cell wall characterization of transgenic <i>Y. lipolytica</i> strains for <i>O</i> -acetylated 4-glucan backbone production.	131
4.3	Discussion	139
4.3.1	<i>O</i> -acetylated glucan backbone production in <i>Y. lipolytica</i>	139
4.3.2	Functional interplay of CSLC4 and XXT2 in glucan chain production	140
4.3.3	Improving the efficiency of heterologous <i>O</i> -acetylated glucan backbone production	141
5.	<i>Conclusion and outlook</i>	142
6.	<i>References</i>	145
7.	<i>Appendix 1: Gene sequences</i>	161
8.	<i>Appendix 2: Vector maps</i>	165
9.	<i>Appendix 3: Miscellaneous data</i>	175
10.	<i>Acknowledgement</i>	190

List of Figures

Figure 1-1. Model of the primary cell wall and its polymers. -----	3
Figure 1-2. Cell wall polysaccharide structures.-----	4
Figure 1-3. Schematic representation of hemicellulose xylan and proteins involved in its biosynthesis. -----	9
Figure 1-4. Schematic representation of hemicellulose heteromannan and proteins involved in its biosynthesis. -----	10
Figure 1-5. Schematic representation of hemicellulose mixed-linkage glucan. -----	11
Figure 1-6. Xyloglucan (XyG) side-chain composition and diversity. -----	13
Figure 1-7. Schematic representation of hemicellulose xyloglucan and proteins involved in its biosynthesis. -----	17
Figure 1-8. Pectin structures.-----	19
Figure 1-9. Model of the cell wall polysaccharide O-acetylation mechanism in plants. -----	25
Figure 3-1. Growth phenotype and acetate content of <i>pAXY</i> and <i>axy9</i> . -----	62
Figure 3-2. <i>pAXY</i> suppressor mutants (<i>saxy</i>) showing rescued phenotype in M ₃ generation. -----	67
Figure 3-3 Genotyping for <i>AXY9</i> and <i>pAXY</i> T-DNA insertion in <i>saxy</i> mutants. -----	70
Figure 3-4 Bulk Segregant Analysis workflow. -----	72
Figure 3-5 Representative image for visualizing SNP in IGV. -----	73
Figure 3-6. Targeted sequencing of candidate mutations in BCF ₂ DNA pools of <i>saxy</i> mutants. -----	82
Figure 3-7. Targeted sequencing on <i>saxy</i> BCF ₂ individuals for the candidate mutations. -----	86
Figure 3-8. Growth phenotype of suppressor mutants. -----	89
Figure 3-9 Gene structures indicating T-DNA insertion site and the SNP position induced by EMS.-----	90
Figure 3-10. Gene expression analysis of <i>AXY9</i> and suppressor genes.-----	92
Figure 3-11. Total wall-bound acetyl ester content from 6-week-old stem of suppressor mutants, WT and <i>pAXY</i> . -----	93
Figure 3-12. Effect of <i>wd40</i> suppressor mutation in the cell wall monosaccharide composition. -----	95
Figure 3-13. Effect of <i>phox3</i> suppressor mutation in the cell wall monosaccharide composition. -----	96
Figure 3-14. Effect of <i>atkh26</i> suppressor mutation in the cell wall monosaccharide composition. -----	97
Figure 3-15 Crystalline cellulose content in the cell wall of suppressor mutants. -----	98
Figure 3-16. Freezing tolerance assay for <i>pAXY</i> suppressor mutants. -----	99
Figure 3-17. Predicted subcellular localization of <i>AtWD40</i> . -----	100
Figure 3-18. Subcellular localization of GFP tagged <i>AtWD40</i> . -----	101
Figure 3-19. Structural comparison of <i>AtWD40</i> and <i>AtWD40</i> ^{H15Y} . -----	102
Figure 3-20. Protein-Protein interaction of <i>AtWD40</i> (AT3G15610).-----	104
Figure 3-21. Structure and sequence alignment of <i>AtWD40</i> and <i>OsWDRP3</i> . -----	105
Figure 3-22. Model used to study protein-protein interaction. -----	107
Figure 3-23. Mammalian 2-hybrid interaction assay between <i>AtWD40</i> and predicted interaction candidate proteins. -----	107
Figure 3-24. Predicted subcellular localisation of <i>AtKH26</i> . -----	109
Figure 3-25. Domain architecture and Structural comparison of <i>AtKH26</i> and <i>AtKH26</i> ^{G411E} . -----	109
Figure 3-26. Predicted protein-protein interaction of <i>AtKH26</i> (AT5G46190). -----	111

Figure 3-27. Predicted subcellular localisation of <i>AtPHOX3</i> .-----	112
Figure 3-28. Predicted protein-protein interaction of PHOX3 (AT5G20360)-----	113
Figure 3-29 Predicted cis-acting regulatory elements in the 2kb promoter region of <i>AtPHOX3</i> . -----	113
Figure 3-30. Simplified model showing involvement of WD40, PHOX3 and KAK in BR signaling pathway.-----	120
Figure 4-1. Genotyping <i>Y. lipolytica</i> transgenic strains.-----	128
Figure 4-2. OLIMP Spectra of E-CELBA digested transgenic <i>Y. lipolytica</i> AIR.-----	130
Figure 4-3. OLIMP spectra of fraction 9 and 10 obtained through SEC separation of E- CELBA digested transgenic <i>Y. lipolytica</i> AIR.-----	133
Figure 4-4. Glycosidic linkage analysis of transgenic <i>Y. lipolytica</i> strains.-----	138
Figure 8-1. Vector map for <i>Y. lipolytica</i> constructs with <i>TmCSLC4</i> in expression cassette.-----	165
Figure 8-2. Vector map for <i>Y. lipolytica</i> constructs with <i>TmCSLC4</i> and <i>TmXXT2</i> in expression cassette.-----	166
Figure 8-3. Vector map for <i>Y. lipolytica</i> constructs with <i>TmCSLC4</i> and <i>BdXyBAT1</i> in expression cassette.-----	167
Figure 8-4. Vector map for <i>Y. lipolytica</i> constructs with <i>TmCSLC4</i> , <i>TmXXT2</i> and <i>BdXyBAT1</i> in expression cassette.-----	168
Figure 8-5. Vector map for mammalian 2 hybrid assay constructs with <i>AtDAAR2</i> attached to the C-terminus of <i>Egene</i> in expression cassette.-----	169
Figure 8-6. Vector map for mammalian 2 hybrid assay constructs with <i>AtSKI1</i> attached to the C-terminus of <i>Egene</i> in expression cassette.-----	170
Figure 8-7. Vector map for mammalian 2 hybrid assay constructs with <i>AtUBQ3</i> attached to the C-terminus of <i>Egene</i> in expression cassette.-----	171
Figure 8-8. Vector map for mammalian 2 hybrid assay constructs with <i>VPI6</i> domain attached to the C-terminus of <i>AtWD40</i> in expression cassette.-----	172
Figure 8-9. Vector map for mammalian 2 hybrid assay constructs with <i>VPI6</i> domain attached to the N-terminus of <i>AtWD40</i> in expression cassette.-----	173
Figure 8-10. Vector map for subcellular localisation of <i>AtWD40</i> -GFP in <i>N. benthamiana</i> .-----	174
Figure 9-1. Stem cross sections of the WT and <i>pAXY</i> genotypes.-----	175
Figure 9-2. Sanger sequencing alignment of AT4G05612 amplicons from <i>saxy59</i> BCF ₂ recovered and dwarf pool.-----	175
Figure 9-3. Growth phenotype of selected suppressor mutants.-----	176
Figure 9-4. Growth phenotype of discarded suppressor mutants.-----	177
Figure 9-5. Growth phenotype of <i>pAXY max4-7</i> mutant.-----	178
Figure 9-6. SEC Chromatograms of <i>Y. lipolytica</i> transgenic strains-----	179
Figure 9-7. OLIMP spectra of SEC fractions of E-CELBA digested transgenic <i>Y. lipolytica</i> AIR.-----	189

List of Tables

Table 1. List of all plant lines used and/or created in this work -----	28
Table 2. List of microbial strains used and/or created in this work -----	30
Table 3. List of all plasmids used and/or created in this work -----	31
Table 4. List of primers -----	34
Table 5. List of cultivation media -----	35
Table 6. List of chemicals -----	36
Table 7. List of Kits -----	37
Table 8. List of equipment and hardware -----	39
Table 9. List of software and tools -----	40
Table 10. Segregation pattern and causal mutation characteristics in <i>saxy</i> mutants of BCF ₂ generation. -----	69
Table 11. Mapping statistics of NGS data. -----	75
Table 12. List of candidate genes obtained for <i>saxy59</i> , <i>saxy85</i> , <i>saxy171</i> , <i>saxy42</i> , <i>saxy161</i> , and <i>saxy38</i> . -----	76
Table 13. Monosaccharide compositional analysis of <i>Y. lipolytica</i> transgenic strains. -----	137

1. Introduction

The plant cell wall is a complex polymer composite crucial for a variety of essential cellular functions. It must be robust enough to provide mechanical support to the cell and the entire plant, resist osmotic pressure, and serve as a barrier against pathogens and environmental stressors. Simultaneously, it needs to be adaptable, allowing for remodeling to facilitate cell elongation (Cosgrove, 2005). The diversity of these functions, which can vary according to developmental stage, tissue type, and species, is reflected in the wide range of wall compositions and structures observed (Burton et al., 2006; Knox, 2008). Despite this variability, most plant cell walls consist primarily of three major components: glycoproteins, polyphenols, and polysaccharides. Among these, polysaccharides are the most abundant, structurally complex, and predominant structural element, especially in the primary cell wall, which is the extensible wall produced by a plant cell during growth (McNeil et al., 1984).

Cell walls exhibit distinct divisions: the middle lamella, primary, and secondary walls (Carpita and Gibeaut, 1993). Positioned between adjacent cell's primary walls, the middle lamella, rich in pectic polymers, plays a pivotal role in cell-to-cell adhesion (Chipuk et al., 2006; Knox et al., 1990). The primary cell wall further delineates into type I and type II. Type I, prevalent in dicots and non-graminaceous monocots, boasts a composition rich in pectin, xyloglucan hemicellulose, structural proteins, and cellulose (Carpita and Gibeaut, 1993). In contrast, type II primary walls, found in grasses, contain lower levels of pectin, and are predominantly enriched in glucurono-arabinoxylan hemicellulose (Carpita and Gibeaut, 1993). After elongation cessation, the secondary cell wall formation commences. This phase involves the synthesis of abundant crystalline cellulose, hemicellulose, and lignin (Carpita and McCann, 2002). These modifications are prevalent in vascular and structural tissues, imparting rigidity, and hydrophobic properties to the wall (Albersheim et al 2010).

1.1 Plant cell wall polysaccharides

1.1.1 Structures

Plant cell wall polysaccharides are classified into three primary categories based on structure and chemical properties: cellulose, hemicellulose, and pectic polysaccharides. Cellulose

comprises β -1,4 linked glucan chains forming semi-crystalline microfibrils, a major component of the cell wall (Somerville, 2006). These microfibrils create an essential framework, and to maintain an extensible wall network, other wall components fill the spaces between cellulose microfibrils, preventing their aggregation (Figure 1-1) (Somerville et al., 2004).

Hemicelluloses are polymers with a β -1,4 linked glycan backbone featuring additional substitutions or linkages (Pauly et al., 2013; Scheller and Ulvskov, 2010). While the backbone allows molecular interaction through hydrogen bonds, the additional substitutions grant partial solubility, preventing aggregation. Identified types of hemicellulose include xyloglucan, xylan, heteromannans, and mixed-linkage glucans (Figure 1-2) (Pauly et al., 2013). Xylan stands out as the most prevalent hemicellulose in primary and secondary walls of grasses, and in the secondary wall of most angiosperms. It consists of a backbone of β -1,4 linked xylosyl residues, often *O*-acetylated or substituted with glucuronosyl-, arabinosyl-, or additional xylosyl-residues depending on the plant species (Faik, 2010). Mannan, found widely across the plant kingdom and in some algal species, is notably abundant in seeds of certain species where it acts as a storage polymer, such as guar, or in the secondary walls of gymnosperms (Kooiman, 1971; Samuels et al., 2002). Its backbone consists entirely of β -1,4 linked mannosyl residues or a combination of mannosyl and glucosyl residues, potentially modified by *O*-acetylation or galactosylation (Moreira and Filho, 2008). Xyloglucan, detailed below, comprises a β -1,4 linked glucan backbone with regular xylosyl substitutions that can further vary depending on position, tissue, and species (Pauly et al., 2013). Mixed-linkage glucans feature a backbone with both β -1,3 and β -1,4 linked glucosyl residues, devoid of observed side branches or other substituents unlike other hemicelluloses (Sørensen et al., 2008).

Pectin, being the most structurally diverse polysaccharide group, encompasses a total of 12 identified monosaccharides, involving 67 distinct enzymatic activities for biosynthesis (Mohnen, 2008). Among the three major pectic polysaccharides—homogalacturonan (HG), rhamnogalacturonan I (RGI), and rhamnogalacturonan II (RGII)—there's a high likelihood of partial covalent linkage between them within the wall, as evidenced by enzymatic treatments with α -1,4-endo-polygalacturonase releasing these fractions (Figure 1-2) (Harholt et al., 2010). HG consists of an α -1,4 linked galacturonosyl residue backbone, often modified with methyl esters that neutralize the charged galacturonosyl-moiety. The formation of gels occurs via calcium bridges between free galacturonosyl residues. Control over the degree of methylesterification, and consequently the ability of the polymer to form calcium bridges, is

regulated by apoplastic pectin methylesterases and pectin methylesterase inhibitors. This influences the strength of the pectin matrix (Anthon and Barrett, 2010; Jarvis, 1984; Saez-Aguayo et al., 2013). Modifications with xylosyl and apiosyl substituents result in xylogalacturonan (XG) and apiogalacturonan, respectively (Harholt et al., 2010). RGI's backbone comprises alternating rhamnose and galacturonic acid residues. Rhamnosyl residues within the backbone are often substituted with galactose or arabinose, with potential branching, while galacturonosyl residues may undergo *O*-acetylation (Mohnen, 2008). RGII's backbone comprises α -1,4 linked galacturonic acid residues and complex sidechains containing various glycosyl units, including apiose, aceric acid, 3-deoxy-D-manno-oct-2-ulosonic acid (KDO), and 3-deoxy-D-lyxo-heptulosaric acid (DHA). These sidechains encompass rare monosaccharides alongside more common ones like galacturonic acid, rhamnose, galactose, and fucose (Figure 1-2) (Pérez et al., 2003). The multitude of monosaccharide constituents and diverse linkages in RGII make it the most structurally diverse polysaccharide identified to date (Pérez et al., 2003).

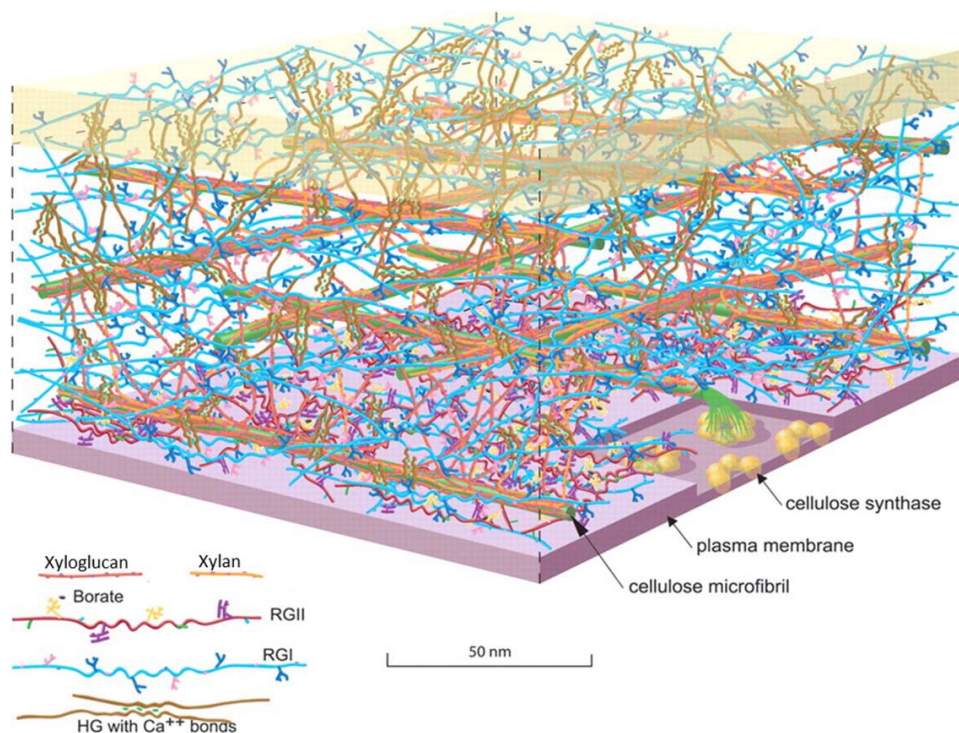


Figure 1-1. Model of the primary cell wall and its polymers.

Cellulose microfibrils stand as the principal load-bearing elements within plant cell walls. These microfibrils interconnect through hemicelluloses like xylan and XyG. Pectin, on the other hand, create an amorphous matrix wherein the hemicellulose and cellulose network reside. Among the pectic polysaccharides are rhamnogalacturonan I (RGI), rhamnogalacturonan II (RGII), and

homogalacturonan (HG). RGII and HG have the capability to form borate and calcium-mediated crosslinks, respectively. These crosslinks significantly contribute to fortifying the wall's strength. Figure reprinted from Somerville et al., 2004.

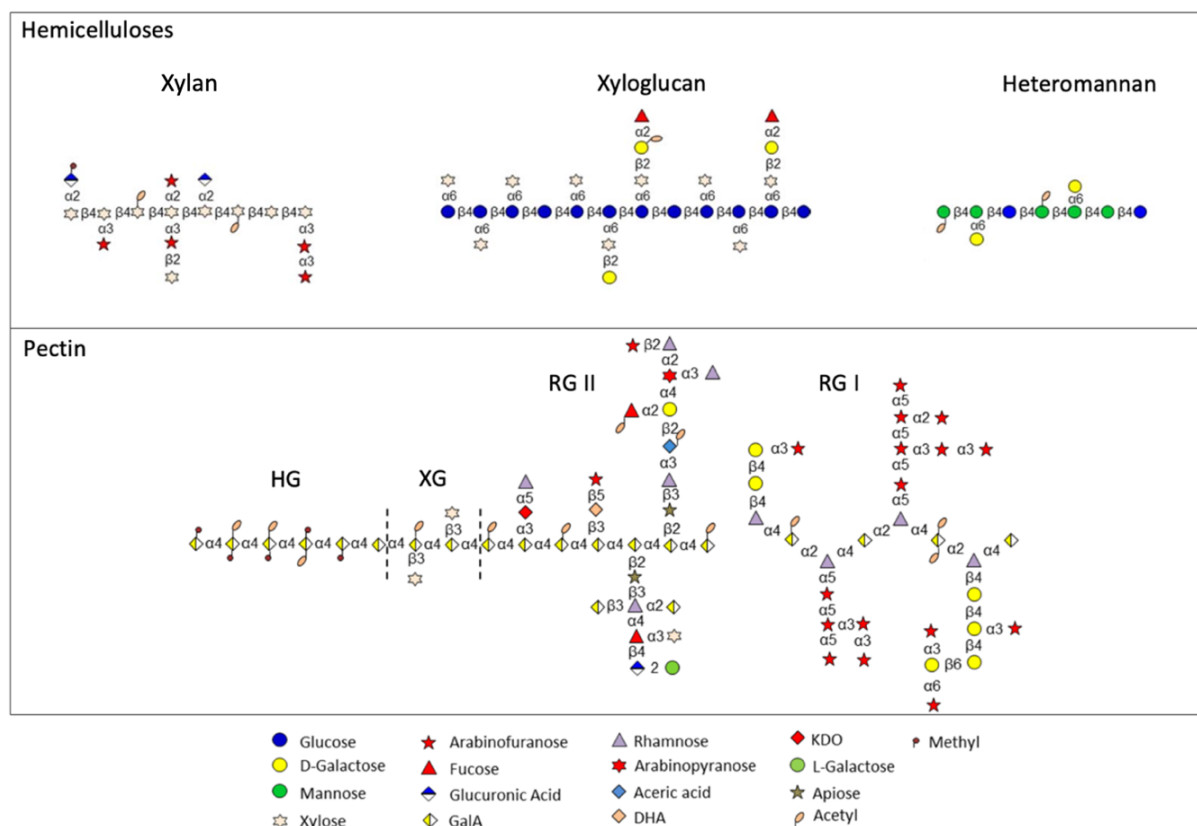


Figure 1-2. Cell wall polysaccharide structures.

Representative structures of hemicelluloses (xylan, heteromannan, and xyloglucan) and pectins [homogalacturonan (HG), Xylogalacturonan (XG), rhamnagalacturonan I (RGI), rhamnagalacturonan II (RGII)] are depicted. The text between the glycosyl moieties denotes the orientation of the glycosidic linkage (α or β) and the associated carbon number related to the acceptor oxygen atom. It's important to note that the actual side-chain composition and arrangement can differ between polymers, plant tissues, and plant species. The structures of hemicelluloses are adapted with modifications from Pauly et al., 2013 (Pauly et al., 2013). Pectin structures have been adapted from Harholt et al., 2010 and Mohnen 2008 (Harholt et al., 2010; Mohnen, 2008). Abbreviations: GalA – Galacturonic acid, DHA – deoxy-D-lyxo--2-heptulosaric acid, KDO – 3-deoxy-D-manno-2-octulosonic acid.

1.1.2 Biosynthesis

The biosynthesis of plant cell wall polysaccharides is driven by the activity of glycosyltransferases (GTs), which use activated sugars, typically nucleotide sugars, to create glycosidic bonds. A key nucleotide sugar, uridine diphosphate glucose (UDP-G), plays a crucial role in the synthesis of cellulose and xyloglucan (XyG) (Delmer and Amor, 1995). It is

generated by the enzyme sucrose synthase, which converts sucrose into UDP-glucose or adenosine diphosphate glucose (ADP-G) and fructose (Delmer and Amor, 1995). UDP-glucose is then processed by a series of enzymes, both in the cytosol and within the Golgi apparatus, to produce various nucleotide sugars essential for wall polysaccharide synthesis (Bar-Peled and O'Neill, 2011; Seifert, 2004). Cellulose biosynthesis occurs at the plasma membrane, where cellulose synthases are organized into large complexes called rosette structures (Mueller and Brown, 1980). In contrast, matrix polysaccharides are synthesized in the Golgi apparatus (Lerouxel et al., 2006). Some enzymes, such as cellulose synthases (CSC) and cellulose synthase-like enzymes (CSL), possess multiple transmembrane domains and typically use a cytosolic pool of nucleotide sugars, with the assembled polymer being extruded through the membrane to the exterior. Other GTs in the Golgi apparatus are type II transmembrane proteins characterized by a single N-terminal transmembrane helix (Lerouxel et al., 2006). These enzymes likely utilize luminal pools of nucleotide sugars, which are transported into the Golgi lumen by nucleotide sugar transporters (Seifert, 2004). The polysaccharides synthesized in the Golgi are delivered to the cell wall via exocytosis, where they become part of the extracellular matrix (Sandhu et al., 2009). Once in the apoplast, wall polysaccharides can undergo further modification by apoplastic esterases and/or glycosyl hydrolases or transglycosylases (Giovane et al., 2004; Günl et al., 2011; Kerr and Fry, 2003). The detailed biosynthesis of each type of polysaccharide is further explained in the sections below.

1.1.2.1 Cellulose

Cellulose, the most abundant sugar polymer on Earth, is the primary component of plant cell walls (Somerville, 2006). Annually, an estimated 180 billion tons of cellulose are produced globally (Delmer, 1999). Synthesized at the plasma membrane, cellulose is formed by large protein complexes called rosettes, which convert UDP-glucose into individual β -1,4-linked D-glucose chains. These chains are then assembled into larger crystalline structures known as microfibrils (Somerville, 2006). Comprising 18-36 glucan chains, microfibrils serve as the main scaffolding structure of the cell wall (Albersheim et al., 2010; Somerville, 2006). The genes responsible for cellulose synthesis are known as *CESA*, an acronym for cellulose synthase, with "A" indicating the presumed catalytic subunit, homologous to bacterial catalytic subunits. In *A. thaliana*, the rosette complexes in primary and secondary cell walls are composed of different but homologous CESA proteins. Specifically, CESA1, CESA3, and CESA6 form the primary wall rosette complex, while CESA4, CESA7, and CESA8 are

involved in the secondary wall complex (Persson et al., 2007; Taylor et al., 2004). This synthetic machinery is highly conserved across plant species, including monocots like rice. Mutations in any of these *CESA* genes lead to severe phenotypes such as brittle stems, dwarfism, collapsed xylem tissue, and growth abnormalities (Arioli et al., 1998; Somerville et al., 2004; Tanaka et al., 2003; Zhang et al., 2009). Given their high sequence similarity across species, the discovery of CESA proteins was pivotal in understanding cellulose synthesis. For instance, heterologously expressed poplar CESA8 has been shown to catalyze β -(1,4) linked glucan biosynthesis in reconstituted proteoliposomes, confirming the biochemical activity of CESA in vitro (Purushotham et al., 2020). CSCs are believed to be assembled in the Golgi apparatus and transported to the plasma membrane (PM) through vesicle trafficking. This hypothesis is supported by the discovery of STELLO, a glycosyltransferase-like protein localized in the Golgi (Zhang et al., 2016). Once at the PM, only CSCs can synthesize cellulose. The direction and speed of CSC movement on the PM are critical in determining the physicochemical properties of the cellulose produced (Zhang et al., 2021). CSCs move along cortical microtubules (CMTs), with cellulose synthase interactors (CSII–3) facilitating the tethering of CSCs to CMTs (Gu et al., 2010; Li et al., 2012; Paredez et al., 2006). The connection between CSCs and CMTs can be disrupted by cellulose synthase microtubule uncoupling (CMU) proteins, whose activity is regulated by the kinesin protein fragile fiber1 (FRA1) (Ganguly et al., 2020; Z. Liu et al., 2016; Zhong et al., 2002). While several proteins involved in different trafficking pathways for cellulose biosynthesis have been identified such as the dynamin protein BC3 (Xiong et al., 2010), TPLATE complex members (Sánchez-Rodríguez et al., 2017), and the AP2 complex (Bashline et al., 2015, 2013), the exact secretion routes of CSCs remain unclear. Additionally, accessory proteins are essential for cellulose production. For example, COBRA (COB) and COB-like proteins are thought to participate in cellulose assembly by binding to cellulose and influencing the crystallization of cellulosic microfibrils (Liu et al., 2013). Similarly, *A. thaliana* chitinase-like proteins *AtCTL1* and *AtCTL2* (Sánchez-Rodríguez et al., 2012), along with the CSC-associated protein KORRIGAN, a glycosyl hydrolase 9 (GH9) protein, are involved in cellulose production, although their precise roles remain to be fully understood (Vain et al., 2014).

1.1.2.2 Hemicellulose

Second to cellulose, hemicelluloses and pectic polymers vary in abundance and composition. Types of hemicelluloses identified to date include xyloglucan, xylan, heteromannans, and

mixed-linkage glucans (Pauly et al., 2013). Hemicelluloses can represent up to one-third of the wall biomass (Albersheim et al., 2010). One of their major features is a backbone composed of β -1,4 glycosidic bonds (Pauly et al., 2013). In contrast to cellulose, some of these polymers are decorated with side chains that render them amorphous and soluble (Carpita and McCann, 2002). There is ample diversity in structure amongst these groups of polymers, varying in tissue types (Gille et al., 2011b) and in plant species (Albersheim et al. 2011; Pauly et al., 2013).

1.1.2.2.1 Xylan

Xylans are the most abundant hemicellulosic polymers in vascular plants, featuring a conserved β -(1,4)-linked xylosyl backbone across various species, indicating a universally preserved biosynthetic machinery in plants. Unlike the hexose-containing backbones found in other polysaccharides, the pentose-based backbone of xylan is synthesized through a distinct process (Smith et al., 2017). The xylan backbone, composed of β -1,4-linked xylosyl residues, undergoes several modifications on its sidechains, including arabinosylation at the C-3 position (Anders et al., 2012), methylation at the O-4 position (Urbanowicz et al., 2012), xylose substitution at C-2 (Chiniquy et al., 2012), acetylation at O-2 and/or O-3 (Xiong et al., 2013), and feruloylation (Faik, 2010). Genetic studies have identified IRREGULAR XYLEM 10 (IRX10) and its homolog IRX10L, members of the GT47 family, as putative β -(1,4) xylosyl transferases responsible for xylan backbone elongation (Brown et al., 2009; Wu et al., 2009). Biochemical analyses have confirmed these enzymes' roles in elongating the xylan backbone (Urbanowicz et al., 2014). Additionally, homologs of *IRX10* from rice and other plant species were able to complement *A. thaliana irx10* mutants, highlighting the cross-species conservation of their function in xylan biosynthesis (X. Chen et al., 2013). Another set of crucial components for xylan backbone synthesis includes IRX9, IRX9L, IRX14, and IRX14L, all members of the GT43 family. Mutations in these proteins have been linked to reduced xylan content (Brown et al., 2007; Wu et al., 2010). Plants with defective xylan structures often display irregular xylem and dwarfed growth, as observed in numerous *irx* mutants (Brown et al., 2009, 2007). However, no GT43 family member has yet been enzymatically validated. The involvement of these multiple components suggests that they may form protein complexes, although the exact organization of xylan synthase complexes remains unclear (Zeng et al., 2016).

Most xylosyl residues of the xylan backbone are substituted with (4-*O*-methyl) glucuronic acids at the *O*-2 sites in dicot plants and with L-arabinose at the *O*-3 sites in grasses (Poaceae). The L-arabinosyl side chain may be further substituted plant cell wall construction with D-xylosyl residues at the *O*-2 site or modified at the *O*-5 site with ferulate esters that can be oxidatively cross-linked in a variety of ways (Chiniquy et al., 2012; Scheller and Ulvskov, 2010). The xylosyl substituent is also present in some secretory xylan backbones, such as mucilage (Zhong et al., 2018a). GTs are required for the formation of these side chains. In *A. thaliana*, glucuronic acid substitution of xylan1–3 (GUX1–3) from the GT8 family are capable of adding glucuronic acid substitutions onto xylan, which can be further methylated by glucuronoxylan methyltransferases (GXMT1–2; from domain of unknown function family 579) to produce (methyl)glucuronic xylan (GX) (Mortimer et al., 2010; Urbanowicz et al., 2012). Xylan arabinosyl transferases (XATs) from the GT61 family transfer arabinosyl residues onto the xylan backbone to form arabinoxylan (Anders et al., 2012). Xylose arabinosyl substitution of xylan 1 (XAX1) (another GT61 family member) mediates the substitution of xylosyl residue onto the arabinosyl side chain (Chiniquy et al., 2012), while XYLAN XYLOSYLTRANSFERASE 1 (XYXT1) catalyzes the substitution of xylosyl residue on the xylan backbone (Zhong et al., 2018a). The diversified enzymatic activities of GT61 family members are in agreement with the expansion of this family in grasses (Mitchell et al., 2007). Xylan is a highly acetylated polysaccharide, which incorporates a majority of cell wall acetyl esters (Gille and Pauly, 2012; Xiong et al., 2013). Monoacetylation at the *O*-3 or *O*-2 sites is a dominant acetyl profile on the xylan backbone; diacetylation at both sites *O*-3 and *O*-2 is also present in plant xylans (Zhang et al., 2017). Earlier studies on provided direct biochemical evidence that TRICHOME BIREFRINGENCE-LIKE 29 (TBL29/ESK1) is a xylan specific *O*-acetyltransferase that catalyzes the addition of *O*-acetyl groups to the 2-position of xylosyl backbone residues in vitro, establishing the precise molecular function of this enzyme (Urbanowicz et al., 2014), and led to the proposed name XYLAN *O*-ACETYLTRANSFERASE 1 (XOAT1). Further studies has shown that even pattern of xylan acetylation is absent in the *tbl29/esk1* mutant, indicating that XOAT1 is necessary for patterning of acetyl esters on xylan in *A. thaliana* (Grantham et al., 2017). Since the initial biochemical analysis of XOAT1, several other members of the TBL family have also been shown to play a role in the regiospecific acetylation of xylan in *A. thaliana*, including TBL3 (XOAT4), TBL28 (XOAT2), TBL30 (XOAT3), TBL31 (XOAT5), TBL32 (XOAT6), TBL33 (XOAT7), TBL34 (XOAT8), and TBL35 (XOAT9) (Yuan et al., 2016b, 2016a; Zhong et al., 2017).

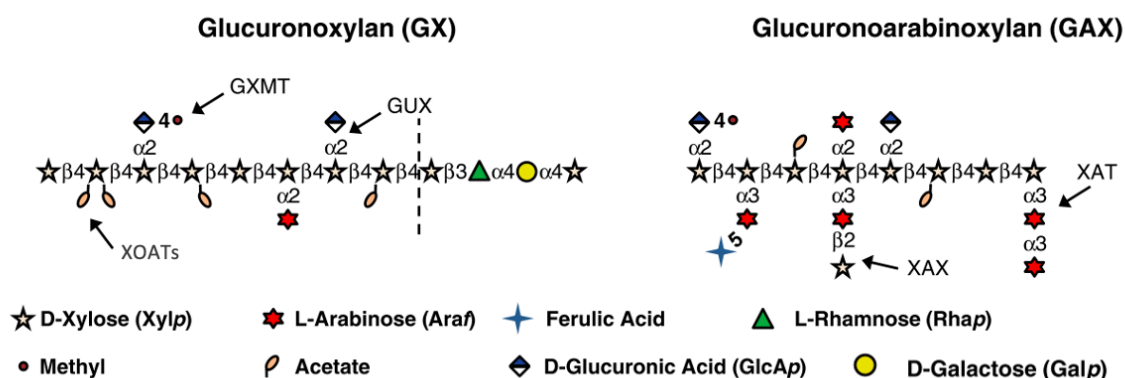


Figure 1-3. Schematic representation of hemicellulose xylan and proteins involved in its biosynthesis.

The symbols representing various monosaccharides were adopted from the Nomenclature Committee of the Consortium for Functional Glycomics (Varki et al., 2009). Glycosidic linkages between monosaccharides are denoted by their anomeric configurations (α or β) and their position; for example, $\beta 4$ indicates a $\beta(1\rightarrow 4)$ linkage. When specific glycosyltransferases are known to add a sugar in a particular linkage, they are indicated by their protein abbreviations. In this context, IRX9, IRX14, and IRX10 are involved in xylan backbone elongation. IRX8 adds galacturonic acid residues, while GUX proteins add glucuronic acid residues. GXMT specifically transfers a methyl group to the *O*-4 position of glucuronosyl residues linked to xylan. XAX adds xylosyl units to form the β -Xylp-1-2- α -Araf sidechain, XAT is involved in arabinosyl substitution of xylan, and XOATs are responsible for xylan *O*-acetylation. The structures of hemicelluloses are adapted with modifications from Pauly et al., 2013 (Pauly et al., 2013)

1.1.2.2.2 Heteromannan

Mannans, considered the most ancient hemicellulose, have been identified in some algal cell walls (Domozych et al., 2012; Rodríguez-Gacio et al., 2012). These polymers are present in the secondary cell walls of dicots (Scheller and Ulvskov, 2010), serve as storage polymers in certain species (Buckeridge, 2010; Rodríguez-Gacio et al., 2012), and are abundant in the secondary walls of gymnosperms (Pauly and Keegstra, 2008). Heteromannans are categorized into four groups: mannan, galactomannan, glucomannan, and glucogalactomannan (Pauly et al., 2013; Scheller and Ulvskov, 2010). Mannans and galactomannans have a β -1,4-linked mannose backbone, while glucomannans also incorporate β -1,4-linked glucose into their backbone. In *A. thaliana*, the CSLA (Dhugga et al., 2004; Gille et al., 2011a; Goubet et al., 2009; Liepman et al., 2005; Suzuki et al., 2006) and CSLD (Verhertbruggen et al., 2011) enzymes from the GT family 2 are involved in mannan backbone synthesis. In vitro activity of other mannan synthases, such as glucoManS, has also been demonstrated, including *At*CSLA2,

AtCSLA3, *AtCSLA9* (Liepman et al., 2005), and *PtCSLA1* from *Populus trichocarpa* (Suzuki et al., 2006). The *AtCSLA9* protein, with its catalytic domain facing the Golgi lumen, suggests that nucleotide sugars like guanosine diphosphate (GDP)-mannose and GDP-glucose must be imported into the Golgi (Davis et al., 2010). A galactosyltransferase activity responsible for galactosylation of mannan by galactomannan galactosyl transferase (GMGT) has been identified in *Trigonella foenum-graecum* (Mary E. Edwards et al., 1999). Additionally, a protein from *Trigonella foenum-graecum* and *A. thaliana*, termed mannan synthase related (MSR), is implicated in mannan biosynthesis. Co-expression of the *A. thaliana* cofactor *AtMSR1* enhanced the catalytic activities of *AkCSLA3* and *AtCSLA2*, enabling *AtCSLA2* to produce glucomannan instead of mannan in yeast *Pichia pastoris* (Goubet et al., 2009; Voiniciuc et al., 2019). However, *CcMANS1* from coffee cannot synthesize mannan without *CcMSR1*, highlighting the flexibility in (gluco)mannan biosynthesis in plants (Voiniciuc et al., 2019). Furthermore, mannan *O*-acetyltransferases (MOATs) modify mannosyl residues on the mannan backbone with acetyl groups (Zhong et al., 2018b).

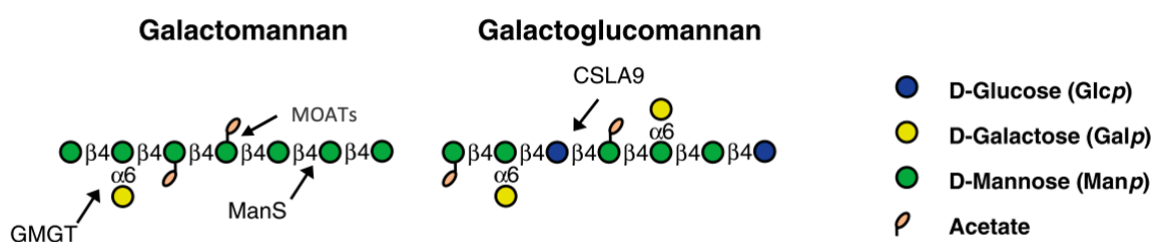


Figure 1-4. Schematic representation of hemicellulose heteromannan and proteins involved in its biosynthesis.

Symbols representing various monosaccharides were adopted from the Nomenclature Committee of the Consortium for Functional Glycomics (Varki et al., 2009). Glycosidic linkages between monosaccharides are denoted by their anomeric configurations (α or β) and their positions; for example, $\beta 4$ indicates a $\beta(1\rightarrow 4)$ linkage. When specific glycosyltransferases are known to add a sugar in a particular linkage, they are indicated by their protein abbreviations. Mannan synthases, such as CSLA and CSLD, are involved in the synthesis of the mannan backbone, with CSLA9 specifically adding glucose residues in the synthesis of glucomannan. GMGT performs galactosyl transferase activity, while MOATs are proposed to act as mannan acetyltransferases. The structures of hemicelluloses are adapted with modifications from (Pauly et al., 2013)

1.1.2.2.3 Mixed-linkage glucan

In higher plants, mixed-linkage glucans (MLGs) are found exclusively in the cell walls of species within the Poales order (Sørensen et al., 2008). These polymers are also present in

certain algal species (Popper et al., 2011), ancient plant lineages like liverworts (Popper and Fry, 2003), and the genus *Equisetum*, as well as in some bacteria and fungi (Oehme et al., 2019). In grasses, MLGs are notably abundant in young tissues such as coleoptiles (Carpita, 1996) and in the endosperm (Pauly et al., 2013), where they are rapidly degraded by licheninases during development (Pauly et al., 2013). This observation has led to the hypothesis that MLGs might serve as storage polysaccharides. Furthermore, some MLGs remain in the cell wall throughout the plant's life cycle, indicating a potential role as a structural polymer (Gibeaut et al., 2005). β -(1,3;1,4)-glucans are composed of unbranched β -(1,4)-linked glucans with β -(1,3)-glucosyl linkages interspersed (see Figure 4). Typically, cellotriosyl (DP3) and cellotetrasy (DP4) units are connected by β -(1,3) linkages, which can be specifically cleaved by lichenases. The ratio of these units (DP3:DP4) affects the physicochemical properties of β -(1,3;1,4)-glucans. The successful production of β -(1,3;1,4)-glucan in *A. thaliana* tissues was achieved by expressing rice CSLF6, a protein not naturally present in *A. thaliana* (Burton et al., 2006). Another group of proteins, the CSLH family members, are also involved in synthesizing this polymer (Doblin et al., 2009). Research into the membrane pore structure of CSLF6 has shed light on how β -(1,3;1,4)-glucan structures are formed (Jobling, 2015). Moreover, the observation that CSLF6 can target the plasma membrane suggests that β -(1,3;1,4)-glucan synthesis may occur in multiple cellular locations beyond the Golgi apparatus (Wilson et al., 2015). Despite these insights, many aspects of β -(1,3;1,4)-glucan synthesis remain to be fully understood.

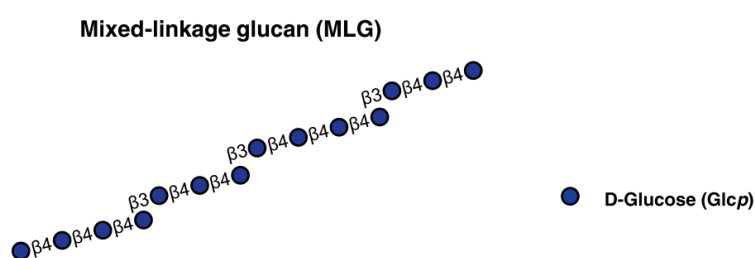


Figure 1-5. Schematic representation of hemicellulose mixed-linkage glucan.

Figure represents the structure of mixed-linkage glucan. Symbols representing various monosaccharides were adopted from the Nomenclature Committee of the Consortium for Functional Glycomics (Varki et al., 2009). Glycosidic linkages between monosaccharides are denoted by their anomeric configurations (α or β) and their position, for instance, β 4 indicates a β (1 \rightarrow 4) linkage. The structures of hemicelluloses are adapted with modifications from Pauly et al., 2013 (Pauly et al., 2013)

1.1.2.2.4 Xyloglucan

Xyloglucan (XyG) is a β -1,4 linked glucan that exhibits a diverse array of glycosyl and nonglycosyl substitutions (Pauly and Keegstra, 2016). The nature and sequence of these XyG substituents depend on factors like plant species, tissue type, cell category, and developmental stage (Obel et al., 2009; Schultink et al., 2014). To simplify the depiction of XyG's side chains, a nomenclature based on one-letter codes has been developed (Fry et al., 1993; Tuomivaara et al., 2015) (Figure 3 and 4). In this system, the letter 'G' signifies the unaltered glucosyl residue of the backbone. The primary substituent in XyG is an α -D-xylopyranose linked to the glucan backbone at *O*-6, represented by the letter 'X' when attached to a backbone glucosyl residue. Further modifications include D- and L-galactosyl, L-fucosyl, D-galacturonosyl, L-arabinopyranosyl, and/or L-arabinofuranosyl moieties at specific positions and linkages. This diversity has led to the identification of 24 unique structures, each designated by a one-letter code (Figure 1-6) (Pauly and Keegstra, 2016). Additionally, XyG can carry *O*-acetyl substituents, often overlooked because these moieties hydrolyze during XyG solubilization with alkali (York et al., 1986). The *O*-acetyl groups can reside either at the glucosyl backbone residue in place of a xylosyl residue (indicated by an underlined 'G') or at the sidechain galactosyl or arabinofuranosyl residue (underlined corresponding to the side-chain letter) (Figure 1-6). These acetyl groups may migrate among the free hydroxyl groups of a single glycosyl residue in aqueous solutions, resulting in varied locations (Kabel et al., 2003; Kamerling et al., 1987).

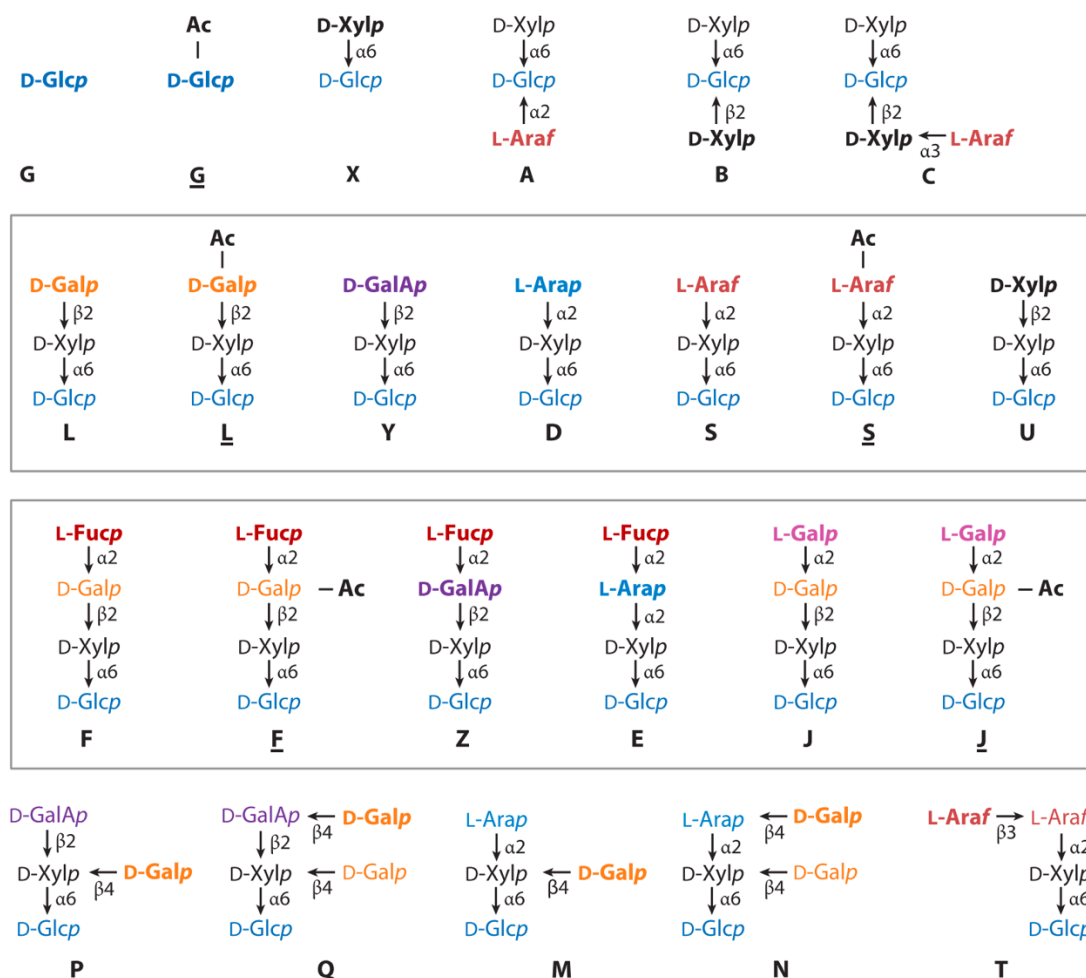


Figure 1-6. Xyloglucan (XyG) side-chain composition and diversity.

A one-letter code-based nomenclature has been established for all known XyG side chains (Fry et al., 1993; Tuomivaara et al., 2015). Notably, *O*-acetylated side chains are denoted by underlining. The depicted oligosaccharide structures, where the terminal glycosyl moiety is believed to be added by glycosyltransferases from the same Carbohydrate-Active Enzymes (CAZy) family, are highlighted within boxes (GT47 for L, L, Y, D, S, S, and U; GT37 for F, F, Z, E, J, and J). Additional abbreviations utilized include Ac for acetyl group; Ara for arabinose; Fuc for fucose; Gal for galactose; GalA for galacturonic acid; Glc for glucose; and Xyl for xylose. The figure has been reprinted from Pauly and Keegstra, 2016.

The availability of enzymes capable of hydrolyzing XyG from wall material has significantly aided the study of XyG structures. Non-specific endoglucanases (Bauer et al., 2006) or XyG-specific endoglucanases, specifically targeting the XyG glucan backbone at unsubstituted glucosyl residues containing substituted glucosyl residues in the aglycone (Pauly et al., 1999), are employed for this purpose. Solubilized oligosaccharides derived from this process can undergo analysis using mass spectrometry, HPLC, and NMR spectroscopy. These techniques help determine their identity and abundance, providing deeper insights into the structure and

substitution patterns of the polysaccharide (Lerouxel et al., 2002). Based on the structure of released XyG oligosaccharides, XyG polymers are generally categorized into two types. The first type, known as XXXG-type XyG, involves three out of four backbone glucosyl residues being xylosylated (Vincken et al., 1997) (Figure 4). This type often undergoes galactosylation and fucosylation, resulting in fucogalactoxyloglucan, commonly found in various tissues across most dicots (Zabackis et al., 1995). The second type of XyG exhibits reduced xylosylation, with only two out of four or more backbone glucosyl residues being xylosylated, forming the XXGGn-type XyG. This variant frequently contains *O*-acetyl substituents on the glucan backbone, leading to acetoxylloglucan, commonly present in numerous grass species (Carpita, 1996; Gibeaut et al., 2005). While most identified XyG structures align with these two classes, exceptions exist. For instance, seed storage XyG in *Hymenaea courbaril* displays a higher degree of backbone xylosylation, seen in XXXXG- or XXXXXG-type XyG (Dos Santos et al., 2004).

Numerous genes are essential in XyG (xyloglucan) biosynthesis, including glycosyltransferases (GTs) which add various glycosyl moieties, and glycosyl hydrolases (GHs) that are crucial for polymer maturation and integration into the extracellular matrix (Günl et al., 2011; Günl and Pauly, 2011; Sampedro et al., 2012; Zabolina et al., 2012). The xyloglucan backbone is synthesized by cellulose synthase-like C (CSLC) family members. A significant milestone in this field was the identification of CSLC4, a XyG synthase from GT family 2, in developing *Tropaeolum majus* (*Nasturtium*) seeds through transcriptomics (Cocuron et al., 2007). To verify whether CSLC4 encodes XyG:glucan synthase activity, researchers expressed the *Nasturtium* gene (*TmCSLC4*) and a homologous *A. thaliana* gene (*AtCSLC4*) in the methylotrophic yeast *Pichia pastoris*. This heterologous expression produced short β -1,4-linked glucan oligosaccharides in the soluble fraction of *Pichia* extracts, supporting the role of CSLC4 as a XyG:glucan synthase (Cocuron et al., 2007). Additionally in *A. thaliana* *cslc4* mutant and the quintuple mutant *cslc4 cslc5 cslc6 cslc8 cslc12* exhibit undetectable xyloglucan levels (Kim et al., 2020). The exact mechanism for the patterning of xylosyl substitutions is still unclear, but several XyG xylosyl transferases (XXTs) have been identified. *A. thaliana* contains seven genes in GT family 34, with five likely functioning as XXTs (Faik et al., 2002; Vuttipongchaikij et al., 2012). The transfer of radiolabeled xylose from UDP-xylose onto cellobiose acceptors has been detected for *AtXXT1*, *AtXXT2*, and *AtXXT4*. Analysis of single, double, and triple mutants of *AtXXT1*, *AtXXT2*, and *AtXXT5* in *A. thaliana* indicates that all three genes are involved in XyG biosynthesis (Cavalier et al., 2008; Zabolina

et al., 2012). Double *xxt1 xxt2* knockout mutants lacked detectable XyG in their walls and exhibited abnormal root hairs and slow growth compared to wild-type plants (Cavalier et al., 2008). The requirement of both *AtCSLC4* and *AtXXT2* for heterologous glucan synthase (GlcS) activity when expressed in *Pichia* indicates these proteins likely form a complex, as demonstrated by bimolecular fluorescence complementation and immuno-coprecipitation (Chou et al., 2012). The proposed XyG synthase complex consists of at least two glucan synthases, with their N and C termini closely colocalized, and includes two XXT2 proteins that interact via disulfide bonds, along with XXT5 and XXT1, which associate with the XXT2-XXT2 and CSLC4-CSLC4 homocomplexes (Chou et al., 2012). XXT2, XXT5, and XXT1 physically interact through their catalytic domains within the Golgi lumen (Chou et al., 2012). Furthermore, XXT1 and XXT2 are responsible for synthesizing XXGG-type XyGs, while XXT3, XXT4, and XXT5 together complete the synthesis of XXXG patterns (N. Zhang et al., 2023).

Discovered via a forward genetic screen for *A. thaliana* mutants with altered monosaccharide composition, MUR3 stands as a XyG galactosyltransferase within the GT family 47. Despite its identity as a XyG:galactosyltransferase, the *mur3* mutant was initially characterized by its deficiency in fucose due to the absence of galactose, a crucial component for XyG:fucosylation (Kong et al., 2015; Madson et al., 2003; Peña et al., 2012). In vitro activity assays conducted by heterologously expressing and purifying MUR3 established its role as a galactosyltransferase employing UDP-galactose to act specifically at the third xylose of the XXXG motif within the XyG polymer (Madson et al., 2003). Surprisingly, the *mur3-3* mutant retained substantial galactosylated XyG, indicating that MUR3 did not galactosylate the middle position of XyG oligosaccharides. Similarly housed within family GT47, XyG L-sidechain galactosyl transferase position 2 (XLT2), akin to MUR3, exhibited selectivity by adding galactosyl units specifically at the second position of XyG oligosaccharides and significantly upregulated during *Nasturtium* XyG seed filling (Jensen et al., 2012). This specificity was further evident in the *A. thaliana* insertional knockout mutant, which lacked XLXG and XLFG oligosaccharides but retained galactosylated XXFG (Jensen et al., 2012). The *A. thaliana mur3-1 xlt2* double mutant revealed XyG nearly devoid of galactosyl residues (Jensen et al., 2012). Heterologous expression of XyG beta-xylopyranosyltransferase from *vaccinium corymbosum* (*VcXBT*) in the *A. thaliana* double mutant *mur3 xlt2*, where xyloglucan consists only of an unsubstituted xylosylated glucan core structure, results in the production of the xylopyranose-containing “U” sidechain (Immelmann et al., 2023). The introduction of the

additional xylopyranosyl residue rescued the dwarfed phenotype of the *A. thaliana mur3 xlt2* mutant (Immelmann et al., 2023). Further XyG:galacturonosyltransferase (XUT1) responsible for introducing galacturonic acid residues onto XyG. The *xut1* mutant lacked galacturonosyl moieties on both xylose positions of XyG oligosaccharides. Notably, expression of *XUT1* under a ubiquitous promoter resulted in XyG galacturonosylation in various *A. thaliana* tissues on both positions of the XyG oligosaccharide (Peña et al., 2012). MUR3 and XLT2 display specificity in adding galactosyl units at distinct positions, while XUT1 exhibits broader activity. Interestingly, the removal of galacturonic acid residues from XyG in the *xut1* mutant led to shorter root hairs, with no significant impact on overall plant growth under the conditions tested (Peña et al., 2012).

The discovery of the XyG fucosyltransferase *FUT1* gene emerged through two distinct avenues. Initially, the protein was purified from pea, and subsequent analysis of partial peptide sequences led to the identification of the *FUT1* gene (Perrin et al., 1999). Simultaneously, the gene was also uncovered in a forward genetic screening aimed at mutants displaying altered cell wall monosaccharide content, earning it the alias *MUR2* (Vanzin et al., 2002). Apart from its primary role in fucosylating the galactosyl residue at the third position of the XXXG motif, MUR2 exhibits the ability to fucosylate galacturonic acid present at the first position of the motif (Peña et al., 2012). While acetyl substituents are present on the XyG backbone in certain plant species, in *A. thaliana*, acetyl groups have only been observed on the galactosyl residue at the third position of the XXXG motif (Kiefer et al., 1989; Maruyama et al., 1996; Sims et al., 1996; York et al., 1996). The ALTERED XYLOGLUCAN 4 (AXY4) and AXY4-like specifically mediate the addition of acetyl residues onto the galactosyl side chains of xyloglucans (Gille et al., 2011b). *Brachypodium* XyBAT1 adds acetyl residues onto the xyloglucan backbone, thereby modulating the xylosylation patterns on xyloglucans (L. Liu et al., 2016; Zhong et al., 2020b). Indeed, much more is known about the biosynthesis of xyloglucans compared to other hemicellulosic polymers.

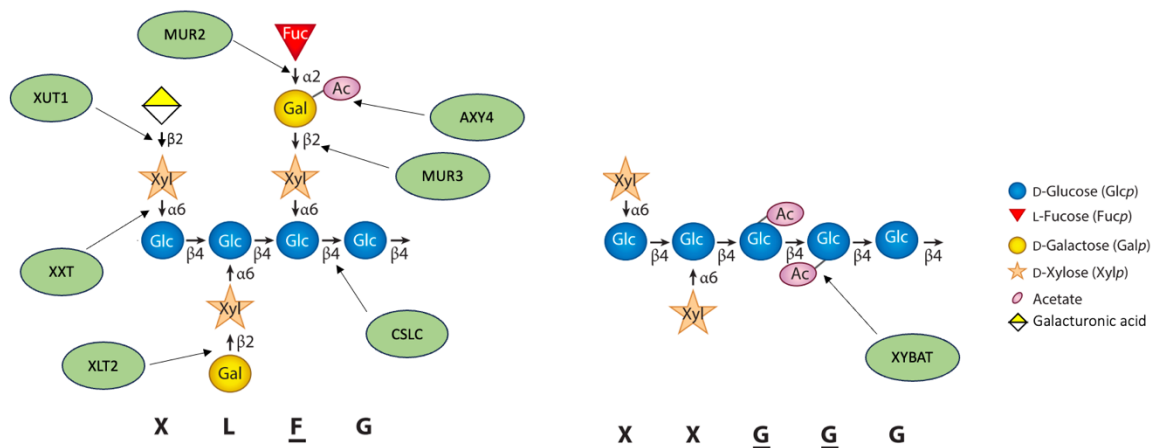


Figure 1-7. Schematic representation of hemicellulose xyloglucan and proteins involved in its biosynthesis.

Symbols representing various monosaccharides were adopted from the Nomenclature Committee of the Consortium for Functional Glycomics (Varki et al., 2009). Glycosidic linkages between monosaccharides are denoted by their anomeric configurations (α or β) and their position, for instance, β_4 indicates a $\beta(1\rightarrow4)$ linkage. If specific glycosyltransferases are known to add a sugar in a particular linkage, they are indicated by their protein abbreviations. The diagram displays the fully substituted XyG motif XLFG and XXGG alongside the known genes essential for its synthesis. CSLC and XXTs are involved in glucan backbone synthesis and xylosyl transfer, respectively. MUR3 and XLT2 enzymes facilitate galactose transfer to the third and second xylosyl units, respectively. XUT1 is responsible for galacturonosyl transfer to the first xylosyl unit. AXY4 functions as an acetyltransferase, acetylating the galactose residue in the third xylosyl unit and XYBAT functions as XyG backbone acetyltransferase. This representation illustrates linkages and their associated known genes from *A. thaliana*, but various other linkages have been reported in different species. The figure has been adapted and modified from (Pauly and Keegstra, 2016).

1.1.2.3 Pectin

Pectin, being the most structurally diverse polysaccharide group, encompasses a total of 12 identified monosaccharides, involving 67 distinct enzymatic activities for biosynthesis (Mohnen, 2008). Among the three major pectic polysaccharides—homogalacturonan (HG), rhamnogalacturonan I (RGI), and rhamnogalacturonan II (RGII)—there's a high likelihood of partial covalent linkage between them within the wall, as evidenced by enzymatic treatments with α -1,4-endo-polygalacturonase releasing these fractions (Figure 2) (Harholt et al., 2010). HG consists of an α -1,4 linked galacturonosyl residue backbone, often modified with methyl esters that neutralize the charged galacturonosyl-moiety. The formation of gels occurs via calcium bridges between free galacturonosyl residues. Control over the degree of methyl esterification, and consequently the ability of the polymer to form calcium bridges, is regulated

by apoplastic pectin methyl esterases and pectin methyl esterase inhibitors. This influences the strength of the pectin matrix (Anthon and Barrett, 2010; Jarvis, 1984; Saez-Aguayo et al., 2013). Modifications with xylosyl and apiosyl substituents result in xylogalacturonan (XG) and apio galacturonan, respectively (Harholt et al., 2010). RGI's backbone comprises alternating rhamnose and galacturonic acid residues. Rhamnosyl residues within the backbone are often substituted with galactose or arabinose, with potential branching, while galacturonosyl residues may undergo *O*-acetylation (Mohnen, 2008). RGII's backbone comprises α -1,4 linked galacturonic acid residues and complex sidechains containing various glycosyl units, including apiose, aceric acid, 3-deoxy-D-manno-oct-2-ulosonic acid (KDO), and 3-deoxy-D-lyxo-heptulosaric acid (DHA). These sidechains encompass rare monosaccharides alongside more common ones like galacturonic acid, rhamnose, galactose, and fucose (Figure 2) (Pérez et al., 2003). The multitude of monosaccharide constituents and diverse linkages in RGII make it the most structurally diverse polysaccharide identified to date (Pérez et al., 2003). Pectin can establish covalent bonds with hemicellulose, particularly xylan and xyloglucan, thereby reinforcing the strength of the cell wall matrix (Deng et al., 2013; Vukelić et al., 2024). Studies suggest that these covalent interactions, which may involve ester and ether linkages, play a crucial role in forming a complex network essential for maintaining the structural integrity of the cell wall (Broxterman and Schols, 2018). Notably, modifications to pectin through acetylation and methylation influence its ability to form covalent bonds with hemicellulosic components such as xylan, facilitating structural connections that are vital for cell wall stability (Broxterman and Schols, 2018).

HG is synthesized by galacturonosyl transferases (GAUTs) from the GT8 family (Amos et al., 2018; Atmodjo et al., 2013; Sterling et al., 2006). Unlike processive glycosyltransferases such as CESAs and CSLs, GAUT1 and GAUT7 work together in a heteromeric complex to initiate the formation of HG de novo. They begin with a slow phase and transition to a rapid phase once the intermediates reach a chain length of DP11, which is an unusual mechanism for synthesizing polysaccharide polymers (Amos et al., 2018; Atmodjo et al., 2011). Rhamnosyl transferases (RRTs), part of the newly identified GT106 family, transfer rhamnose residues to RG-I oligosaccharides (Takenaka et al., 2018). However, the specific enzyme for RG-I:galacturonosyl transfer has not yet been discovered. Additionally, many glycosyltransferases are involved in side-chain formation. For example, Xylogalacturonan deficient1 (XGD1) is essential for the xylosylation of xylogalacturonan (Jensen et al., 2008), while four

rhamnogalacturonan xylosyl transferases (RGXTs) add xylosyl residues to L-fucose in RG-II side chain A (Egelund et al., 2006; Liu et al., 2011). Two sialyl transferase-like proteins are believed to incorporate the rare sugars 2-keto-3-deoxy-D-lyxo-heptulosaric acid (Dha) and/or 2-keto-3-deoxy-D-manno-octulosonic acid (Kdo) into side chains C and D (Dumont et al., 2014). Galacturonosyltransferase-like5 (GATL5) is crucial for mucilage RG-I synthesis in *A. thaliana* (Kong et al., 2013). Galactan synthase1-3 (GALS1-3), from the GT92 family, acts as a galactosyl transferase for pectic galactan (Liwanag et al., 2012), while Arabinan deficient1 (ARAD1) and ARAD2 are responsible for synthesizing pectic arabinan (Harholt et al., 2012). Before HG is secreted into the apoplast, it undergoes methylation by methyltransferases like QUASIMODO2/TUMOROUS SHOOT DEVELOPMENT2 in the Golgi apparatus (Du et al., 2020). Pectin methyl-esterases (PMEs) then remove these methyl-ester groups from HG, with their activity being antagonistically regulated by PME inhibitors (Peaucelle et al., 2011). Polygalacturonases (PGs) and pectate lyases (PLs) further cleave HG (Ogawa et al., 2009; Xiao et al., 2014). These enzymes modify the physicochemical properties of pectin, thereby influencing cell wall structure and function, which is essential for plant growth and development.

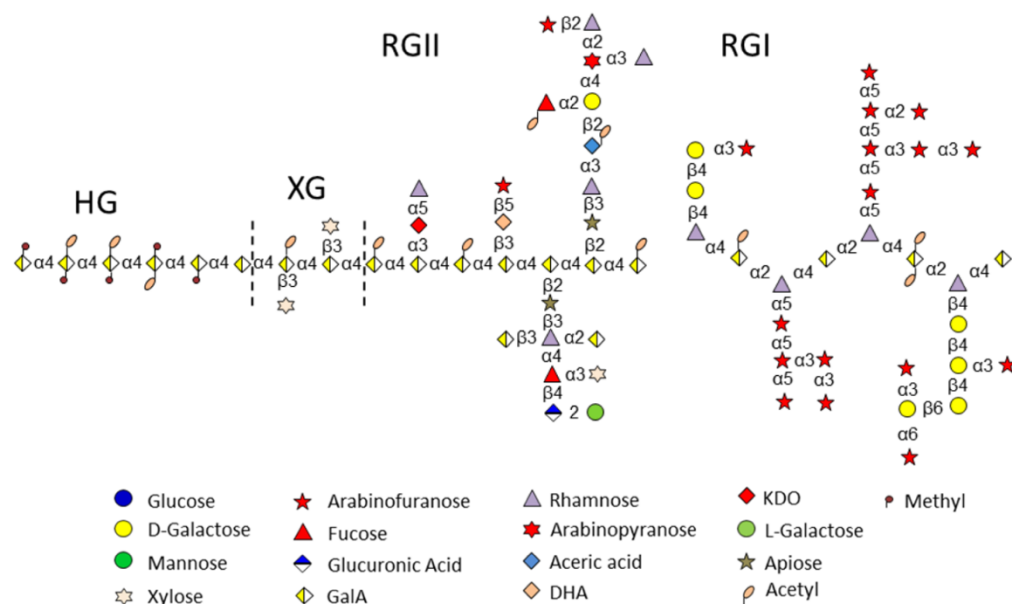


Figure 1-8. Pectin structures.

Representative structures of pectin [homogalacturonan (HG), Xylogalacturonan (XG), rhamnogalacturonan I (RGI), rhamnogalacturonan II (RGII)] are depicted. The text between the glycosyl moieties denotes the orientation of the glycosidic linkage (α or β) and the associated carbon

number related to the acceptor oxygen atom. It's important to note that the actual side-chain composition and arrangement can differ between polymers, plant tissues, and plant species. The dashed lines delimit XG structure. Pectin structures have been adapted from Harholt et al., 2010 and Mohnen 2008. Abbreviations: GalA – Galacturonic acid, DHA – deoxy-D-lyxo--2-heptulosaric acid, KDO – 3-deoxy-D-manno-2-octulosonic acid.

1.2 Lignin

Lignin is an amorphous polymer composed of aromatic monomers derived from phenylalanine (and tyrosine in grasses), making it a key component of cell walls in vascular plants (Barros et al., 2016; Vanholme et al., 2019). Although lignin lacks a regular structure, it strengthens cell walls and acts as a physical barrier against pathogens. Typically, lignin consists of guaiacyl (G), syringyl (S), and occasionally *p*-hydroxyphenyl (H) monomers, which are produced through complex phenylpropanoid metabolic pathways (Vanholme et al., 2019). At least 35 natural lignin monomers have been identified, highlighting the metabolic complexity involved in lignin biosynthesis. Phenylalanine ammonia lyases (PALs) convert phenylalanine into cinnamic acids, which are then processed by 4-Coumarate:CoA ligase (4CL), Cinnamoyl-CoA reductase (CCR), and Cinnamyl alcohol dehydrogenase (CAD) to produce CoA-thioester, aldehyde, and alcohol intermediates, respectively (Mottiar et al., 2016). These intermediates can undergo hydroxylation by cytochrome P450 enzymes such as Cinnamate 4-hydroxylase (C4H), *p*-Coumarate 3-hydroxylase (C3H), and Ferulate 5-hydroxylase (F5H). Further methylation at the 3-*O* and 5-*O* positions by *O*-methyltransferases, including Caffeoyl-CoA *O*-methyltransferase (CCoAOMT) and Caffeic acid *O*-methyltransferase (COMT), results in various lignin monomers (Vanholme et al., 2019). Additionally, Caffeoyl shikimate esterase (CSE) hydrolyzes caffeoyl shikimate to produce caffeic acid, representing a unique but non-essential reverse reaction in the monolignol pathway (Vanholme et al., 2013). The variety of substrates and the complex metabolic pathways contribute to the diverse composition of lignin monomers across different plant species and tissues. Recent research has revealed the role of scaffold proteins that may enhance enzyme activity by facilitating substrate channeling, potentially offering new ways to manipulate lignin content and properties (Gou et al., 2018). Lignin monomers are passively transported to the apoplast via unidentified transporters (Perkins et al., 2019; Vermaas et al., 2019), where they form hydrophobic polymers linked by ester/ether bonds. Lignification is further regulated by local oxidation systems activated by laccases/oxygen and peroxidases/hydrogen peroxide in lignifying cells (Lee et al., 2018, 2013; Lu et al., 2013; Tobimatsu and Schuetz, 2019). Ferulic acid (FA) residues can attach via ester

linkages to the α -1,3-arabinosyl residues of grass GAX (Glucurono arabinoxylan). Ferulated xylan then connects with monolignols, further extending lignin polymers through enzymatic radical coupling reactions (de Oliveira et al., 2015; Terrett and Dupree, 2019). This covalent cross-link of lignin to GAX forms a matrix network embedding cellulose microfibrils, enhancing the hydrophobicity and rigidity of the cell wall.

1.3 *O*-acetylation mechanism and its biological significance in plant cell wall

Considerable proportions of plant biomass, such as poplar wood (5%) and corn stover (4.5%), are comprised of acetyl esters, offering advantages in industrial applications by influencing viscosity and gelation (Chundawat et al., 2011; Huang et al., 2002; Johnson et al., 2017). However, *O*-acetylation of plant polymers can present challenges during processing, resulting in the release of bound acetate. This can acidify the medium and hinder microbial fermentation, particularly in applications like biofuel production (Helle et al., 2003; Selig et al., 2009). *O*-acetylation is predominantly found in the form of *O*-linked acetate in various wall polysaccharides, especially in matrix polysaccharides like pectin and hemicellulose. Notably, it is absent in cellulose, callose, mixed-linkage glucans, and structural glycoproteins (Gille and Pauly, 2012). However, the position and extent of acetylation can vary among plant species, tissue types, and developmental stages (Günl and Pauly, 2011). *O*-acetylation can occur on both the glucan backbone (e.g., XyG or heteromannans) and the side-chain sugar moieties of the polymer (e.g., XyG). The *O*-acetylation of the polymer backbone has a more pronounced effect on polymer features, such as conformation and hydrophobicity, than side chain modification. Additionally, several polymers can be mono- or di-*O*-acetylated, contributing to the structural diversity of plant cell wall components (Gille and Pauly, 2012).

Hemicelluloses, including xylan and xyloglucan, exhibit diverse acetylation patterns that influence their interactions with cellulose. The addition of acetyl groups increases the hydrophobicity of hemicellulose, improving its compatibility with the hydrophobic lignin present in plant cell walls (Berglund et al., 2020). This hydrophobic modification disrupts inter-fibrillar hydrogen bonding in cellulose, thereby enhancing hemicellulose binding to cellulose microfibrils (Park et al., 2014). Maintaining a balance between hydrophilic and hydrophobic properties is critical for cell wall integrity and the adhesion of its components (Winter et al.,

2017). The degree of acetylation (DA) of hemicellulose plays a crucial role in cellulose-hemicellulose binding. A well-regulated DA enhances flexibility and reduces hemicellulose crystallinity, facilitating better integration into the cellulose network. Studies indicate that increased binding of xyloglucan and xylan to cellulose can influence cellulose crystallization and packing (Park et al., 2014; Sánchez-Rodríguez et al., 2012). Notably, a uniform distribution of acetyl groups enables xylan to adopt a stable twofold helical screw conformation when interacting with cellulose, strengthening the stability of this association (Simmons et al., 2016; Tryfona et al., 2023). Hemicelluloses also act as coupling agents, bridging hydrophilic cellulose with the more hydrophobic lignin matrix, thereby improving overall cell wall stability (Winter et al., 2017). The spatial arrangement of acetyl groups affects both hemicellulose-cellulose binding strength and the enzymatic accessibility of the cell wall, which is particularly relevant for biofuel production efficiency (J. Liu et al., 2022). Research on acetylation patterns suggests that a uniform distribution of acetyl groups optimizes hemicellulose function within the cell wall. For instance, *A. thaliana* mutants with disrupted acetylation patterns displayed defects in hemicellulose-cellulose interactions, highlighting the essential role of precise acetylation in maintaining cell wall integrity (Busse-Wicher et al., 2014).

Multiple lines of evidence suggest that *O*-acetylation of wall polysaccharides occurs during polysaccharide biosynthesis in the Golgi lumen (Obel et al., 2009; Pauly and Scheller, 2000). All proteins implicated in this modification are predicted to be located in the Golgi membrane, with putative catalytic domains facing the Golgi lumen (Gille et al., 2011a; Schultink et al., 2015). It is noteworthy that the degree and pattern of polysaccharide *O*-acetylation can also be influenced by apoplastic plant *O*-acetyltransferases, likely acting post-deposition in the wall (de Souza et al., 2014; J. Y. Gou et al., 2012; Orfila et al., 2012; Zhang et al., 2017). The study of plant mutants affected in *O*-acetylation has been pivotal in unravelling the molecular mechanisms, revealing the involvement of three protein families: TRICHOME BIREFRINGENCE-LIKE (TBL) protein family, ALTERED XYLOGLUCAN 9 (AXY9), and REDUCED WALL *O*-ACETYLATION (RWA) protein family (Pauly and Ramírez, 2018).

The TBL protein family, consisting of 46 members in *A. thaliana*, plays a crucial role in the *O*-acetylation of specific wall polymers and is characterized by three distinct signatures (Bischoff et al., 2010). These signatures include an N-terminus transmembrane domain, along with two plant-specific domains: DUF231 and TBL. The DUF231 domain, marked by a conserved DxxH motif, while the TBL motif is defined by the presence of an esterase GDS

motif (Zhong et al., 2017). Mutagenic analysis of *AtXOAT1* revealed that these domains containing conserved GDS and DxxH motifs together form a putative catalytic triad comprising Ser216-His465-Asp462, positioned at the bottom of the active site cleft (Lunin et al., 2020). In this catalytic triad, the Ser residue in the GDS motif and the Asp and His residues in the DxxH motif are essential for catalytic activity (Lunin et al., 2020). The *axy4/tbl27* loss-of-function mutant in *A. thaliana* displayed a complete absence of *O*-acetyl substituents on the hemicellulose XyG, with no impact on the acetylation status of other wall polymers (Gille et al., 2011b). The paralogous gene *AXY4-like (AXY4L/TBL22)* performs the same function in seeds, underscoring its role as an XyG-specific acetyltransferase (Gille et al., 2011b). Another *A. thaliana* mutant, *tbl29/eskimo1*, exhibited a 46% reduction in xylan *O*-acetylation in the stem (Xiong et al., 2013). TBL29/ESKIMO1 was confirmed to catalyze the transfer of *O*-acetyl groups to β -(1 \rightarrow 4) xylooligosaccharides in vitro, substantiating its role as a xylan *O*-acetyltransferase (Urbanowicz et al., 2014). Essential residues for TBL29/ESK1 function include the Ser residue from the GDS motif and the Asp and His residues of the DxxH motif; mutations in these residues lead to a loss of enzyme activity (Zhong et al., 2017). To summarize, nine different TBLs in *A. thaliana* contribute to xylan 2-*O*-acetylation, 3-*O*-acetylation, and/or 2,3-di-*O*-acetylation (Zhong et al., 2017). In rice, 66 TBLs are implicated in *O*-acetylation, with *OsXOAT1-7* able to complement defects in xylan *O*-acetylation in the *A. thaliana* *tbl29/esk1* mutant (Zhong et al., 2018c). Among these 66 TBLs in rice, 14 TBLs exhibit xylan 2-*O*- and 3-*O*-acetylation (*OsXOAT1-14*) (Zhong et al., 2018c). In poplar, 64 different TBLs were identified, and 12 of them demonstrated xylan acetylation when expressed heterologously (Zhong et al., 2018c). Other TBL family members, such as *AtPMR5/AtTBL44*, *AtTBR*, and *AtTBL3*, are believed to be involved in pectin *O*-acetylation, and *AtTBL25/AtTBL26* are thought to be involved in mannan *O*-acetylation (Bischoff et al., 2010; Gille et al., 2011b; Vogel et al., 2004).

Similar to TBLs, a second family of protein involved in polysaccharide *O*-acetylation is *AXY9*, which also contains an N-terminus transmembrane domain and a C-terminus with GDS and DxxH domains facing the Golgi lumen (Schultink et al., 2015). The *A. thaliana* *axy9* mutant exhibits a significant reduction in total wall *O*-acetylation in stem and leaf tissues. In contrast to the polysaccharide substrate specificity of TBLs, *AXY9* appears to be non-specific in polysaccharide *O*-acetylation, as the corresponding *axy9* mutant plants show reduced *O*-acetylation in multiple hemicelluloses such as xyloglucan or xylan but not pectin (Schultink et al., 2015). Due to these characteristics, *AXY9* has been proposed to be involved in generating

an intermediate acetyl donor substrate later utilized by TBL proteins (Schultink et al., 2015). The presence of the GDS and DxxH domains suggests that AXY9 could also function as an *O*-acetyltransferase, although the enzymatic activity is yet to be determined.

RWA represents the third group of proteins involved in plant polysaccharide *O*-acetylation (Manabe et al., 2011). The *A. thaliana* genome contains four RWA proteins, and quadruple *rwa* mutants exhibit a 63% reduction in total wall *O*-acetylation. These proteins are required for *O*-acetylation of both pectic and non-pectic polysaccharides, including xyloglucan, xylan, and mannan (Manabe et al., 2013). In contrast to AXY9 and TBLs, which have a single transmembrane domain, RWA proteins are characterized by 10 predicted transmembrane domains (Manabe et al., 2011). The cytosolic pool of acetyl-CoA is likely the source for the *O*-acetylation of polysaccharides in plants, as it is used for alkaloids, anthocyanins, isoprenoids, or phenolics (Oliver et al., 2009). Genetic evidence shows that RNAi downregulation of *ATP-CITRATE LYASE (ACL)* expression leads to a significant reduction in the acetylation of xylan, glucomannan, xyloglucan, and pectin. This indicates that cytosolic acetyl-CoA, produced by ACL, acts as the acetyl donor for the acetylation of cell wall polysaccharides (Zhong et al., 2020b). Microsomal preparations isolated from potato cells and incubated with radiolabeled acetyl-CoA were able to incorporate and transfer radioactive acetate to proteins and cell wall polysaccharides, suggesting that acetyl-CoA serves as a donor substrate for the *O*-acetylation of wall polysaccharides (Pauly and Scheller, 2000). As acetyl-CoA cannot diffuse through the membrane and is not produced by the Golgi (Oliver et al., 2009), it has been proposed that RWA is responsible for the translocation of acetyl groups across the membrane to supply the substrate to other *O*-acetyltransferases (AXY9 and various TBLs). Although no experimental evidence has been reported yet, the existence of an intermediary acetyl donor is a likely option (Manabe et al., 2013, 2011; Schultink et al., 2015).

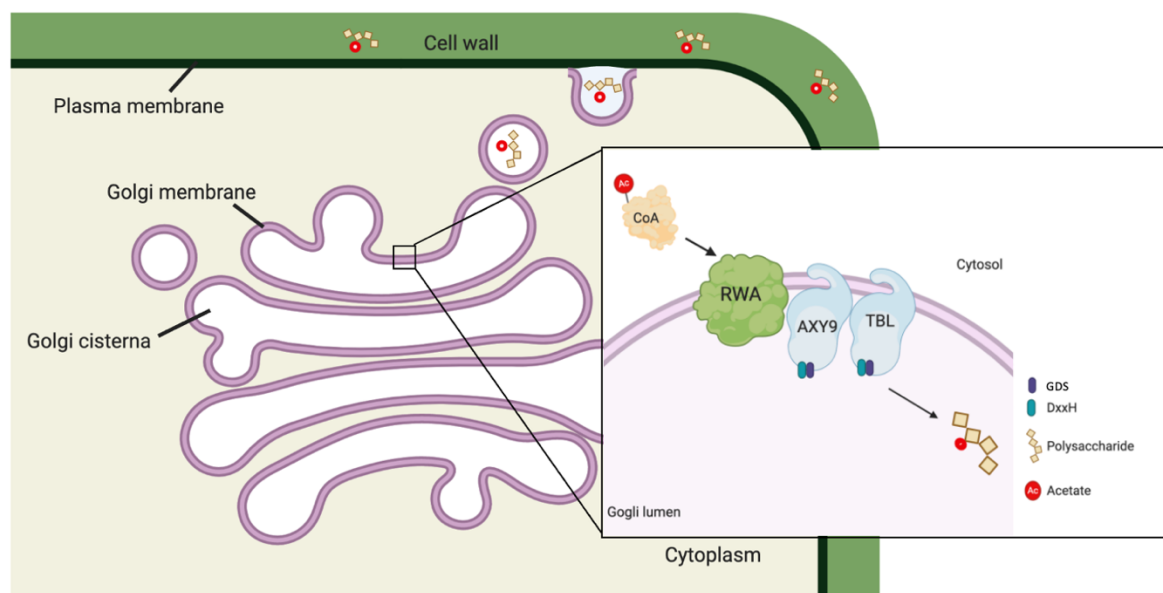


Figure 1-9. Model of the cell wall polysaccharide O-acetylation mechanism in plants.

RWA proteins are distinguished by possessing multiple transmembrane domains, suggesting their potential role in acetyl-moiety translocation. In contrast, *AXY9* and *TBL*s feature a single-transmembrane domain. *AXY9* is suggested to play a role in generating an intermediate acetyl donor substrate, subsequently utilized by *TBL* proteins. The presence of *GDS* and *DxxH* sequences is believed to be essential for enzymatic activity. This figure is adapted and modified from (Pauly and Ramírez, 2018).

1.4 Thesis objectives

Identifying genes essential for the *O*-acetylation of various wall polysaccharides has been largely advanced through mutant screening. However, deciphering the biological significance of this modification remains challenging due to the pleiotropic phenotypes exhibited by these mutants (Schultink et al., 2015). Notably, the loss of function of the *AXY9* gene significantly reduces *O*-acetylation in multiple wall polysaccharides, leading to severe developmental and stress-related defects (Schultink et al., 2015). Investigating this unique mutant is technically challenging because of its extreme growth defects and male sterility associated with the homozygous *axy9* mutation. To overcome these obstacles, a conditionally complemented *axy9* line, *pAXY*, was developed. This line utilizes an inducible promoter (*pER8::AXY9*) to control the expression of *AXY9*. The leaky expression of *AXY9* from the inducible promoter, even without the addition of the inducer, partially restored growth, and fertility. This resulted in a significant improvement in developmental defects, such as extreme dwarfism and male sterility, though wall acetylation levels remained lower than normal. Chapter 3 of this thesis

focuses on leveraging forward genetics to unravel the complex nature of cell wall acetylation and its impact on plant growth and stress responses. The specific goal is to identify novel genes involved in *pAXY* suppression through a forward genetic screen on *pAXY* EMS mutants and to uncover independent pathways that contribute to the growth recovery of the *pAXY* mutant.

Despite significant advances in identifying the molecular components involved in plant cell wall polymer synthesis, the cooperative functioning of these components in determining the length and decoration pattern of a polysaccharide remains largely unclear (Pauly et al., 2019). Synthetic biology offers a powerful approach to tackle these questions by enabling the reconstruction of entire biosynthetic machineries required for producing complete wall polysaccharides. Thus, Chapter 4 of this thesis aims to reconstruct the xyloglucan backbone *O*-acetylation pathway in *Yarrowia lipolytica*, a non-conventional yeast species. By rebuilding this machinery, it is possible to assess whether all essential factors have been identified by comparing the synthetic polysaccharide's structure to that found in native walls. Specifically, this project involves the heterologous expression and functional characterization of the *CSLC4*, *XXT2*, and *XyBAT1* genes, which are responsible for synthesizing the *O*-acetylated glucan backbone. This work not only enhances our understanding of plant cell wall biology but also explores the broader potential of *Y. lipolytica* as a versatile platform for synthetic biology and metabolic engineering.

2 Materials and methods

2.1 Materials

2.1.1 Plant lines

Generation	Label	Background	Species	Source
	Col-0/WT	Col-0	<i>A. thaliana</i>	Dr. Vicente Ramirez, HHU
	<i>axy9</i>	<i>axy9</i>	<i>A. thaliana</i>	Dr. Vicente Ramirez, HHU
	<i>pAXY</i>	<i>pAXY, axy9</i>	<i>A. thaliana</i>	Dr. Vicente Ramirez, HHU
M ₂	<i>pAXY EMS Pool 7</i>	<i>pAXY, axy9</i>	<i>A. thaliana</i>	Dr. Vicente Ramirez, HHU
M ₂	<i>pAXY EMS Pool 20</i>	<i>pAXY, axy9</i>	<i>A. thaliana</i>	Dr. Vicente Ramirez, HHU
M ₂	<i>pAXY EMS Pool 21</i>	<i>pAXY, axy9</i>	<i>A. thaliana</i>	Dr. Vicente Ramirez, HHU
M ₃	<i>saxy38</i>	<i>pAXY, axy9 (EMS Pool 7)</i>	<i>A. thaliana</i>	This work
M ₃	<i>saxy57</i>	<i>pAXY, axy9 (EMS Pool 21)</i>	<i>A. thaliana</i>	This work
M ₃	<i>saxy42</i>	<i>pAXY, axy9 (EMS Pool 7)</i>	<i>A. thaliana</i>	This work
M ₃	<i>saxy163</i>	<i>pAXY, axy9 (EMS Pool 20)</i>	<i>A. thaliana</i>	This work
M ₃	<i>saxy161</i>	<i>pAXY, axy9 (EMS Pool 20)</i>	<i>A. thaliana</i>	This work
BCF ₂	<i>pAXY*saxy38</i>	<i>pAXY, axy9</i>	<i>A. thaliana</i>	This work
BCF ₂	<i>pAXY*saxy57</i>	<i>pAXY, axy9</i>	<i>A. thaliana</i>	This work
BCF ₂	<i>pAXY*saxy42</i>	<i>pAXY, axy9</i>	<i>A. thaliana</i>	This work
BCF ₂	<i>pAXY*saxy163</i>	<i>pAXY, axy9</i>	<i>A. thaliana</i>	This work
BCF ₂	<i>pAXY*saxy161</i>	<i>pAXY, axy9</i>	<i>A. thaliana</i>	This work

M ₃	<i>saxy59</i> / <i>pAXY</i> <i>WD40-1</i>	<i>pAXY, axy9</i> (EMS Pool 21)	<i>A. thaliana</i>	This work
BCF ₂	<i>pAXY*saxy59</i>	<i>pAXY, axy9</i>	<i>A. thaliana</i>	This work
Ordered line	<i>SALK</i> <i>071771/WD40-2</i>	<i>at3g15610(WD40-2)</i>	<i>A. thaliana</i>	NASC repository
BCF ₄	<i>pAXY WD40-2</i>	<i>pAXY, axy9, at3g15610</i>	<i>A. thaliana</i>	This work
M ₃	<i>saxy85</i> / <i>pAXY</i> <i>phox3-1</i>	<i>pAXY, axy9</i> (EMS Pool 21)	<i>A. thaliana</i>	This work
BCF ₂	<i>pAXY*saxy85</i>	<i>pAXY, axy9</i>	<i>A. thaliana</i>	This work
Ordered line	<i>SAIL 1247</i> <i>D08/phox3-2</i>	<i>at5g20360 (phox3-2)</i>	<i>A. thaliana</i>	NASC repository
BCF ₃	<i>pAXY phox3-2</i>	<i>pAXY, axy9, phox3-2</i>	<i>A. thaliana</i>	This work
M ₃	<i>saxy171/pAXY</i> <i>atkh26-1</i>	<i>pAXY, axy9</i>	<i>A. thaliana</i>	This work
BCF ₂	<i>pAXY*saxy171</i>	<i>pAXY, axy9</i>	<i>A. thaliana</i>	This work
Ordered line	<i>SALK</i> <i>051182/atkh26-2</i>	<i>at5g46190 (atkh26-2)</i>	<i>A. thaliana</i>	NASC repository
BCF ₃	<i>pAXY atkh26-2</i>	<i>pAXY, axy9, atkh26-2</i>	<i>A. thaliana</i>	This work
	<i>Nicotiana WT</i>	<i>Nicotiana benthamiana</i>	<i>N. benthamiana</i>	HHU Greenhouse

Table 1. List of all plant lines used and/or created in this work

2.1.2 Microbial strains

Strain	Genotype/description	Source
<i>E. coli</i> DH5 α	<i>fhuA2</i> Δ (<i>argF-lacZ</i>)U169 <i>phoA glnV44</i> Φ 80 Δ (<i>lacZ</i>)M15 <i>gyrA96 recA1 relA1</i> <i>endA1 thi -1 hsdR17</i>	New England Biolabs
<i>E. coli</i> TOP10F'	<i>F -mcrA</i> Δ (<i>mrr-hsdRMS - mcrBC</i>) Φ 80LacZ Δ M15 Δ <i>LacX74 recA1 araD139</i> Δ (<i>araleu</i>) 7697 <i>galU galK rpsL (StrR)</i> <i>endA1 nupG</i>	Thermo Fisher Scientific
<i>Y. lipolytica</i> Po1d (called NG17)	<i>MatA, ura3 -302, leu2 -270, xpr2 -322</i>	(Barth and Gaillardin, 1997)
<i>Y. lipolytica</i> NG17+Cas9- <i>ylcas1</i>	<i>MatA, ura3 -302, leu2 -270, xpr2 -322 ,</i> <i>SpCa9, Δ yali0c00187</i>	Nina Boots, HHU
<i>Y. lipolytica</i> NG17+ pEYK <i>TmCSLC4</i> +pEYK <i>BdXyBAT1</i>	Derived from NG17 with pEYK inducible expression of <i>TmCSLC4</i> and <i>BdXyBAT1</i>	This work
<i>Y. lipolytica</i> NG17+Cas9- <i>ylcas1</i> + pEYK <i>TmCSLC4</i> +pEYK <i>BdXyBAT1</i>	Derived from NG17+Cas9- <i>ylcas1</i> with pEYK inducible expression of <i>TmCSLC4</i> and <i>BdXyBAT1</i>	This work
<i>Y. lipolytica</i> NG17+ pEYK <i>TmCSLC4</i>	Derived from NG17 with pEYK inducible expression of <i>TmCSLC4</i>	This work
<i>Y. lipolytica</i> NG17+ <i>Cas9-ylcas1</i> +pEYK <i>TmCSLC4</i>	Derived from NG17+Cas9- <i>ylcas1</i> with pEYK inducible expression of <i>TmCSLC4</i>	This work
<i>Y. lipolytica</i> NG17+ pEYK <i>TmCSLC4</i> +pEYK <i>TmXXT2</i> +pEYK <i>BdXyBAT1</i>	Derived from NG17 with pEYK inducible expression of <i>TmCSLC4</i> , <i>TmXXT2</i> and <i>BdXyBAT1</i>	This work
<i>Y. lipolytica</i> NG17+Cas9- <i>ylcas1</i> + pEYK <i>AtCSLC4</i> +pEYK <i>TmXXT2</i> +pEYK <i>BdXyBAT1</i>	Derived from NG17+Cas9- <i>ylcas1</i> with pEYK inducible expression of <i>TmCSLC4</i> , <i>TmXXT2</i> and <i>BdXyBAT1</i>	This work
<i>Y. lipolytica</i> NG17+ pEYK <i>TmCSLC4</i> +pEYK <i>TmXXT2</i>	Derived from NG17 with pEYK inducible expression of <i>TmCSLC4</i> and <i>TmXXT2</i>	This work
<i>Y. lipolytica</i> NG17+Cas9- <i>ylcas1</i> + pEYK <i>TmCSLC4</i> +pEYK <i>TmXXT2</i>	Derived from NG17+Cas9- <i>ylcas1</i> with pEYK inducible expression of <i>TmCSLC4</i> and <i>TmXXT2</i>	This work
<i>E. coli</i> + pCfB4780 pEYK <i>AkTBL25</i> + pEYK <i>AkCSLC3</i>	Derived from <i>E. coli</i> DH5 α + pCfB4780 construct cloned with <i>AkTBL25</i> and <i>AkCSLC3</i> along with pEYK promoter	Nina Boots, HHU
<i>E. coli</i> + pCfB4780 pEYK <i>TmCSLC4</i> + pEYK <i>TmXXT2</i>	Derived from <i>E. coli</i> DH5 α + pCfB4780 construct cloned with <i>TmCSLC4</i> and <i>TmXXT2</i> along with pEYK promoter	This work
<i>E. coli</i> + pCfB4780 pEYK <i>TmCSLC4</i>	Derived from <i>E. coli</i> DH5 α + pCfB4780 construct cloned with <i>TmCSLC4</i> along with pEYK promoter	This work

<i>E. coli</i> + pCfB4780 pEYK <i>TmXXT2</i>	Derived from <i>E. coli</i> DH5 α + pCfB4780 construct cloned with <i>TmXXT2</i> along with pEYK promoter	This work
<i>E. coli</i> + pCfB4780 pEYK <i>TmCSLC4</i> + pEYK <i>BdXyBAT1</i>	Derived from <i>E. coli</i> DH5 α + pCfB4780 construct cloned with <i>TmCSLC4</i> and <i>BdXyBAT1</i> along with pEYK promoter	This work
<i>E. coli</i> + pCfB4780 pEYK <i>TmCSLC4</i> + pEYK <i>TmXXT2</i> +pEYK <i>BdXyBAT1</i>	Derived from <i>E. coli</i> DH5 α + pCfB4780 construct cloned with <i>TmCSLC4</i> , <i>TmXXT2</i> and <i>BdXyBAT1</i> along with pEYK promoter	This work
<i>A. tumefaciens</i> strain GV3101	C58 rifr pMP90RK (disarmed Ti plasmid lacking tumor-inducing genes)	Dr. Vicente Ramirez, HHU
<i>A. tumefaciens</i> GV3101 + pB7FW2G p35S <i>WD40 GFP</i>	Derived from <i>A. tumefaciens</i> GV3101 transformed with pB7FW2G construct cloned with <i>WD40</i> gene with C terminal <i>GFP</i> tag under p35S promoter	This work

Table 2. List of microbial strains used and/or created in this work

2.1.3 Plasmids

Constructs	Antibiotic resistance	Source
<i>pBC47</i> +pAOX1 <i>TmCSLC4</i> +pAOX1 <i>TmXXT2</i>	Amp, Zeo	Dr. Balakumaran Chandrasekar, HHU
pCfB4780	Amp, Nat	Holkenbrink et al., 2018
pCfB4780+pEYK <i>AkTBL25</i> +pEYK <i>AkCSLA3</i>	Amp, Nat	Nina Boots
pCfB4780+pEYK <i>TmCSLC4</i> +pEYK <i>BdXyBAT1</i>	Amp, Nat	This work
pCfB4780+pEYK <i>TmCSLC4</i>	Amp, Nat	This work
pCfB4780+pEYK <i>TmCSLC4</i> +pEYK <i>TmXXT2</i>	Amp, Nat	This work
pJET1.2/Blunt	Amp	Thermo Fisher Scientific
pJET1.2+ <i>BdXyBAT1</i>	Amp	This work
pCfB4780+pEYK <i>BdXyBAT1</i> +pEYK <i>TmCSLC4</i> +pEYK <i>TmXXT2</i>	Amp, Nat	This work
pJS207+ <i>VP16</i>	Amp	Jonas Schön, HHU
pJS025+ <i>VP16</i>	Amp	Jonas Schön, HHU
pJS204+ <i>Egene</i>	Amp	Jonas Schön, HHU
pJET1.2+ <i>AtDAAR2</i>	Amp	This work
pJET1.2+ <i>AtSK11</i>	Amp	This work
pJET1.2+ <i>AtUBQ3</i>	Amp	This work
pJET1.2+ <i>AtWD40</i>	Amp	This work
pJS207+ <i>AtWD40</i> + <i>VP16</i>	Amp	This work
pJS207+ <i>AtDAAR2</i> + <i>VP16</i>	Amp	This work
pJS207+ <i>AtSK11</i> + <i>VP16</i>	Amp	This work
pJS025+ <i>VP16</i> + <i>AtWD40</i>	Amp	This work
pJS025+ <i>VP16</i> + <i>AtSK11</i>	Amp	This work
pJS204+ <i>Egene</i> + <i>AtWD40</i>	Amp	This work

pJS204+ <i>Egene</i> + <i>AtDAAR2</i>	Amp	This work
pJS204+ <i>Egene</i> + <i>AtSK11</i>	Amp	This work
pJS204+ <i>Egene</i> + <i>AtUBQ3</i>	Amp	This work
pDONOR207+ <i>AtWD40</i>	Amp	This work
pMDC107+p35S: <i>GFP</i>	Kan, Gen, Rif	Amancio de Souza, HHU
pDONOR207	Amp	Dr. Vicente Ramirez, HHU

Table 3. List of all plasmids used and/or created in this work

2.1.4 Primers

Name	Sequence 5'->3'	Application
axy9 WT F	TGGGTCAGACTTTTGCATTC	<i>axy9</i> genotyping
axy9 WT R	TTGAATCTTGTTTTGGGTTTCG	<i>axy9</i> genotyping
axy9 T-DNA	TGGTTCACGTAGTGGGCCATCG	<i>axy9</i> genotyping
pAXY WT F	GATGGTTCCTCATCGTTCATTGC	<i>pAXY</i> genotyping
pAXY WT R	CGTCTCCATTGAACTCACAACCATC	<i>pAXY</i> genotyping
pAXY T-DNA	TCGCCCTTCCCAACAGTTGC	<i>pAXY</i> genotyping
RN83 WT F	ATACCTGAGAGAAGGCGCATG	<i>wd40-2</i> genotyping
RN83 WT R	AAGACAAAGAAATAGCTTCCCG	<i>wd40-2</i> genotyping
Lbb1.3	ATTTTGCCGATTCGGAAC	<i>wd40-2</i> genotyping
RN104 85 20360SWTF	TGGCCAACAACATTTAGTTCC	<i>phox3-2</i> genotyping
RN104 85 20360SWTR	CAGCTCAGCAATTCCAAGAAG	<i>phox3-2</i> genotyping
RN104 85 20360SMu	GCCTTTTCAGAAATGGATAAATAGCCTTGCTTCC	<i>phox3-2</i> genotyping
tbl29 WT F	AATTTGCAAGCAAAGCATCAC	<i>tbl29</i> genotyping
tbl29 WT R	TGGGTTTTTGATAACGAGACG	<i>tbl29</i> genotyping
tbl29 tDNA	GCCTTTTCAGAAATGGATAAATA	<i>tbl29</i> genotyping
RN108 171 051182F	CAAAATTGGTCGTGTTATCGG	<i>atkh26-2</i> genotyping
RN108 171 051182R	AGAGAGGGCACATACCATGTG	<i>atkh26-2</i> genotyping (use lbb1.3 for tDNA)
pJET1.2 F	CGACTCACTATAGGGAGAGCGGC	pJET1.2 genotyping
pJET1.2 R	AAGAACATCGATTTTCCATGGCAG	pJET1.2 genotyping
RN157 pDon Gen F	CTGAGCCTTTCGTTTTATTTGATGCCT	PDONOR207 genotyping
RN157 pDON Gen R	AGCATCAGATGGTTTCTCTGCGG	PDONOR207 genotyping
RN156 pDONOR WD F	GGGGACAAGTTTGTACAAAAAAGCAGGCTTCGAAGG AGATAGAACCATGGATGGAGAAGAAGAAAGTCGCG AC	pDONOR207+ <i>WD40</i> genotyping
RN156 pDONOR WD R	GGGGACCACTTTGTACAAGAAAGCTGGGTCAGCATC AGATGGTTTCTCTGCGG	pDONOR207+ <i>WD40</i> genotyping
RN121 GAPDH qPCR F	ACCACTGTCCACTCTATCACTGC	qPCR for <i>GAPDH</i>

RN121 GAPDH qPCR R	TGAGGGATGGCAACACTTTCCC	qPCR for <i>GAPDH</i>
RN ACT F	TTTGTGGGAATGGAAGCTGC	qPCR for <i>ACTIN</i>
RN ACT R	ACCTGCCTCATCATACTCGG	qPCR for <i>ACTIN</i>
RN atkh26 RTF	GTGGGCAATACAAGTTATGG	qPCR for <i>AtKH26</i>
RN atkh26 RTR	TGGAACAAGTTCTCTGCGGT	qPCR for <i>AtKH26</i>
RN TRP RT F	AACCGATTGCCTGACACATG	qPCR for <i>PHOX3</i>
RN TPR RT R	AACTGGTCTGAAGGGATCCC	qPCR for <i>PHOX4</i>
RN WD40RT F	ATGGAGAAGAAGAAAGTCGC	qPCR for <i>WD40</i>
RN WD40RT R	TGCAGAAGCTGCACGTAAAG	qPCR for <i>WD40</i>
VR qPCR axy9F	ACGCCAAAGGAGCAAGAAGGAG	qPCR for <i>AXY9</i>
VR qPCR axy9R	AACCGGCATCCCAATCCAGAAC	qPCR for <i>AXY9</i>
AT2G38940 F	ATGGCTGGTGGTATTTTCGC	AT2G38940 SNP genotyping
AT2G38940 R	AGGTTGTAGCATTGGGTCCA	AT2G38940 SNP genotyping
AT3G15610 F	CAAGAACTCCACACAGCACC	SNP genotyping
AT3G15610 R	CATGTAACACTTCTCTTGAGGCA	SNP genotyping
AT4G16144 F	CTGAATTGTCCGCAGAACCC	SNP genotyping
AT4G16144 R	ACCGACATCTCAACCATCCT	SNP genotyping
AT4G04930F	ATTTGGTTTCCACTAGTCCGGAT	SNP genotyping
AT4G04930R	AGTTTTAATGTTTACTTCCTCAA	SNP genotyping
AT5G20360F	AAAACCAAAGTCAGATGTA	SNP genotyping
AT5G20360R	TACATTTAAATTTAATTGTA	SNP genotyping
AT4G36860F	GAATTACATGTTCTTG	SNP genotyping
AT4G36860R	ATGCAATCTCCCTATAATA	SNP genotyping
AT2G25710F	TGTGGTAATATACAATGGTA	SNP genotyping
AT2G25710R	TCGAACCAGACCTTTGAAA	SNP genotyping
AT5G46190F	CTCAGAACTATCTGAATAA	SNP genotyping
AT5G46190R	ATGGAGAAAATGCTGCAAAT	SNP genotyping
AT2G01008F	GTGTTGAGGGAGTCTGGG	SNP genotyping
AT2G01008R	ACCTCGCTCACACTCGG	SNP genotyping
AT2G07722F	ACAGCTTCAAGGTTAGGTC	SNP genotyping
AT2G07722R	AGAATTGCACGAAGTCCGAT	SNP genotyping
AT2G39620F	TATCTCTAAACAAAGAGATA	SNP genotyping
AT2G39620R	CTTGAGTCTGATGTTTATATAG	SNP genotyping
AT2G46250F	TGGAGAGAGAGTGTGAAGAA	SNP genotyping
AT2G46250R	GAACTGCTGCTGCTGCTGCA	SNP genotyping

AT3G48430F	TTTTCTCTTGTTACATGT	SNP genotyping
AT3G48430R	CAAGACAAAACACGTGCAAC	SNP genotyping
AT5G53330F	CAGGGTGTAGATCATGTAGT	SNP genotyping
AT5G53330R	AAATTTAGGAAGAACCATGG	SNP genotyping
AT4G15150F	AAAGCTCGACTTGTGCCTCA	SNP genotyping
AT4G15150R	TCACCGTAACTCGTAAGAAT	SNP genotyping
AT4G16770F	CCTATTATATTTTCATTTGGA	SNP genotyping
AT4G16770R	AATATATAGTCGGAATTCCA	SNP genotyping
AT4G36849F	TTGTAAGAGCTGCAATTGTAT	SNP genotyping
AT4G36849R	TAAATTCTTGATTGGAATCG	SNP genotyping
RN49F	TCCGTTGCTATATCCTCGCA	tPEX20 binding pCfB4780
RN83F	CTTACACATCTACTTGGGATATGAAGCTCCATTCTT GGTGAAG	<i>BdXyBAT1</i> Gibson
RN83R	AGGAATGCACGCGATGCGATGCGATGCGCTAGACGA GGATCAT	<i>BdXyBAT1</i> Gibson
RN53F	CACATCTACTTATGATTGAACGATGCCTTG	<i>TmXXT2</i> Gibson
RN53R	AAAGTAGATGCATCGGCGATCAGATGCATTCTTGGG CG	<i>TmXXT2</i> Gibson
RN50F	CACATCTACTTATGGCCCCTAACTCCGTTG	<i>TmCSLC4</i> Gibson
RN50R	ACAGAAGGAATGCACGCGATGGATTTAAGACATTTG TTCTCC	<i>TmCSLC4</i> Gibson
NG 54 XXT F	TAAGCCTGACCCTTCAAAGC	Genotyping <i>TmXXT2</i>
NG 54 XXT R	GTAACCAAGGGCCATCTGTG	Genotyping <i>TmXXT2</i>
NG53F	GAGGAGCATCCAAAGAGTCG	Genotyping <i>TmCSLC4</i>
NG53R	GGTGCAATCTCCTCCTGTTC	Genotyping <i>TmCSLC4</i>
RN78 int F	GGCCATCCTCATCCTCTTCA	Genotyping <i>BdXyBAT1</i>
RN78 int R	TTGCGCTGGGAGTAGTAGAG	Genotyping <i>BdXyBAT1</i>
E gene F	CGGATCGAATTGCGGCCGCGAATTCCCACCATGCCC CGC	Cloning for M2H
WD40 E gene R	TCTTCTCCATGCGGCTGTACGCGGACGC	Cloning for M2H
E gene wd40 F	GTACAGCCGCATGGAGAAGAAGAAAGTCG	Cloning for M2H
E gene WD40 R	GCTTGGGCTGCAGGTCGACTCTACACCTTCCGCTTTT TCTTGGGAGCATCAGATGGTTTC	Cloning for M2H
UBQ E gene F	GCGTCCGCGTACAGCCGCATGCAAATCT	Cloning for M2H
E gene UBQ F	GTACAGCCGCATGCAAATCTTCGTGAAAAC	Cloning for M2H
E gene UBQ R	CGTGGTGGAAGCTTCCCCAAGAAAAGCGGAAGGTG TAGAGTCGACCTGCAGCCCAAGC	Cloning for M2H
SK11 E gene F	CTGACGCCATGCGGCTGTACGCGGACGC	Cloning for M2H
E gene SK11 F	GTACAGCCGCATGGCGTCAGTGGGTATAG	Cloning for M2H

E gene SK11 R	GCTTGGGCTGCAGGTCGACTCTACACCTTCCGCTTTT TCTTGGGCAAACCGAGCCAAGGACAC	Cloning for M2H
DAAR2 E gene F	CATCACACATGCGGCTGTACGCGGACGC	Cloning for M2H
E gene DAAR2 F	GTACAGCCGCATGTGTGATGGAAAGAAAGAAAAA AC	Cloning for M2H
E gene DAAR2 R	GCTTGGGCTGCAGGTCGACTCTACACCTTCCGCTTTT TCTTGGGGACCAAGACATGGCC	Cloning for M2H
207 WD F	TTATTTCAAGTCCCGGATCGCCACCATGGAGAAGAA GAAAG	Cloning for M2H
207 WD R	GTACGCGCGGCAGCATCAGATGGTTTCTC	Cloning for M2H
207 VP16 wd40 F	ATCTGATGCTGCCGCGGTACGAAAAACAATTAC	Cloning for M2H
207 VP16 wd40 r	TCTTATCATGTCTGGATCGATGGGCTGCAGGTCGACT C	Cloning for M2H
207 UBQ F	TTATTTCAAGTCCCGGATCGCCACCATGCAAATCTTC G	Cloning for M2H
207 UBQ R	TACGCGCGGCGAAGCTTCCACCACGAAG	Cloning for M2H
207 VP16 UBQ F	TGGAAGCTTCGCCGCGGTACGAAAAAC	Cloning for M2H
207 VP16 UBQ r	TCTTATCATGTCTGGATCGATGGGCTGCAGGTCGACT C	Cloning for M2H
207 SK11 F	TTATTTCAAGTCCCGGATCGCCACCATGGCGTCAGTG GGTATAG	Cloning for M2H
207 SK11 R	GTACGCGGCCAAACCGAGCCAAGGACAC	Cloning for M2H
207 VP16 SK11 F	GCTCGGTTTGGCGCGGTACGAAAAACAATTAC	Cloning for M2H
207 VP16 SK11 r	GAGTCGACCTGCAGCCATCGATCCAGACATGATAA GA	Cloning for M2H

Table 4. List of primers**2.1.5 Cultivation media**

Name	Component	Concentration	Application
Liquid LB-Media	Yeast Extract Peptone NaCl	10.0 g/l 5.0 g/l 5.0 g/l	<i>E. coli</i> liquid culture
LB-Agar	Yeast Extract Peptone NaCl Bacto Agar	10.0 g/l 5.0 g/l 5.0 g/l 15.0 g/l	<i>E. coli</i> plate culture
Liquid YPD-Medium	Yeast Extract Peptone Glucose Monohydrate	10 g/l 20 g/l 20 g/l	<i>Y. lipolytica</i> liquid culture
YPD-Agar	Yeast Extract Peptone Glucose Monohydrate Bacto Agar	10 g/l 20 g/l 20 g/l 20 g/l	<i>Y. lipolytica</i> plate culture
Liquid YNB-Medium	Yeast Nitrogen Base (without amino acid) NH ₄ Cl Phosphate Buffer (pH 6.8) Glucose Monohydrate L-Leucine Uracil	1.7 g/l 5.3 g/l 0.05 M10 g/l 0.1 g/l 0.1 g/l	<i>Y. lipolytica</i> induction pre- culture

Liquid YNBE-Medium	Yeast Nitrogen Base (without amino acid) NH ₄ Cl Phosphate Buffer (pH 6.8) Erythritol L-Leucine Uracil	1.7 g/l 5.4 g/l 0.05 M 10 g/l 0.1 g/l	<i>Y. lipolytica</i> induction medium
--------------------	---	---	---------------------------------------

Table 5. List of cultivation media**2.1.6 Chemicals**

Name	Manufacturer	Application
2,5-Dihydroxybenzoic Acid	Sigma Aldrich	MALDI-matrix
2-Propanol	Fisher Chemical	Carbohydrate Analysis
Acetic Acid Glacial	VWR chemicals	Carbohydrate Analysis
Acetic Anhydride	Sigma Aldrich	Carbohydrate Analysis
Acetone	AppliChem	Carbohydrate Analysis
Agarose	Bio-Budget Technologies GmbH	Gel Electrophoresis
Amicon® Ultra-15 Centrifugal Filter Unit	Merck	HPAEC-Sample filtration
Ammoniumchloride	ROTH	Culture Media Preparation
Ammonium hydroxide	RVWR Chemicals	Carbohydrate Analysis
Ampicillin sodium salt	ROTH	Resistance Screening
Anthrone (ACS reagent, 97%)	Sigma Aldrich	Anthrone Assay
BD Bacto Agar	Thermo Fisher Scientific	Culture Plates
Carrier DNA of single- stranded DNA from Salmon testes	Sigma Aldrich	<i>Y. lipolytica</i> Transformation
Chloroform	Sigma Aldrich	Carbohydrate Analysis & RNA Extraction
D-Arabinose	Sigma Aldrich	HPAEC-Standard
D-Galacturonic acid	Sigma Aldrich	HPAEC-Standard
D-Galactose	Sigma Aldrich	HPAEC-Standard
D-Glucuronic acid	Sigma Aldrich	HPAEC-Standard
D-Glucosamine	Sigma Aldrich	HPAEC-Standard
D-Glucose	Sigma Aldrich	HPAEC-Standard
D-Mannose	Sigma Aldrich	HPAEC-Standard
D-Rhamnose	Sigma Aldrich	HPAEC-Standard
D-Ribose	Sigma Aldrich	Internal HPAEC-Standard
D-Xylose	Sigma Aldrich	HPAEC-Standard
Dextran (2.5 kDa)	ROTH	SEC-Standard
Dextran (5 kDa)	ROTH	SEC-Standard
Dextran (12.5 kDa)	ROTH	SEC-Standard
Dextran (25 kDa)	ROTH	SEC-Standard
Dichloromethane	Fisher Chemical	Carbohydrate Analysis
di-Potassium Hydrogen Phosphate 3-hydrate	Appllichem	Phosphate Buffer
Dithiothreitol	Sigma Aldrich	<i>Y. lipolytica</i> Transformation
DMSO	Fisher Chemical	Carbohydrate Analysis
DNA Gel Loading Dye (6X)	Thermo Fisher Scientific	Gel Electrophoresis
EDTA	AppliChem	TAE-buffer preparation

Ethanol	Sigma Aldrich	Carbohydrate Analysis & Disinfectant
Ethyl Acetate	Merck	Carbohydrate Analysis
FastDigest AsiSI	Thermo Fisher Scientific	Plasmid Digestion Buffer
FastDigest Buffer	Thermo Fisher Scientific	Plasmid Digestion Buffer
FastDigest NotI	Thermo Fisher Scientific	Plasmid Digestion Enzyme
FastDigest Sall	Thermo Fisher Scientific	Plasmid Digestion Enzyme
FastDigest XhoI	Thermo Fisher Scientific	Plasmid Digestion Enzyme
GelRed	GeneON	Gel Electrophoresis
GeneRuler 1 kb DNA Ladder	Thermo Fisher Scientific	Gel Electrophoresis
GeneRuler 1 kb Plus DNA Ladder	Thermo Fisher Scientific	Gel Electrophoresis
GeneRuler 100 bp DNA Ladder	Thermo Fisher Scientific	Gel Electrophoresis
Glucose monohydrate	Sigma Aldrich	Culture Media Preparation
HEPES	Roth	HEPES-buffer preparation
HyClone water	VWR	Water for Cloning purposes
Hydrochloric Acid	VWR Chemicals	Acetic Acid Assay
IC-vials with inserts	VWR	HPAEC-Injection
LB-Agar (Luria/Miller)	Roth	Culture Plates Preparation
LB-Medium (Luria/Miller)	Roth	Culture Media Preparation
Methanol	VWR	Carbohydrate Analysis
Methylene Chloride	Roth	Carbohydrate Analysis
meso-Erythritol, 99%	Thermo Fisher Scientific	YNBE-medium Preparation
Poly(ethylene glycol) 4000 BioUltra	Sigma Aldrich	<i>Y. lipolytica</i> Transformation
Potassium Phosphate monobasic	Sigma Aldrich	Phosphate Buffer Preparation
Sodium Hydroxide Solution	Sigma Aldrich	Carbohydrate Analysis, Acetic Acid Assay
L-Leucine	Sigma Aldrich	Culture Media Preparation
Nourseothricin	Jena Bioscience	Resistance Screening
Nuclease Free Water	Roth	RNA work
Nitric Acid	Roth	Cellulose Content Measurement
Phusion High Fidelity DNA Polymerase	Thermo Fisher Scientific	PCR
Pyridine	AppliChem	Carbohydrate Analysis
RedTaq DNA Polymerase	VWR	PCR
Sodium Bordeuteride	Sigma Aldrich	Carbohydrate Analysis
Sulfuric acid (95-98%, p.a.)	Sigma Aldrich	Anthrone Assay
Trifluoroacetic acid	Sigma Aldrich	Carbohydrate Hydrolysis
Tris-(hydroxymethyl) aminomethane	VWR	TAE-buffer preparation
Uracil	Sigma Aldrich	Culture Media Preparation
Bacto Yeast Extract	Thermo Fisher Scientific	Culture Media Preparation
Yeast Nitrogen Base without Amino Acids	Sigma Aldrich	Culture Media Preparation
Yeast Nitrogen Base without Amino Acids and Ammonium Sulfate	Sigma Aldrich	Culture Media Preparation
YPD Medium	Roth	Culture Media Preparation
Zymolyase, 2000 U	Zymo Research	AIR-Digestion

Table 6. List of chemicals

2.1.7 Kits

Name	Manufacturer	Application
Acetic Acid Assay Kit (ACS Manual Format)	Megazyme	Acetic Acid Assay
DNeasy Plant Mini Kit	Qiagen	Genomic DNA extraction from plants tissues
EasyCloneYALI – Integrative Vector Set	addgene	Source for <i>Y. lipolytica</i> plasmids
Gibson Assembly Cloning Kit	NEB	Gibson Cloning
iScript Reverse Transcription Supermix	BioRad	For cDNA synthesis from RNA
RNeasy Plant Mini Kit (Qiagen)	Qiagen	RNA extraction from plant tissues
Quick-DNA Fungal/Bacterial Mini prep kit	Zymo Research	Miniprep of plasmid DNA from <i>Y. lipolytica</i>
SsoAdvanced™ Universal SYBR® Green Supermix	BioRad	For qPCR
Turbo DNA-Free kit	ThermoFisher Scientific	For DNaseA treatment
Zymoclean DNA Clean & Concentrator Kit	Zymo Research	PCR-cleanup
Zymoclean Gel DNA Recovery Kit	Zymo Research	DNA-extraction from agarose gel
Zyppy Plasmid Miniprep Kit	Zymo Research	Miniprep of plasmid DNA from <i>E. coli</i>

Table 7. List of Kits

2.1.8 Equipment

Product	Manufacturer
1 mm μ Cuvette G1.0	Eppendorf
1.5 ml tubes	VWR
2 ml screw cap tubes	Sarstedt
2.0 ml tubes	VWR
3-Speed Mini-Centrifuge	neoLab
7890B GC System	Agilent Technologies
96 well plate	VWR
Agarose Gel Casters	Bio-Rad Laboratories
Agarose Gel Combs	Bio-Rad Laboratories
Autosampler+GC+MS	Agilent Technologies
Balance XSR204DR	Mettler Toledo
BioSpectrometer® basic 613500009	Eppendorf
Camera	Canon EOS 2000D SLR
CFX96 Real-Time PCR Detection System w/ C1000 Touch Thermal Cycler	Bio-Rad
C1000 Touch Thermal Cycler	Bio-Rad Laboratories
Centrifuge 5424 R	Eppendorf
Centrifuge 5427 R	Eppendorf
Centrifuge 5430 R	Eppendorf

Centrifuge 5810R	Eppendorf
ChemiDoc XRS+ Imaging System	Bio-Rad Laboratories
Clean bench SAFE 2020	Thermo Fisher Scientific
Combitips advanced 1.0 ml	Eppendorf
Combitips advanced 10.0 ml	Eppendorf
Combitips advanced 5.0 ml	Eppendorf
Combitips advanced 50.0 ml	Eppendorf
CryoPure tubes	Sarstedt
Culture Tubes	VWR
Cuvettes	Sarstedt
Dionex CarboPac Pa20 column	Thermo Fisher Scientific
Dri-Block DB200/3	Techne
Easypet 3, 1-Kanal	Eppendorf
Filter units with PES-membrane (0.2 µm pore, 250 mL volume, 50 mm membrane ø)	VWR
FiveEasy Plus pH meter FP20	Mettler Toledo
Giffy plant substrate	Giffy-7
Glass beads, acid washed, 0.1 mm	Sigma Aldrich
Grinding balls Glass beads, 3mm	VWR
Grinding balls stainless steel, 3mm	VWR
Heraeus Multifuge X3R Centrifuge	Thermo Fisher Scientific
HOBOWare	Onset computer corporation
Incubator Innova 42	New Brunswick Scientific
Injekt 10 ml	Braun
Injekt 20 ml	Braun
Injekt 5 ml	Braun
MALDI TARGET PLATE MTP 384 polished steel	Bruker Daltonik
MALDI-TOF system rapifleX	Bruker Daltonik
Metrohm 940 Professional IC Vario HPAEC-system	Metrohm
Metrohm 889 IC Sample Center	Metrohm
Micropore 1530 tape	VWR
Milli-Q System	Merck
Mini-Sub Cell GT Systems	Bio-Rad Laboratories
Minisart Syringe Filter 0.22 µm	Sartorius
Nalgene Rapid Flow	Thermo Fisher Scientific
NGC Fraction Collector	Bio-Rad Laboratories
NGC Scout 10 Chromatography System	Bio-Rad Laboratories
Nitril Gloves	VWR
PCR stripes	VWR
Petri dish, 92 x 16 mm	Sarstedt
Pipette Tips, 10 µl, transparent	Sarstedt

Pipette Tips, 1000, µl blue	Sarstedt
Pipette Tips, 2-200 µl, yellow	Sarstedt
Pipette Tips with filter, 10 µl, box	Sarstedt
Pipette Tips with filter, 1000 µl, box	Sarstedt
Pipette Tips with filter, 200 µl, box	Sarstedt
Schwingmühle (Mixer Mill) MM 400	Retsch
Multipette E3, 1-Kanal	Eppendorf
Multipette M4, 1-Kanal	Eppendorf
PowerPac Basic Power Supply	Bio-Rad Laboratories
Research plus, 1-Kanal, variable, 0.1 – 2.5 µl Pipette, dunkelgrau	Eppendorf
Research plus, 1-Kanal, variable, 0.5 – 10.0µl Pipette, mittelgrau	Eppendorf
Research plus, 1-Kanal, variable, 100.0 – 1000.0 µl Pipette, blau	Eppendorf
Research plus, 1-Kanal, variable, 2.0 – 20.0 µl Pipette, gelb	Eppendorf
Research plus, 1-Kanal, variable, 20.0 – 200.0 µl Pipette, gelb	Eppendorf
Sample Concentrator SBHCONC/1	Stuart
SC 950 vacuum pump	KNF
Serological Pipets 10 ml	Eppendorf
Serological Pipets 25 ml	Eppendorf
Serological Pipets 5 ml	Eppendorf
Serological Pipets 50 ml	Eppendorf
Single Use Inoculation Loops	VWR
Single Use Spatulas	VWR
SPECORD200 Plus spectrophotometer	Analytik Jena
SpectraMax Plus 384 Microplate Reader	Molecular Devices LLC
Superdex Peptide Column 10/300 GL	Cytiva
Syringe Filter (0.2 µm)	Sartorius
ThermoMixer 5350	Eppendorf
UV-Transparent Gel Trays	Bio-Rad Laboratories
Vacuubrand MZ 2C NT +2AK	Vacuubrand GmbH + Co KG
Vortex-Genie 2	Scientific Industries
Water Bath VWB6	VWR
Walk-in Plant chamber SON05-11	Regineering
Wide Mini Ready Sub-Cell GT Horizontal Electrophoresis System	Bio-Rad Laboratories

Table 8. List of equipment and hardware

2.1.9 Software/tools

Software	Developer
MSD Chemstation Classic Data Analysis (G1701FA)	Agilent Technologies
Benchling	Benchling Inc.
ChimeraX	RBVI, UCSF
flexAnalysis	Bruker Daltonics
flexControl	Bruker Daltonics
Galaxy	Galaxy Europe
Image Lab™ Software	Bio-Rad Laboratories
R studio	Posit, PBC
OMERO	CAi, HHU
GCMSD MassHunter Acquisition Software for GC/MS Systems	Agilent Technologies
Microsoft Office suite	Microsoft
Primer BLAST	NCBI
PubChem Drawer	NCBI

Table 9. List of software and tools

2.2 Methods

2.2.1 Media and growth conditions

2.2.1.1 Soil grown *Arabidopsis thaliana*

Seeds were stratified for 3 days at 4°C in a 0.1% plant agar solution (Roth) before being transferred to soil or Jiffy pellets (Jiffy-7 CatLog: 789005). The pots were placed in a Walk-in Plant chamber SON05-11 (regineering) set to 22°C with a light intensity of 8000 lux and a humidity level of 45% during the light period, and 19°C with a humidity level of 70% during the dark period, following a 16-hour light/8-hour dark cycle. After one-week, excess plants were removed to leave one plant per pot. Leaf tissues were harvested 21 days post-germination, and stem tissues were collected after 35 days. Plant height was measured using a 30 cm ruler. For the freezing tolerance assay, 4-week-old plants were exposed to -5°C for 18 hours, then returned to the plant chambers at 22°C, with data collected after 3 days.

2.2.1.2 Soil grown *Nicotiana benthamiana*

Nicotiana benthamiana plants utilized for transient gene expression were sourced as 3-week-old plants from the greenhouse of HHU Düsseldorf. These plants were kept under short-day conditions, consisting of 10-hour light periods and 14-hour dark periods, within a plant chamber set at 23°C. The light intensity during the day was maintained at 8000 lux, with a humidity level of 65%. During the dark periods, the temperature was adjusted to 18°C, and the humidity was increased to 90%.

2.2.1.3 Bacterial growth conditions

Bacterial liquid cultures of transformed *E. coli* NEB 5-alpha competent cells or One Shot® OmniMAX™ 2 T1 Phage-Resistant Cells (Catalog no. C8540-03) or TOP10' F calcium competent cells or *Agrobacterium tumefaciens* strain GV3101 were cultured in LB medium (Table 5) supplemented with an appropriate antibiotic (Table 2 and 3). The cultures were incubated at 37°C with constant agitation (225 rpm) in 14 mL tubes containing 5 mL of media. For solid LB media, 1.5% (w/v) agar was added to grow cultures in petri dishes.

2.2.1.4 *Yarrowia lipolytica* growth conditions

The *Y. lipolytica* strain Po1d was employed in this study. Originally obtained from (Barth and Gaillardin, 1997), a strain carrying a mutation in the *YICASI* gene was created and provided by Nina Boots. All strains were cultivated on Yeast Extract Peptone Dextrose (YPD) agar plates or in liquid medium (Table 5). For selection after transformation (2.2.2.13), the medium was supplemented with 250 µg/mL Nourseothricin (Nat) (Jena Bioscience, AB-102L). Colonies on plates were grown without shaking for 2 days at 30°C, while liquid cultures were grown in a rotating shaker at 225 rpm for two days, with the incubator set to 30 °C for both media.

For gene induction under the control of the *pEYK* promoter, 50 mL of Yeast Nitrogen Base (YNB) liquid medium (Table 5) were pipetted into sterile Erlenmeyer flasks and inoculated with sterile inoculation loops. Two loops of cell material from re-streaked colonies grown on YPD plates or glycerol stocks were used for inoculation. The flasks were mixed and placed for incubation at 30°C and 225 rpm for three days. Subsequently, the liquid cultures were

centrifuged for 2 min at 3000 rpm (Eppendorf, 5810R), the supernatant was discarded, and the cell pellet was resuspended in 50 mL of Yeast Nitrogen Base Erythritol (YNBE) liquid medium (Table 5), initiating gene induction. The tubes were incubated for one more day, then centrifuged for 2 min at 3000 rpm (Eppendorf, 5810R) to harvest the cell material, and the media were replaced with fresh YNBE. Similarly, the media were replaced for 2 more days, and after the third day, the cells were harvested by centrifuging the cultures at 4000 rpm for 10 mins for Alcohol Insoluble Residue (AIR) preparation (2.2.5.2).

2.2.2 Molecular biology methods

2.2.2.1 Plant nucleic acid extraction

2.2.2.1.1 DNA extraction from leaf tissues for genotyping

The DNA extraction method was adapted from Lunde, 2018. Leaf tissue (2 cm²) (Table 1) was collected in a 2 mL tube (Eppendorf), and 3 glass beads (3 mm) were added. The material was ground in a Retch-mill 2 times at 30 Hz for 30 sec. The ground tissue was then spun down, and 500 µL of extraction buffer (100mM Tris-HCl, pH 8.0; 50 mM EDTA; 100 mM NaCl; 0.35% w/v SDS) was added, followed by vortexing for 30 sec. Cold 5M potassium acetate (130 µL) was added, and the samples were mixed by inverting the tubes prior to centrifugation for 15 mins at 15,000 g. The supernatant (450 µL) was transferred to a new tube, and 350 µL of cold isopropanol was added and mixed by inverting. The samples were centrifuged for 10 mins at 16,000 g. The supernatant was discarded, and 750 µL of 70% v/v ethanol was added to the leftover pellet and centrifuged again for 5 mins at 16,000 g. The supernatant was discarded, and any remaining ethanol was removed using a pipette carefully. The pellet was dried and dissolved in 100 µL TE buffer (10mM Tris and 1mM EDTA with pH 8.0).

2.2.2.1.2 DNA extraction from leaf tissues for Whole Genome Sequencing

Leaf tissues of equal size (2 cm²) (Table 1) were pooled from 50 recovered suppressor BCF₂ plants of *A. thaliana*, and a similar pooling was performed for 50 *pAXY*-like dwarf BCF₂ plants. DNA extraction from these pools was conducted using the DNeasy Plant Mini Kit (Qiagen CatLog no: 69104) according to the manufacturer's protocol. The quality of the extracted DNA

was assessed through DNA fragment analysis (DNF-488) at BMFZ, HHU, with 20 ng of DNA sent for quality check. Upon passing the quality check, the samples were submitted for standard Illumina DNA library preparation and sequencing.

2.2.2.1.3 RNA extraction from stem tissues

Stem material from *A. thaliana* WT and mutant lines (Table 1) was extracted using the RNeasy Plant Mini Kit (Qiagen CatLog no: 74904). For each line, stem material from 5 individual plants was pooled and ground using liquid nitrogen, and the resulting powdered samples were stored at -60°C until further use for RNA extraction. The extraction protocol provided by the kit was followed, and the extracted RNA underwent DNase treatment using the TURBO DNA-free™ Kit (ThermoFisher Scientific CatLog no: AM1907) to eliminate any remaining DNA traces in the samples.

2.2.2.2 Genomic DNA extraction from *Y. lipolytica*

Genomic DNA was extracted from *Y. lipolytica* liquid cultures, which were incubated for two days, using the Quick-DNA™ Fungal/Bacterial Mini prep kit (Zymo Research CatLog no: D6005). The manufacturer's protocol was followed with a minor modification. Prior to starting the provided protocol, liquid cultures were centrifuged for 10 min at 4000 rpm (Eppendorf, 5810R), and the pellets were resuspended in 1 mL of HyClone water. The extracted genomic DNA was used as a template for PCR (2.2.2.7) to genotype the transgenic *Y. lipolytica* strains.

2.2.2.3 Plasmid DNA extraction

Plasmid DNA was extracted from *E. coli* liquid cultures (2.2.2.3) using the Zyppy™ Plasmid Miniprep Kit (Zymo Research CatLog no: D4019) following the manufacturer's protocol. Each centrifugation step was performed at 16000 x g (Eppendorf, 5430R). The DNA was eluted with 40 µL of elution buffer, and the concentration was measured afterward (2.2.2.6). In cases where plasmid preparation was conducted on *E. coli* strains not created during this thesis, the strains were re-streaked from glycerol stocks, grown on LB agar plates (Table 5), and single colonies were picked for liquid culture inoculation (2.2.1.3) before proceeding with plasmid DNA extraction.

2.2.2.4 Gel DNA extraction

After gel electrophoresis (2.2.2.7), the desired DNA fragments were identified by size and purified using the Zymoclean™ Gel DNA Recovery Kit (Zymo Research CatLog no: D4001) following the manufacturer's protocol. Gel slices were incubated for 10 minutes at 55°C in a thermomixer (Eppendorf, 5350), and all centrifugation steps were performed at 16000 x g (Eppendorf, 5418). For the final elution step, 10 µL of elution buffer was used. Subsequently, the DNA was cleaned and concentrated, and its concentration was determined.

2.2.2.5 DNA clean and concentration

If the purity or concentration of DNA samples was not sufficient, they underwent treatment with the Zymoclean™ DNA Clean & Concentrator Kit (Zymo Research CatLog no: D4003) following the manufacturer's protocol. All centrifugation steps were conducted at 16000 x g (Eppendorf, 5418), and the final elution was carried out with 12 µL of elution buffer. Subsequently, the concentration was re-measured.

2.2.2.6 DNA/RNA concentration measurement

To determine the DNA or RNA concentration following gDNA or plasmid DNA extraction (2.2.2.1 and 2.2.2.2), PCR (2.2.2.7), gel extraction (2.2.2.4), RNA extraction (2.2.2.1.3), and DNA clean-up (2.2.2.5), 1 µL per sample was measured using a 1 mm cuvette in a Bio photometer (Eppendorf, 6138000018). The elution buffer from the associated kits was used as a blank. The concentration was measured at 260 nm and calculated using the Beer-Lambert Law. The absorption ratio of 260/280 nm was determined to assess the DNA or RNA purity. A ratio close to 1.8 for DNA and close to 2.0 for RNA indicates acceptable purity. If a sample did not meet the purity criteria, the extraction process was repeated, or the sample was subjected to cleaning (2.2.2.5).

2.2.2.7 Genotyping PCR and Gel electrophoresis

Genotyping PCRs (see primer list in the Table 4) were performed using the VWR® Red Taq DNA Polymerase Master Mix (CatLog no: 733-1320) following the manufacturer's recommendations. PCR reactions were carried out in a total volume of 20 µL. DNA in TE

buffer was added to a volume of 1 μL (~ 150 ng/ μL), and primers were added to a final concentration of 0.1 μM each. Cycling conditions were adjusted based on primer melting temperatures and amplicon sizes. PCR products were visualized on a UV transilluminator after gel electrophoresis in 1% agarose gels in TAE buffer (40 mM Tris, 20 mM acetic acid, and 1 mM EDTA) containing GelRedTM Nucleic acid stain (10000X in water) (CatLog no: 2G120-BC-0.5ML). Gel electrophoresis was run at 100V for 40 mins in TAE buffer.

2.2.2.8 Transcriptional analysis using qRT-PCR

RNA extraction from *A. thaliana* stem material was carried out using the Plant RNeasy kit from Qiagen according to the manufacturer's instructions (2.2.2.1.3). Subsequently, cDNA was synthesized from this RNA using the GoScriptTM Reverse Transcriptase Mix (Promega CatLog no: A2791). The qRT-PCR reaction was conducted using SsoAdvancedTM Universal SYBR[®] Green Supermix (BioRad CatLog no: 1725271) on the Bio-Rad CFX96 C1000 Touch Thermal Cycler Real-Time PCR System for thermocycling and fluorescence detection. The thermal cycling program comprised an initial denaturation step at 95°C for 3 minutes, followed by 40 cycles of 95°C for 30 seconds and 60°C for 60 seconds. A melting curve analysis was performed after amplification to confirm the specificity of the products. The Ct values were determined using the CFX manager software (version: 3.1.1517.0823) and used to calculate the relative abundance of the transcripts by normalizing to an internal control (transcript abundance of the actin gene AT3G18780). Primer sequences can be found in Table 4.

2.2.2.9 DNA amplification for cloning

To generate DNA amplification fragments for cloning purposes, Phusion High-Fidelity DNA Polymerase (ThermoFisher Scientific CatLog no: F530S) was used. This enzyme possesses proofreading capabilities, enhancing the fidelity of the amplified sequences. PCR optimization was conducted according to the manufacturer's recommendations (refer to primer list Table 4). Templates for these reactions comprised cDNA, genomic DNA, or plasmids.

2.2.2.10 Plasmid linearisation

For the preparation of EasyCloneYALI vectors for cloning, they were linearized/open using the FastDigest (FD) SfaAI/AsiSI enzyme (Thermo Fisher Scientific CatLog no: FD2094). Approximately 1000 ng of the desired EasyCloneYALI vector was mixed with 2 μ L of FD Green Buffer (Thermo Fisher Scientific, B72) and 1 μ L of FD SfaAI enzyme, then filled up to 20 μ L with HyClone water. The incubation was carried out at 37 °C for 60 minutes and stopped by a temperature increase to 80 °C for 5 to 10 minutes using a thermocycler. Subsequently, gel electrophoresis (2.2.2.7), gel extraction (2.2.2.4), and concentration measurement (2.2.2.6) were performed, and the DNA was stored at -20 °C.

To prepare assembled plasmids for *Y. lipolytica* transformation (2.2.2.14), they were linearized using the FD NotI enzyme (Thermo Fisher Scientific CatLog no: FD0593). Approximately 3000 ng of the desired plasmid DNA was mixed with 5.0 μ L of FD buffer (Thermo Fisher Scientific CatLog no: B64) and 0.6 μ L of FD enzyme, then filled up to 50 μ L with HyClone water. The incubation was carried out at 37 °C for 120 minutes and stopped by a temperature increase to 80 °C for 5 to 10 minutes using a thermocycler. Subsequently, gel electrophoresis (2.2.2.7), DNA clean-up (2.2.2.5), and concentration measurement (2.2.2.6) were performed, and the DNA was stored at -20 °C.

2.2.2.11 Cloning methods

Plasmid construction involved several cloning methods, sometimes used in combination, including Gibson Assembly, Gateway, and Blunt-End cloning. Intermediate and final constructs were validated through PCR and Sanger Sequencing.

2.2.2.11.1 Gibson Assembly

Gibson assembly served as one of the cloning strategies, conducted using the Gibson Assembly Cloning Kit (NEB CatLog no: E5510S) following the manufacturer's protocol with slight modifications. All the constructs used for *Y. lipolytica* transformations were created using this method. The total reaction volume was reduced to 10 μ L, leading to a corresponding halving of the volume of Gibson Assembly Master Mix (2x). Fragments totaling 0.01 to 0.25 pmol, including approximately 100 ng of vector and a twofold molar excess of each gene of interest (GOI) fragment, were employed. Calculations were facilitated using the NEBioCalculator®

(<https://nebiocalculator.neb.com/#!/dsdnaamt>). Reactions proceeded at 50 °C for 120 minutes, after which 5 µL of the reaction mixture was directly used for *E. coli* transformation (2.2.2.13) employing the NEB 5-alpha Competent *E. coli* cells. The remaining mixture was incubated overnight and stored at -20 °C, utilizing a thermocycler for incubation. Prior to assembly, the vector backbone fragment was obtained via plasmid linearization (2.2.2.10), while the promoters, genes, or the promoter-gene-terminator cassette were acquired through PCR amplification (2.2.2.9). The final constructs were validated by PCR, Sanger sequencing (2.2.2.12.3) of the insert or Whole plasmid sequencing (2.2.2.12.2). (Gibson et al., 2009)

2.2.2.11.2 Gateway Cloning

Gateway Cloning (Invitrogen CatLog no: 11789020 and 11791020) was initiated by amplifying the gene of interest with attB sites incorporated at the 5' end of the gene-specific primers. Following DNA gel electrophoresis, the PCR product was extracted from the gel. The purified product was then used in a BP reaction with 100 ng of the pDONR207 plasmid and transformed into TopTen Oneshot chemically competent *E. coli* cells (Invitrogen) according to the manufacturer's protocol. After selecting the correct entry plasmids, they were confirmed by PCR and Sanger sequencing. Subsequently, the desired gene fragment(s) were moved into the appropriate destination vector, in this case pB7FW2G, via an LR reaction. The resulting constructs were transformed into TopTen Oneshot chemically competent *E. coli* cells (Invitrogen) as per the manufacturer's protocol. The final constructs were validated by PCR, Sanger sequencing (2.2.2.12.3) of the insert or Whole plasmid sequencing (2.2.2.12.2).

2.2.2.11.3 Blunt-End cloning

The construction of several constructs was facilitated by the CloneJET™ PCR Cloning Kit (ThermoFisher Scientific CatLog no: K123120), which employs the pJET1.2/blunt cloning vector to assist in the cloning of genes or gene fragments. Initially, the desired DNA sequence was amplified by PCR using Phusion DNA Polymerase (ThermoFisher Scientific CatLog no: F530S), resulting in a blunt-end PCR product. Following purification, the resulting product was directly used for the blunt-end cloning reaction with the pJET1.2/blunt vector, following the protocol recommended by the manufacturer. Subsequently, the constructs were transformed into chemically competent TopTen *E. coli* cells and the final constructs were

validated by PCR, Sanger sequencing (2.2.2.12.3) of the insert or Whole plasmid sequencing (2.2.2.12.2).

2.2.2.12 Sequencing methods

2.2.2.12.1 Sample prep from BSA and Whole Genome Sequencing of *A. thaliana*

Genomic DNA of high purity, extracted from *A. thaliana* (2.2.2.1.2), totaling 2 µg, was submitted for Whole Genome Sequencing. For *saxy59* and *saxy42*, leaf samples of equal size were pooled from 50 (recovered) suppressor BCF₂ plants, and a similar pooling approach was applied for 50 *pAXY*-like (dwarf) BCF₂ plants. The DNA samples were analyzed for quality using DNA fragment analysis (method: DNF488) by BMFZ, HHU. Subsequently, DNA extraction was performed from the pooled leaf material for both tall and dwarf pools. The extracted DNA samples were then sent to Genewiz Germany GmbH, where standard Illumina DNA library preparation procedures were employed for all samples. The samples underwent sequencing on Illumina Novaseq platforms with a sequencing depth of 20 million reads and paired end read length of 150bp, resulting in approximately 50 times coverage of the *A. thaliana* genome. Similarly, for *saxy38*, *saxy85*, *saxy171*, and *saxy161*, leaf samples were prepared in a similar manner, with 30 BCF₂ plants utilized per pool. The DNA samples were analyzed for quality using DNA fragment analysis (method: DNF488) by BMFZ, HHU. Subsequent library preparation and sequencing of these samples were conducted by Eurofins Genomics using Illumina Next Generation Sequencing technology, yielding a sequencing depth of 30 million reads and paired end read length of 150bp, providing approximately 30 times coverage of the *A. thaliana* genome.

2.2.2.12.2 Whole plasmid sequencing

Whole plasmid sequencing, leveraging third generation NGS technology, offers a robust and precise method for comprehensive plasmid characterization and analysis. The plasmids used for mammalian 2 hybrid assay were sequenced using this method. Its versatility extends to various applications, including plasmid verification and resequencing, even in the absence of a reference sequence. To initiate this process, 30 ng/µL of plasmid DNA was prepared in a final volume of 20 µL and submitted to Eurofins Genomics for sequencing services. Upon completion, sequencing results were downloaded from their website. Subsequently, alignment

to an in silico generated DNA template was conducted using either the MAFFT or Clustal Omega alignment feature within the Benchling platform (<https://www.benchling.com>) for validation.

2.2.2.12.3 Sanger sequencing

Sanger sequencing, conducted by Eurofins Genomics, was employed to determine the unknown sequences of DNA fragments. For this purpose, 5 μL of purified DNA fragment was utilized, with concentrations of 100 $\text{ng}/\mu\text{L}$ for plasmid DNA, 25 $\text{ng}/\mu\text{L}$ for DNA fragments >1000 bp, 12 $\text{ng}/\mu\text{L}$ for DNA fragments ranging from 300 to 1000 bp, and 2 $\text{ng}/\mu\text{L}$ for DNA fragments spanning 150 to 300 bp. This DNA template was mixed with 5 μL of a 5 μM primer specific to the desired sequence within a 1.5 mL tube. Upon completion, sequencing results were retrieved from their website. Subsequently, alignment to an in silico generated DNA template was conducted using either the MAFFT or Clustal Omega alignment feature within the Benchling platform.

2.2.2.13 Transformation of *E. coli*

Plasmid DNA insertion into calcium competent *E. coli* TOP10F' cells (2.4.2) or NEB 5-alpha Competent *E. coli* cells or TopTen Oneshot chemically competent *E. coli* cells was accomplished through heat shock transformation. Frozen aliquots of 50 μL *E. coli* competent cells were thawed from -60 $^{\circ}\text{C}$ by placing on ice. Then, 5 μL of the ligation reaction (2.2.2.11) or 1 μL of plasmid DNA [10 $\text{ng}/\mu\text{L}$] was added to the cells and gently mixed by tapping. The remaining ligation samples were stored at -20 $^{\circ}\text{C}$. The mixture was incubated for 30 min on ice, then transferred into a 42 $^{\circ}\text{C}$ water bath (VWR CatLog no: VWB6) for exactly 30 sec and quickly returned to ice for 2 min. Throughout the incubation steps, the cells were kept as undisturbed as possible. Next, 500 μL of LB medium for *E. coli* TOP10F' cells or 950 μL of SOC outgrowth medium (NEB CatLog no: B9020S) for NEB 5-alpha Competent *E. coli* cells and TopTen Oneshot chemically competent *E. coli* cells were added to each tube. The tubes were then horizontally incubated at 37°C and 225 rpm for 60 min. After one hour of incubation, 100 μL of each transformation mixture was plated on LB agar plates (Table 5), supplemented with the appropriate antibiotic (Table 2 and 3), using spatulas. The plates were subsequently incubated at 37°C overnight.

2.2.2.14 Preparation of *Y. lipolytica* competent cells and transformation

The transformation protocol utilized in this study was adapted from the method described by Holkenbrink et al. (2018). To obtain sufficient cells for the procedure, two loops of cell material from a plate were resuspended in 200 μL of sterile HyClone water within 1.5 mL tubes (Sarstedt, CatLog no: 72.690.301), plated on a YPD agar plate without antibiotics, and then incubated at 30 °C without shaking for one day. Following incubation, the cells were harvested from the plate using a sterile pipette tip, resuspended in 1 to 2 mL of sterile HyClone water inside a 2 mL tube (Sarstedt CatLog no: 72.691), with one tube prepared per strain. Tubes were centrifuged for 2 min at 3000 x g (Eppendorf, 5430R), the supernatant discarded, and the pellet resuspended in 1 mL HyClone water by briefly vortexing. This washing step was repeated once, and the optical density at 600 nm (OD₆₀₀) was determined by diluting 10 μL of cell resuspension in 990 μL of HyClone water inside cuvettes (Sarstedt, CatLog no: 67.742), with 1 mL of HyClone water used as a blank. The OD₆₀₀ measurement was conducted using a Biospectrometer basic photometer (Eppendorf, 6135000009). An OD₆₀₀ of 9.2 equates to 5×10^7 *Y. lipolytica* cells, which are required for one transformation reaction. The volume of each cell resuspension needed for the transformation was calculated and aliquoted into 1.5 mL tubes, with one tube per strain to be created. The tubes were centrifuged for 2 min at 3000 x g, and the supernatant was discarded.

For the transformation process, 500 ng of NotI-digested (2.2.2.10) vector was added to the cell pellet, and the pellet was resuspended in 100 μL of the following transformation mix by gently flicking. The transformation mix comprised 82.5 μL 50 % Polyethylene glycol (PEG) 4000, BioUltra (Sigma Aldrich CatLog no: 95904-250G-F), 5.0 μL 2.0 M Lithium acetate (LiAc) (Sigma Aldrich CatLog no: 213195), 2.5 μL 10 mg/mL carrier DNA of single-stranded DNA (ssDNA) from salmon testes (Sigma Aldrich CatLog no: D7656-1ML), and 10.0 μL 1.0 M Dithiothreitol (DTT) (Sigma Aldrich CatLog no: 43816). Subsequently, the mixture was incubated at 39 °C for 60 min in a water bath, followed by centrifugation for 2 min at 3000 x g (Eppendorf, 5430R), discarding the supernatant, and resuspending the pellet in 500 μL of YPD medium. The mixture was then incubated at 30 °C and 225 rpm for 2 hours. After incubation, 250 to 500 μL were plated on YPD plates containing 250 $\mu\text{g}/\text{mL}$ Nat, and the plates were incubated at 30 °C without shaking for two days. Following incubation, the colonies were genotyped directly, or the plates were stored at 4 °C.

2.2.2.15 Transformation of *Agrobacterium tumefaciens*

Retrieve the GV3101 competent cells from the -60°C freezer. To the thawed tube, add 1 µg of the desired plasmid DNA and gently mix by tapping. Rapidly freeze the tubes in liquid nitrogen for 2 minutes. Thaw the tubes for 5 minutes at 37°C, then add 1 mL of LB media and incubate for 2 hours at 28°C with constant shaking at 225 rpm. Centrifuge the tubes for 5 minutes at 6000 rpm (Eppendorf, 5430R), discard the supernatant, and carefully resuspend the pellet in 100 µL of LB. Plate the suspension on an LB agar media plate containing the appropriate antibiotics. Incubate the plates for 2 days at 28°C. Following incubation, the colonies were genotyped directly, or the plates were stored at 4 °C.

2.2.2.16 Infiltration in *Nicotiana benthamiana*

Inoculate the *A. tumefaciens* strains in 5 mL LB cultures with appropriate antibiotics and incubate at 28°C for 2 days. Afterward, centrifuge the cultures at 4000 rpm (Eppendorf, 5810R) for 10 minutes, discard the supernatant, and resuspend the pellet in an equal volume of infiltration media (10 mM MES, pH 5.6, 10 mM MgCl₂). Repeat the washing step once more, then resuspend the pellet in half the volume of infiltration media. Measure the OD₆₀₀ and adjust it to 1. Add 100 µM acetosyringone according to the final volume. Incubate the culture in the dark for at least 3 hours without shaking. Finally, infiltrate the abaxial surface of 4-week-old *N. benthamiana* plants using the prepared culture and a 1 mL syringe without a needle.

2.2.2.17 Mammalian 2-hybrid assay for protein-protein interaction

The plasmids were designed to harbor the gene of interest (GOI) fused either to the N or C terminus of the *VPI6* transcription activator domain or the C terminus of the *E*-gene, a DNA binding domain. These plasmids were constructed using the Gibson assembly method (see 2.2.2.11.1). Subsequently, these cloned plasmids were utilized for transfection experiments in HEK cell lines to investigate protein interactions. The transfection and activity assay experiments were conducted by Jonas Schön at the Institute of Synthetic Biology, University of Düsseldorf. The transfection process involved several steps. First, the cells were treated with 2 mL of trypsin for 1 minute in DMEM media (ThermoFischer Scientific CatLog no: 12491015). The trypsin-treated cells were then transferred to a 15 mL falcon tube containing DMEM media and centrifuged at 300g for 3 minutes. The supernatant was discarded, and the pellet was resuspended in 5 mL of fresh DMEM media containing serum using a pipette. Cell

counting was performed using a CASY Counter by pipetting 20 μL of the resuspended cells into 10 mL of CasyTon media, resulting in a cell suspension of 50,000 cells in 500 μL per well. In a separate tube, a mixture of plasmid DNA containing the GOI with activator and DNA binding domains was prepared in OptiMEM media (ThermoFischer Scientific CatLog no: 31985062) to a total volume of 50 μL per well, with a total amount of 0.75 μg plasmid mixture. Additionally, a PEI (Polyethyleneimine, 1 mg/mL) solution of 2.5 μL per well and OptiMEM media were added to the tube to reach a final volume of 50 μL . The solution was vortexed for 10 seconds and incubated for 15-30 minutes at room temperature. Next, 100 μL of the PEI/DNA mix was added dropwise to each well containing the cell suspension culture, and the plates were gently swirled to ensure homogenization. The plates were then incubated at 37°C, and the reporter assay was performed 24 to 48 hours post-transfection. After 24 hours, 200 μL of cell supernatant from each well was transferred to a 96-well microtiter plate, which was sealed tightly and incubated at 65°C for 1 hour followed by cooling to room temperature. Then, 100 μL of SEAP buffer was added to each well, and 80 μL of this mixture was transferred to a new plate. Subsequently, 20 μL of pNPP (p-Nitrophenylphosphate, 120 mM in double-distilled water) was added, and the absorbance at 405 nm was measured every minute for 1 hour in a plate reader.

2.2.3 Subcellular localization using confocal microscopy

Protein localization analysis involved the creation of fluorescent protein fusion constructs for the genes of interest, with subsequent examination of the resulting fluorescent signal in infiltrated *N. benthamiana* plants. The genes were cloned into the vector pB7FW2G using gateway cloning (2.2.2.11.2) to generate C-terminal GFP fusions, following the method described by Curtis and Grossniklaus (2003). These constructs were then transformed into *A. tumefaciens* (2.2.2.15), and the transgenic *A. tumefaciens* was used to infiltrate *N. benthamiana* leaves (2.2.2.16). The leaves were observed at two-, three-, and four-days post-infiltration to determine the optimal time for viewing, considering factors such as protein expression levels and the overall health of the plants following infiltration. Imaging of the fluorescent signal in the leaf epidermal cells was conducted using an Olympus FV3000 confocal laser scanning microscope (DFG-INST 1358/44-1 FUGB) located at the Center for Advanced Imaging (CAi) at Heinrich Heine University Düsseldorf, with assistance from Dr. Sebastian Hänsch. Lasers with excitation wavelengths of 495 nm were utilized to excite the fluorescent GFP protein, while autofluorescence of chloroplasts was detected using a 650 nm excitation wavelength.

2.2.4 Bioinformatic methods

2.2.4.1 Analysis of Whole Genome Sequencing data

The sequencing reads generated using Illumina Next Generation Sequencing platform underwent analysis using the Galaxy platform (<https://usegalaxy.eu/>) as described in figure 3-4. Initial processing involved quality and adapter trimming using the TrimMomatic tool (Bolger et al., 2014). This tool removes all the reads below the average quality score of 20. Following this, the trimmed FASTQ files were aligned to the *Arabidopsis thaliana* reference genome (TAIR10) using Bowtie2 aligner (Langmead and Salzberg, 2012). The resultant aligned sequence files were utilized for variant calling via the MiModD variant caller (Maier et al., 2014), which identified all SNPs and indels, categorizing them as homozygous, heterozygous or WT allele in both DNA pools. To streamline the data, the identified variants were organized into a tabular format using the MiModD extract variant sites tool (Maier et al., 2014). Unique homozygous variants, with at least 90% of the reads containing the variant site in the recovered DNA pool and heterozygous variants with less than 50% containing the variant site in the dwarf pool for recessive mutants, were selected using the MiModD VCF filter tool (Maier et al., 2014). For dominant segregation, variants with at least 60% of the reads containing the variant sites in the recovered DNA pool and 0-10% in the dwarf pool were selected. Subsequently, the SnpEff tool (Cingolani et al., 2012) was employed for genetic variant annotation and functional effect prediction such as missense, non-sense and frameshift mutations in coding sequence and also extended to identify the SNPs present in the intron, untranslated and promoter regions. Further the identified SNPs were visually confirmed for the presence in the reads by using the vcf file obtained from the MiModD variant caller in integrative genome viewer (IGV) (Robinson et al., 2017).

2.2.4.2 Protein structural analysis and interaction prediction

Available protein models were obtained from the AlphaFold2 database (Jumper et al., 2021). The following UniProt IDs were used: AT3G15610: A0A384KUR2, AtPHOX3: F4K487-1, and AtKH26: A0A1P8BC43. For unavailable models, prediction of protein structures was performed using Swiss- Fold (Arnold et al 2006). Rice OsWDRP3 sequence were obtained from (Xi and Wang, 2022). ChimeraX software was used to perform the superposition of predicted structures and obtain the structure images (Pettersen et al., 2004, 2021). Chimera

structural protein alignments were created from structure superposition with a 5 Å residue–residue distance cut-off. Protein sequence alignment was performed using Clustal Omega multiple sequence alignment tool (Sievers et al 2011). The protein-protein interaction was predicted using *Arabidopsis* eFP browser (<https://bar.utoronto.ca/eplant/>). The cis elements in the promoter region were predicted using PlantPAN4.0 (Chow et al 2024) (<http://plantpan.itps.ncku.edu.tw/plantpan4/index.html>)

2.2.5 Analytical methods

2.2.5.1 Preparation of alcohol insoluble residue (AIR) from *A. thaliana* stem material

The protocol for AIR preparation was adapted from Foster et al., 2010. The freeze-dried stem material was ground using a Retch ball mill (Retsch MM400) for 90 seconds at 30 Hz, repeating the process until the material reached a fine powder consistency. The tubes were then spun for 10 seconds, and 10 mg of the ground material was transferred to a new 2 mL screwcap tube (Sarstedt CatLog no: 72.694.007). A steel ball and 1.5 mL of 70% ethanol were added, and the mixture was shaken in the Retch mill for 1 minute. After removing the steel balls, the samples were centrifuged for 10 minutes at 12,000 rpm (Eppendorf, 5810R). The supernatant was replaced with 1.5 mL of chloroform:methanol (1:1, v/v) and vortexed. The tubes were centrifuged again for 10 minutes at 12,000 rpm (Eppendorf, 5810R), and this chloroform:methanol wash step was repeated until the supernatant became clear. Next, 1.5 mL of acetone was added, vortexed, and centrifuged for 10 minutes at 12,000 rpm (Eppendorf, 5810R). The tubes were then dried under airflow in a fume hood. The dried pellet was resuspended in 1 mL of 0.1M citrate buffer (pH 5.0). A steel ball was added, and the samples were shaken in the Retch mill for 30 seconds at 25 Hz to break up the pellet. An enzyme mixture containing 10 µL of sodium azide (0.01 mg/mL), 10 µL of α -amylase (100 µg/mL) (Sigma-Aldrich CatLog no: A6380), 22 µL of pullulanase M2 (Megazyme CatLog: M-PULBL), and 458 µL of water was added to the samples, which were then incubated for 16 hours at 37°C for destarching. After the incubation, the samples were boiled at 80°C for 10 minutes to stop the reaction and then cooled down. They were centrifuged for 10 minutes at 12,000 rpm (Eppendorf, 5810R), and the supernatant was discarded. The pellet was washed with water three more times by centrifugation, followed by a final wash with 1.5 mL of acetone.

The samples were then dried, and a 10 mg/mL stock was prepared by adding water according to the weight of the pellet. Finally, the samples were frozen at -20°C until further use.

2.2.5.2 Preparation of alcohol insoluble residue (AIR) from *Y. lipolytica* cell wall material

The protocol for AIR preparation was adapted from Voiniciuc et al., 2019. The gene-induced liquid cultures underwent centrifugation for 10 minutes at 4000 rpm (Eppendorf, 5810R). After discarding the supernatant, the cell pellet was resuspended in 1 mL of 70% (v/v) ethanol to wash out alcohol-soluble residues. Two small spoons of acid-washed glass beads (Sigma Aldrich CatLog no: G8772) were added to each 2 mL screw cap tube (Sarstedt CatLog no: 72.694.007), and the ethanol-resuspended cells were transferred to the tubes. Subsequently, the samples were ground at 30 Hz for 5 minutes using a Retsch Mill (Retsch MM400). Following grinding, the tubes were centrifuged for 10 minutes at 12000 rpm (Eppendorf, 5810R), and the supernatant was discarded. Then, 1 mL of chloroform:methanol (1:1, v/v) mixture was added, and the tubes were ground again at 30 Hz for 5 to 10 minutes. After centrifugation for 10 minutes at 12000 rpm (Eppendorf, 5810R), the supernatant was carefully aspirated, and 1 mL of acetone was added to wash out any remaining chloroform:methanol mixture. The suspension was vortexed and transferred to a fresh 2 mL screw cap tube to separate the suspension from the glass beads. The tubes were centrifuged again for 10 minutes at 12000 rpm (Eppendorf, 5810R), and the supernatant was carefully aspirated. Then, the tubes were placed open inside a fume hood overnight for acetone evaporation. The dried pellet was resuspended in 1 mL of 0.1M citrate buffer (pH 5.0), and a steel ball was added. The samples were shaken in the Retch mill for 30 seconds at 25 Hz to break up the pellet. An enzyme mixture containing 10 µL of sodium azide (0.01 mg/mL), 10 µL of α -amylase (100 µg/mL) (Sigma-Aldrich CatLog no: A6380), 22 µL of pullulanase M2 (Megazyme CatLog: M-PULBL), and 458 µL of water was added to the samples, which were then incubated for 16 hours at 37°C for destarching. After the incubation, the samples were boiled at 80°C for 10 minutes to stop the reaction and then cooled down. They were centrifuged for 10 minutes at 12,000 rpm, and the supernatant was discarded. The pellet was washed with water three more times by centrifugation, followed by a final wash with 1.5 mL of acetone and dried. The dried pellet was subjected to enzymatic treatment by adding an enzyme mixture composed of 30 µL of 125 µg/mL Zymolyase 20T (Roth CatLog no: 9324.2), 2 µL of sodium azide (0.01 mg/mL), and 368 µL of MilliQ water to remove native yeast β -1,3-glucans. This mixture was then incubated at 37°C for 24 hours. Following the incubation period, the mixture was centrifuged, and the resulting pellet was

washed twice with 70% ethanol and dried. The final weight of the isolated AIR was determined, and a 20 mg/mL slurry was prepared by adding an adequate amount of MilliQ water to the AIR material. The slurry was stored at -20°C until usage.

2.2.5.3 Measurement of acetic acid content in *A. thaliana* AIR material

The method was adapted from Ramírez et al., 2018. The AIR material (see 2.5.1) was suspended in 100 µL water. To saponify the material, 100 µL of 1 M sodium hydroxide was added, and the mixture was incubated at 25°C for 1 hour with shaking at 600 rpm. Saponification was stopped by adding 100 µL of 1 M HCl, and the samples were then centrifuged at 21,000 g for 10 minutes (Eppendorf, 5810R). Next, 10 µL of the supernatant was transferred to a well of a 96-well microtiter plate (VWR CatLog no:735-2002), and the acetic acid content was measured using the Acetic Acid Kit (Megazyme CatLog: K-Acet). The assay was conducted with a scaled-down reaction: 30 µL of Solution 1, 12 µL of Solution 2, and 94 µL of water were added to the 10 µL sample. The absorbance at 340 nm (Spectramax plus 384) was read after 3 minutes, followed by the addition of 12 µL of a 10X dilution of Solution 3. After 4 minutes, another absorbance measurement was taken, and then 12 µL of a 10X dilution of Solution 4 was added. A final absorbance measurement was taken after 12 minutes. These absorbance values were used to calculate the acetic acid content relative to a standard curve, following the formulas provided in the kit's manual.

2.2.5.4 Oligosaccharide Mass Profiling (OLIMP) by MALDI-TOF

For OLIMP analysis, 10 µL of slurry [20 mg/mL] (see 2.5.2) was digested with cellulase. To initiate digestion, 10 µL of endo-1,4-β-D-glucanase from *Bacillus amyloliquefaciens* (Megazyme, E-CELBA) at a concentration of 1 mU/µL and 10 µL of slurry were combined in a 1.5 mL tube. The mixture was then incubated in a thermomixer at 40°C and 1000 rpm for 90 minutes. Following digestion, the sample was diluted by a factor of 1:10 and centrifuged for 2 minutes at 20000 x g (Eppendorf, 5430R). For sample spotting, 1 µL of 2,5-Dihydroxybenzoic acid (DHB) matrix (Sigma Aldrich, 85707-1G-F) at a concentration of 10 mg/mL in 10 mM NaCl in HyClone water was first spotted onto a MALDI plate (Bruker Daltonik, MTP384 polished steel) and dried by applying vacuum (Vacuubrand, MZ 2C NT +2AK). Subsequently, 1 µL of supernatant from each sample was pipetted onto the matrix, incubated for 1 to 2 minutes, and then dried by applying vacuum. Finally, the samples were analyzed using a MALDI-TOF system (Bruker Daltonik, rapifleX). Data acquisition was performed using

FlexControl software version 4.0 (Bruker Daltonik) and processed using FlexAnalysis software version 4.0 (Bruker Daltonik).

2.2.5.5 Separation of oligosaccharides using Size Exclusion Chromatography (SEC)

For the separation of oligosaccharides by SEC, 200 μL (4 mg) of AIR slurry [20 mg/mL] (see 2.5.2) was subjected to cellulase digestion. In a 1.5 mL tube, 200 μL of endo-1,4- β -D-glucanase from *Bacillus amyloliquefaciens* (Megazyme, E-CELBA) at a concentration of 1 mU/ μL was combined with 200 μL of slurry. The mixture was then incubated in a thermomixer at 40°C and 1000 rpm for 90 minutes. Following digestion, the samples were centrifuged for 2 minutes at 20000 x g (Eppendorf, 5430R), and 1 μL of the resulting supernatant containing solubilized oligosaccharides was analyzed under MALDI-TOF (2.2.5.4) for confirmation. Subsequently, the remaining supernatant was injected into the SEC system (Bio-Rad, NGC Scout 10 plus Chromatography system) at a flow rate of 0.5 mL/min using a Supedex peptide 10/300 GL column. The elution was performed with double-distilled water, and 15 fractions (Bio-Rad, BioFrac) were collected, each with a volume of 1.5 mL. The detection was conducted using a RID detector (Refractive Index Detector) (Shimadzu, RID 20A). Following collection, 1 μL from each fraction was subjected to MALDI-TOF analysis to confirm the presence of the desired oligosaccharides. Upon confirmation, the fractions containing the desired oligosaccharides were pooled together and dried using a speedvac (Eppendorf, concentrator plus) at 45°C under vacuum. The resulting dried oligosaccharides were then utilized for monosaccharide compositional analysis using HPAEC-PAD (2.2.5.6) and glycosidic linkage analysis (see 2.5.7).

2.2.5.6 Monosaccharide compositional analysis using HPAEC-PAD

The protocol was adapted from Ramírez et al., 2018. For hemicellulose monosaccharide quantification, the AIR material (100 μL slurry containing 1 mg AIR) from *A. thaliana* was subjected to 150 μL of 3.34 M trifluoroacetic acid (TFA) to make a final concentration of 2M TFA and heated to 121°C for 90 minutes for hydrolysis. Following hydrolysis, the samples were briefly centrifuged, and 100 μL of the supernatant was transferred to a new tube. A stream of dried air using nitrogen was applied to the samples to remove excess TFA. The remaining pellet was reserved for crystalline cellulose content measurement (2.2.5.8). For the *Y. lipolytica* samples, the dried fractions from SEC or the dried AIR pellet (see 2.2.5.5 and 2.2.5.2) were hydrolyzed using 200 μL of 2 M TFA, followed by drying with nitrogen air. The dried samples

were then diluted in 300 μL of double-distilled water, and 25 μg of ribose was added as an internal standard. For both *A. thaliana* and *Y. lipolytica* samples, the sugars were separated using a CarboPac PA20 column in a Knauer HPAEC system (Azura, High-Performance Anion Exchange Chromatography system). The samples were run at a flow rate of 0.4 mL/min, and the gradient consisted of 2 mM NaOH for 23 minutes for the separation of neutral sugars, followed by an 8-minute flush with 490 mM NaOH for the separation of uronic acids. Subsequently, a 4-minute flush with 700 mM NaOH was performed, followed by a 25-minute column wash with 2 mM NaOH. Detection was carried out using a pulse amplitude detector (PAD) (Antec Scientific-Decade Elite). Oligosaccharides were quantified by comparison to a standard curve generated from commercially available monosaccharides.

2.2.5.7 Glycosidic Linkage Analysis

The methodology was adapted from Ciucanu, 2006. The dried oligosaccharides obtained from the fractions separated by SEC (see 2.2.5.5) were dissolved in a suspension of dry dimethyl sulfoxide (DMSO) and sodium hydroxide (NaOH) (12.5 mg/mL). The methylation procedure was initiated by adding 100 μL of methyl iodide with 2.5 hours of stirring following the addition (Ciucanu and Kerek 1984). The reaction was quenched by adding 2 mL of water. Subsequently, dichloromethane (2 mL) was used to extract the partially methylated carbohydrates. The dichloromethane was evaporated under a stream of dry nitrogen, and the residue was hydrolyzed by incubation with 2 M TFA for 90 minutes at 121 $^{\circ}\text{C}$. The trifluoroacetic acid was removed by evaporation under a stream of nitrogen at 40 $^{\circ}\text{C}$, followed by two additions and evaporations of 300 μL of isopropanol. The samples were then reduced by adding 200 μL of 1 M ammonium hydroxide containing 10 mg/mL sodium borodeuteride and incubated at room temperature for one hour. The reduction was stopped by adding 150 μL of acetic acid. Three additions and evaporations of 250 μL of 9:1 (v/v) methanol:acetic acid were performed, followed by four additions and evaporations of methanol to remove resulting borate side-products. Next, the samples were per-O-acetylated by adding 50 μL of acetic anhydride and 50 μL of pyridine, followed by incubation at 121 $^{\circ}\text{C}$ for 20 minutes. The solvents were removed by evaporation at room temperature, followed by two additions and evaporations of toluene (200 μL). The partially methylated alditol acetates were then extracted using 1.2 mL of ethyl acetate and 5 mL of water. The organic phase was transferred to a new tube and dried under nitrogen. The sample was subsequently dissolved in acetone and injected for GC-MS (Gas Chromatography – Mass Spectrometry) analysis using a 7890B GC system (Agilent) with

an SP-2380 column (Supelco) and a 5977 MS detector with quadrupole electric impact ionization (Agilent). The GC program involved holding the column at 80 °C for 3 minutes, then heating to 170 °C and holding for 3 minutes, followed by a gradual increase (20 °C per minute) to 240 °C and holding for 38.5 minutes, with an additional 15-minute run time. Peaks were assigned by comparing retention time and fragmentation patterns to standards and utilizing the CCRC database of partially methylated alditol acetates (<http://www.ccrcc.edu/databases/>).

2.2.5.8 Crystalline cellulose measurement

The protocol was adapted from Ramírez and Pauly, 2019. For the measurement of crystalline cellulose in *A. thaliana* stem material, the leftover pellet from TFA hydrolysis of AIR material (2.2.5.1) was utilized. Initially, the pellet underwent three washes with double-distilled water through centrifugation, followed by drying under ambient air. Subsequently, a Seaman hydrolysis was conducted by adding 175 µL of 72% sulfuric acid to the pellet, which was then incubated at room temperature for 30 minutes, vortexed, and further incubated for 15 minutes. Next, 825 µL of water was added, vortexed again, and the mixture was centrifuged at 10,000 rpm for 15 minutes (Eppendorf, 5810R). The glucose content in the resulting supernatant was assayed using the anthrone assay. For the assay, 10 µL of the supernatant from the Seaman hydrolysis was diluted in 90 µL of water in a new screw cap tube. Additionally, 100 µL of standards with varying concentrations of glucose were prepared in new tubes. Subsequently, 250 µL of anthrone reagent (Sigma Aldrich CatLog no: 319899) (0.2% w/w anthrone in concentrated sulfuric acid) was added to both the samples and standards, thoroughly mixed, and heated for 60 minutes at 80 °C. After heating, the samples were allowed to cool down to room temperature for 15 minutes. Then, 250 µL of each mixture was transferred to a 96-well microtiter plate (VWR CatLog no:735-2002), and the absorbance was measured at 630 nm (Spectramax plus 384). The amount of crystalline cellulose was quantified by comparing the absorbance values to a standard curve generated from the hydrolyzed glucose standards.

2.2.6 Statistical analysis methods

2.2.6.1 Chi-squared test

To assess the statistical significance of the observed versus expected frequencies in our categorical data, a chi-square test (Formula et al., 2021) was performed using Microsoft Excel. The observed and expected frequencies were organized in a tabular format within an Excel

spreadsheet. A new column was created to compute the chi-square component for each category using the formula square of (observed – expected frequencies)/expected frequency, and the chi-square statistic was obtained by summing all the components with the `SUM` function. The degrees of freedom for the test were calculated as the number of categories minus one. The `CHISQ.DIST.RT` function in Excel was used to calculate the p-value, following the syntax `=CHISQ.DIST.RT(chi-square statistic, degrees of freedom)`. This function returns the probability of observing a chi-square statistic at least as extreme as the one calculated, given that the null hypothesis is true. The p-value was then compared against a significance level (0.05). If the p-value was less than the significance level, the null hypothesis (that there is no difference between the observed and expected frequencies) was rejected, indicating a statistically significant difference. This procedure provided a quantitative measure to determine if the differences between observed and expected frequencies were significant or attributable to random chance.

2.2.6.2 Tukey HSD and ANOVA

To determine if there were significant differences between group means, an Analysis of Variance (ANOVA) followed by a Tukey's Honest Significant Difference (TukeyHSD) post-hoc test using RStudio was performed. The dataset was first imported into RStudio, and the appropriate data frame was created. An ANOVA test was conducted using the `aov()` function, specifying the dependent variable and the independent factor in the model formula, e.g., `model <- aov(dependent_variable ~ independent_factor, data = data_frame)`. The summary of the ANOVA test was obtained using the `summary()` function, which provided the F-value, degrees of freedom, and p-value to determine if there were overall significant differences between the groups. To identify which specific group means were significantly different from each other, a TukeyHSD test was performed on the ANOVA model using the `TukeyHSD()` function, e.g., `tukey_results <- TukeyHSD(model)`. The results of the TukeyHSD test, which include the confidence intervals and p-values for each pairwise comparison, were then summarized and interpreted. If the p-value for a comparison was less than the significance level (commonly 0.05), it indicated a statistically significant difference between those group means. This process allowed for a detailed examination of the differences between individual group means following the overall significance detected by the ANOVA.

3. A forward genetic screen to identify genes involved in suppression of growth and stress related defects associated with wall hypoacetylation

3.1 Background

Unlike other characterized *O*-acetylation mutants, the loss of function of the *ALTERED XYLOGLUCAN9 (AXY9)* gene significantly reduces *O*-acetylation in multiple cell wall polysaccharides, leading to severe developmental and stress-related defects (Ramírez et al., 2018; Schultink et al., 2015). Studying this unique mutant is technically challenging due to the extreme dwarfism and male sterility associated with the homozygous *axy9* mutation. Suppressor studies on other *O*-acetylation mutants, such as *tbl29*, indicate that reduced wall *O*-acetylation does not directly cause the collapse of xylem vessels or the related developmental changes (Bensussan et al., 2015; Ramírez et al., 2018). However, comprehensive analysis of the *axy9* mutant has been hindered by its severe dwarfism and male sterility. To address these challenges, researchers at the *Institute for Plant Cell Biology and Biotechnology, HHU* engineered a conditionally complemented *axy9* line known as *pAXY*. This line utilizes an inducible promoter (pER8::*AXY9*) to control the expression of *AXY9*. The leaky expression of *AXY9* from the inducible promoter, even without the addition of the inducer (estradiol), partially restored the growth, and fertility, though wall acetylation levels remained lower than normal (Figure 3-1). Analysis of wall *O*-acetylation levels (Figure 3-1B) shows a 70% reduction in total wall *O*-acetyl ester levels in the *axy9* mutant compared to the WT. The *pAXY* line exhibits wall *O*-acetylation levels 50% lower than WT (Col-0). Thus, the *pAXY* line represents a partially restored *axy9* phenotype, characterized by reduced wall *O*-acetate levels, normal fertility, and stunted growth, as illustrated in Figure 3-1. This chapter of the thesis aims to identify novel genes involved in the suppression of growth and stress-related defects associated with *pAXY* through forward genetic screening. By leveraging forward genetics, researchers can identify previously unknown and non-obvious genes linked to these processes, enabling a detailed analysis of the biological and cellular mechanisms involved in the plant's response to wall *O*-acetylation defects. Ethyl Methane Sulfonate (EMS) mutagenesis was used to induce random point mutations in the *pAXY* line. A subsequent suppressor mutant screen was conducted to identify mutations that suppress the *pAXY* phenotype. Researchers at the Institute for Plant Cell Biology and Biotechnology carried out the mutagenesis and seed pooling, resulting in 22 pools, each containing seeds from 100 first-generation M₁ plants. For this study, three of these pools were screened.

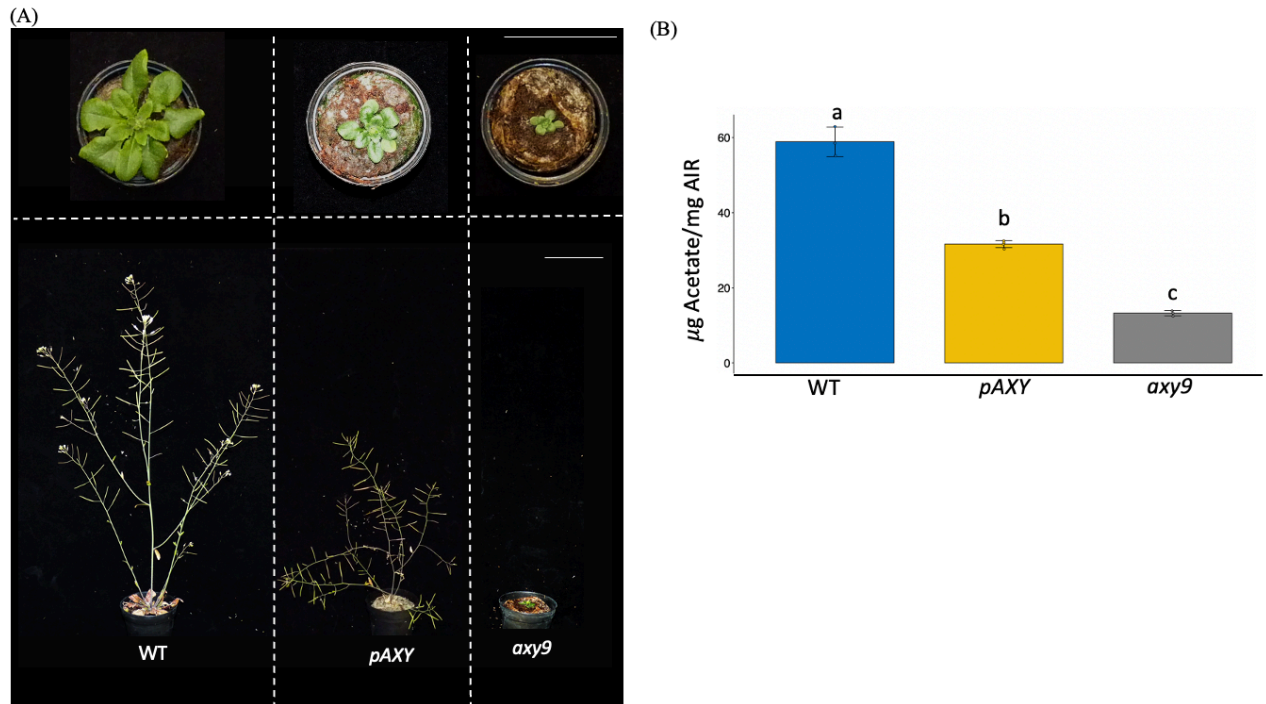


Figure 3-1. Growth phenotype and acetate content of *pAXY* and *axy9*.

(A) Growth phenotype showing the rosette size of four-week-old and stem height of six-week-old *axy9*, *pAXY* and WT. The white bar represents a scale of 5 cm. (B) Total wall-bound acetyl ester content for stem of WT, *pAXY* and whole shoot of *axy9*. Error bars indicates SD (n=3), and the alphabets indicates the significant differences between the mean of different genotypes (Tukey HSD, $p < 0.05$).

3.1.1 Potential and challenges of forward genetic approach in uncovering genetic pathways

Forward genetics relies on populations with genetic variation resulting in mutant phenotypes identifiable in screens. Genetic variability can be induced by chemical mutagenesis (EMS), radiation, T-DNA insertion, or transposon activation. The different methods of mutagenesis lead to different types of alleles, each with its own identification challenges. For instance, T-DNA mutagenesis can disrupt gene function or overexpress genes depending on the insertion site (Weigel et al., 2000), while EMS typically introduces point mutations leading to missense or nonsense mutations (Drake and Baltz, 1976). Forward genetics has been effective in identifying genes involved in cell wall biosynthesis. Screens for *A. thaliana* mutants with altered cell wall monosaccharide compositions have identified glycosyltransferases (MUR2, MUR3, MUR10) and nucleotide sugar interconversion enzymes (MUR1, MUR4) (Bosca et al., 2006; Madson et al., 2003; Reiter et al., 1997; Vanzin et al., 2002). Other screens have identified mutants through various assays, including conditional root expansion phenotypes

(Hauser et al., 1995), radial root swelling (Arioli et al., 1998), and morphological responses to glycosyl hydrolase treatment (Gille et al., 2009). While typical reverse genetics approaches require genomic sequence information, forward genetics can identify genes from families with unknown functions, as prior information about gene function is unnecessary (Gille et al., 2011b). Another advantage of forward genetics is its ability to demonstrate the importance of a previously characterized gene in processes not readily associated with the known function of the corresponding protein. An example is the XyG galactosyltransferase MUR3, which has a direct role in cytoskeleton organization and indirectly activates plant defense responses (Tamura et al., 2005; Tedman-Jones et al., 2008). Forward genetic screens have also been pivotal in uncovering mutants with modified acetylation patterns, such as the *axy* mutants in *A. thaliana*, which exhibited decreased xyloglucan *O*-acetylation (Gille et al., 2011b). Additionally, forward genetic screens have been utilized to identify suppressors of different stress phenotypes, as demonstrated by the discovery of genetic suppressors of chloroplast reactive oxygen species signaling mutants (Lemke and Woodson, 2023). In plant immunity research, a forward genetic screen in immunodeficient mutants revealed loci implicated in plant defense mechanisms (George et al., 2023). The effectiveness of forward genetics in identifying suppressors of *O*-acetylation mutants is a critical area of research. For example, the identification of two *tbl29* suppressors, where xylem collapse and growth arrest are recovered despite reduced wall/xylan acetate, supports the effectiveness of this approach. Loss of function in *KAKTUS* (*KAK*) increases stem diameter and activates the development of larger tracheary elements, almost completely rescuing *tbl29/esk1*-associated dwarfism without affecting wall acetate content. Although *KAK* has been previously described as an endoreduplication repressor affecting trichome morphology, its role in regulating vascular development remains unclear (Bensussan et al., 2015; Downes et al., 2003; El Refy et al., 2004). Additionally, blocking strigolactone (SL) synthesis in *tbl29/esk1* plants (*tbl29 max4* double mutants) completely suppresses both developmental defects and increased freezing tolerance without affecting reduced acetate (Ramírez et al., 2018). Exogenous application of synthetic SL to *tbl29 max4* plants results in dwarfism and collapsed xylem, confirming SL-dependency for these phenotypes (Ramírez et al., 2018).

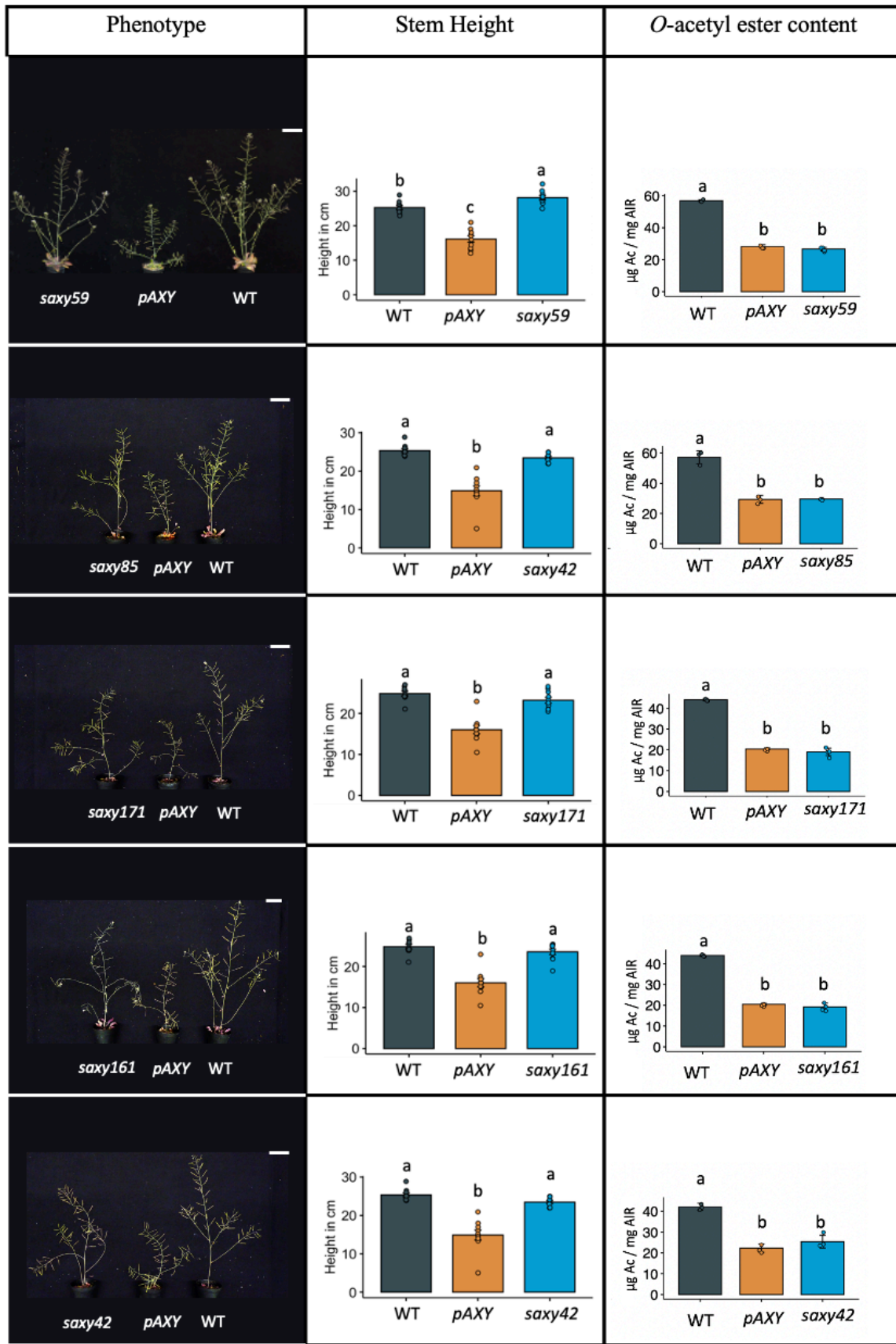
These instances highlight the potential of forward genetics in elucidating the genetic foundation of acetylation patterns, stress responses, and cellular integrity, emphasizing its potential in identifying suppressors of *O*-acetylation mutants. The short generation time, small size, well-annotated genome, and T-DNA collections available for *A. thaliana* have made it a popular

model for forward genetic screens. High-throughput sequencing methods can rapidly re-sequence the entire genome of *A. thaliana* mutants, facilitating the identification of candidate mutations (Austin et al., 2011). One limitation of forward genetics is its difficulty in identifying genes due to genetic redundancy or lethality. In *A. thaliana*, multiple gene copies with similar biochemical activity often result in no observable phenotype when a single gene is knocked out (Cavalier et al., 2008; Jensen et al., 2012; Manabe et al., 2013). Additionally, disrupting cell wall biosynthetic genes often leads to decreased plant fitness or lethality, limiting the identification of these genes (Geshi et al., 2013; Sitaraman et al., 2008). Furthermore, the complexity of genetic interactions and the potential for off-target effects can complicate the identification of suppressors in forward genetic screens (Jankowicz-Cieslak and Till, 2016). Screening under stress conditions can help identify conditionally-sensitive alleles that display phenotypes under specific conditions but function normally otherwise, such as mutants defective for cellulose synthase genes under high temperature or low light (Arioli et al., 1998).

3.2 Results

3.2.1 Identification, growth characterization, and *O*-acetate content of suppressor mutants

From the randomly selected three pools, each containing seeds from 100 first-generation M₁ plants, screenings identified 147 M₂ plants that exhibited a clear reversal of the *pAXY* growth phenotype, characterized by reaching a height threshold of over 20 cm and increased rosette size compared to *pAXY*. The progeny of these 147 M₂ lines were further analyzed for consistent growth with increased rosette size compared to *pAXY* and height above the 20 cm threshold, resulting in the selection of 40 M₂ lines based on their height to identify potential suppressor mutants. At least 20 plants per M₂ line were screened for homogenous height recovery. Mutants displaying uneven growth phenotypes among progeny or intermediate suppression were excluded (Appendix Figure 9-4). Subsequent validation in the M₃ generation for homogenous increased height above the threshold led to the identification of nine clear suppressor mutants of *pAXY*, characterized by a distinct increase in stem height compared to *pAXY* (Figure 3-2). These mutants were designated *saxy59*, *saxy85*, *saxy171*, *saxy161*, *saxy42*, *saxy71*, *saxy57*, *saxy163*, and *saxy38*. When comparing the phenotypes of WT and *pAXY* under long-day conditions, it is evident that *pAXY* exhibits stunted growth and a dwarf phenotype. In Figure 3-2, all the suppressor (*saxy*) mutants demonstrated an increase in height, corresponding to a recovered growth phenotype when compared to the *pAXY* line (see Appendix Figure 9-3 for rosette images). Investigation of the *O*-acetate levels in 6-week-old stem material of the selected M₃ *saxy* mutants, alongside *pAXY* and WT (Figure 3-2), revealed that the wall acetylation levels of *saxy* mutants closely resembled those observed in *pAXY*, both approximately 50% lower than WT levels. This observation underscores that changes in *O*-acetate levels do not necessarily correlate with the increase in plant height of *saxy* mutants.



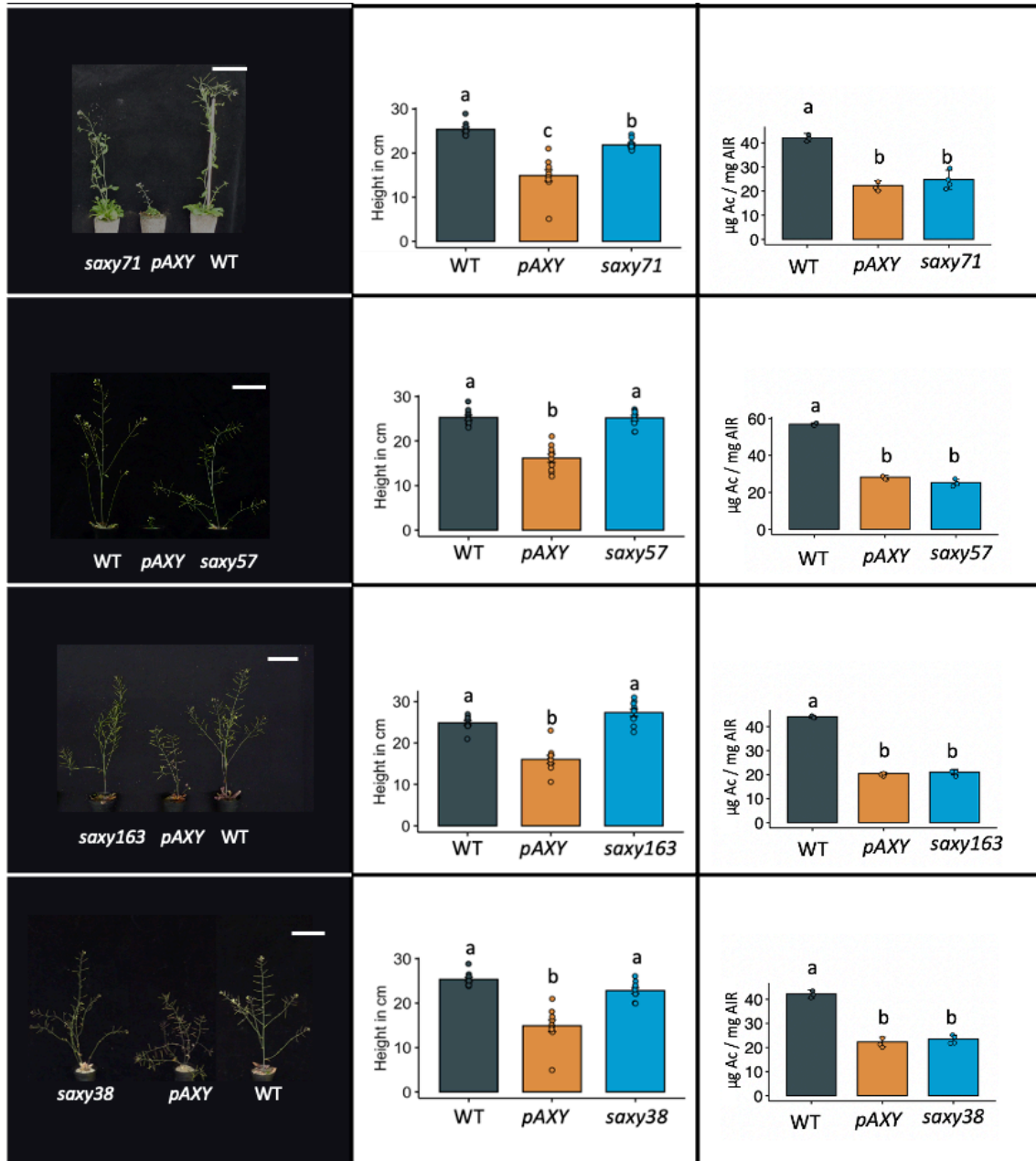


Figure 3-2. *pAXY* suppressor mutants (*saxy*) showing rescued phenotype in M₃ generation.

Representative images of six-week-old plants from the indicated genotypes in the left column: WT, *pAXY* and *saxy* M₃ suppressor mutants grown in long day conditions. All selected suppressor mutants show rescue in growth phenotype. White scale bars in the plant pictures represents 5cm. The bar plots in the middle column represent the average height of 10 individual plants from each genotype. The bar plots in the right column represents average total wall-bound acetyl ester content from stem material of 4 individual plants from each genotype. Error bars indicate standard deviation, and the alphabets indicates the significant differences between the mean of genotypes (Tukey HSD, $p < 0.05$).

3.2.2 Inheritance pattern of suppressor mutations

The identification of *saxy* mutants prompted further genetic assessment to determine the inheritance patterns of their suppressor mutations. All nine *saxy* mutants were backcrossed (BC) with the original parental *pAXY* line. In the subsequent BCF₁ generation, observing a dwarf phenotype would suggest a recessive mutation, while a recovered *saxy* phenotype would suggest a dominant mutation. However, this initial observation does not exclude the possibility of more complex inheritance patterns, such as linked or non-linked genomic locations, semi-dominant traits, and incomplete penetrance. To accurately determine the inheritance pattern, phenotypic segregation was analyzed in the BCF₂ generation, produced by selfing the BCF₁ plants. The observed segregation ratios in the BCF₂ generation allowed to infer whether the suppressor mutations were recessive or dominant. For instance, a 3:1 segregation ratio favoring the *pAXY* phenotype would indicate a recessive suppressor mutation, whereas a 3:1 ratio favoring the suppressor *saxy* phenotype would suggest a dominant mutation. To assess the segregation patterns, a chi-square test for goodness of fit was employed, comparing the observed and expected populations. For a hypothesis of Mendelian segregation to hold, the chi-square value (χ^2) should be lower than 3.84, corresponding to a significance level p-value. Table 10 shows that suppressor mutants *saxy59*, *saxy85*, *saxy171*, *saxy161*, and *saxy38* exhibited a recessive segregation of phenotype, while *saxy42* showed a dominant segregation. Conversely, *saxy71*, *saxy57*, and *saxy163* deviated from the expected Mendelian 3:1 segregation ratio. Notably, the number of dwarf plants or those exhibiting the *pAXY* phenotype closely matched the number of plants with the recovered or suppressor phenotype. This discrepancy could result from various non-Mendelian inheritance patterns, such as epigenetic modifications, cytoplasmic inheritance, or tighter linkage of the causal mutations (Mittelsten Scheid, 2022). Consequently, these three suppressors were not considered for further analysis. The remaining six suppressors, which followed a consistent Mendelian inheritance pattern, were chosen for more detailed investigation (Table 10).

<i>saxy</i> Mutant	Dwarf plants	Recovered plants	Total (n)	Chi.sq value	Dominant/ Recessive
<i>saxy59</i>	122	44	166	0.2	Recessive
<i>saxy85</i>	106	37	143	0.05	Recessive
<i>saxy171</i>	273	96	369	0.2	Recessive
<i>saxy161</i>	287	108	395	1.15	Recessive
<i>saxy42</i>	99	248	347	2.3	Dominant
<i>saxy71</i>	58	45	103	19.18	No fit
<i>saxy57</i>	43	58	101	16.6	No fit
<i>saxy163</i>	101	92	193	52.8	No fit
<i>saxy38</i>	104	38	142	0.23	Recessive

Table 10. Segregation pattern and causal mutation characteristics in *saxy* mutants of BCF₂ generation.

Dwarf plants - phenotype akin to *pAXY*; Recovered plants – phenotype similar to suppressor; Total (n) – represents total number of plants used for observation; Chi.sq – Chi-squared test value for goodness of fit, for a hypothesis to fit the chi-squared value χ^2 should be lower than 3.84, corresponding to a significance level p-value; Dominant/Recessive – inheritance pattern of causal mutation based on phenotype and chi square test; No fit – The segregation did not fit the hypothesis for dominant or recessive mutation. The *saxy* mutants displaying mendelian segregation are highlighted in bold.

3.2.3 Bulk segregant analysis and whole genome sequencing on *saxy* mutants

The Bulk Segregant Analysis (BSA) strategy was employed to identify the causal mutation responsible for the observed phenotype in *saxy* mutants. In this method, a segregating BCF₂ population was divided into two pools: one pool containing individuals exhibiting the suppressor phenotype (recovered), and the other comprising individuals displaying the parental *pAXY* phenotype (dwarf). The mutant background selected for the suppressor mutant screening was *pAXY*, where the *pER8::AXY9* transgene was transformed into the *axy9* (SALK_090612) T-DNA insertion mutant. To ensure that the BCF₂ plants chosen for the bulked segregant analysis were not contaminated with WT seeds, these selected BCF₂ plants underwent genotyping for the presence of T-DNA in the *AXY9* gene and the additional *pAXY* transgene insertion through PCR. For *axy9* genotyping, DNA was extracted from 4-week-old BCF₂ plant leaves, and two distinct PCR reactions were performed for each sample: Reaction A employed primers LP and RP flanking the T-DNA insertion in the *AXY9* gene, with the presence of a ~1100 bp band indicating the absence of T-DNA insertion. Reaction B included one primer (RP) flanking the *AXY9* gene and another primer (LBb1.3) binding in the T-DNA, with the presence of a ~800 bp signal indicating the presence of the T-DNA (Figure 3-3 A and C). A similar strategy was used to genotype the *pAXY* insertion present in the chromosome 4

(position: 15022454) using the primers: WT_F and WT_R flanking the *pER8::AXY9* insertion, with the presence of a ~1100 bp band indicating the absence of transgene insertion. Reaction B included one primer (RP) flanking the genomic region and another primer (LBb1.3) binding in the *pER8::AXY9* transgene, with the presence of a ~800 bp signal indicating the presence of the transgene (Figure 3-3 B and D). The primer sequences are listed in Table 4. The genotyping determined that all BCF₂ mutants were homozygous for the T-DNA insertion in *AXY9* and the *pAXY* transgene, thus eliminating the possibility of WT-like phenotypes resulting from seed contamination or heterozygosity for the T-DNA. It is important to highlight that the *pAXY* line, regulated by an inducible promoter (*pER8::AXY9*), includes a copy of *AXY9*, and the suppressors were developed on this *pAXY* background. To prevent misinterpretation of WT amplicons, the LP primer for *axy9* genotyping was designed to bind to the 5' UTR region of the *AXY9* gene, which is not present in the *pAXY* transgene insertion.

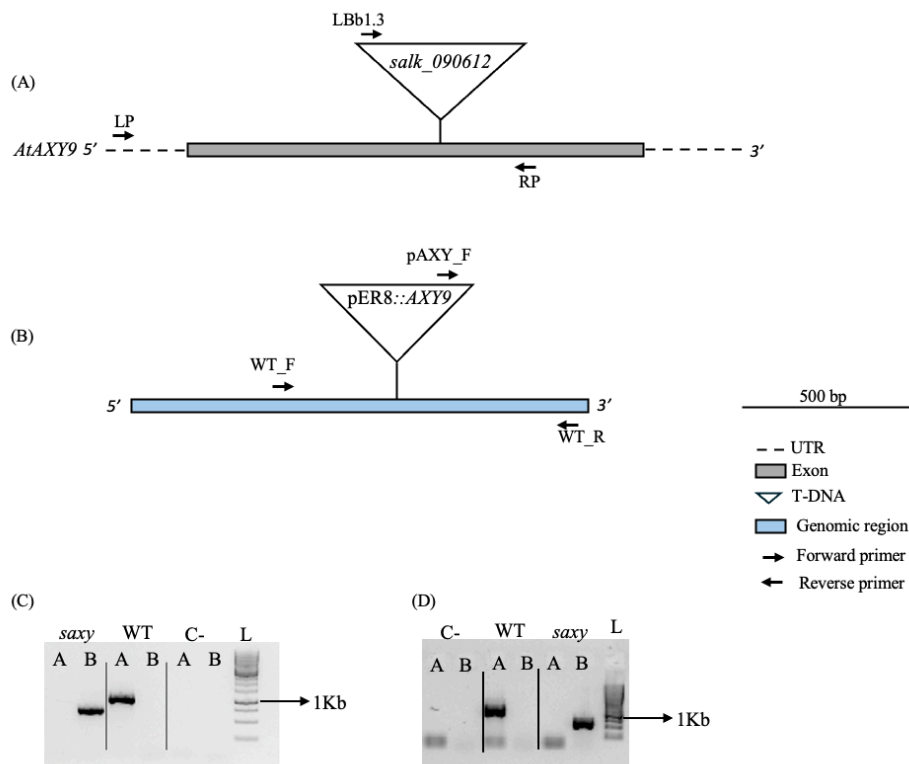


Figure 3-3. Genotyping for *AXY9* and *pAXY* T-DNA insertion in *saxy* mutants.

(A) Schematic representation of *AXY9* gene structure, position of T-DNA insertion and genotyping primer binding sites. (B) Schematic representation of *pAXY* insertion and genotyping primer binding sites. (C) Representative picture of *AXY9* genotyping in *saxy* and WT samples. (D) Representative picture of *pAXY* genotyping in *saxy* and WT samples. The LP, RP, LBb1.3, WT_F, WT_R and pAXY_F indicates the primers used for genotyping. A Generuler 1kb ladder was used as size markers indicated as L in the picture. The C- indicate the negative control where no DNA was added for the PCR reaction.

The leaf samples from BCF₂ population were then pooled according to the phenotype (see section 2.2.2.12.1) and DNA was extracted, which underwent standard Illumina DNA library preparation (refer section 2.2.2.1.2, 2.2.2.12.1, and 2.2.4.1 for sequencing specification). Subsequently, the samples were sequenced on the Illumina Next Generation Sequencing platform. The sequencing reads generated underwent analysis using the Galaxy platform (<https://usegalaxy.eu/>) as described in figure 3-4. Initial processing involved quality and adapter trimming using the TrimMomatic tool (Bolger et al., 2014). This tool removes all the reads below the average phred quality score of 20. Following this, the trimmed FASTQ files were aligned to the *A. thaliana* reference genome (TAIR10) using Bowtie2 aligner (Langmead and Salzberg, 2012). The alignment showed a mapping coverage of above 95% in all *saxy* mutants, except the dwarf pool of *saxy85* where the coverage of aligned reads was 89.95% (Table 11). This discrepancy could be due to the loss of reads in quality trimming process, technical variations or more complex genomic changes affecting alignment efficiency. For each *saxy*, the BCF₂ DNA pool of recovered plants and dwarf plants was sequenced, yielding the following results: In the case of *saxy38*, the recovered pool had 40,651,010 total reads, with 98.01% mapped, while the dwarf pool had 39,358,642 reads, with 96.27% mapped. For *saxy42*, the recovered pool comprised 23,619,005 reads, with 98.91% mapped, and the dwarf pool had 33,491,404 reads, with 98.91% mapped. Likewise, for *saxy59*, the recovered pool contained 33,445,722 reads, with 96.42% mapped, and the dwarf pool had 33,218,760 reads, with 95.61% mapped. In the analysis of *saxy85*, the recovered pool had 30,566,206 reads, with 95.10% mapped, whereas the dwarf pool had 29,972,422 reads, with 89.95% mapped. Regarding *saxy161*, the recovered pool had 29,958,254 reads, with 97.64% mapped, while the dwarf pool had 40,489,410 reads, with 96.73% mapped. For *saxy171*, the recovered pool had 33,129,392 reads, with 97.48% mapped, and the dwarf pool had 34,529,714 reads, with 96.56% mapped. The close similarity in total number of reads and mapping percentages between recovered and dwarf pools within each *saxy* mutant suggests that the sequencing was consistent across samples. The resultant aligned sequence files were utilized for variant calling via the MiModD variant caller (Maier et al., 2014), which identified all SNPs and indels, categorizing them as homozygous, heterozygous or WT allele in both DNA pools. To streamline the data, the identified variants were organized into a tabular format using the MiModD extract variant sites tool (Maier et al., 2014). Given the previous observation that all recessive *saxy* mutants exhibited a 3:1 segregation ratio for *pAXY* and suppressor phenotypes, it was concluded that the causal mutations must be recessive, except for *saxy42*, which showed dominant inheritance. Consequently, unique homozygous variants, with at least 90% of the reads containing the

variant site in the recovered DNA pool and heterozygous variants with less than 50% containing the variant site in the dwarf pool, were selected using the MiModD VCF filter tool (Maier et al., 2014). For dominant segregation, variants with at least 60% of the reads containing the variant sites in the recovered DNA pool and 0-10% in the dwarf pool were selected. Subsequently, the SnpEff tool (Cingolani et al., 2012) was employed for genetic variant annotation and functional effect prediction such as missense, non-sense and frameshift mutations in coding sequence and also extended to identify the SNPs present in the intron, untranslated and promoter regions. Further the identified SNPs were visually confirmed for the presence in the reads by using the vcf file obtained from the MiModD variant caller in integrative genome viewer (IGV) (Figure 3-5) (Robinson et al., 2017).

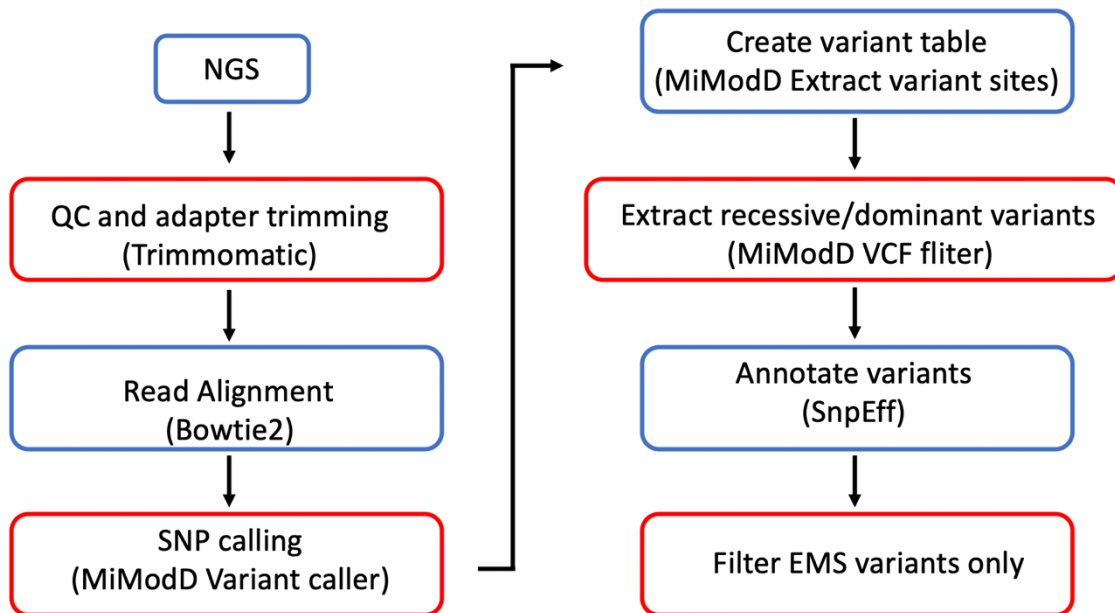


Figure 3-4. Bulk Segregant Analysis workflow.

Galaxy based workflow to identify the genetic variations responsible for the *saxy* phenotype caused by EMS mutation. Specific tool used are indicated in the brackets. NGS – Next Generation Sequencing reads, QC – Quality Check, SNP – Single Nucleotide Polymorphism, EMS – Ethyl Methane Sulphonate.

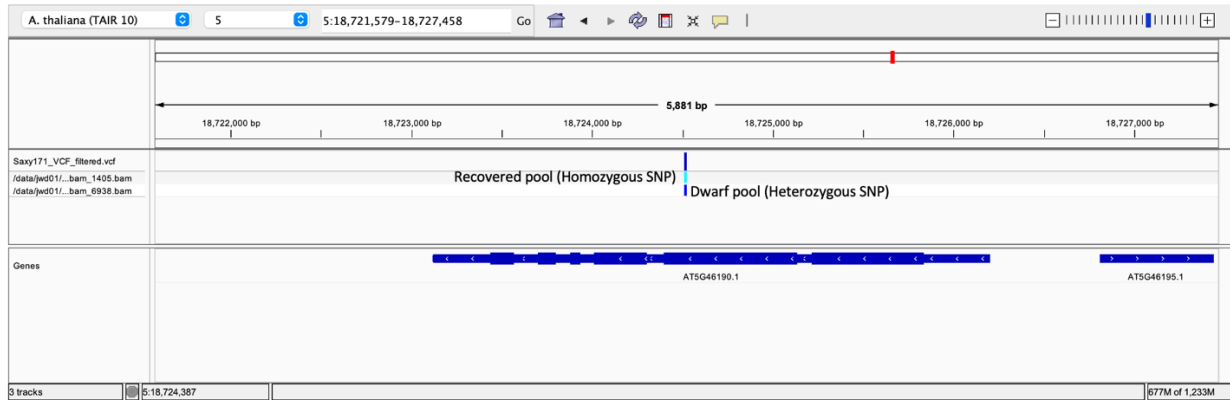


Figure 3-5. Representative image for visualizing SNP in IGV.

This representative image shows a SNP on chromosome 5 of the *saxy171*, visualized using the Integrative Genome Viewer (IGV). The SNP is homozygous in the recovered pool (sky-blue bar) and heterozygous in the dwarf pool (dark blue bar). Gene structure is represented below, with exons as thicker regions and introns as thinner regions. The SNP position is indicated by the scale above the SNP.

The NGS analysis for recessive segregation of SNPs in *saxy59* identified potential candidate mutation in the genes AT4G16144, AT4G05612, AT3G15610, and AT2G38940 associated with the recovered growth phenotype (Table 12). Notably, the missense mutation in the AT2G38940 gene showed a strong association with the recovered phenotype, as indicated by the read counts for the reference and altered variant (Ref/Alt) between the dwarf (18/7) and recovered pools (2/25). Similarly, mutations in the AT3G15610 (recovered 1/11 and dwarf 6/15) and AT4G16144 (recovered 1/22 and dwarf 2/16) genes exhibited notable differences in read counts, suggesting potential associations with the phenotype. For *saxy85*, NGS pinpointed candidate mutations in AT4G04930 (recovered 0/5 and dwarf 3/5) and AT5G20360 (recovered 1/20 and dwarf 4/10) that might be responsible for the observed phenotype (Table 12). The mutation in the 3' UTR of a AT4G04930 and the promoter region of AT5G20360 indicate a possible links to the *saxy85* phenotype. In *saxy171*, potential candidate mutations were identified in AT4G36860, AT2G25710, and AT5G46190 (Table 12). The missense mutation in AT5G46190, supported by read counts between the dwarf (15/10) and recovered pools (1/13), suggests a potential connection to the *saxy171* phenotype especially since other candidate mutations show lower read counts.

For *saxy161*, the genes AT4G15150 and AT4G16770 were identified as likely containing the causal mutation, while in *saxy38*, only one gene AT4G36849 was identified (Table 12). However, all the reads in the dwarf pool for these genes contain the altered variant for these

candidates, suggesting that they might not be associated with the observed phenotype or could be false positives occurred due to sequencing errors, misalignment, or low coverage in that region. In *saxy42*, NGS analysis for dominant segregation of SNPs identified six genes: AT2G01008, AT2G07722, AT2G39620, AT2G46250, AT3G48430, and AT5G53330 (Table 12). The mutations in AT2G01008 and AT2G07722 showed higher read counts for the altered variants in both recovered and dwarf pools, which could indicate that these genes are not directly involved in the recovered phenotype. Another possibility is that the high read counts are due to overrepresentation of these reads by repetitive regions, which often contain sequences that are similar or identical across different parts of the genome. Sequencing reads from such regions can be challenging to align accurately, potentially leading to an overrepresentation of reads. The other four candidates AT2G39620, AT2G46250, AT3G48430, and AT5G53330 displayed relatively low numbers of reads in the dwarf pool, with all reads displaying altered variants, indicating they might be false positives. The identified mutations across all lines included missense variants, UTR, promoter, and intron mutations, each potentially affecting protein function or gene expression differently although some with lower read counts. Further validation is required through additional methods such as targeted sequencing of the amplicons from variant regions to confirm the SNPs, as well as through knockout mutants and complementation tests.

Genotype	DNA pool	Total reads after trimming	Paired reads	Unpaired reads	Unmapped reads	Mapped reads	% of reads aligned
<i>saxy38</i>	Recovered	40651010	25157306	9907781	809399	39841611	98.01%
	Dwarf	39358642	23453050	9470259	1469736	37888906	96.27%
<i>saxy42</i>	Recovered	23619005	17762733	5856272	477648	23141357	98.91%
	Dwarf	33491404	25368366	8123038	642921	32848483	98.91%
<i>saxy59</i>	Recovered	33445722	24927679	8177508	340535	33105187	96.42%
	Dwarf	33218760	23154830	8644060	357119	32861641	95.61%
<i>saxy85</i>	Recovered	30566206	20192080	7861081	1233843	29332363	95.10%
	Dwarf	29972422	18515928	7705480	2753292	27219130	89.95%
<i>saxy161</i>	Recovered	29958254	19210080	7735173	706553	29251701	97.64%
	Dwarf	40489410	26974506	10708736	1325787	39163623	96.73%
<i>saxy171</i>	Recovered	33129392	22158662	8548099	835343	32294049	97.48%
	Dwarf	34529714	22925726	9080975	1187685	33342029	96.56%

Table 11. Mapping statistics of NGS data.

The table shows total number of reads after trimming, number of paired reads, number of unpaired reads, number of mapped and unmapped reads, and percentage of mapping coverage in both recovered and dwarf DNA pools of different *saxy* mutants used in the analysis.

saxy	Gene	Gene description	Position	Chromosome	Consequence	Amino acid	Base or codon change	Reads (Dwarf pool REF/ALT)	Reads (recovered pool REF/ALT)
<i>saxy59</i>	AT2G38940	<i>Arabidopsis thaliana</i> phosphate transporter 2, ATPT2,	16259539	2	Missense variant	ALA-VAL	gCg/gTg	18/7	2/25
	AT3G15610	Transducin/WD40 repeat-like superfamily protein	5292754	3	Missense variant	HIS-TYR	Gta/Ata	6/15	1/11
	AT4G05612	Hypothetical protein	2961614	4	Missense variant	ASP-ASN	Gat/Aat	1/1	0/7
	AT4G16144	AMSH3, associated molecule with the SH3 domain of STAM 3	9139901	4	Missense variant	MET-ARG	cAt/cCt	2/16	1/22
<i>saxy85</i>	AT4G04930	Encodes a sphingolipid delta4-desaturase	2506789	4	3'UTR	N/A	A/G	3/5	0/5
	AT5G20360	PHOX3, encodes one of the 36 carboxylate clamp (CC)-tetratricopeptide repeat (TPR) proteins	6886187	5	Promoter	N/A	G/A	4/10	1/20
<i>saxy171</i>	AT4G36860	DAR1, a member of a small (7 member) ubiquitin binding protein family	17361281	4	Intron	N/A	C/T	1/1	0/3
	AT2G25710	HCS1, holocarboxylase synthase 1	10954682	2	Intron	N/A	T/C	2/9	0/8
	AT5G46190	ATKH26 RNA-binding KH domain-containing protein	18724519	5	Missense variant	GLY-GLU	cCt/cTt	15/10	1/13
<i>saxy42</i>	AT2G01008	Encodes maternal effect embryo arrest protein	2019	2	Missense variant	SER-PRO	Tcc/Ccc	11/410	29/491
	AT2G07722	Encodes transmembrane protein	3438797	2	Missense variant	LEU-SER	tTg/tCg	8/94	9/57
	AT2G39620	Pentatricopeptide repeat (PPR) superfamily protein	16520623	2	Missense variant	LEU-PHE	Cca/Tca	0/8	7/7
	AT2G46250	myosin heavy chain-like protein	18991603	2	Missense variant	ARG-LYS	aGa/aAa	0/5	20/8
	AT3G48430	REF6, Relative of Early Flowering 6	17938132	3	Missense variant	GLY-GLU	gGg/gAg	0/9	4/8
	AT5G53330	Ubiquitin-associated/translation elongation factor EF1B protein	21640588	5	Missense variant	GLU-LYS	aGa/aAa	0/4	7/9
<i>saxy161</i>	AT4G15150	Glycine rich protein	8643599	4	5'UTR	N/A	C/T	0/21	4/19
	AT4G16770	2-oxoglutarate (2OG) and Fe(II)-dependent oxygenase superfamily protein	9437468	4	5'UTR	N/A	T/C	0/6	1/4
<i>saxy38</i>	AT4G36840	Galactose oxidase/kelch repeat superfamily protein	17351281	4	5'UTR	N/A	T/C	0/11	4/9

Table 12. List of candidate genes obtained for *saxy59*, *saxy85*, *saxy171*, *saxy42*, *saxy161*, and *saxy38*.

Table 12 presents a compilation of candidate SNPs and their annotated genes isolated from BSA conducted on the BCF₂ segregating population for *saxy59*, *saxy85*, *saxy171*, *saxy42*, *saxy161*, and *saxy38*. The NGS analysis for recessive segregation of SNPs in *saxy59* identified potential candidate mutations in the

genes AT4G16144, AT4G05612, AT3G15610, and AT2G38940. Similarly, for *saxy85*, BSA and NGS pinpointed candidate mutations in the genes AT4G04930 and AT5G20360 that could be responsible for the *saxy85* phenotype. For *saxy171*, potential candidate mutations were identified in the genes AT4G36860, AT2G25710, and AT5G46190. For *saxy161*, the genes AT4G15150 and AT4G16770 were identified as containing the causal mutations. For *saxy38*, only one gene was identified as containing the causal mutation: AT4G36849. For *saxy42*, the NGS analysis for dominant segregation of SNPs identified six genes: AT2G01008, AT2G07722, AT2G39620, AT2G46250, AT3G48430, and AT5G53330. The table includes details such as gene name, description, SNP location, mutation consequence, amino acid alteration, and specific changes in the codon sequence. The "Reads" column denotes the total number of reads obtained for each SNP, where "REF" indicates the number of reads showing no variants, and "ALT" indicates the number of reads displaying variants. "N/A" signifies not applicable.

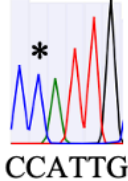
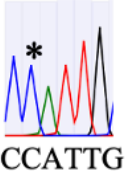
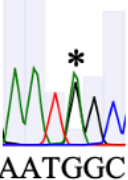
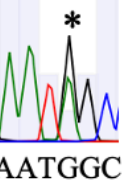
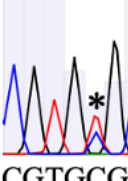
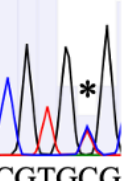

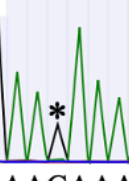
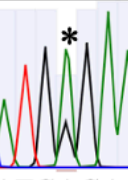
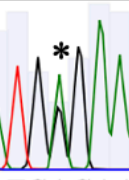
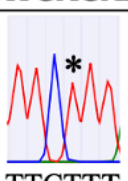
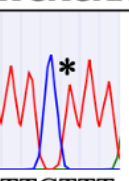
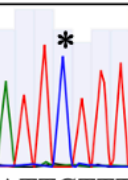
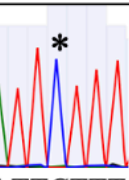
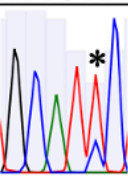
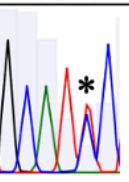
3.2.4 Validation of SNPs identified by BSA and NGS

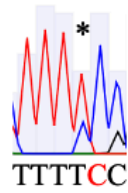
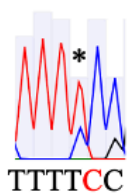
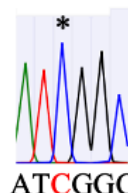
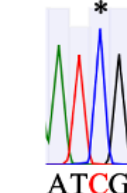
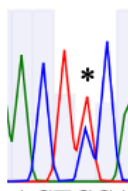
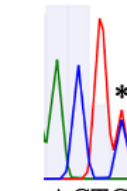
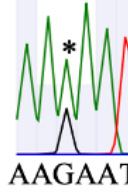
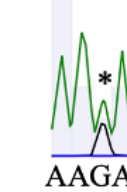
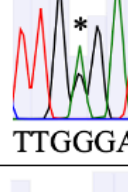
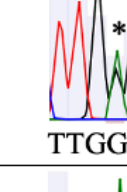
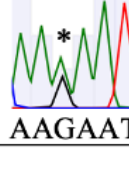
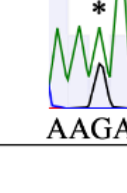
To refine the list of candidate mutations, sanger sequencing was conducted on DNA pools extracted from recovered and dwarf BCF₂ plants used in the initial BSA analysis. In the sanger sequencing analysis to determine the presence of SNP identified from NGS analysis, the genes AT3G15610, AT2G38940, AT5G20360, AT5G46190, AT2G39620, AT2G46250, AT3G48430, and AT5G53330 showed heterozygous SNPs in both recovered and dwarf pools (Figure 3-6). The presence of heterozygous SNPs in both pools means that none of these SNPs showed a clear difference in allelic composition that could be directly associated with the phenotypic difference (recovered vs. dwarf). As a result, the analysis could not definitively confirm any of these SNPs as the causal mutation. However, it also did not completely rule out the possibility that these SNPs might still be involved in the phenotype, possibly due to misinterpretation of phenotype during the selection of plants for DNA pooling. Hence a additional sequencing for the presence of SNPs in these genes on BCF₂ individual recovered and dwarf plants with clear phenotype is necessary to identify the true causal mutation. The candidate mutations in AT4G16144, AT4G04930, AT4G36860, AT2G25710, AT2G01008, AT2G07722, AT4G15150, AT4G16770, and AT4G36840 were eliminated as possible candidate genes since the identified SNP appeared as a polymorphism in the reference genome utilized for the analysis and was present in both recovered and dwarf pools (Figure 3-6). Similarly, the sanger sequencing results for AT4G05612 did not provide any conclusive evidence for the presence of SNP due to the multiple repetitive sequences within the gene causing unspecific amplification during PCR (refer appendix 9-2). Therefore, confirmation using a knock-out line of AT4G05612 line will be necessary to determine if the SNP in this gene is indeed responsible for suppression of *pAXY* phenotype in *saxy59*.

To further investigate the potential causal SNPs in genes that showed heterozygous SNPs in both pools, additional sequencing was performed on three individual BCF₂ recovered and dwarf plants with clear phenotypes during a second phase of the study. In this targeted Sanger sequencing, DNA was extracted from three distinct recovered and dwarf plants displaying clear phenotypes in the BCF₂ generation of the corresponding *saxy* mutants. This targeted approach led to the exclusion of AT2G38940 as a candidate because two plants in the recovered pool lacked the SNP (Figure 3-7 A) indicating that this SNP is segregating independently of the phenotype and is unlikely to be the causal mutation. In the case of AT3G15610, all recovered plants exhibited the homozygous SNP, while the dwarf plants displayed a heterozygous SNP

(Figure 3-7 A), consistent with a recessive segregation. This suggests that the mutation in AT3G15610 might be the causal SNP for the phenotype observed in *saxy59*. Similarly, for *saxy85* and *saxy171*, analysis of AT5G20360 and AT5G46190 showed that all three recovered plants exhibited a homozygous SNP, while the dwarf plants displayed a heterozygous or WT allele of the SNP (Figures 3-7 B and 3-7 C). This strengthens the evidence that the SNP in AT5G20360 might be the causal mutation for *saxy85* and the SNP in AT5G46190 might be the causal mutation responsible for suppressing the *pAXY* phenotype in *saxy171*. For *saxy42*, the causal mutation was expected to show a heterozygous or homozygous SNP in recovered plants and a WT allele in dwarf plants, given its dominant segregation (Table 10). However, since the candidates showed at least one homozygous SNP in the analyzed dwarf plants, AT2G39620, AT2G46250, AT3G48430, and AT5G53330 were eliminated as possible candidates (Figure 3-7 D).

Although the candidate mutations identified in *saxy161*, *saxy38*, and *saxy42* showed lower read counts for variants and predominantly altered variants in the dwarf pools, Sanger sequencing was performed to confirm these results. The identified SNPs turned out to be polymorphism in the reference genome used for the analysis, or they were segregating independently of the phenotype. Consequently, these mutants were excluded from further analysis. Several factors could explain the absence of definitive candidate mutations from the NGS analysis in these mutants, including inheritable epigenetic changes that modify gene expression without altering the DNA sequence (Law and Jacobsen, 2011), biased library preparation, or sample contamination, which could have affected the NGS results. To identify the causal suppressor gene in these mutants, further steps such as resequencing the DNA pools or performing a second backcross of these *saxy* mutants with *pAXY* are recommended. These additional analyses could help uncover the gene responsible for the observed phenotype. Whereas the SNPs identified to be segregating according to the phenotype in *saxy59*, *saxy85* and *saxy171* BCF₂ plants a second allele confirmation is necessary to validate that these SNPs are indeed causal mutation responsible for the suppression of *pAXY* phenotype.

Suppressor	Gene	WT/Mutant allele	Recovered pool sequence	Dwarf pool sequence
<i>saxy59</i>	AT4G16114	A/C	 CCATTG	 CCATTG
	AT3G15610	G/A	 AATGGC	 AATGGC
	AT2G38940	G/T	 CGTGCG	 CGTGCG
<i>saxy85</i>	AT4G04930	A/G	 GAAGAAA	 GAAGAAA
	AT5G20360	G/A	 ATGAGAA	 ATGAGAA
<i>saxy171</i>	AT4G36860	C/T	 TTCTTT	 TTCTTT
	AT2G25710	T/C	 ATTCTTT	 ATTCTTT
	AT5G46190	C/T	 GCATTC	 GCATTC

Suppressor	Gene	WT/Mutant allele	Recovered pool sequence	Dwarf pool sequence
<i>saxy42</i>	AT2G01008	T/C	 TTTTCC	 TTTTCC
	AT2G07722	T/C	 ATCGGC	 ATCGGC
	AT2G39620	C/T	 ACTCCA	 ACTCCA
	AT2G46250	G/A	 AAGAAT	 AAGAAT
	AT3G48430	G/A	 TTGGGA	 TTGGGA
	AT5G53330	G/A	 AAGAAT	 AAGAAT

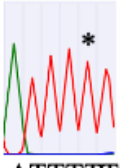
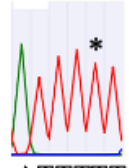
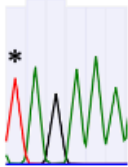
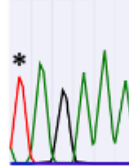
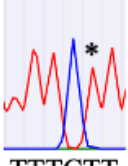
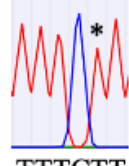
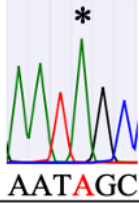
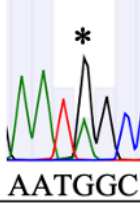
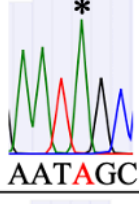
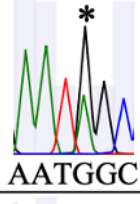
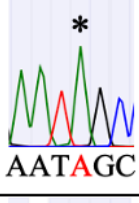
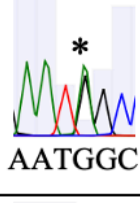
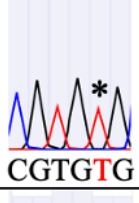
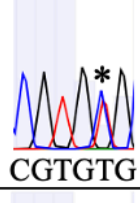
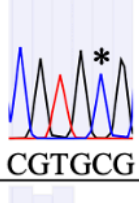
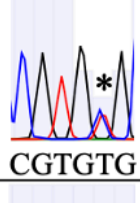
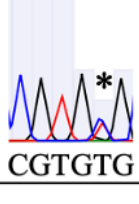
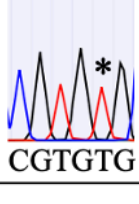
<i>saxy161</i>	AT4G15150	C/T		
	AT4G16770	T/C		
<i>saxy38</i>	AT4G36840	C/T		

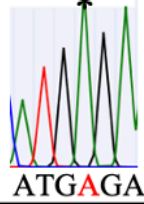
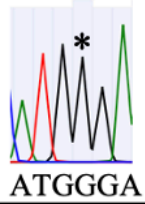
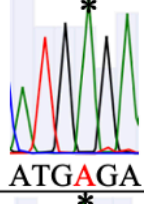
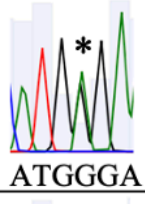
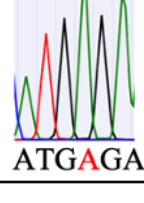
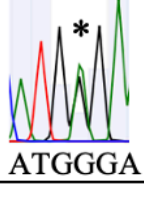
Figure 3-6. Targeted sequencing of candidate mutations in BCF₂ DNA pools of *saxy* mutants.

Figure shows list of *saxy59*, *saxy85*, *saxy171*, *saxy42*, *saxy161*, and *saxy38* candidate mutations identified from BSA which underwent targeted sanger sequencing on the amplicons from BCF₂ DNA pools. The table contains columns for the suppressors, gene name, WT and mutant allele variant, screenshot of sanger sequencing chromatograms. The SNPs are highlighted in red color and the position of SNP is indicated with the symbol *.

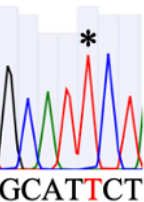
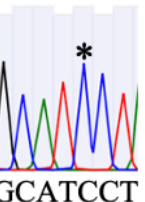
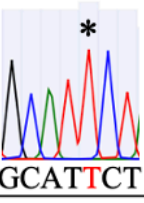
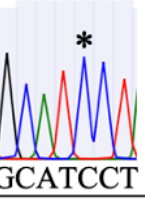
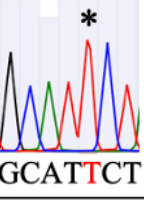
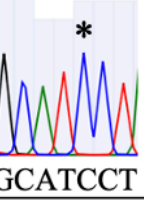
(A)

Suppressor	Gene	WT/Mutant allele	Recovered BCF ₂ individuals	Dwarf BCF ₂ individuals
<i>saxy59</i>	AT3G15610	G/A		
				
				
	AT2G38940	C/T		
				
				

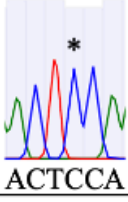
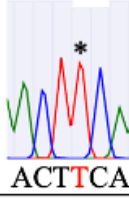
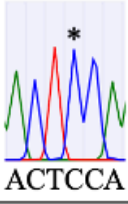
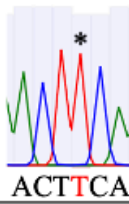
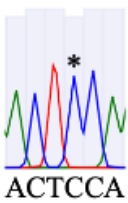
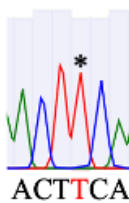
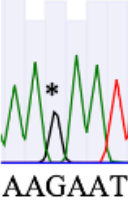

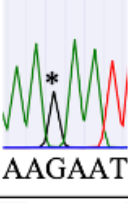
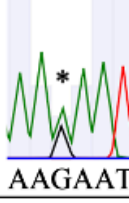
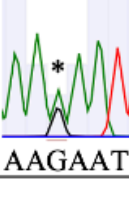
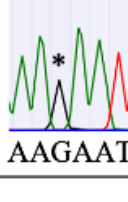
(B)

Suppressor	Gene	WT/Mutant allele	Recovered BCF ₂ individuals	Dwarf BCF ₂ individuals
<i>saxy85</i>	AT5G20360	G/A	 ATGAGA	 ATGGGA
			 ATGAGA	 ATGGGA
			 ATGAGA	 ATGGGA

(C)

Suppressor	Gene	WT/Mutant allele	Recovered BCF ₂ individuals	Dwarf BCF ₂ individuals
<i>saxy171</i>	AT5G46190	C/T	 GCATTCT	 GCATCCT
			 GCATTCT	 GCATCCT
			 GCATTCT	 GCATCCT

(D)

Suppressor	Gene	WT/Mutant allele	Recovered BCF ₂ individuals	Dwarf BCF ₂ individuals
<i>saxy42</i>	AT2G39620	C/T	 ACTCCA	 ACTTCA
			 ACTCCA	 ACTTCA
			 ACTCCA	 ACTTCA
	AT2G46250	G/A	 AAGAAT	 AAGAAT
			 AAGAAT	 AAGAAT
			 AAGAAT	 AAGAAT

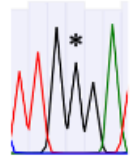
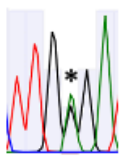
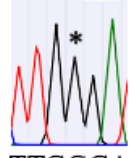
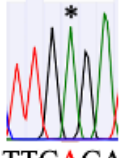
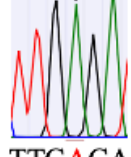
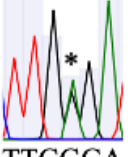
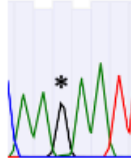
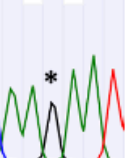

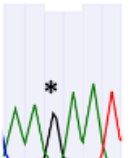

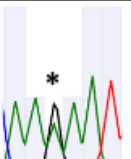
<i>saxy42</i>	AT3G48430	G/A		
				
				
	AT5G53330	G/A		
				
				

Figure 3-7. Targeted sequencing on *saxy* BCF₂ individuals for the candidate mutations.

The figures illustrate the results of targeted sequencing conducted on (A) AT3G15610 and AT2G38940 in *saxy59* BCF₂ individuals (n=3). (B) AT5G20360 in *saxy85* BCF₂ individuals (n=3). (C) AT5G46190 in *saxy171* BCF₂ individuals (n=3). (D) AT2G39620, AT2G46250, AT3G48430 and AT5G53330 in *saxy42* BCF₂ individuals (n=3). This sequencing was carried out using Sanger sequencing methodology. The table contains columns for the suppressors, gene name, WT, and mutant allele variant, as well as screenshots of the Sanger sequencing chromatograms. Notably, the identified SNPs are highlighted in red within the chromatograph images and the position of SNP is indicated with the symbol *.

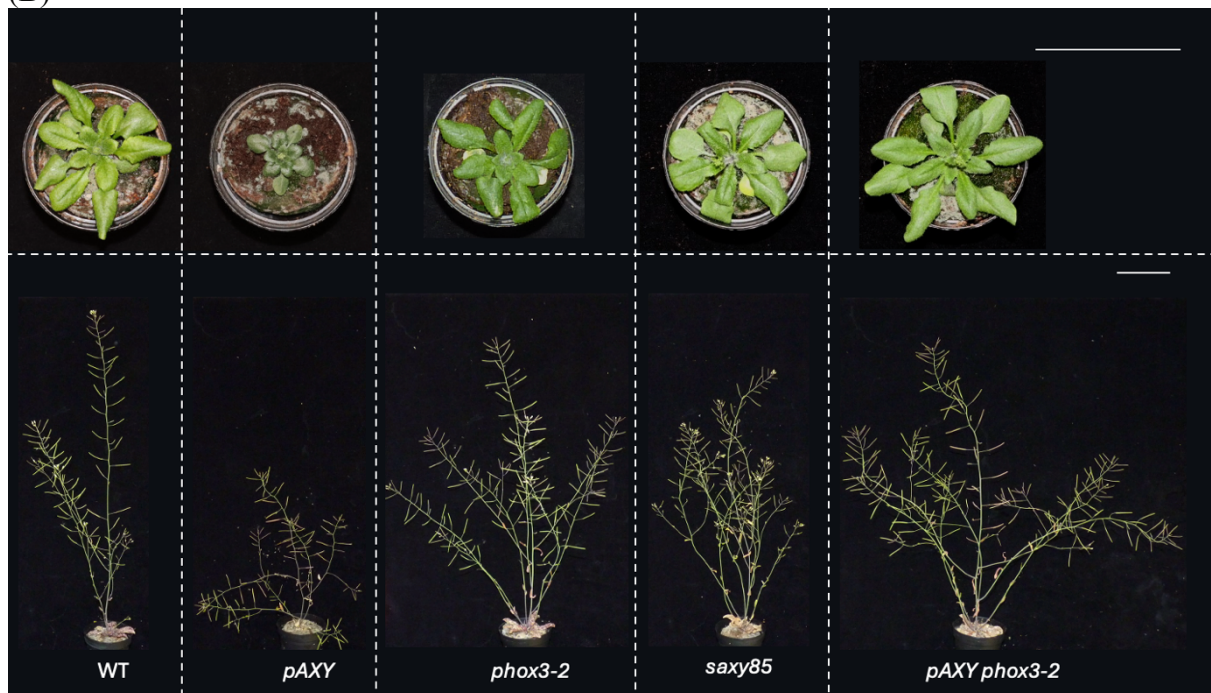
3.2.5 Validation of suppressor mutations by second allele approach

To confirm whether SNPs in AT3G15610 (WD40^{H15Y}), AT5G46190 (AtKH26^{G411E}), and the SNP in the 2 kb promoter region of AT5G20360 (*PHOX3*) are indeed responsible for suppressing the *pAXY* phenotype in *saxy59*, *saxy171*, and *saxy85*, a second allele approach was utilized. The T-DNA insertion lines corresponding to the candidate genes were identified and ordered from the NASC database (<https://arabidopsis.info/>). The lines *Salk_071771* (referred to as *wd40-2*), *SAIL_1247_D08* (referred to as *phox3-2*), and *Salk_051182* (referred to as *atkh26-2*) were used as second alleles to evaluate the suppression of the *pAXY* phenotype, thereby providing conclusive evidence of their role in the suppression mechanism. Subsequently, these T-DNA lines were individually crossed with the *pAXY* line to obtain second alleles of the *saxy* mutants. Mutants containing homozygous *axy9*, *pAXY*, and T-DNA insertions in the respective candidate genes were identified in the F₂ and F₃ segregating populations by genotyping for all T-DNA insertions (*axy9*, *pAXY*, and *wd40-2/phox3-2/atkh26-2*), following the methodology described in section 3.1.3 and refer figure 3-9 for the location of T-DNA insertions. When comparing the stem height of six-week-old T-DNA insertion suppressor mutants to *pAXY*, there was a notable increase of approximately 40% in stem height, bringing it closer to the WT (Figure 3-8). Additionally, when comparing the rosette size of four-week-old suppressor mutants, an increase in rosette size nearly equal to that of WT was observed (Figure 3-8 A, B, and C). These results clearly indicate that the second allele of the suppressor mutations identified through BSA significantly suppressed the *pAXY* phenotype by increasing both stem height and rosette size.

(A)



(B)



(C)



(D)

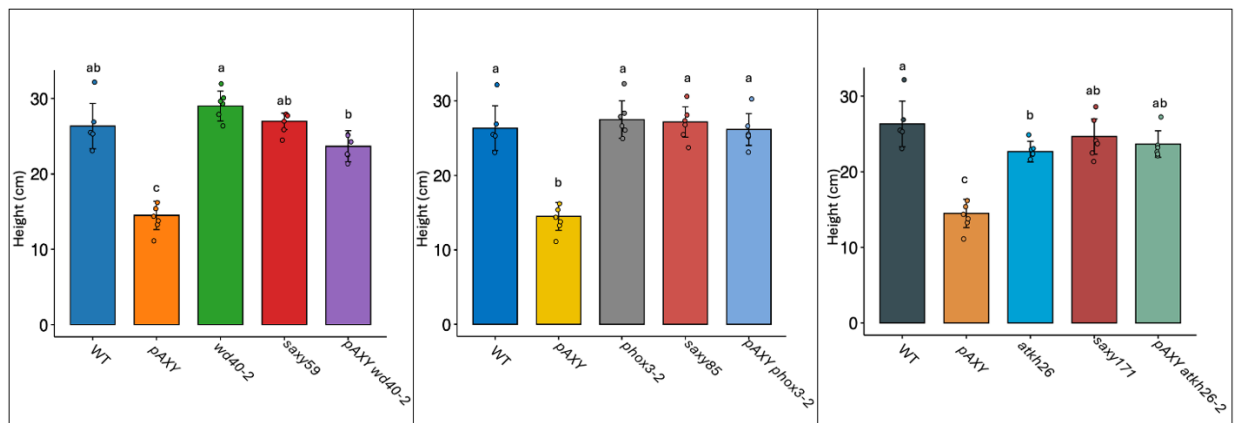


Figure 3-8. Growth phenotype of suppressor mutants.

(A) Growth phenotype showing the rosette size of four-week-old and stem height of six-week-old WT, *pAXY*, *wd40-2*, *saxy59* and *pAXY wd40-2*. (B) Growth phenotype showing the rosette size of four-week-old and stem height of six-week-old WT, *pAXY*, *phox3-2*, *saxy85* and *pAXY phox3-2*. (C) Growth phenotype showing the rosette size of four-week-old and stem height of six-week-old WT, *pAXY*, *atkh26-2*, *saxy171* and *pAXY atkh26-2*. The white bar represents a scale of 5 cm. (D) Height measurements of six-week-old suppressor mutants, *pAXY* and WT. Error bars indicate standard deviation ($n = 6$), and the alphabets indicates the significant differences between the mean of genotypes (Tukey HSD, $p < 0.05$).

The missense mutation in the *WD40* gene (AT3G15610), resulting in $WD40^{H15Y}$ in the *saxy59* suppressor mutant, impacts a critical structural tetrad in the first exon. In contrast, the second allele, the *pAXY wd40-2* mutant, has a T-DNA insertion in the 5' UTR just before the first exon of *WD40* (Figure 3-9 A), potentially affecting transcription. Consequently, the *saxy59* mutant

was renamed *pAXY wd40-1*. Similarly, the causal SNP identified in *saxy85* is located in the 2 kb promoter region of the *PHOX3* gene (AT5G20360) and is expected to mis-regulate *PHOX3* expression (Figure 3-9 B). The second allele, *pAXY phox3-2* carries a T-DNA insertion in the first exon of the *PHOX3* gene, possibly affecting transcription from the start. As a result, the *saxy85* mutant was renamed *pAXY phox3-1*. The missense mutation leading to AtKH26^{G411E}, discovered in the *AtKH26* gene (AT5G46190) of the *saxy171* suppressor mutant, affects a putative nucleic acid binding site within the fourth KH domain. The second allele, the T-DNA insertion suppressor mutant *pAXY atkh26-2*, has a T-DNA insertion at the end of the third exon, disrupting the protein from the third KH domain onward (Figure 3-9 C). Therefore, the *saxy171* mutant was renamed *pAXY atkh26-1*.

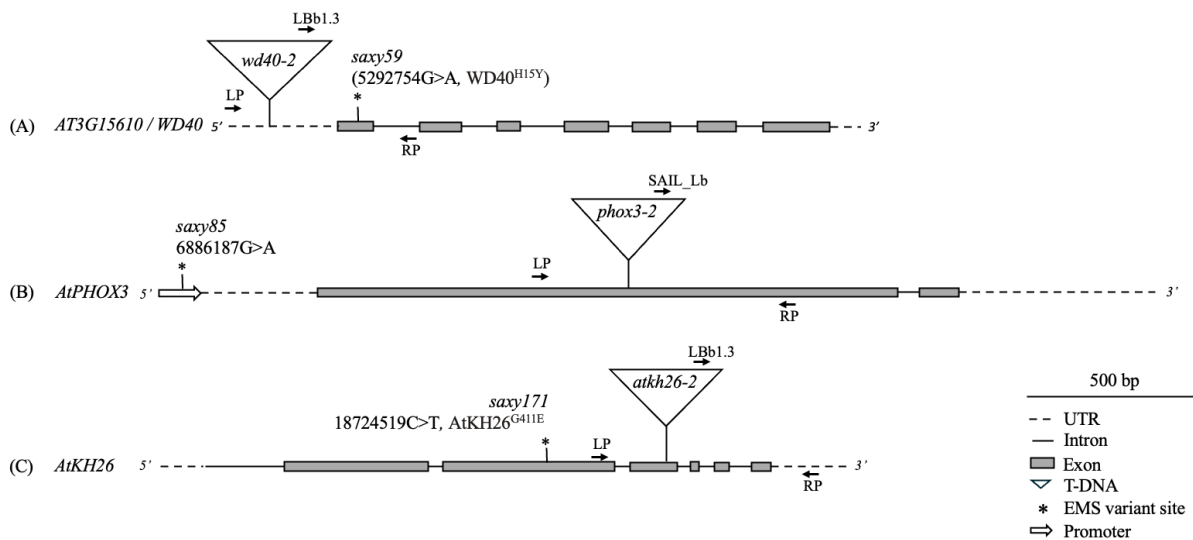


Figure 3-9. Gene structures indicating T-DNA insertion site and the SNP position induced by EMS.

(A) Gene structure of *AT3G15610 / WD40* (B) Gene structure of *AtPHOX3* (C) Gene structure of *AtKH26*. In each structure, the black triangle denotes the T-DNA insertion site, while * marks the position of the SNP in the respective *saxy* mutants as indicated above the symbol. The LP, RP, LBb1.3 and SAIL_Lb indicated by arrows are the primers used for genotyping the presence or absence of T-DNA. Abbreviations used: UTR- Untranslated region, T-DNA- Transfer DNA, EMS- Ethyl methane sulfonate, bp- base pairs.

3.2.5.1 Gene expression analysis of suppressor genes

To determine whether the T-DNA insertion disrupts the expression of target genes in the suppressor mutants, qRT-PCR analysis was performed. This analysis used stem material from 5-week-old plants and revealed a significant reduction in *AXY9* transcript levels in *pAXY* and the suppressor mutants (Figure 3-10 A). The reduction was approximately 5-fold compared to the WT and single mutants (*wd40-2*, *phox3-2*, and *atkh26-2*), confirming that reduced *AXY9* gene expression correlates with observed lower wall acetylation levels (Figure 3-11). The *WD40* gene, expression was not completely abolished in the *wd40-2* mutant; transcripts were still detectable but reduced by 2-fold compared to WT and *pAXY*. This reduced expression was also seen in the *pAXY wd40-2* mutant (Figure 3-10 B), characterizing *wd40-2* mutants as knock-down mutants. However, the *pAXY wd40-1* mutant showed transcript levels similar to WT and *pAXY* (Figure 3-10 B), suggesting that the EMS-induced change in *pAXY wd40-1* does not affect transcript levels but likely results in a defective protein due to an amino acid change. Similarly, the *phox3-2* mutant displayed a 2-fold reduction in *PHOX3* gene expression compared to WT and *pAXY*, with the *pAXY phox3-2* mutant showing a similar decrease (Figure 3-10 C). Additionally, the SNP in the 2kb promoter region of the *PHOX3* gene reduces its expression by approximately 2-fold in the *pAXY phox3-1* mutant (Figure 3-10 C). In contrast to the other suppressor mutants, the *atkh26-2* mutant showed abolished *AtKH26* gene expression compared to WT and *pAXY* (Figure 3-10 D), classifying it as a knock-out mutant. However, the *pAXY atkh26-1* mutant, which has a missense mutation in the *AtKH26* gene, displayed gene expression levels comparable to WT and *pAXY* (Figure 3-10 D). This suggests that the *AtKH26*^{G41E} mutation does not affect gene expression but likely impacts the protein's fourth KH domain, potentially resulting in a defective protein.

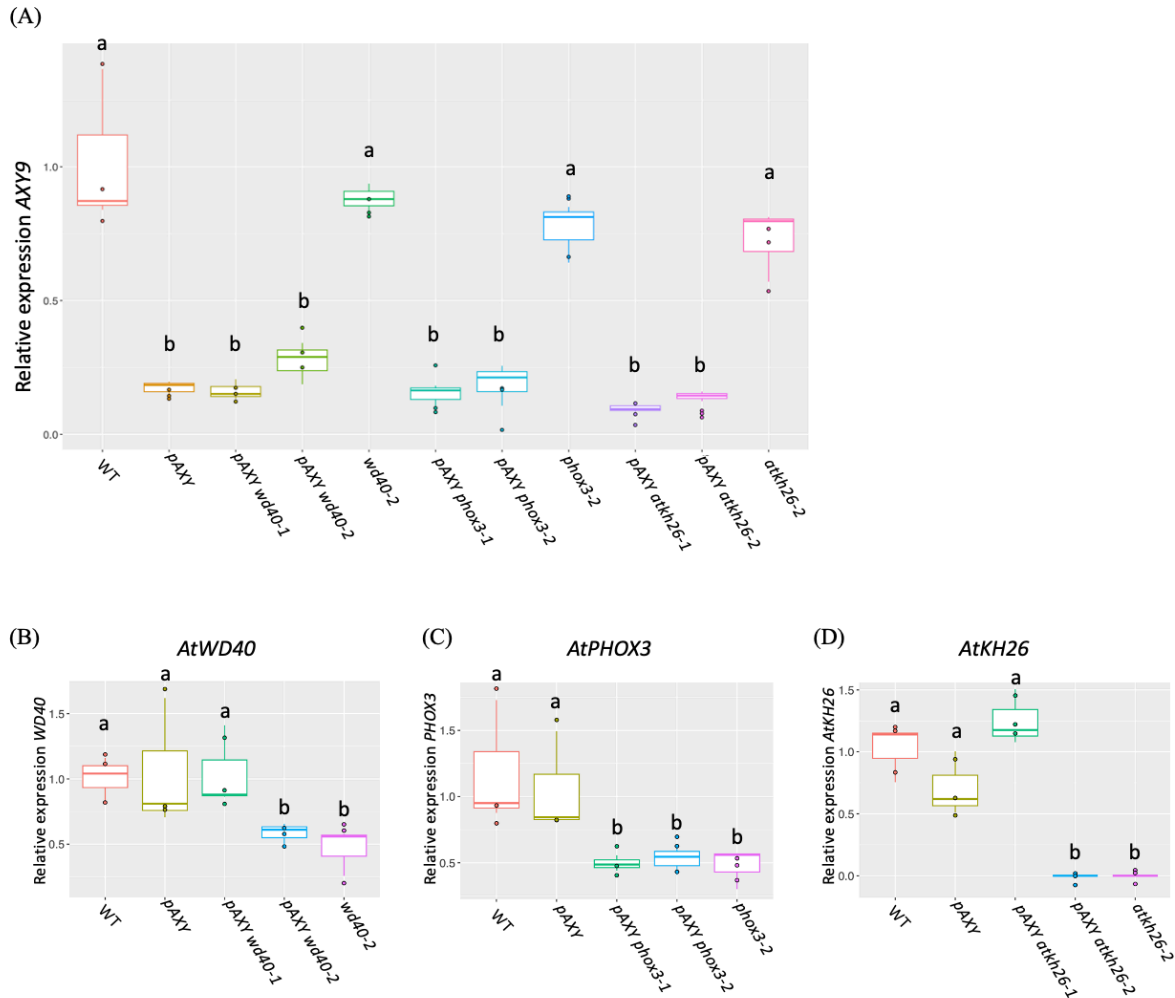


Figure 3-10. Gene expression analysis of *AXY9* and suppressor genes.

Transcript levels of *AXY9* in 4-week-old stem material of (A) WT, *pAXY*, *wd40*, *wd40-1* and *wd40-2*, *phox3-2*, *pAXY phox3-1* and *pAXY phox3-2*, *atk26-2*, *pAXY atkh26-1* and *pAXY atkh26-2*. (B) Transcript levels of *WD40* in 4-week-old stem material of WT, *pAXY*, *wd40-2*, *pAXY wd40-1*, and *pAXY wd40-2*. (C) Transcript levels of *PHOX3* in 4-week-old stem material of WT, *pAXY*, *phox3-2*, *pAXY phox3-1* and *pAXY phox3-2*. (D) Transcript levels of *AtKH26* in 4-week-old stem material of WT, *pAXY*, *atk26-2*, *pAXY atkh26-1* and *pAXY atkh26-2*. *ACT* gene expression was used as an internal normalization control (n=6). The alphabets indicate the significant differences between the mean of genotypes (Tukey HSD, $p < 0.05$).

3.2.5.2 Cell wall characterization of *pAXY* suppressor mutants

To determine whether suppression of the *pAXY* phenotype involved alterations in cell wall components, the levels of hemicellulosic monosaccharides, crystalline cellulose, and wall *O*-acetate levels were quantified. Wall acetate content was measured using an acetic acid assay (see Section 2.2.5.3), and the monosaccharide content of hemicellulose was analyzed through TFA (trifluoroacetic acid) hydrolysis, followed by high-performance anion exchange

chromatography (see Section 2.2.5.6). Crystalline cellulose content was estimated from the residual pellet of TFA hydrolysis using Saeman hydrolysis and anthrone assay (see Section 2.2.5.8). These analyses were performed on 6-week-old stem material. The quantitative analysis revealed that wall *O*-acetate levels in all suppressor mutants, including both EMS and T-DNA alleles, were similar to those observed in *pAXY*, with approximately 50% lower acetylation compared to WT (Figure 3-11). This highlights that the increase in plant height observed in the suppressor mutants (Figure 3-8) is not necessarily associated with changes in *O*-acetate levels.

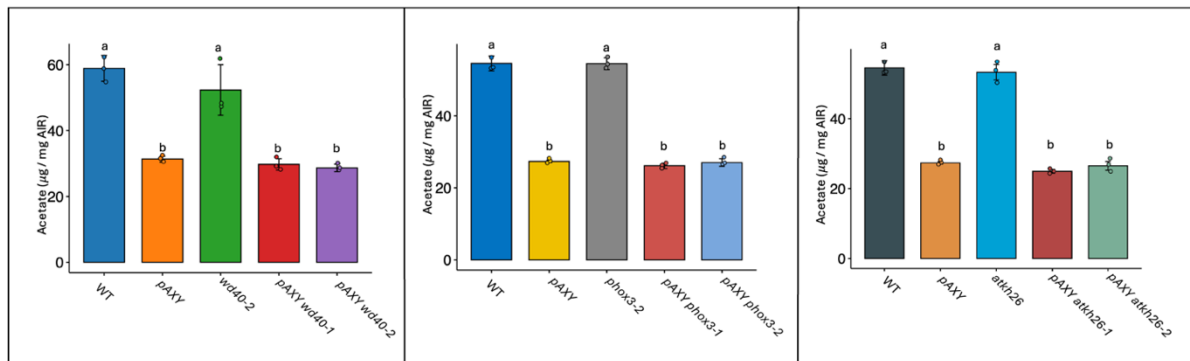


Figure 3-11. Total wall-bound acetyl ester content from 6-week-old stem of suppressor mutants, WT and *pAXY*.

Total wall-bound acetyl ester content for stem of WT, *pAXY* and suppressor mutants per mg AIR. Bars represent the average mean \pm the standard deviation (n=3). Error bars indicates SD, and the alphabets indicates the significant differences between the mean of genotypes (Tukey HSD, $p < 0.05$).

When comparing the absolute monosaccharide levels in the cell wall of stem tissues between WT and *pAXY* lines, a significant increase was observed in all sugars except glucose in the *pAXY* line (Figures 3-12B, 3-13B, 3-14B). Additionally, the overall crystalline cellulose content in *pAXY* was reduced compared to WT (Figure 3-15). This reduction in crystalline cellulose and glucose levels within the hemicellulose content appears to be offset by a relative increase in other cell wall components as reflected in the significant rise of all other monosaccharides in *pAXY*. In certain suppressor mutants, a relative decrease in glucose levels compared to WT was observed, bringing them closer to the levels found in *pAXY*. This reduction was notably significant in the *pAXY atkh26-2* mutant (Figure 3-14), which also exhibited decreased crystalline cellulose content (Figure 3-15 C). This reduction was compensated by a relative increase in other monosaccharides, such as xylose, and suggests a compensatory mechanism possibly involving modification of xylan levels (Figure 3-14). Although the *pAXY phox3-2* and *pAXY phox3-1* lines also showed a relative decrease in glucose

levels (Figures 3-13 A), the crystalline cellulose levels were partially restored but did not reach WT levels (Figure 3-15 B). Consequently, a relative increase in other non-cellulosic monosaccharides such as galactose, rhamnose, and galacturonic acid was observed, indicating a compensatory mechanism likely through pectic polysaccharides (3-13 A). A consistent trend across *pAXY* and all suppressor lines was the elevated levels of glucuronic acid compared to WT or single mutants, with this increase being significant in *pAXY*, *pAXY phox3-2*, *pAXY atkh26-1*, and *pAXY atkh26-2* (Figures 3-13, 3-14, and 3-15). This increase may be attributed to the substitution of missing acetyl groups with glucuronic acid, similar to what observed in the *tbl29* mutant, where acetyl groups were replaced by glucuronic acid moieties upon the expression of the *AtGUX1* glycosyl transferase (Xiong et al., 2015). In contrast, the *pAXY wd40-1* and *pAXY wd40-2* suppressor mutants did not show any significant differences in hemicellulose monosaccharide levels, suggesting that the recovery mechanism in these mutants might rely solely on the increased crystalline cellulose content (Figures 3-12 and 3-15 A). Overall, these results suggest that the recovery mechanism of the *pAXY* phenotype in the *pAXY atkh26-2* mutant altered the xylan content without affecting the crystalline cellulose levels, while the *pAXY phox3-1* and *pAXY phox3-2* mutants had altered pectic monosaccharide levels and partial restoration of crystalline cellulose levels, all while maintaining low wall *O*-acetylation. The recovery in *pAXY wd40-1* and *pAXY wd40-2* appears to involve only partial restoration of crystalline cellulose content, with no significant changes in hemicellulose or pectic monosaccharide levels and consistently low wall *O*-acetylation levels.

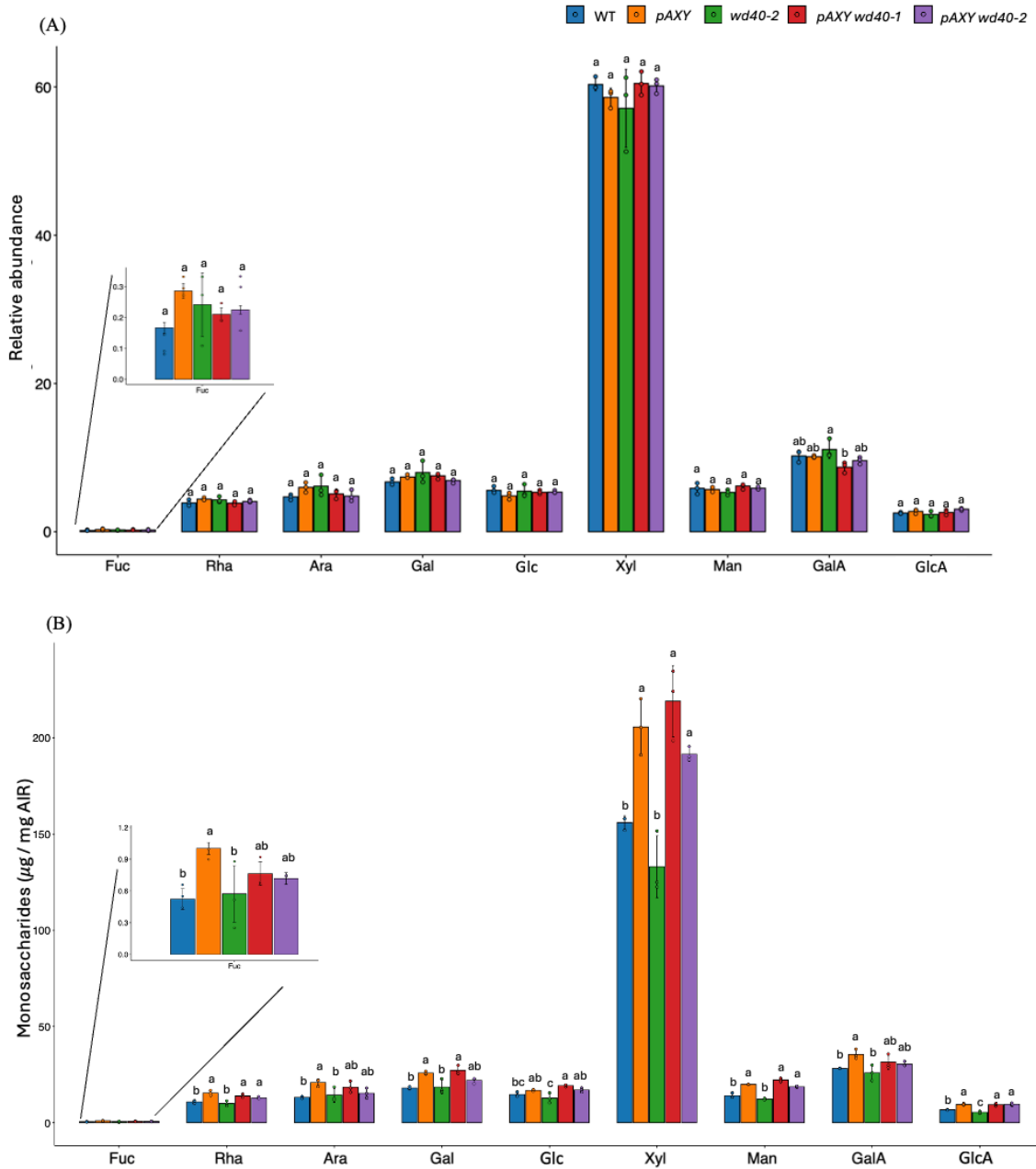


Figure 3-12. Effect of *wd40* suppressor mutation in the cell wall monosaccharide composition.

(A) Relative abundance of cell wall monosaccharides in WT, *pAXY*, *wd40-2*, *pAXY wd40-1* and *pAXY wd40-2*. (B) Absolute levels of cell wall monosaccharides in µg per mg AIR of WT, *pAXY*, *wd40-2*, *pAXY wd40-1* and *pAXY wd40-2*. Bars represent the average mean ± the standard deviation (n=6). Alphabets indicates the significant differences between the means of different genotypes (Tukey HSD, p<0.05).

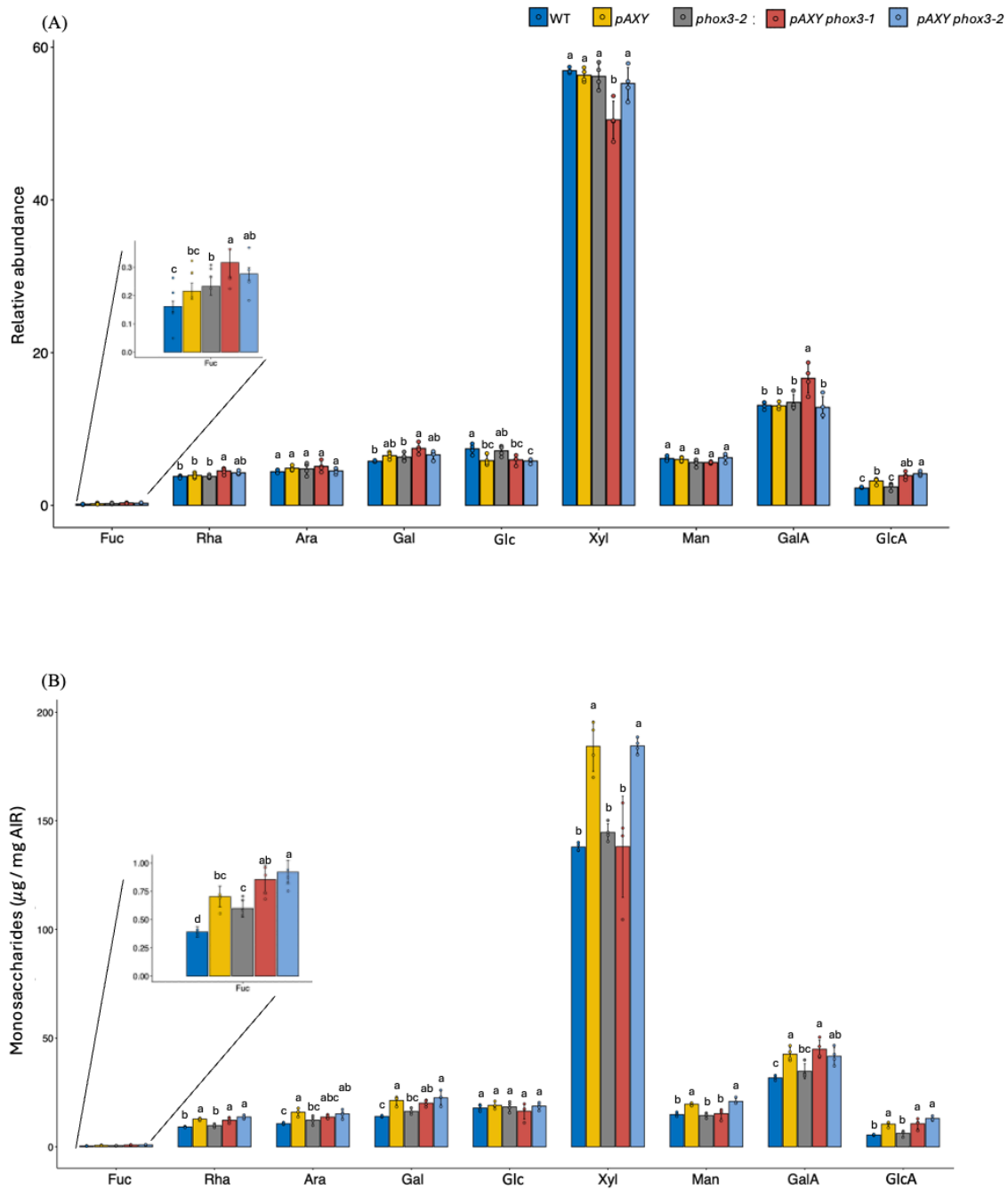


Figure 3-13. Effect of *phox3* suppressor mutation in the cell wall monosaccharide composition.

(A) Relative abundance of cell wall monosaccharides in WT, *pAXY*, *phox3-2*, *pAXY phox3-1* and *pAXY phox3-2*. (B) Absolute levels of cell wall monosaccharides in µg per mg AIR of WT, *pAXY*, *phox3-2*, *pAXY phox3-1* and *pAXY phox3-2*. Bars represent the average mean ± the standard deviation (n=8). Alphabets indicates the significant differences between the means of different genotypes (Tukey HSD, p<0.05).

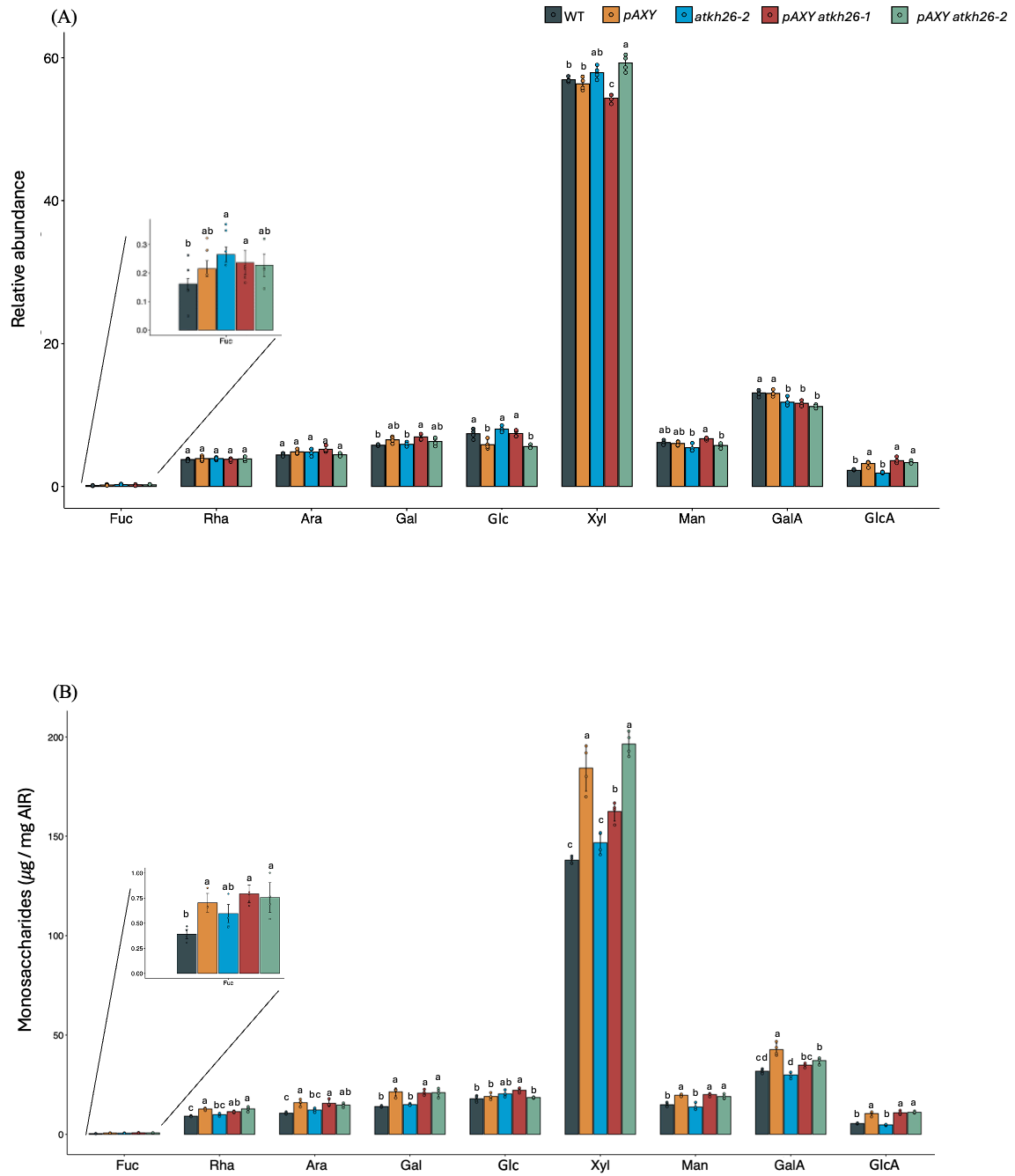


Figure 3-14. Effect of *atkh26* suppressor mutation in the cell wall monosaccharide composition.

(A) Relative abundance of cell wall monosaccharides in WT, *pAXY*, *atkh26-2*, *pAXY atkh26-1* and *pAXY atkh26-2*. (B) Absolute levels of cell wall monosaccharides in µg per mg AIR of WT, *pAXY*, *atkh26-2*, *pAXY atkh26-1* and *pAXY atkh26-2*. Bars represent the average mean ± the standard deviation (n=8). Alphabets indicates the significant differences between the means of different genotypes (Tukey HSD, p<0.05).

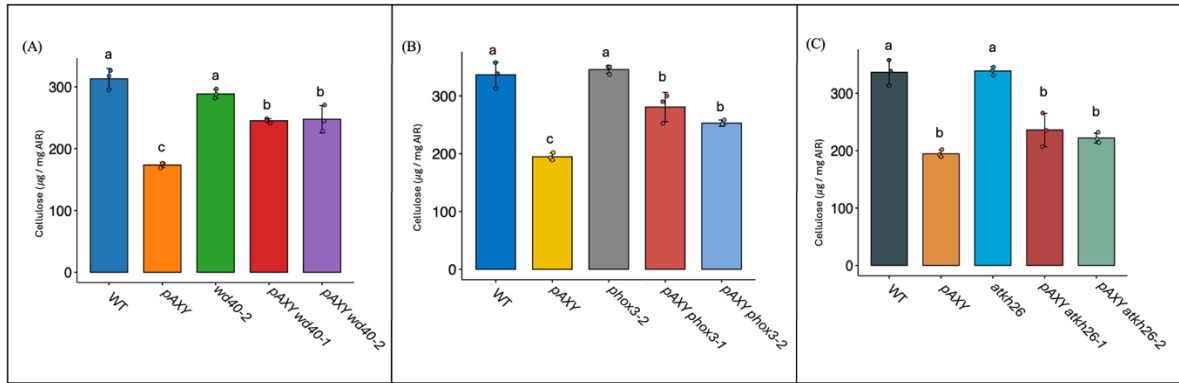


Figure 3-15. Crystalline cellulose content in the cell wall of suppressor mutants.

(A) Crystalline cellulose per mg AIR of WT, *pAXY*, *wd40-2*, *pAXY wd40-1* and *pAXY wd40-2*. (B) Crystalline cellulose per mg AIR of WT, *pAXY*, *phox3-2*, *pAXY phox3-1* and *pAXY phox3-2*. (C) Crystalline cellulose per mg AIR of WT, *pAXY*, *atkh26-2*, *pAXY atkh26-1* and *pAXY atkh26-2*. Bars represent the average mean \pm the standard deviation (n=6). Alphabets indicates the significant differences between the means of different genotypes (Tukey HSD, $p < 0.05$).

3.2.5.3 Freezing tolerance of suppressor mutants

Several secondary wall-deficient mutants have been shown to exhibit increased freezing tolerance, a phenotype commonly observed in plants with modified xylan composition and altered cellulose content (Ramírez & Pauly, 2019). To determine whether the *pAXY* mutant, which exhibits altered cellulose content (see section 3.2.5.2 and Figure 3-15), also shows enhanced freezing tolerance, and whether the suppressor mutants could mitigate this tolerance, a freezing tolerance experiments was conducted on *pAXY* and its suppressor mutants. The *tbl29* mutant, known for its high freezing tolerance among cell wall-deficient mutants as reported by Ramírez & Pauly (2019), was included as a control. Four-week-old plants were exposed to -5°C for 18 hours, then returned to growth chambers at 22°C, with survival data collected after three days. The results revealed that *tbl29* had a freezing survival rate of 80-90%, whereas no WT plants survived. The *pAXY* mutant showed a survival rate of approximately 50-60%, indicating higher freezing tolerance than WT but lower than *tbl29* (Figure 3-16). In contrast, all suppressor mutants exhibited a survival rate of less than 25%, with no WT plants surviving (Figure 3-16). This reduction in survival rates among the suppressor mutants correlates with the partial restoration of monosaccharides in the hemicellulose and crystalline cellulose (Section 3.2.5.3). These findings suggest that the *pAXY* suppressor mutants were able to reduce the freezing tolerance associated with the altered cellulose content of the *pAXY* mutant.

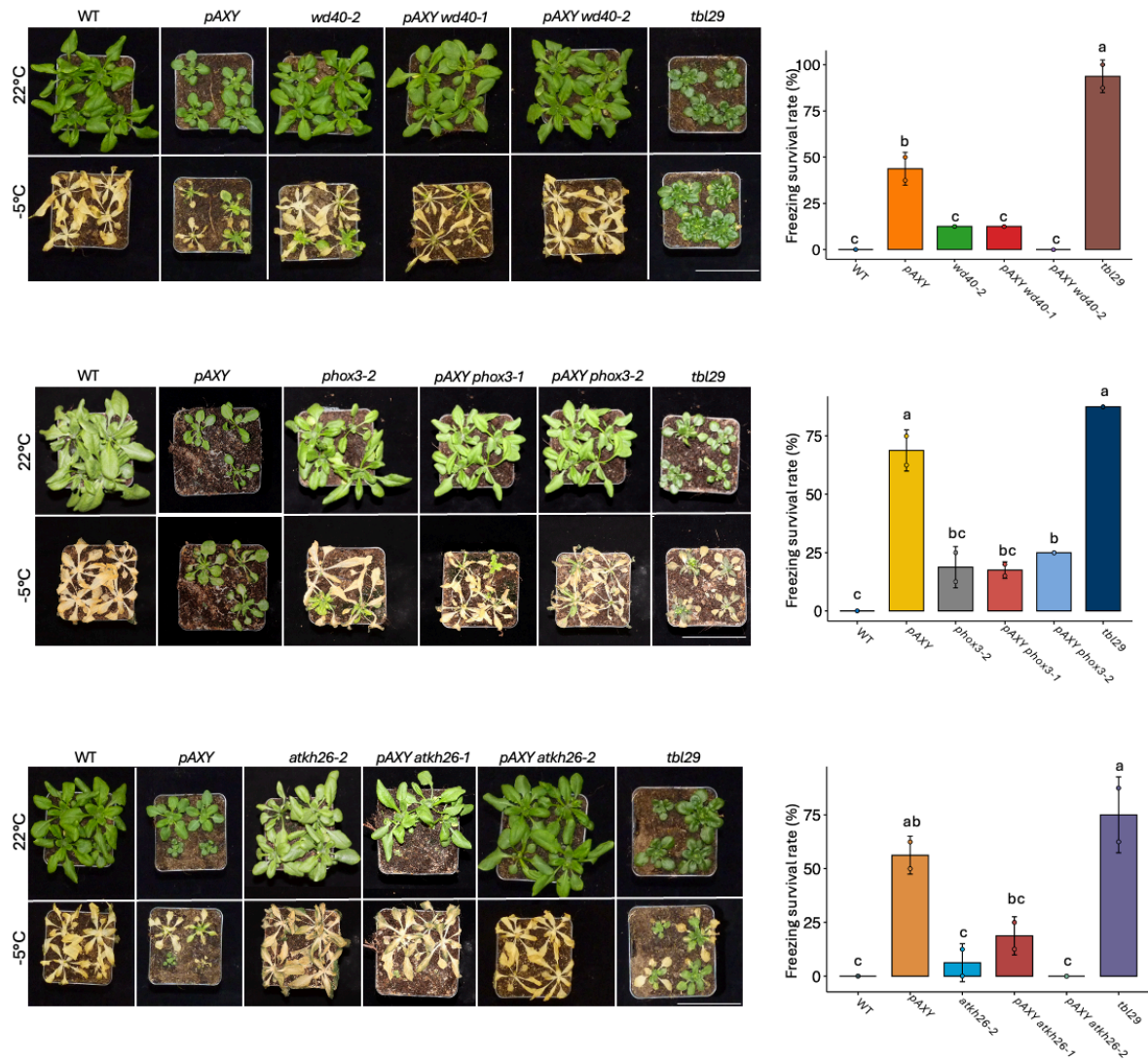


Figure 3-16. Freezing tolerance assay for *pAXY* suppressor mutants.

Representative pictures of 4-week-old plants of indicated genotypes before (upper panel) and after freezing experiment (lower panel). White bars indicate the scale 5 cm. The bar plots indicate survival rate after freezing assay. Data represented as mean (AVG) \pm the standard deviation (SD) of two independent experiments (≥ 10 plants/experiment). Means with different alphabets are statistically significant (Tukey's HSD, $p < 0.05$).

3.2.6 Functional implications of *pAXY* suppressor mutations

3.2.6.1 Localization and interaction profiling of *AtWD40*

The WD40 repeat-like superfamily proteins, known for their sequences rich in tryptophan and aspartic acid, form seven β -propeller structures crucial for assembling large multiprotein complexes (Smith et al., 1999). These proteins play a crucial role in mediating the assembly of

nucleopore complex scaffold subdomains, thereby facilitating interactions between transport complexes and the nucleopore complex (Cronshaw et al., 2002). The nucleopore complex serves as the gateway between the nucleus and cytoplasm, regulating the trafficking of proteins and RNA (Xu and Meier, 2008; Meier and Brkljacic, 2009a). Determining the localization of a protein can provide significant insights into its function. The cell eFP viewer tool from the eFP browser (<https://bar.utoronto.ca/eplant/>) was utilized to predict the subcellular localization of the suppressor genes. According to predictions from the cell eFP viewer, AT3G15610 (*AtWD40*), a transducin/WD40 repeat-like superfamily protein localizes to both the nucleus and cytoplasm (Figure 3-17), implying a role in the trafficking of proteins and RNA between these two cellular compartments. The subcellular localization prediction of WD40 was validated by transient expression with GFP fusion in *Nicotiana benthamiana* using *Agrobacterium tumefaciens* and visualized through confocal microscopy. The coding sequence of the *AtWD40* gene was cloned into the pB7FW2G vector to create a GFP fusion at the C-terminus of *AtWD40*. The resulting constructs were transformed into *A. tumefaciens*, and the transformed bacteria were subsequently infiltrated into 4-week-old *N. benthamiana* leaves. Confocal microscopy was performed four days after infiltration, revealing fluorescence signal for GFP fused *AtWD40* distributed around the periphery of the cells and concentrated in discrete spots (indicated by red arrows) (Figure 3-18 A-C). This localization pattern mirrors that observed with the free GFP control (Figure 3-18 D-F), which is known to reside in both the cytosol and nucleus (Chiu et al., 1996), suggesting that *AtWD40* may also localize to these compartments. The autofluorescence of chloroplasts was visible in all images, including the negative control, which consisted of *N. benthamiana* plants infiltrated with non-transformed *A. tumefaciens*. No fluorescence was observed in the negative control (Figure 3-18 G-I). These results support the hypothesis that *AtWD40* may localizes to both the nucleus and cytoplasm, aligning with predictions from the cell eFP viewer (Figure 3-17).



Figure 3-17. Predicted subcellular localization of *AtWD40*.

Predicted subcellular localization of *AtWD40* according to cell eFP viewer (<https://bar.utoronto.ca/eplant/>). The local max linear indicates the confidence score calculated from the computational experiments and molecular experiments (Winter et al., 2007). The higher confidence score for a given subcellular compartment, the more intense the red color in the output.

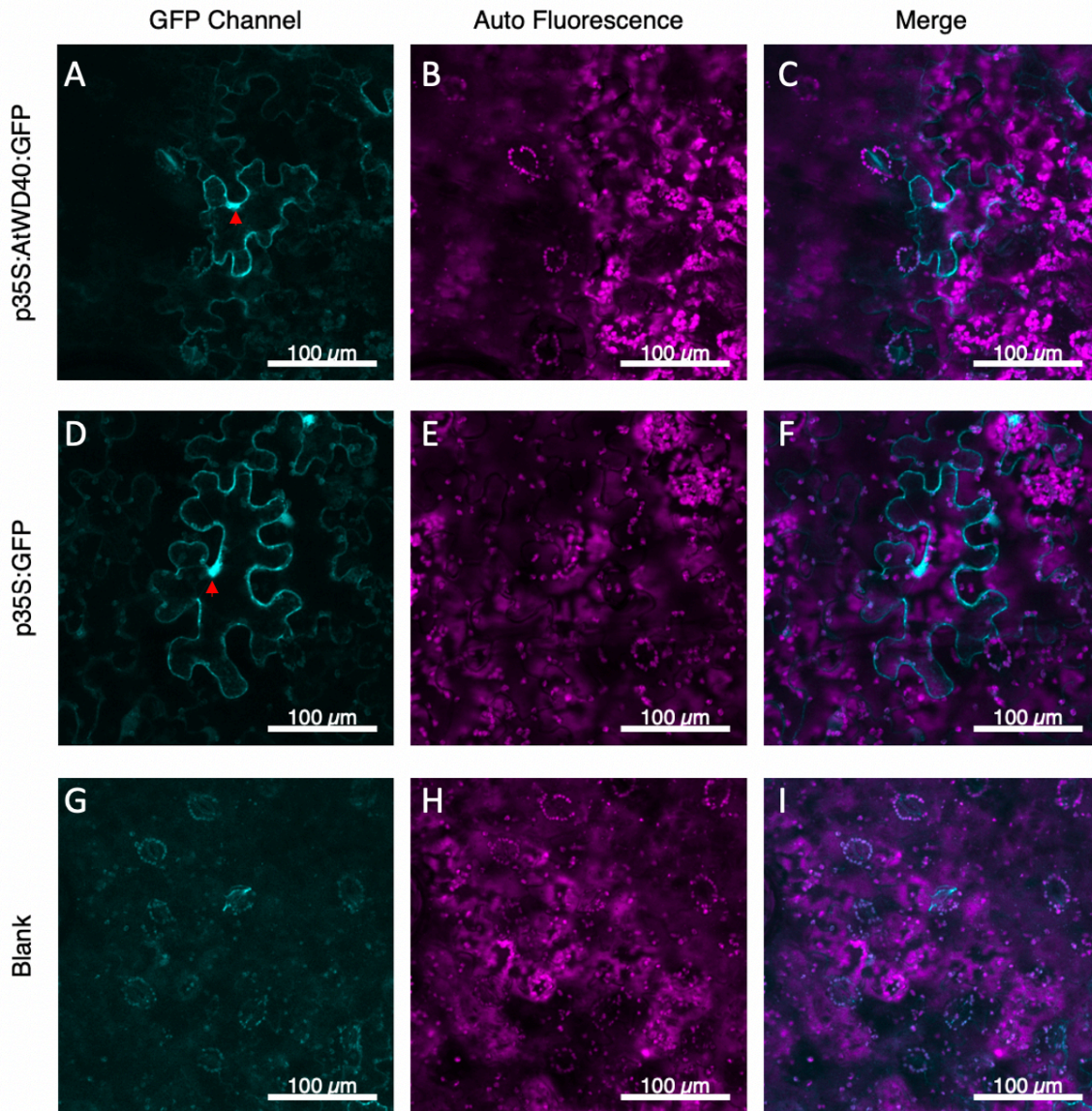


Figure 3-18. Subcellular localization of GFP tagged *AtWD40*.

Subcellular localization of GFP tagged WD40 in *N. benthamiana*. Columns indicate channels used for visualization: GFP channel (A, D, and G); Auto fluorescence (B, E, and H); Merge of GFP and autofluorescence (C, F, and I). Rows exhibit microscopy images of GFP fused *AtWD40*, free GFP and negative control. Red arrow indicates the areas of interest possibly showing nuclear localization.

The *AtWD40*^{H15Y} missense mutation identified in the *pAXY wd40-1* suppressor mutant alters the histidine residue of glycine-histidine peptide to glycine-tyrosine peptide, immediately

following the first β -sheet of the protein's initial propeller structure which is one of the three distinct surfaces involved in protein-protein interactions (Stirnemann et al., 2010). Histidine and tyrosine have different side chains, with tyrosine being bulkier due to its aromatic ring and hydroxyl group (Figure 3-19 B). This difference in size can affect the local structure of the protein, potentially causing steric hindrance or altering how the protein folds (Tokuriki and Tawfik, 2009). However, there is no overall structural differences observed when aligning the 3D protein structures of *AtWD40* and EMS induced *AtWD40*^{H15Y} (Figure 3-19 A). Nevertheless, the change in side chain properties might still influence the protein's interactions with other proteins or ligands, potentially disrupting existing binding sites or creating new ones (Guerois et al., 2002). This could possibly affect signaling pathways, structural integrity, or the ability of the protein to function in its biological role. Thus, it is plausible to speculate that the *AtWD40*^{H15Y} missense mutation might affect the protein's interactions with other molecules or its subcellular localization, ultimately leading to altered trafficking of proteins and RNA between the cytoplasm and the nucleus.

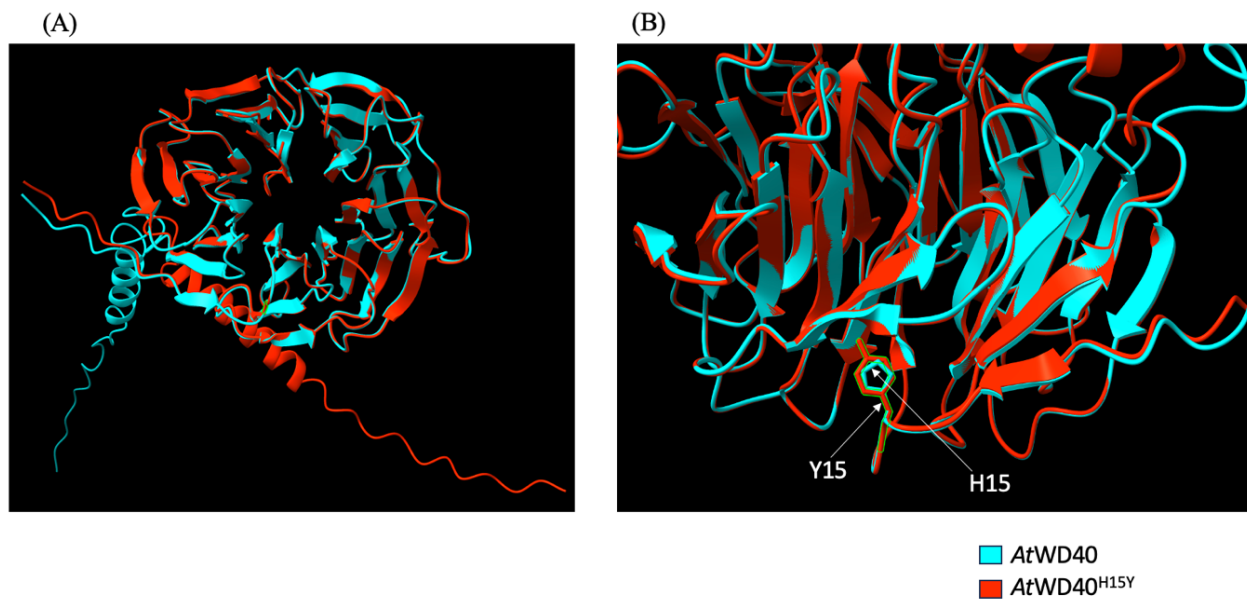


Figure 3-19. Structural comparison of *AtWD40* and *AtWD40*^{H15Y}.

(A) Superimposed model of *AtWD40* (cyan) and *AtWD40*^{H15Y} (red). (B) Detailed overview of differences between *AtWD40* (cyan) and *AtWD40*^{H15Y} (red) superimposed model shown in A. The amino acid residues are highlighted using the arrow and the structural difference induced by missense mutation highlighted in green. The superimposed model was created using ChimeraX-1.8, Needleman-Wunsch algorithm and the 3D structures were predicted using Alpha Fold algorithm.

The eFP browser's interaction viewer tool determines interactive network and aids visualizing interactions between genes, proteins, or other molecular entities. Predictions indicate potential interactors of *AtWD40*, shedding light on the pathways in which *AtWD40* might be involved. One predicted interactor of *AtWD40* is AT5G03240 (UBQ3), a POLYUBIQUITIN 3 protein involved in the targeted degradation of other proteins (Figure 3-20). Although the exact function of *AtWD40* (AT3G15610) has not been experimentally characterized, its rice homolog, *OsWDRP3* (WD Repeat Protein 3), shares 79% sequence similarity (Figure 3-21 A). *OsWDRP3* regulates brassinosteroid signaling by mediating the degradation of the receptor kinase *OsBAK1* (BRI1-associated kinase 1) (Xi and Wang, 2022). BAK1 is involved in brassinosteroid-related signaling and acts as a coreceptor in multiple pathways, including brassinosteroid signaling and pathogen-associated molecular pattern (PAMP)-triggered immunity (He et al., 2013). Structural alignment of protein *AtWD40* and *OsWDRP3* reveals high similarity, with a structural alignment score of 1461.2 (Figure 3-21 B). This suggests a potential role for AT3G15610 in similar pathways. Protein-protein interaction prediction suggests a potential interaction between AT3G15610 and UBQ3, a member of Cul4-RING E3 Ubiquitin ligase complex supporting its involvement in BAK1 degradation (Kim et al., 2013).

Another predicted interactor of *AtWD40*, with low confidence (Figure 3-20), is AT5G26751 (SK11), a shaggy-related kinase involved in meristem organization, redox stress response, and regulation of salt stress tolerance through glucose-6-phosphate dehydrogenase 6 phosphorylation (Dal Santo et al., 2012). SK11 regulates the phosphorylation of TRANSPARENT TESTA GLABRA1 (TTG1), a WD40 repeat transcription factor that mediates carbon flow to fatty acid synthesis and seed coat traits in *A. thaliana* seeds (C. Li et al., 2018). However, the exact mechanism of how and why AT3G15610 and SK11 interact is unknown and no experimental data are available. Another predicted interactor of *AtWD40* again with low confidence value is AT4G02860 (DAAR2), a D-amino acid racemase involved in lateral root growth under low nitrate conditions facilitated by auxin transport (Figure 3-20) (Lv et al., 2021; Gifford et al., 2013; Rosas et al., 2013; Kamali and Singh, 2022). However, the precise link between *AtWD40* and DAAR2 remains elusive, with no experimental data supporting this interaction. To validate *AtWD40*'s interaction with these predicted proteins, a mammalian-2-hybrid assay was employed.

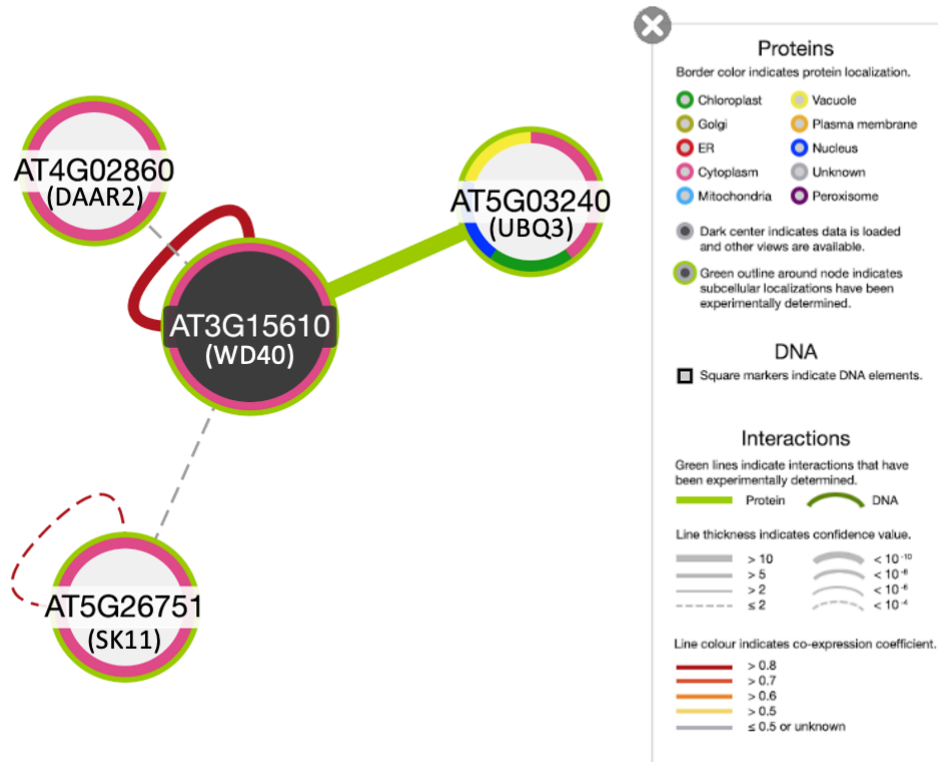


Figure 3-20. Protein-Protein interaction of *At*WD40 (AT3G15610).

Predicted protein-protein interaction candidates of *At*WD40 according to interaction viewer of eFP browser (<https://bar.utoronto.ca/eplant/>). The green line indicates experimentally proven interaction, and the dotted lines indicate the prediction based on confidence score. The color of the circle indicates predicted subcellular localization and the color code for various compartments are mentioned in the figure.

(A)

AtWD40	MEKKKVATPLVCHGHSRPVVDLFYSPITPDGFFLISASKDSQPMLRNGETGDWIGTFEGH	60
OsWDRP3	MDRKKAGVPLVCHGHSRPVVDLFYSPVTPDGCFLISASKDSNPMIRNGDTGDWIGTFEGH	60
	:. . .*****:**** *****:*.**:*****	
AtWD40	KGAVWSSCLDNNALRAASASADFSAKLWDALTDVLSFEHKHIVRACAFSQDTKYLITG	120
OsWDRP3	KGAVWSSCLDTNALRAASGSADFSAKVWDALTDGELHSFEHKHIVRACAFSEDTHLLLTG	120
	*****.***.******.******:*****:*****:*****:*.**:**	
AtWD40	GFEKILRVFDLNRDAPPEIDKSPGSIKTLTWLHGDQTISSCTDIGGVRLWDVRSKGI	180
OsWDRP3	GLEKILRIYDMNRDAPPEIDKSPGSIKTLTWLHSDQSISSCTDMGGVRLWDVRSKGI	180
	*:*****:*.**:** ** * *****:*.**:***.***:***.***.******	
AtWD40	VQTLETKSPVTSAEVSQDGRYIITADGSTVKFWDANHFGLVKSYPNIESASLEPKSG	240
OsWDRP3	AQTLETKATVTSAEVSQDGRYIITADGSSVKFWDANYFGLVKSYPNIESASLEPKYK	240
	.*****:***** *****:*****:*****:*****:***** *	
AtWD40	NKFVAGGEDMWRLFDFTGKEIGCNKGHHGPVHCVRFPAGTESYASGSEDGTIRIWQTG	300
OsWDRP3	NKFIAGGEDMWHVDFDFTGEEITCNKGHHGPVHCVRFPAGGESYASGSEDGTIRIWQLG	300
	:**:***.***:** ***** ***** ***** ***** *	
AtWD40	PVNP EEISES-----KPKQSVDEVARKIEGFHINKEGKTAEKPSDA	341
OsWDRP3	PATSDEQESPPNANGKLVNTVSDAARKIEGFHLPKDGQTEG-----	342
	.. : .. :*.**:*****:*.**:**	

(B)



Figure 3-21. Structure and sequence alignment of *AtWD40* and *OsWDRP3*.

(A) Protein sequence alignment of *AtWD40* and *OsWDRP3* performed using Clustal Omega multiple sequence alignment tool. ‘*’ indicates positions with identical residues in both sequences. ‘.’ indicates positions with conserved substitutions and ‘:’ indicates positions with semi-conserved substitutions. (B)

Superimposed model of *AtWD40* and *OsWDRP3* performed using ChimeraX-1.8, Needleman-Wunsch algorithm and the 3D structures were predicted using Alpha Fold algorithm.

The 2-hybrid system operates by utilizing a reporter gene, *SEAP* (Secreted Alkaline Phosphatase), fused with a DNA binding domain (*E* gene). When a transcription activator domain (*VPI6*) interacts with the E protein, it drives the *etr8-pCMV* minimal hybrid promoter to transcribe the *SEAP* gene. Plasmids were constructed to incorporate the gene of interest (GOI) fused either to the N or C terminus of the *VPI6* transcription activator domain, and the C terminus of the *E*-gene. When proteins interact, the *etr8-pCMV* minimal hybrid promoter activates the *SEAP* gene, leading to the production of secreted alkaline phosphatase (Figure 3-22). Interaction can be quantified colorimetrically, where the measurable signal is proportional to the amount of SEAP present. To investigate interactions between *AtWD40* and the listed candidate proteins (Figure 3-20), the coding sequences of these genes were cloned into vectors containing *E*-gene and *VPI6* domains, driven by the SV40 promoter and terminator. Both N and C termini of the domains were utilized for cloning, as the specific interaction pattern between the candidate proteins and *AtWD40* was not clearly defined. These constructs were then transfected into CHO (Chinese Hamster Ovary) cell lines, followed by SEAP assays to quantify the level of interaction. All candidates were tested against *AtWD40* for both N and C terminal interaction. However, the results depicted in Figure 3-23 indicate that none of the predicted interactions were substantiated in this experiment. No significant increase was observed in interactions between candidate proteins and any N or C terminal combination of the *AtWD40* protein, suggesting a lack of evident interaction in this context. Nevertheless, the positive controls showed a significant increase in interaction where *E*-gene and *VPI6* domains without any fused genes were used. Negative controls utilized *E*-gene fused candidates against stuffer which is a block of DNA without the *VPI6* domain; thus, no signal was expected, and the observed results indicate the same (Figure 3-23). Consequently, this experiment failed to provide conclusive evidence regarding the interacting partners of *AtWD40* and potential pathways it might regulate.

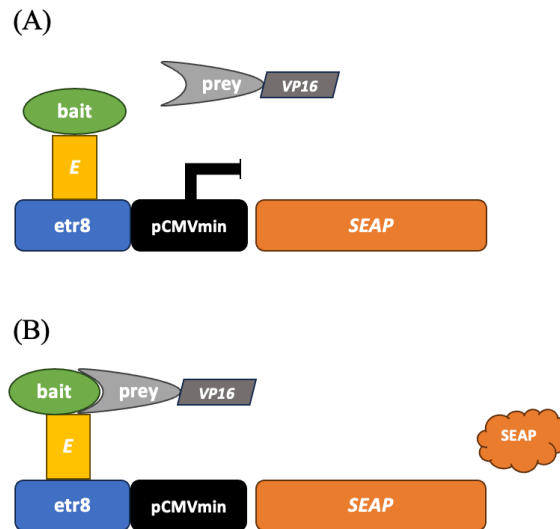


Figure 3-22. Model used to study protein-protein interaction.

(A) In the absence of interaction between candidate bait and prey proteins, SEAP production is not initiated. (B) SEAP is produced when bait and prey proteins interact. Description: E- E gene DNA binding domain; VP16- transactivation domain; bait and prey – candidate proteins to be tested for interaction; etr8:pCMVmin- promoter; SEAP - Secreted Alkaline Phosphatase.

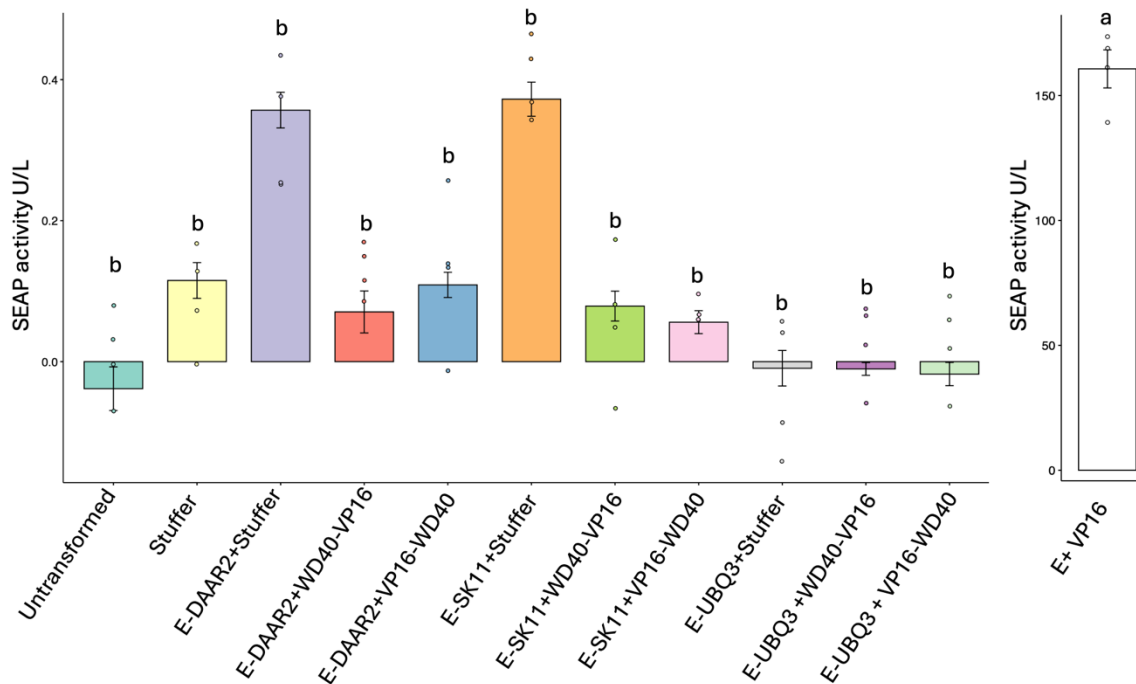


Figure 3-23. Mammalian 2-hybrid interaction assay between *At*WD40 and predicted interaction candidate proteins.

The plot represents SEAP activity for determining protein-protein interactions of WD40 with various predicted interaction candidate proteins (SK11, DAAR2, and UBQ3). The combinations labeled as "stuffer" serve as negative controls. Stuffer is a block of DNA without the *VP16* domain. Additionally, the positive controls utilized are E -VP16 protein interactions without any cloned candidate proteins.

Bars represent the average mean of SEAP activity measured in U/L \pm the standard deviation (n=4). Alphabets indicates the significant differences between the means of combinations used (Tukey HSD, $p < 0.05$).

3.2.6.2 Localization and interaction profiling of *AtKH26*

KH domain proteins play a crucial role in regulating various biological processes, including RNA binding, splicing, transcription, and translation, with potential localization in the nucleus (Nazarov et al., 2019)). Subcellular localization predictions further support this, indicating that *AtKH26* is predominantly found in the nucleus and chloroplast, with some presence in the cytoplasm and mitochondria (Figure 3-24). However, these predictions require validation through subcellular localization studies using GFP-tagged *AtKH26*, despite earlier reports suggesting that *AtKH26* is primarily nuclear localized (Bridgen, 2022). In *pAXY atkh26-1* mutant the missense mutation leading to the G411E substitution in *AtKH26* occurs in the fourth KH domain of the protein (Figure 3-25 A). The KH domain, approximately 70 amino acids long, is known to bind RNA and single-stranded DNA (Valverde et al., 2008). Proteins containing KH domains have been shown to regulate various biological processes, such as mRNA stability, splicing, and the enhancement or silencing of translation (Nazarov et al., 2019). The glycine-to-glutamate missense mutation in the fourth KH domain could potentially disrupt the local structure, impacting the domain's ability to interact with RNA (Figure 3-25 B and C). Glycine, being the smallest amino acid, provides flexibility in protein structures due to its minimal steric hindrance (Voet et al., 2013). It is often found in regions that require tight turns or close packing, such as loops or near hinge points in protein domains. In contrast, glutamate is larger, negatively charged, and hydrophilic. Replacing glycine with glutamate introduces a bulky side chain with a negative charge, which can disrupt the local topology, especially in regions requiring tight packing or those involved in hydrophobic interactions (Voet et al., 2013). If the KH domain's RNA-binding ability is compromised due to the G411E substitution, the overall function of the *AtKH26* protein could be affected, potentially impairing its roles in RNA processing, transport, or regulation, leading to downstream effects on gene expression or cellular processes (Nicastro et al., 2015).

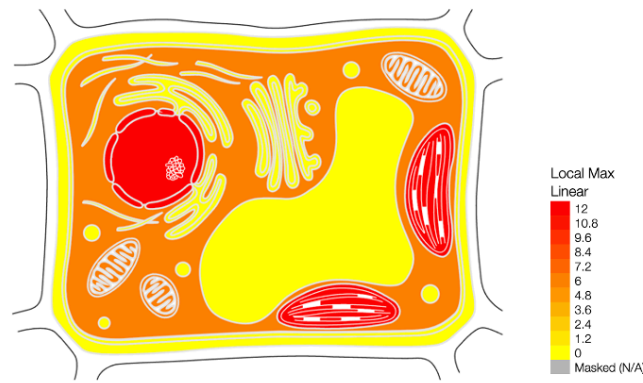


Figure 3-24. Predicted subcellular localization of *AtKH26*.

Predicted subcellular localization of *AtKH26* according to cell eFP viewer (<https://bar.utoronto.ca/eplant/>). The local max linear indicates the confidence score calculated from the computational experiments and molecular experiments (Winter et al., 2007). The higher confidence score for a given subcellular compartment, the more intense the red color in the output.

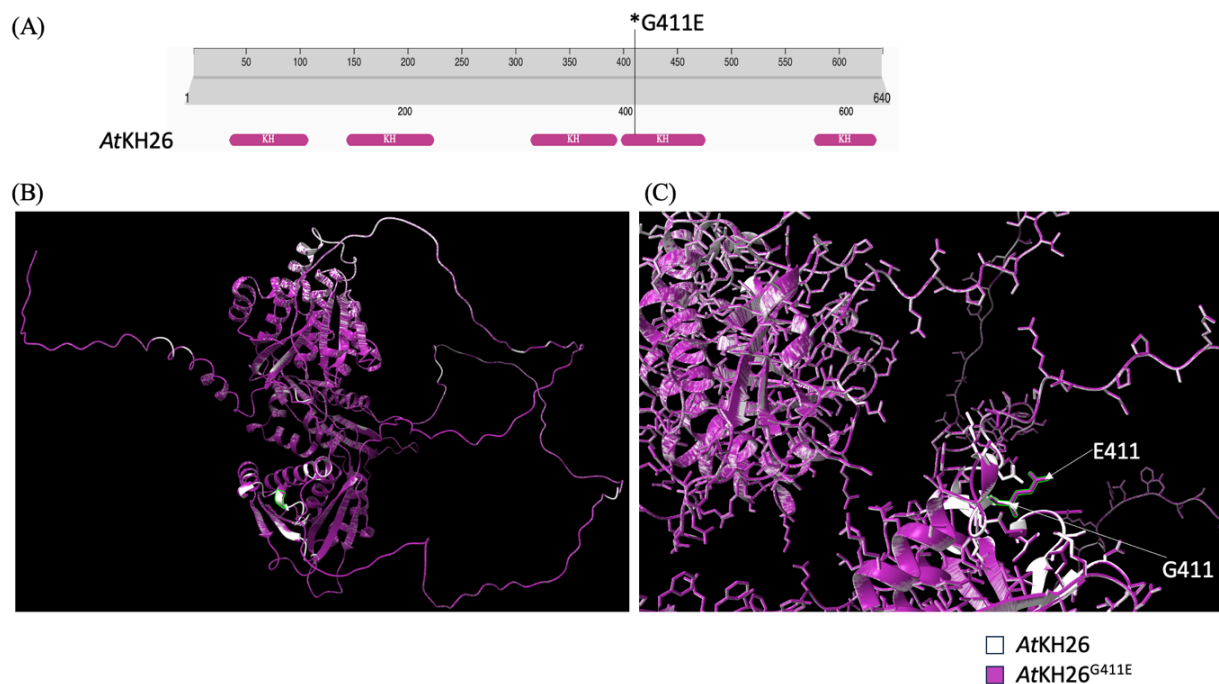


Figure 3-25. Domain architecture and Structural comparison of *AtKH26* and *AtKH26*^{G411E}.

(A) The domain organization of the *AtKH26* protein is depicted based on InterPro predictions. The analysis identified five K homology (KH) domains, located at positions 42-112, 148-226, 315-392, 397-492 and 572-627, represented by purple bars. Additionally, the substitution G411E induced by EMS is indicated using the symbol (*). (B) Superimposed model of *AtKH26* (white) and *AtKH26*^{G411E} (purple). The structural difference induced by missense mutation highlighted in green (C) Detailed overview of differences between *AtKH26* (white) and *AtKH26*^{G411E} (purple) superimposed model shown in A. The amino acid residues are highlighted using the arrow. The superimposed model was created using ChimeraX-1.8, Needleman-Wunsch algorithm and the 3D structures were predicted using Alpha Fold algorithm.

The eFP browser's interaction viewer tool was utilized to predict the interacting partners of *AtKH26* (AT5G46190), providing insights into the potential pathways involving *AtKH26* (Figure 3-26). The analysis identified two possible interactors: ORRM2 (AT5G54580) and AT3G21215. ORRM2 is associated with the FLOWERING CONTROL LOCUS A (FCA) protein, a critical regulator of floral transition (Macknight et al., 1997). The FCA protein contains two RNA-binding domains (RRMs), which are highly conserved across different plant species (Sun et al., 2012). Interestingly, these RRM domains have been implicated in promoting plant growth (Sun et al., 2012). Overexpression of the FCA-RRM1 and FCA-RRM2 domains has been shown to increase cell size in rice and cotton, thereby improving the yield. Notably, in transgenic rapeseed overexpressing FCA-RRM2, there was a significant downregulation of the *CYCLIN-B2-1* gene (Qi et al., 2012). However, it remains unclear whether the increase in cell size is directly caused by the reduced expression of *CYCLIN-B2-1*. Defects in *CYCLIN B* are known to delay mitotic entry, resulting in an increased cell size (Nigg, 1993). Based on these findings, it could be speculated that *AtKH26* may play a role in repressing ORRM2. A loss of function in *AtKH26* might lead to a mis-regulated repression, potentially contributing to the recovery of the *pAXY* phenotype through cell expansion. However, further experimental validation is required to substantiate this hypothesis. Another predicted interaction partner of *AtKH26* is AT3G21215 (Figure 3-26), an RNA-binding protein that also contains an RRM domain. However, there is no available experimental or predictive data regarding the function of this protein, leaving the significance of its interaction with *AtKH26* unclear.

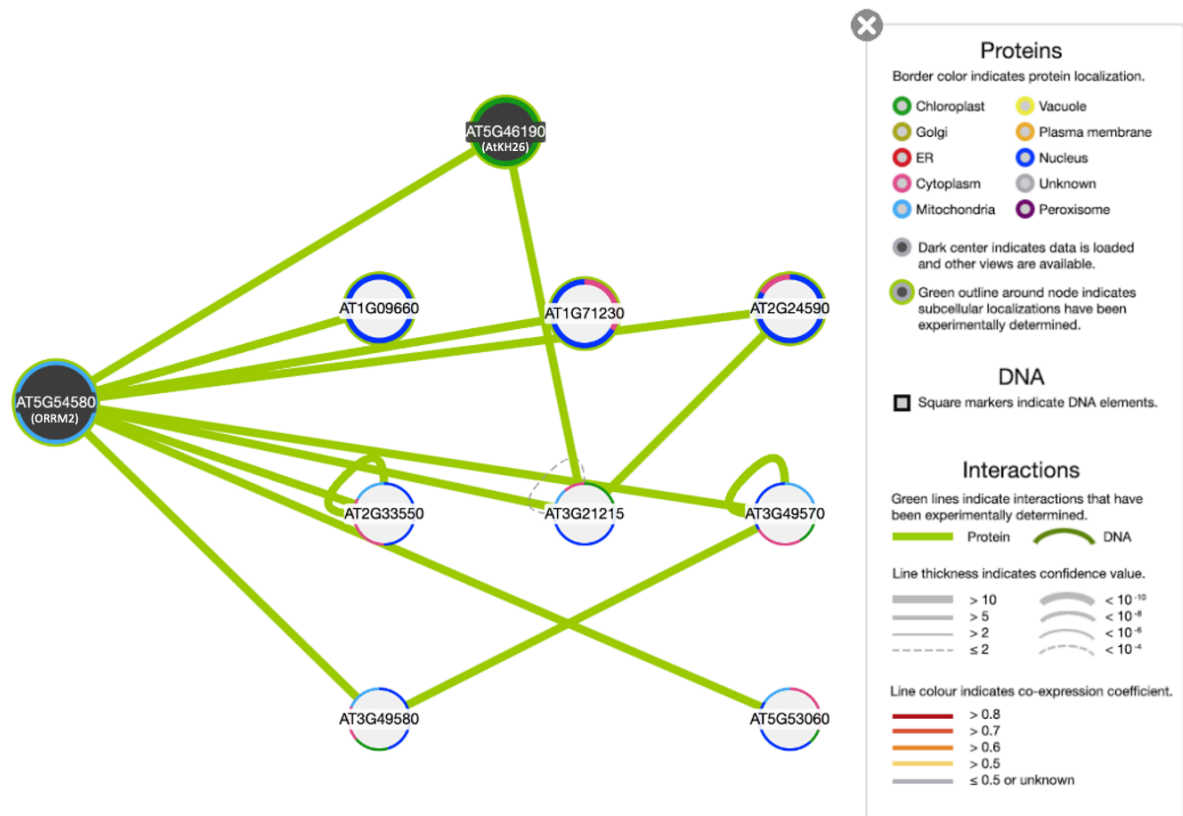


Figure 3-26. Predicted protein-protein interaction of *AtKH26* (AT5G46190).

Predicted protein-protein interaction candidates of *AtKH26* according to interaction viewer of eFP browser (<https://bar.utoronto.ca/eplant/>). The green line indicates experimentally proven interaction, and the dotted lines indicate the prediction based on confidence score. The color of the circle indicates predicted subcellular localization and the color code for various compartments are mentioned in the figure.

3.2.6.3 Localization and interaction profiling of PHOX3

PHOX3, belonging to the Carboxylate clamp (CC)-tetratricopeptide repeat (TPR) protein family, plays a significant role in mediating protein-protein interactions that are critical for various cellular processes (Prasad et al., 2010). The CC-TPR proteins are characterized by the presence of tetratricopeptide repeats (TPRs), which are 34-amino acid sequence motifs that form a helix-turn-helix structure (Causier et al., 2012). PHOX3 has been identified to interact with the MEEVD motif of HSP90, suggesting a possible role as an interactor of HSP90 for co-chaperon formation, primarily localized in the nucleus (Prasad et al., 2010). While eFP browser did not predict this interaction, STRING database provided support for the involvement of PHOX3 in co-chaperones (Figure 3-28), which are essential components of the HSP90/HSP70 chaperone machinery (Pearl et al., 2008; Pearl and Prodromou, 2006; Whitesell and Lindquist,

2005). Subcellular localization predictions also indicate that PHOX3 is mainly localized in the nucleus with some presence in the cytoplasm (Figure 3-27). However, validation through GFP fusion and yeast 2 hybrid assay is necessary to confirm these predictions.

A mutation caused by EMS that leads to the substitution of G to A at position 6886187, occurs in a potential cis-acting element of NF-Y (Nuclear Factor Y) within the 2kb promoter region of *PHOX3* in the *pAXY phox3-1* mutant (Figure 3-29). The *PHOX3* gene is located on the antisense strand. NF-Y transcription factors are crucial in regulating gene expression, particularly those involved in cell cycle control, development, and stress responses in plants (Laloum et al., 2013). The NF-Y complex consists of three subunits: NF-YA, NF-YB, and NF-YC. NF-YA is the DNA-binding subunit that recognizes and binds to the CCAAT box, a common promoter element in many genes and CCCAT is identified as another variant (Laloum et al., 2013). NF-YB and NF-YC form a heterodimer that interacts with NF-YA, stabilizing its DNA interaction (Myers et al., 2016). This complex is essential for the proper function of NF-Y in gene regulation. In *A. thaliana*, NF-YA is involved in regulating processes like flowering time, seed development, and stress responses. NF-YB forms a dimer with NF-YC, facilitating NF-YA recruitment to the CCAAT box, and can also interact with other transcription factors to modulate gene expression (Laloum et al., 2013). The EMS-induced mutation in *pAXY phox3-1* changes cCcat to cTcat, potentially disrupting the NF-Y binding site, which may alter the regulation of *PHOX3* by the NF-Y complex. This mutation is supported by the observed two-fold reduction in *PHOX3* gene expression in the *pAXY phox3-1* mutant compared to the WT (Figure 3-10 E), suggesting an impact on the gene's regulation by the NF-Y complex.

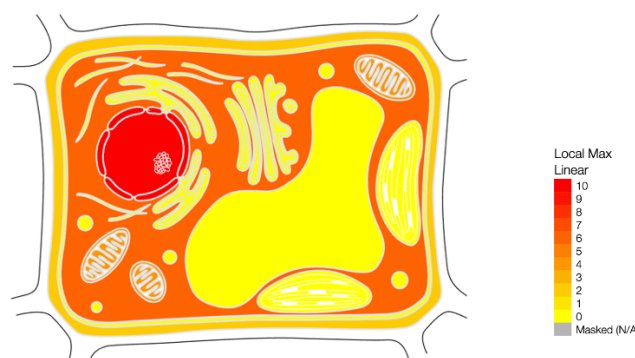


Figure 3-27. Predicted subcellular localisation of *AtPHOX3*.

Predicted subcellular localization of *AtPHOX3* according to cell eFP viewer (<https://bar.utoronto.ca/eplant/>). The local max linear indicates the confidence score calculated from the

computational experiments and molecular experiments (Winter et al., 2007). The higher confidence score for a given subcellular compartment, the more intense the red color in the output.

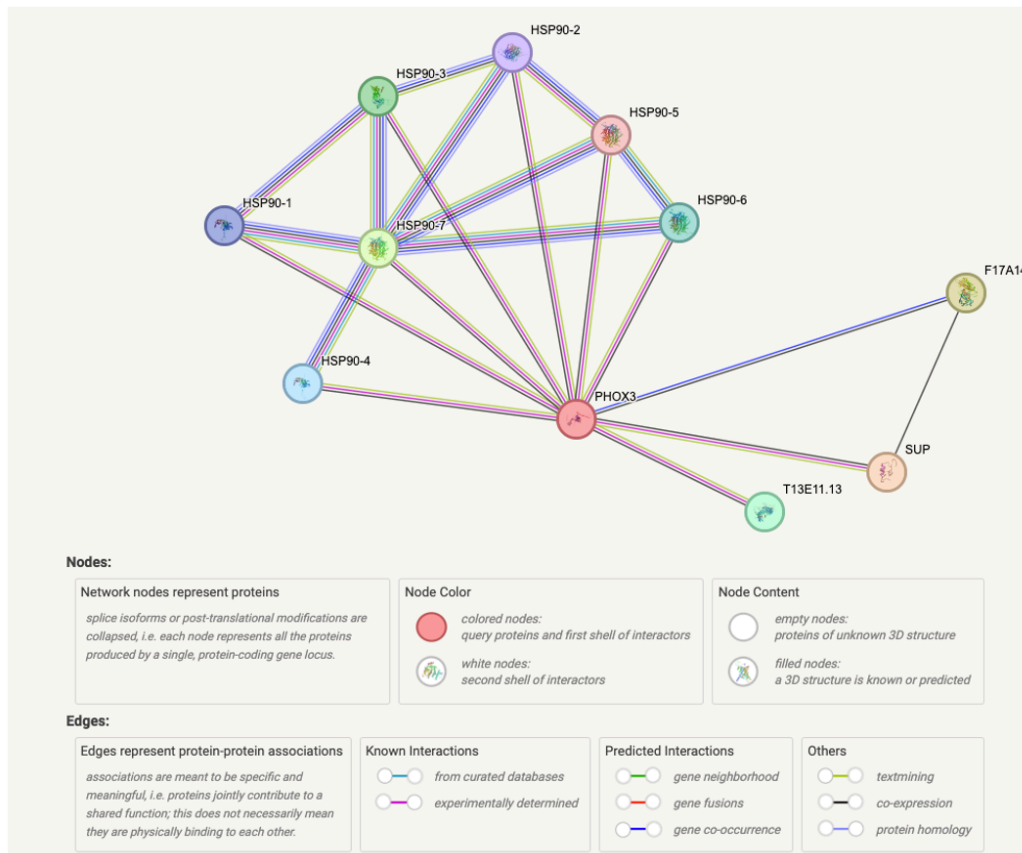


Figure 3-28. Predicted protein-protein interaction of PHOX3 (AT5G20360)

Predicted protein-protein interaction candidates of PHOX3 according to STRING interaction viewer (<https://string-db.org/>). The color code indicates the experimentally proven interaction, and the prediction based on confidence score.

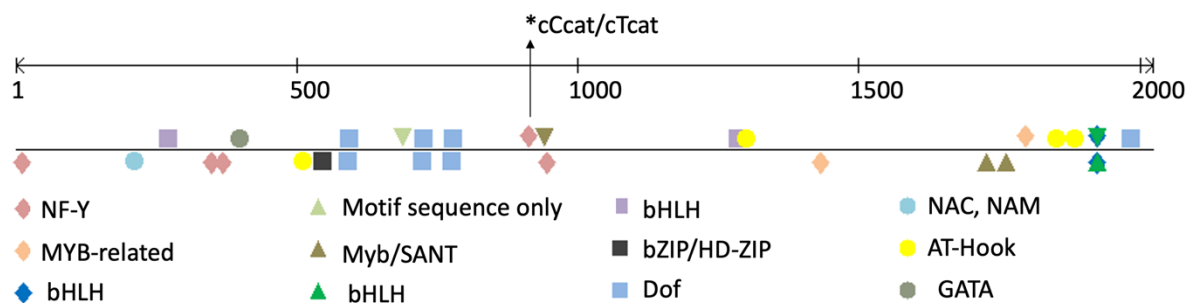


Figure 3-29. Predicted cis-acting regulatory elements in the 2kb promoter region of *AtPHOX3*.

The figure illustrates the regulatory cis-acting elements identified using PlantPAN 4.0, a tool that predicts potential transcription factor binding sites based on sequence similarity and established motifs. These cis-regulatory elements are represented along the promoter region, with different transcription factor binding sites distinguished by specific color-coded markers. The EMS-induced mutation

affecting the NF-Y binding site is specifically marked with an asterisk (*), highlighting its location within the promoter sequence.

3.3 Discussion

3.3.1 Genetic basis of growth recovery in *O*-acetylation mutants

The complex biological function of *O*-acetylation has been challenging to study due to the diverse characteristics exhibited by wall acetylation mutants. Notably, the loss of function of *AXY9* gene drastically reduces *O*-acetylation of multiple wall polysaccharides, leading to severe developmental and stress-related defects (Schultink et al., 2015). In WT *A. thaliana* stems, the xylem vessels are typically large, well-formed, and patent whereas in the *axy9* mutant, the xylem vessels are severely collapsed (Schultink et al., 2015). Similar, though less severe, phenotypes are observed in mutants with loss of function in *TBL29* (Xiong et al., 2013) and in an *rwa* quadruple mutant (Lee et al., 2011). The study of the *axy9* mutant has been technically challenging because the homozygous *axy9* mutation leads to extreme dwarfism and complete male sterility. To overcome these challenges, a conditionally complemented *axy9* line, *pAXY*, was established. This line retains reduced levels of wall-bound acetate and a dwarf stature but is normally fertile and has a xylem structure comparable to that of the WT (Figure 3-1 and Appendix 9-1). This characteristic overcomes some of restrictions of *axy9* mutant such as male sterility. Therefore, this mutant provides an excellent tool for suppressor screening and for studying other genes involved in growth and stress-related defects associated with wall hypoacetylation. In our study, all nine suppressor mutants showed increased height, leading to a recovered phenotype closely resembling that of the WT (Figure 3-2). Analysis of *O*-acetate levels in the *pAXY* suppressor mutants shows that wall acetylation levels are indistinguishable from those observed in *pAXY*, being approximately 50% lower than in the WT (Figure 3-2). This highlights that reduced *O*-acetate levels do not necessarily correlate with the observed developmental defects associated with *pAXY* mutant. This hypothesis is supported by previously identified two *tbl29* suppressors (*tbl29 kak* and *tbl29 max4*), where the xylem collapse and growth arrest are recovered but the wall/xylan acetate remains reduced (Bensussan et al., 2015; Ramírez et al., 2018).

Altered biosynthesis of plant hormone strigolactone have been suggested to play a role in the recovery of the pleiotropic phenotype observed in *tbl29/esk1*. Inhibiting strigolactone (SL)

synthesis in *tbl29/esk1* plants (i.e., *tbl29 max4* double mutants) completely suppresses both developmental defects and increased freezing tolerance without affecting the reduced acetate content (Ramírez et al., 2018). Additionally, exogenous applications of a synthetic SL to *tbl29 max4* plants result in dwarfism and collapsed xylem, further confirming that these phenotypes are SL-dependent. This suggests that an altered SL pathway could be directly involved in the pleiotropic phenotypes associated with the hypoacetylation mutants. As SLs are hormones involved in regulating multiple plant processes, including stem elongation, secondary growth, leaf expansion, and adaptation to abiotic stress (Waters et al., 2017), this opens the possibility that xylan hypoacetylation could be perceived by an unknown mechanism, triggering the activation of an SL-dependent response regulating xylem development (Ramírez et al., 2018). However, loss of function of *MAX4* in *pAXY* did not restore the dwarf phenotype associated with *pAXY* (Appendix Figure 9-5) suggesting that the recovery mechanism among wall acetylation mutants may differ and operate independently of each other. In conclusion, our results highlight the complex relationship between *O*-acetylation levels and various plant traits. The *pAXY* line serves as an important tool for unravelling the mechanisms underlying growth and stress response in plants with modified *O*-acetylation, while the suppressor mutants identify genetic elements that can influence these effects. The dissociation of *O*-acetylation levels from height recovery in suppressor mutants suggests that compensatory mechanisms or pathways may contribute to the observed phenotypic alterations.

3.3.2 Correlation between cell wall composition and growth recovery

The analysis of cell wall composition indicated that lower levels of crystalline cellulose in the *pAXY* line led to a relative increase in other non-cellulosic cell wall-related sugars as a compensatory response (section 3.2.5.2). This observation aligns with several studies showing that a reduction in cellulose content is often accompanied by an increase in non-cellulosic cell wall sugars (Song, 2013; Chantreau, 2015; Li F, 2017). However, in the suppressor mutants, this reduction in glucose levels was particularly significant in the *pAXY atkh26-2* mutant (Figure 3-14 A), which also exhibited decreased crystalline cellulose content (Figure 3-15 C). This reduction was compensated by a relative increase in other monosaccharides, such as xylose (5% increase), suggesting a compensation mechanism possibly altered xylan content. In contrast, other suppressor mutants like *pAXY wd40* and *pAXY phox3* showed partial restoration of crystalline cellulose levels in the recovery mechanism (Figure 3-15 A and B). Additionally, compensatory alterations in sugar levels, particularly those involving pectic

polysaccharides, were observed in *pAXY phox* mutants (Figure 3-13). Whereas in *pAXY wd40* the hemicellulose monosaccharide levels were similar to that of *pAXY* suggesting that recovery mechanism only altered crystalline cellulose content (Figure 3-12). A consistent observation across *pAXY* and all suppressor lines was the elevated levels of glucuronic acid (GlcA) compared to WT, with significant increases noted in *pAXY*, *pAXY phox3-2*, *pAXY atkh26-1*, and *pAXY atkh26-2* (Figures 3-12, 3-13, and 3-14). Interestingly, expression of the *GUX1* gene in vascular tissue, driven by a tissue-specific promoter, successfully rescues the growth defects in the *tbl29/esk1* mutant, suggesting that xylan functionality is restored (Xiong et al., 2015). In the absence of *O*-acetyl groups in *tbl29*, GUX1 facilitates glucuronosylation at additional available positions on the xylan backbone. This glucuronosylation can be considered functionally equivalent to *O*-acetylation in vivo (Ramirez and pauly 2019). This implies that the observed increase in glucuronic acid in the *pAXY* and its suppressor mutants may compensate for the missing *O*-acetyl groups by glucuronosylating additional positions on the xylan backbone. However, this increase alone is not sufficient to recover the phenotype, as similar elevations were also seen in *pAXY*. Mutant studies have shown that altered xylan composition, reduced xylan *O*-acetylation, and modified cellulose content often correlate with improved freezing tolerance (Ramírez and Pauly, 2019). It is hypothesized that the increased freezing tolerance in these mutants results from a transpiration imbalance caused by xylem collapse (Ramírez and Pauly, 2019). Notably, the *pAXY* mutant, with reduced cellulose and *O*-acetylation levels, showed an improved freezing tolerance of around 50-60% survival, even though the xylem structure remained intact (Figure 3-17, Appendix Figure 9-1). Freezing tolerance, despite the intact xylem could be attributed to stress related responses induced by altered crystalline cellulose levels and *O*-acetylation levels. While all suppressor mutants exhibited a survival rate of less than 25%, indicating that partial restoration of hemicellulose monosaccharides or cellulose in the wall might have reduced freezing tolerance in these mutants.

3.3.3 Proposed regulatory interactions in BR signaling and their role in *pAXY* growth phenotype suppression

The loss of function of *WD40* (AT3G15610) was able to suppress the growth and stress related defects associated with *pAXY* phenotype. WD40 repeat proteins typically feature a ~40 amino acid core region with a glycine-histidine (GH) dipeptide at the N-terminus and a tryptophan-aspartate (WD) dipeptide at the C-terminus (Migliori et al., 2012). Despite their generally low

sequence conservation, WD40 proteins have diverse functions (Jain and Pandey, 2018). Genome-wide studies of WD40 protein families have been conducted in various organisms, including *A. thaliana* (van Nocker and Ludwig, 2003), cotton (Haron et al., 2018), foxtail millet (Mishra et al., 2014), rice (Ouyang et al., 2012), wheat (Cheng et al., 2018), humans (Ouyang et al., 2012), peach (Feng et al., 2019), and mango (Tan et al., 2021). The function of *AtWD40* (AT3G15610) has not been experimentally characterized yet. However, its rice homolog, *OsWDRP3* (WD Repeat Protein 3), shares 79% sequence similarity and regulates brassinosteroid (BR) signaling by mediating the degradation of the receptor kinase *OsBAK1* (BRI1-associated kinase 1) (Xi and Wang, 2022) (Figure 3-21). This suggests a potential role for *AtWD40* in similar pathways. Protein-protein interaction analysis suggests a potential interaction between WD40 and POLYUBIQUITIN 3 (UBQ3, AT5G03240), a member of Cul4-RING E3 Ubiquitin ligase complex supporting that *AtWD40* might recruit UBQ3 to degrade BAK1 (Kim et al., 2013) (Figure 3-20). This suggests that the loss of function of *AtWD40* in the *pAXY* mutant may hinder BAK1 degradation, leading to enhanced BR signaling through its interaction with BRI1 (Figure 3-31). BAK1, involved in BR-related signaling, and serves as a coreceptor in multiple signaling pathways pathogen-associated molecular pattern (PAMP)-triggered immunity (He et al., 2013). Brassinosteroid-insensitive-1 (BRI1) is a plasma membrane-localized receptor that binds BRs, leading to its activation and interaction with BAK1, which enhances BR signaling (Li and Chory, 1997; Li and Jin, 2007). Overexpression of BAK1 can rescue the growth phenotype of *bri1* mutants, highlighting BAK1's importance as a coreceptor in BR signaling pathway (X. Gou et al., 2012). The BR-BRI1 binding also releases BRI1 from its inhibitor BKI1, allowing BAK1 binding and promoting signal transduction (Kim et al., 2011; Li and He, 2013). Activated BRI1 triggers phosphorylation cascades involving BR-Signaling Kinase 1 (BSK1) and constitutive differential growth 1 (CDG1), which activate BRI1-suppressor 1 (BSU1). BSU1 deactivates brassinosteroid-insensitive 2 (BIN2), a negative regulator of BR signaling that usually inhibits the transcription factors BES1 and BZR1 by phosphorylation (Abbas et al., 2022; Peng et al., 2010). When dephosphorylated by protein phosphatase 2A (PP2A) through BR signaling, BES1 and BZR1 enter the nucleus to regulate BR-responsive genes (Sun, 2010; Yu et al., 2011). These dephosphorylated transcription factors regulate BR-target genes, enhancing plant stress tolerance by increasing the capacity of antioxidant enzymes (Vardhini and Anjum, 2015), regulating the accumulation of endogenous hormones (Abbas et al., 2022), and upregulating numerous genes (Li et al., 2018). Furthermore, BIN2 has been shown to phosphorylate CESA1, reducing the CSC activity (Sánchez-Rodríguez et al., 2017), which could explain the reduced

cellulose content in *pAXY* (Figure 3-15). This highlights BIN2 as a key regulator of cellulose synthesis, directly linking a crucial hormonal signal transduction pathway with a fundamental process in plant growth and development. The loss of function of *KAKTUS* has been shown to alleviate the stress-related defects associated with the xylan acetylation mutant *tbl29/esk1* (Bensussan et al., 2015). Recent research indicates that *KAKTUS* (UPL3) plays a role in the degradation of the BZR1 transcription factor (Z. Zhang et al., 2023). *KAKTUS* functions as an E3 ubiquitin protein ligase 3 (UPL3) and acts as a negative regulator of brassinosteroid (BR) signaling (Z. Zhang et al., 2023). It is involved in growth attenuation under stress and starvation conditions to enhance plant survival. This suggests that BR response genes are indeed crucial for the suppression of stress-related defects linked to hypoacetylation. To further confirm the involvement of *KAKTUS* and BR signaling and in mitigating these stress-related defects, generating a *pAXY kak* mutant would be necessary.

Another identified suppressor mutation in *PHOX3* gene, might also influence the regulation of BR mediated genes through modulation of HSP90 (Figure 3-28). HSP90 has also emerged as a crucial player in BR signaling, interacting directly with BIN2, BZR1, and BES1 (Samakovli et al., 2014; Shigeta et al., 2015). *PHOX3* belongs to the Carboxylate clamp (CC)-tetratricopeptide repeat (TPR) protein family, which is crucial in protein-protein interactions that drive various cellular processes (Prasad et al., 2010). These proteins contain tetratricopeptide repeats (TPR), a 34-amino acid sequence repeat structure of helix-turn-helix conformation (Causier et al., 2012). In plants, computational analysis has unveiled CC-TPR proteins in *A. thaliana* and rice, potentially interact with heat shock proteins HSP90/HSP70 in co-chaperon binding (Prasad et al., 2010). Co-chaperones are obligatory partners of the HSP90/HSP70 chaperone in cellular protein folding machinery, which drives a wide range of cellular processes (Pearl et al., 2008; Pearl and Prodromou, 2006; Pratt et al., 2004; Smith-Jones et al., 2004; Whitesell and Lindquist, 2005). *PHOX3* has been identified to interact with the MEEVD motif of HSP90, indicating a potential role as an interactor of HSP90 or HSP70 in co-chaperone binding, with primary localization in the nucleus. (Prasad et al., 2010). However, the specific regulatory mechanism of HSP90 by *PHOX3* remains unclear, as no other interacting proteins of *PHOX3* have been experimentally characterized yet. HSP90 plays a vital role in BR signaling, with its inhibition affecting the expression of BR-responsive genes. Specifically, HSP90.3 maintains BES1 in a dephosphorylated state, while both HSP90.1 and HSP90.3 assist in the nucleocytoplasmic export of BIN2, thereby reducing its inhibitory effect on BZR1 and BES1 during BR signaling (Samakovli et al., 2014; Shigeta et al., 2015). Another

protein, TWISTED DWARF 1 (TWD1), interacts with HSP90 and contributes to BR signaling by binding to the kinase domains of BRI1 and BAK1, enhancing their signal transduction activity by promoting efficient auto-phosphorylation upon BR perception (Chaiwanon et al., 2016; Zhao et al., 2016). Besides, TWD1 acts as a positive regulator of BR signaling upstream of BIN2, possibly by maintaining the conformational state of the BR coreceptor complex (Chaiwanon et al., 2016). So, it is plausible to speculate that positive regulation of HSP90 by loss of function of *PHOX3* would upregulate the BR signal transduction or BR response genes, thus increasing the growth regulation in *pAXY* suppression. The simplified model in Figure 3-30 illustrates the involvement of WD40, PHOX3, and KAK in the BR signaling pathway.

To validate the hypothesis that BAK1 and HSP90 contribute to the suppression of the *pAXY* phenotype through enhanced BR signaling, several critical experiments are proposed. Firstly, overexpressing BAK1 and HSP90 independently in the *pAXY* background could help determine whether these interventions rescue the *pAXY* phenotype. If overexpression results in improved growth and stress responses, it will indicate that BAK1, HSP90, and BR signaling are indeed involved in the defects observed in the *pAXY* mutant. Conversely, knocking out *BAK1* in the *pAXY wd40-2* background and *HSP90* in the *pAXY phox3* background could reveal whether this leads to a dwarf phenotype. If the knockout of *BAK1* or *HSP90* causes a return to dwarfism, it would suggest that the enhanced BR signaling in the *pAXY wd40* and *pAXY phox3* suppressor mutants depends on BAK1 and HSP90. However, if the dwarf phenotype persists or worsens, this might indicate more complex interactions or the involvement of additional pathways. Additionally, performing interaction assays such as co-immunoprecipitation (Co-IP) with WD40, UBQ3, and BAK1 could clarify whether WD40 recruits UBQ3 to facilitate BAK1 degradation. Similarly, using yeast two-hybrid (Y2H) assays to confirm the interaction between HSP90 and PHOX3 would help support the hypothesis that PHOX3 is involved in modulating BR signaling through its effects on HSP90. Further experiments, such as RNA-seq or qRT-PCR, could reveal differences in the expression of BR signal transduction and response genes. If PHOX3 negatively regulates HSP90 and WD40 facilitates BAK1 degradation, then their loss of function should lead to the upregulation of these BR-related genes at the transcriptional level. These experiments are essential for elucidating the roles of BAK1 and HSP90 in BR signaling within the *pAXY* mutant phenotype and for understanding the underlying molecular mechanisms.

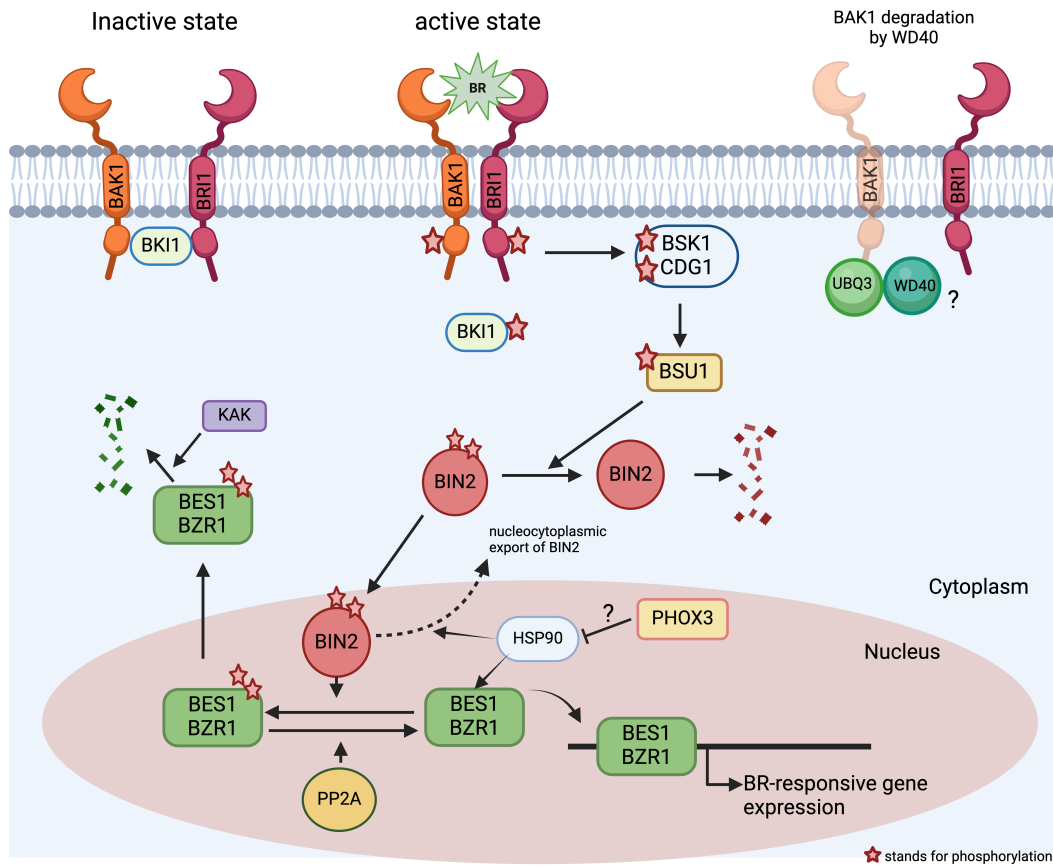


Figure 3-30. Simplified model showing involvement of WD40, PHOX3 and KAK in BR signaling pathway.

This figure illustrates the proposed roles of WD40, PHOX3 and KAK in the brassinosteroid (BR) signaling pathway, focusing on their potential modulation of key proteins. In the absence of BR, the BRI1 receptor is inhibited by BKI1, preventing its interaction with the coreceptor BAK1 (Abbas et al., 2022; Peng et al., 2010). BR binding releases BKI1, enabling BRI1-BAK1 interaction and triggering a phosphorylation cascade that activates BSU1 and deactivates the negative regulator BIN2 (He et al., 2013). This allows dephosphorylated BES1 and BZR1 to regulate BR-responsive genes (Sun, 2010; Yu et al., 2011). WD40 is hypothesized to recruit UBQ3 for BAK1 degradation, potentially modulating BR signaling (Xi and Wang, 2022). HSP90 maintains BES1 in a dephosphorylated state and aids in BIN2's nucleocytoplasmic export (Samakovli et al., 2014; Shigeta et al., 2015). PHOX3's role in repressing HSP90, indicated in the nucleus remains uncertain. KAK, an E3 ubiquitin ligase, targets BES1/BZR1 for degradation, acting as a negative regulator and highlighting the pathway's regulatory complexity in balancing growth and stress responses (Z. Zhang et al., 2023). Figure adapted and modified from Abbas et al., 2022.

3.3.4 Loss of ORRM2 repression in *pAXY atkh26* mutants may rescue *pAXY* growth phenotype

Another identified suppressor mutation in *AtKH26* gene restored *pAXY* phenotype. KH domain proteins have emerged as critical regulators of various biological processes, where they regulate splicing, transcription, translation, and RNA stability (Nazarov et al., 2019). A recent

genome-wide search and phylogenetic analysis identified 30 KH family genes in *A. thaliana* (S. Liu et al., 2022). These KH domain proteins are involved in several essential developmental programs, such as flowering time control, reproductive organ development, vegetative growth, seed germination and environmental stress response pathways in plants (T. Chen et al., 2013; Cheng et al., 2003; Dai, 2011; Karlsson et al., 2015; S. Liu et al., 2022; Ripoll et al., 2009). Protein-protein interaction predictions have shown that *AtKH26* interacts with ORRM2 (Figure 3-26). Its homologue FCA-RRM2 protein, containing two highly conserved RNA-recognition motifs (RRMs) across different plant species, has been implicated in promoting plant growth (Karamat et al., 2021; Sun et al., 2012). Overexpression of the FCA-RRM1 and FCA-RRM2 domains in rice and cotton has been shown to increase cell size, leading to improved yield. In transgenic rapeseed overexpressing FCA-RRM2, there was a notable downregulation of the *CYCLIN-B2-1* gene, although it remains unclear whether the increase in cell size is directly due to reduced *CYCLIN-B2-1* expression (Qi et al., 2012). Defects in CYCLIN B are known to delay mitotic entry, resulting in an increased cell size (Nigg, 1993). Interestingly, the human homologue of *AtKH26*, IGF2BP, has been shown to bind to m⁶A-modified RNA (N⁶-methyladenylation) through its KH3-4 domains and regulate mRNA, miRNAs, and lncRNAs (Bridgen, 2022; Huang et al., 2018). IGF2BP has also been demonstrated to promote an aggressive tumor cell phenotype by inhibiting miRNA-directed downregulation of oncogenic factors, suggesting a repressive role in gene regulation (Müller et al., 2018). This raises the possibility that *AtKH26* might have a similar repressive function in *A. thaliana*, potentially repressing ORRM2. A loss of function in *AtKH26* might lead to abolished repression of ORRM2, contributing to the recovery of the *pAXY* phenotype through cell expansion. To validate this hypothesis, several experiments are proposed. First, analyzing cell size and growth patterns in the *atkh26-2* and *pAXY atkh26* suppressor mutants would help assess the impact of *AtKH26* loss on cell expansion and overall plant development. A qRT-PCR analysis of *ORRM2* and *CYCLIN-B2-1* expression levels could be conducted. If *AtKH26* is indeed responsible for repressing ORRM2, one would expect to see upregulated *ORRM2* expression and downregulated *CYCLIN-B2-1* expression in the *pAXY atkh26* suppressor mutants and the opposite in *pAXY* mutant. Further a Co-IP or Y2H assay could then be employed to confirm the interaction between ORRM2 and *AtKH26*. Additionally, RNA-Seq analysis could identify other potential binding partners of *AtKH26*.

4. Heterologous production of *O*-acetylated xyloglucan backbone in *Yarrowia lipolytica*

4.1 Background

Plant cells are encased within an extracellular matrix primarily composed of polysaccharides. While significant progress has been made in identifying the molecular components involved in plant cell wall polymer synthesis, the collaborative functioning of these components in determining the length and decoration pattern of a polysaccharide remains largely unclear (Pauly et al., 2019). Synthetic biology offers a powerful approach to address these questions, allowing for the reconstruction of entire biosynthetic machineries necessary for producing complete wall polysaccharides. By reconstructing these machineries, it is possible to determine whether all essential factors have been identified based on whether the synthetic polysaccharide matches the structure found in native walls. Discrepancies in substitution patterns could indicate the presence of unidentified or uncharacterized factors that are still to be discovered and studied. Previous research has achieved success in expressing plant cell wall biosynthetic genes in *Pichia pastoris*, including the *CSLC4* glucan synthase, which plays a role in xyloglucan (XyG) biosynthesis (Cocuron et al., 2007). Enzymes such as XyG xylosyltransferases, and heteromannan mannan synthase have also been expressed in this yeast (Cocuron et al., 2007; Voiniciuc et al., 2019). However, the reconstruction of *O*-acetylation machinery in yeast has not been achieved, likely due to the absence of an innate *O*-acetylation mechanism in *P. pastoris*. This chapter focuses on the primary objective of reconstructing and elucidating the plant xyloglucan backbone *O*-acetylation pathway within *Yarrowia lipolytica*, a non-conventional yeast species that may naturally possess an *O*-acetylation mechanism. Specifically, the project involves the heterologous expression and functional characterization of the *CSLC4*, *XXT2*, and *XyBAT1* genes, which are responsible for synthesizing the *O*-acetylated glucan backbone.

4.1.1 Advantages of heterologous expression over other conventional methods

Understanding the mechanisms and regulation of plant cell wall biosynthetic enzymes is essential for advancing the study of plant cell walls (Keegstra, 2010). Various traditional methods have been employed to identify genes involved in this complex process. Reverse genetics approaches, such as those used by Brown et al. (2011) and Cocuron et al. (2007),

involve disrupting candidate genes and analyzing the resulting phenotypes, while forward genetics relies on screening mutant populations for specific phenotypes, as demonstrated by studies like Arioli et al., (1998) and Madson et al., (2003). Additionally, protein purification followed by partial peptide sequencing has been a valuable method for identifying specific enzymes involved in cell wall biosynthesis, as seen in the work of Crombie et al., (1998) and Edwards et al., (1999). Although these methods have successfully identified many key enzymes, they come with significant limitations. For instance, direct protein purification from host tissue involves extracting enzymes and then sequentially fractionating them using techniques such as size exclusion or ion exchange chromatography. The enzyme of interest is identified using specific enzymatic assays, and the peptides are partially sequenced after obtaining an enriched fraction. This approach has led to the identification of several important enzymes, such as mannan galactosyltransferase (Edwards et al., 1999) and XyG glucosidase (Crombie et al., 1998). However, this method has notable challenges, including the need for highly specific and sensitive activity assays, and the necessity of fully solubilizing the enzyme. Moreover, the availability of specific donor or acceptor substrates, like radiolabeled nucleotide sugars, is critical. Given that many glycosyltransferases are membrane-bound and part of multi-enzyme complexes, solubilizing these enzymes without losing their functionality can be particularly challenging (Atmodjo et al., 2011; Chou et al., 2012; Zeng et al., 2010). Forward genetics, another powerful approach, is well-suited for identifying genes based on observable mutant phenotypes. This method has been instrumental in discovering genes with previously unknown functions, as exemplified by the identification of TBL proteins in polysaccharide acetylation (Gille et al., 2011b). Additionally, forward genetics can reveal unexpected roles for known genes, such as the involvement of the XyG galactosyltransferase MUR3 in cytoskeleton organization (Tamura et al., 2005). However, forward genetics is inherently time-consuming and is limited to species with short generation times that are capable of being crossed and transformed. The method is also constrained by the available assay techniques and may fail to identify essential genes or those with redundant functions. The availability of insertional mutants in model species like *Arabidopsis thaliana*, *Brachypodium distachyon*, and maize has facilitated forward genetic approaches, leading to the identification of genes involved in the biosynthesis of important cell wall components like XyG, xylan, mannan, and lignin. Despite its effectiveness, this approach is less useful in cases of gene redundancy and mutant lethality (Goubet et al., 2003; Jensen et al., 2012).

Heterologous expression of plant cell wall biosynthetic genes offers a complementary or alternative approach to traditional methods. By expressing these genes in a different host system, researchers can study the enzymes *in vivo* and directly observe the products of their activity. This method has successfully identified enzymes such as xylan arabinosyltransferase (Anders et al., 2012) and has demonstrated that proteins like CSLH, CSLF, and ManS can function as β -1,3;1,4 glucan synthases (Doblin et al., 2009). However, using plant hosts for heterologous expression presents several challenges. The plant must provide appropriate acceptor and donor substrates for the enzymes to act upon, and the expression levels of the candidate genes often do not reach saturating levels of activity, which can limit the effectiveness of functional assays. Additionally, the process of creating transgenic plants is both time-consuming and technically demanding. While species like *A. thaliana* (Clough and Bent, 1998) can be transformed relatively easily using methods such as floral dip with *Agrobacterium tumefaciens*, other species, including *Brachypodium distachyon*, maize, rice, wheat, and sugarcane, require tissue culture stages that can extend the process to 4-5 months (Shrawat and Lörz, 2006). To overcome some of these limitations, non-plant systems offer a faster and potentially more efficient alternative. For instance, *Escherichia coli* can be used for rapid gene expression, but it lacks an endomembrane system and protein glycosylation pathways, which are critical for the proper functioning of many plant enzymes. Additionally, bacterial systems like *E. coli* lack a Golgi apparatus, where plant *O*-acetylation machinery is localized, making it an unsuitable environment for some plant proteins (Baker et al., 2014; Jones et al., 2021). *Neurospora crassa*, a genetically tractable filamentous fungus, presents another option, but its hydrolytic enzymes could degrade the target polysaccharides, complicating the analysis unless these genes are knocked out (Bauer et al., 2006; Tian et al., 2009). Insect cell cultures, such as S2 cells, have been successfully used to express plant proteins like CSLA for *in vitro* demonstration of mannan synthase activity (Liepman et al., 2005). However, these systems are slow growing compared to other alternatives. While mammalian cell culture offers another eukaryotic expression system, it has not been widely used for plant glycosyltransferases due to its high cultivation costs, slower growth rates, and more complex genetic manipulation requirements (Gray, 2001). Yeast expression systems, particularly *Pichia pastoris*, provide a more balanced alternative. Yeast offers the advantages of a eukaryotic system that is more similar to plants while maintaining simpler and faster culturing requirements. Previous studies have successfully expressed plant cell wall biosynthetic genes in *Pichia pastoris*, including the CSLC4 glucan synthase involved in XyG biosynthesis (Cocuron et al., 2007), as well as enzymes like MUR3, XyG xylosyltransferases,

XyG xylosidase, XyG fucosidase, and heteromannan mannan synthase (Cavalier and Keegstra, 2006; Günl and Pauly, 2011; Madson et al., 2003; Voiniciuc et al., 2019). These successes highlight yeast as a versatile and effective system for the heterologous expression of plant proteins, enabling detailed in vitro activity assays and advancing our understanding of plant cell wall biosynthesis.

4.1.2 Advantages of *Yarrowia lipolytica* for *O*-acetylation studies over *Pichia pastoris*

In synthetic orthogonal metabolic engineering initiatives, various yeast species have been evaluated as model organisms for studying *O*-acetylation of plant cell wall polysaccharides. Initially, attention was on *P. pastoris*, a non-conventional yeast, not for *O*-acetylation but for investigating heteromannan synthesis. The aim was to understand the properties of these polymers and the role of CELLULOSE SYNTHASE LIKE A (CSLA) proteins responsible for their heteromannan synthesis in plants. Through expression of *CSLA* gene family members from plants like *A. thaliana* and *A. konjac*, synthesis of heteromannans such as linear mannan and glucomannan was achieved (Voiniciuc et al., 2019). However, *P. pastoris* was found unsuitable for *O*-acetylation studies due to its lack of a natural acetylation mechanism. Attempts to introduce *AkTBL25*, an acetylation enzyme from *Amorphophallus konjac* responsible for acetylating heteromannan, did not result in successful acetylated mannan production (Tim Niedzwetzki, unpublished). Consequently, *Y. lipolytica* emerged as a promising alternative due to its similar cell wall structure to *P. pastoris* and *S. cerevisiae*, along with its natural acetylation capability (Pauly et al., 2019; Vicente Ramírez, unpublished). *Y. lipolytica* emerged with the highest cell wall-bound acetate content compared to other yeast species, making it the most promising candidate, likely harboring an *O*-acetylation mechanism (Vicente Ramirez, unpublished). A protein BLAST analysis to identify an *AtRWA2* ortholog revealed *Yarrowia lipolytica* CAPSULE SYNTHASE 1 (*YICAS1*), further confirming *Y. lipolytica* as a suitable candidate. Subsequent analyses demonstrated that *YICAS1* shares GDS and DxxH motifs with *CnCas1* (Patrick Micke, unpublished). Additionally, the *ylcas1* knockout strain exhibited a complete lack of acetate in the cell wall compared to the WT strain, providing a valuable tool to study the *O*-acetylation mechanism in vivo (Nina Boots, unpublished).

Yarrowia lipolytica offers several advantages over plant hosts, being easy to transform, growing rapidly, and lacking endogenous plant cell wall components. Molecular biology tools,

such as efficient gene cassettes and plasmids, have been developed for engineering non-conventional yeasts like *Y. lipolytica* (Ma et al., 2020). The TEF (pTEF) promoter, a native and widely used promoter, has been employed for the expression of the gene of interest (GOI) (Müller et al., 1998). To get advantage over gene induction by inducers inducible promoters were developed to dissociate the growth phase and GOI production phase. The pEYK300A3B (pEYK) hybrid promoter induced by erythritol with pEYK being the strongest known inducible promoter for *Y. lipolytica*, resulting in five-fold higher expression compared to pTEF (Trassaert et al., 2017). The terminators XPR2 and LIP2, known to influence mRNA stability and half-life, are commonly used in *Y. lipolytica* (Curran et al., 2015; Madzak et al., 2000; Pignéde et al., 2000). For selection of transformed cells, markers such as LEU2, URA3 (auxotrophic markers), and antibiotics like nourseothricin (Nat) are available. *Y. lipolytica* is sensitive to phleomycin, hygromycin, and nourseothricin (Kretzschmar et al., 2013; Tsakraklides et al., 2018; Wagner et al., 2018). Both replicative and integrative vectors are available for *Y. lipolytica*, with integrative vectors being suitable for stable GOI integration into the yeast genome. Targeted integration is achieved by homologous recombination into specific integration sites, and knockout mutation of *KU70* improves homologous recombination success rates (Holkenbrink et al., 2018; Kretzschmar et al., 2013). Eleven integration sites have been identified for targeted integration. The EasyCloneYALI vector set comprises plasmids suitable for constructing multiple insertion vectors at four distinct loci (Holkenbrink et al., 2018).

4.1.3 Considerations for reconstruction of glucan *O*-acetylation pathway in *Y. lipolytica*

For the heterologous production of *O*-acetylated glucan backbone, the plant cell wall biosynthetic genes of interest are selected. Transcriptomics identified a XyG synthase, *CSLC4*, in developing *Tropaeolum majus* seeds (Cocuron et al., 2007) (see section 1.1.3.4). To confirm the XyG:glucan synthase activity of *CSLC4*, the *Nasturtium* gene (*TmCSLC4*) and a homologous *A. thaliana* gene (*AtCSLC4*) were expressed in *Pichia pastoris*. Heterologous expression resulted in the appearance of short β -1,4-linked glucan oligosaccharides, confirming *CSLC4*'s function as a XyG:glucan synthase (Cocuron et al., 2007). Despite the absence of xylose addition to the polymer due to *Pichia* cells' inability to produce UDP-xylose, the mere presence of the XXT protein seemed to facilitate glucan production (Pauly and Keegstra, 2016). The genes *TmCSLC4* and *TmXXT2* were selected based on their involvement

in XyG glucan backbone biosynthesis (see section 1.1.2.2.4). A study from 2016 uncovered a XyG glucan backbone *O*-acetyltransferase (XYBAT) specific to the grass species *Brachypodium distachyon* through the examination of grass-specific TBLs (Liu et al., 2016). Upon heterologous expression of the *XyG backbone acetyltransferase (BdXyBAT)* in *A. thaliana* plants, the glucan backbone undergoes *O*-acetylation, a process that doesn't naturally occur in non-transformed plants (Liu et al., 2016). Thus, *BdXyBAT1* gene is selected with an aim of producing *O*-acetylated glucan backbone.

4.2 Results

4.2.1 Engineering *Y. lipolytica* strains for xyloglucan backbone *O*-acetylation pathway integration

To reconstruct and functionally characterize the *O*-acetylation mechanism of the plant xyloglucan backbone, the genes *TmCSLC4*, *TmXXT2*, and *BdXyBAT1* were introduced into *Yarrowia lipolytica* strains (Figure 4-1 B). Four different gene combinations were transformed into both the WT and the *ylcas1* strains: *CSLC4*; *CSLC4* and *XXT2*; *CSLC4* and *XyBAT1*; and *CSLC4*, *XXT2*, and *XyBAT1*. The *ylcas1* strain serves as a control to determine whether XyBAT1 alone is sufficient to *O*-acetylate the glucan backbone, or if a native machinery is required for XyBAT1 functionality. All genes were cloned into the pCfB4780 integrative vector, driven by the pEYK promoter—an inducible promoter activated in the presence of erythritol as the carbon source. The pCfB4780 vector should guide the integration of the expression cassette at a specific locus (D-1) within chromosome D of the host strain through homologous recombination (Figure 4-1 A). However, genotyping results depicted in Figure 4-1C revealed that the integration occurred randomly, rather than at the intended loci within chromosome D. The amplicon observed in reaction A in all the strains (Figure 4-1 C) indicates that the original integration site remained intact, suggesting that homologous recombination with the transformed expression cassette did not occur. The presence of an amplicon in reaction C in all the strains (Figure 4-1 C), generated using internal primers binding to the transgenes, confirms successful integration, but not at the intended D-1 site, indicating random integration. This discrepancy could be due to inefficient homologous recombination, potentially caused by insufficient homology between the vector and the target locus, or the cell's reliance on alternative DNA repair pathways, such as non-homologous end joining (NHEJ), leading to random integration.

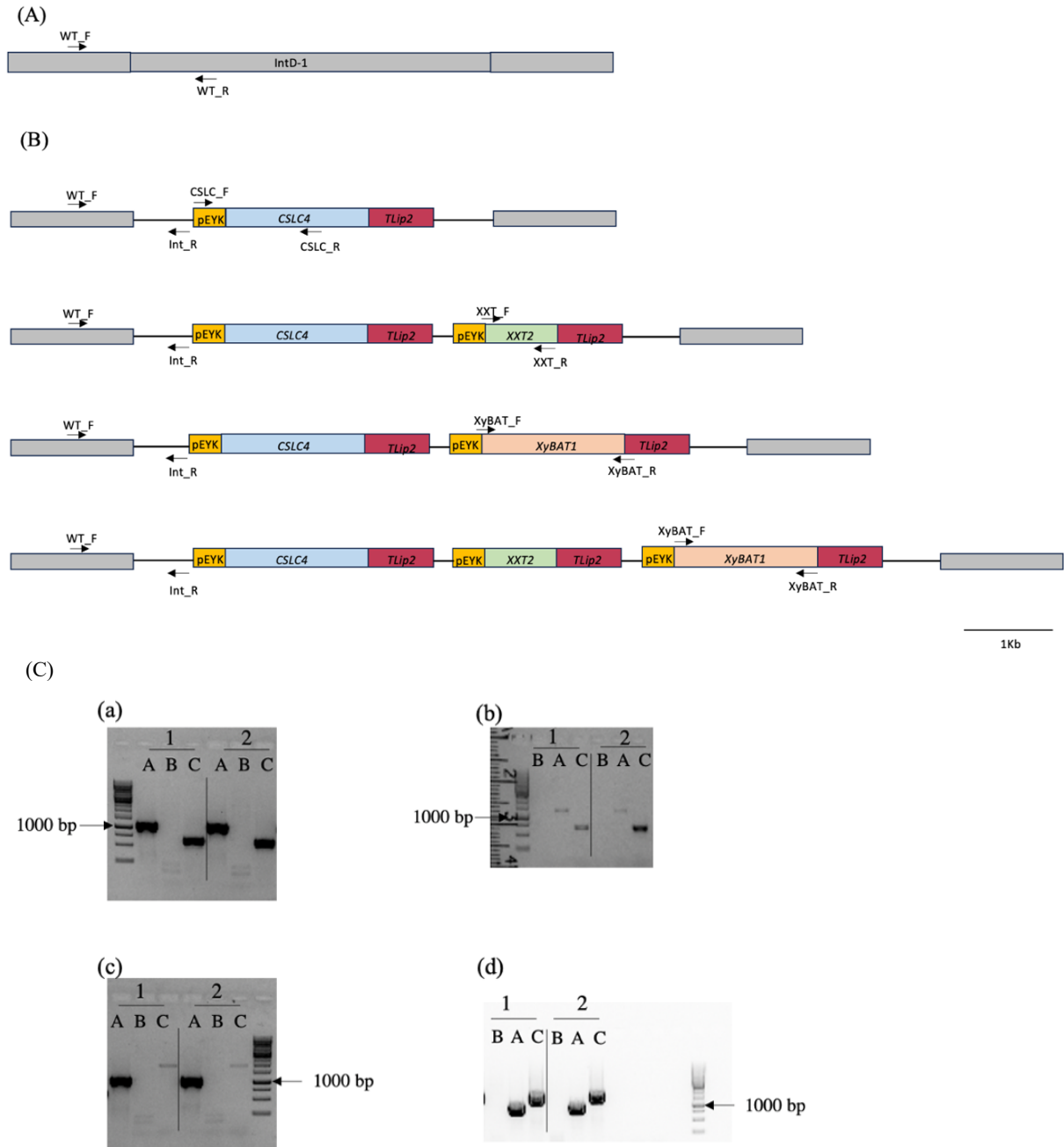


Figure 4-1. Genotyping *Y. lipolytica* transgenic strains.

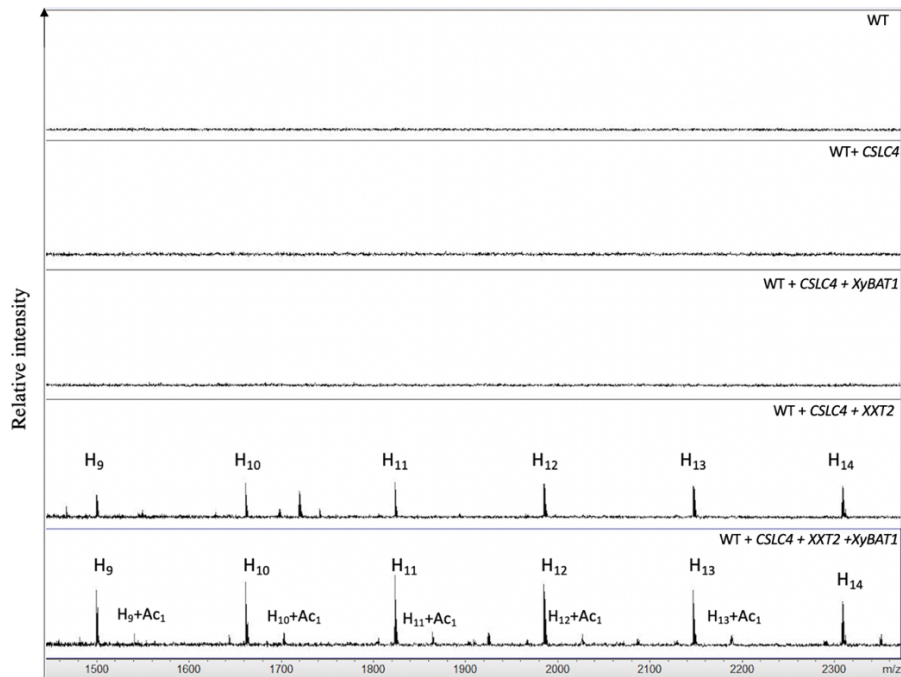
(A) Depiction of integration site D-1 in *Y. lipolytica* genome. (B) Depiction of integration site D-1 after transformation of expression cassette with transgenes. The arrows indicate the binding sites of genotyping primers. (C) Representative image of genotyping PCR results aimed at detecting the presence of transgenes in *Y. lipolytica*. (a) Genotyping PCR conducted for strains transformed with the *CSLC4* gene. (b) Genotyping PCR carried out for strains transformed with both *CSLC4* and *XXT2* genes. (c) Genotyping PCR executed for strains transformed with *CSLC4* and *XyBAT1* genes. (d) Genotyping PCR performed for strains transformed with *CSLC4*, *XXT2*, and *XyBAT1* genes. The numbers 1 and 2 within each gel picture indicate the WT and *ylcas1* strains transformed with the expression cassette. The alphabets A, B, and C within each gel picture represent the amplicons used to assess the WT genotype (WT_F and WT_R), integration site-specific transformed genotype (WT_F and Int_R), and

internal primers binding in the transgene (CSLC_F, CSLC_R, XXT_F, XXT_R, XyBAT_F, and XyBAT_R).

4.2.2 Oligosaccharide mass profiling (OLIMP) analysis of *O*-acetylated glucan synthesis in engineered *Y. lipolytica* strains

OLIMP utilizes the specificity of glycosylhydrolases to cleave distinct polysaccharides from cell wall material, releasing oligosaccharides that are subsequently analyzed via mass spectrometry. Although OLIMP can estimate the overall composition of an oligosaccharide by analyzing the mass-to-charge ratio of its monosaccharide units, it cannot distinguish between isomeric monosaccharides (those with the same mass but different structures) or determine the glycosidic linkages between them, as it relies solely on mass-to-charge ratio without providing details on structural variations. To analyze the production of an *O*-acetylated glucan backbone in the *Y. lipolytica* transgenic strains, the AIR material obtained after 3 days of induction was digested with endo- β -1,4-glucanase (E-CELBA), which releases β -1,4-glucan oligosaccharides with varying degrees of polymerization (DP). The WT strains expressing *CSLC4* and *XXT2* exhibited a clear hexose ladder (Figure 4-2 A), consistent with the presence of a glucan backbone. When *XyBAT1* was co-expressed with *CSLC4* and *XXT2*, the strains produced an additional *O*-acetylated hexose ladder, which might be an *O*-acetylated glucan. However, in the *ylcas1* strains expressing same genes, this *O*-acetylated hexose ladder was absent (Figure 4-2 B), suggesting that *YICAS1* functionality is essential for *XyBAT1* activity. Strains expressing *CSLC4* alone or in combination with *XyBAT1* did not show a detectable hexose ladder (Figure 4-2), indicating that *XXT2* is necessary for glucan oligosaccharide production (Cocuron et al., 2007). Additionally, no pentose side-chain decoration was detected in any of the strains, suggesting the possible absence of xylosylation (Cocuron et al., 2007; Schultink, 2013). To further confirm and quantify whether the produced hexose ladders consist of 1,4-linked glucans, a monosaccharide compositional analysis and a glycosidic linkage analysis were performed on the oligosaccharides released after glucanase digestion.

(A)



(B)

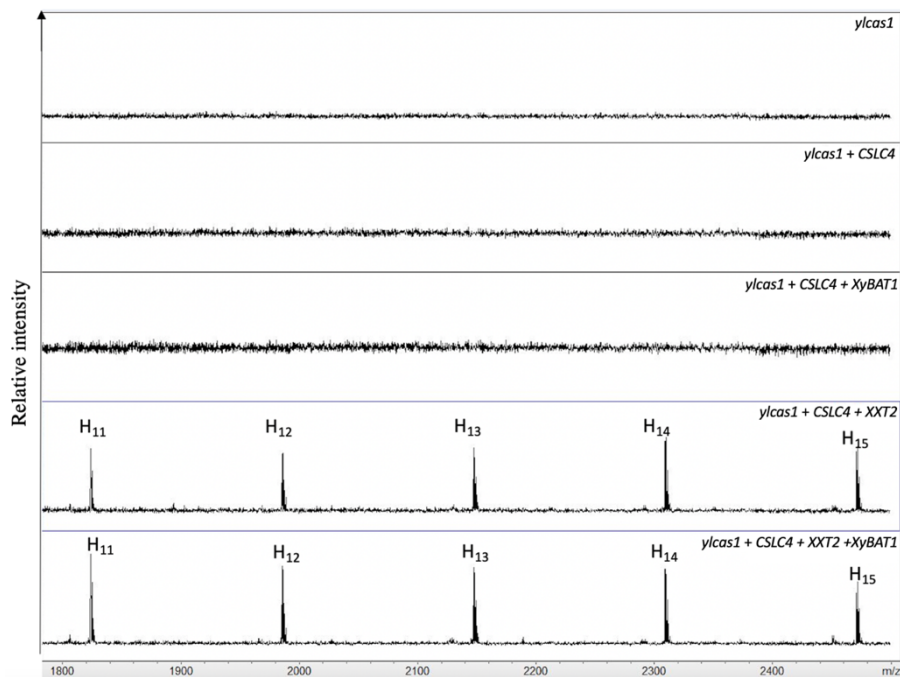


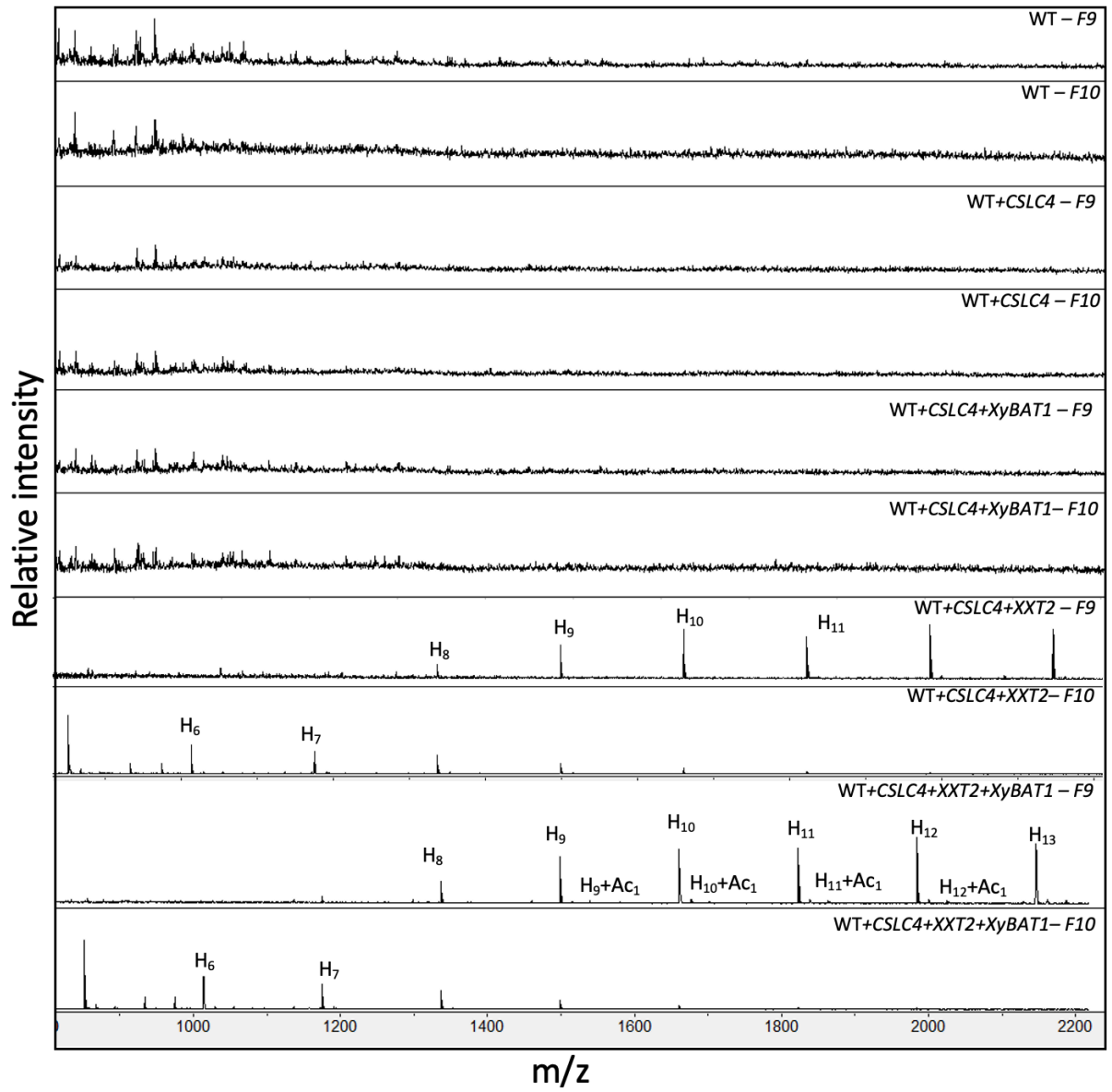
Figure 4-2. OLIMP Spectra of E-CELBA digested transgenic *Y. lipolytica* AIR.

(A) OLIMP spectrum of transgenic *Y. lipolytica* strains expressing *CSLC4*; *CLSC4* and *XXT2*; *CSLC4* and *XyBAT1*; *CSLC4*, *XXT2* and *XyBAT1* on WT background after E-CELBA enzymatic digest on AIR material. (B) OLIMP spectrum of transgenic *Y. lipolytica* strains expressing *CSLC4*; *CLSC4* and *XXT2*; *CSLC4* and *XyBAT1*; *CSLC4*, *XXT2* and *XyBAT1* on *ylcas1* background after E-CELBA enzymatic digest on AIR material. H_n-number of hexoses; Ac_n-number of *O*-acetyl substituents. The spectra show (M+Na⁺) adducts.

4.2.3 Cell wall characterization of transgenic *Y. lipolytica* strains for *O*-acetylated 4-glucan backbone production

To further confirm and quantify whether the hexose ladders produced by transgenic strains co-expressing *CSLC4* and *XXT2* or *CSLC4*, *XXT2*, and *XyBAT1* consist of 1,4-linked glucans, a monosaccharide compositional analysis and glycosidic linkage analysis were performed on the oligosaccharides released after E-CELBA digestion. The procedure involved separating 75% of the supernatant from the E-CELBA digested 4 mg AIR based on molecular weight using size exclusion chromatography (SEC). The resulting fractions from SEC were then analyzed using OLIMP to identify those containing hexose or acetylated hexose oligosaccharides. These fractions were pooled and subjected to monosaccharide composition analysis and glycosidic linkage analysis. The remaining 25% of the E-CELBA digested AIR supernatant was used as a control without SEC separation for monosaccharide composition analysis. Additionally, the leftover pellet from the E-CELBA digestion also underwent monosaccharide compositional analysis. The total monosaccharides from the SEC fractions, supernatant, and pellet were then compared with those in undigested samples as control. During OLIMP analysis the WT strains expressing *CSLC4* and *XXT2*, a distinct hexose ladder appeared in fractions 9 and 10 (Figure 4-2A), indicating the presence of a glucan backbone (see appendix Figure 9-6 and 9-7 for the spectra of remaining 13 fractions and SEC chromatograms). When *XyBAT1* was co-expressed with *CSLC4* and *XXT2*, the strains produced an additional *O*-acetylated hexose ladder. However, in the *ylcas1* strains expressing the same genes, the *O*-acetylated hexose ladder was absent (Figure 4-2B), consistent with the results observed in section 4.2.2. Strains expressing *CSLC4* alone or in combination with *XyBAT1* did not exhibit a detectable hexose ladder. Consequently, fractions 9 and 10 were pooled for all samples and further analyzed for monosaccharide composition. The glycosidic linkage analysis was also performed on the SEC separated fractions 9 and 10.

(A)



(B)

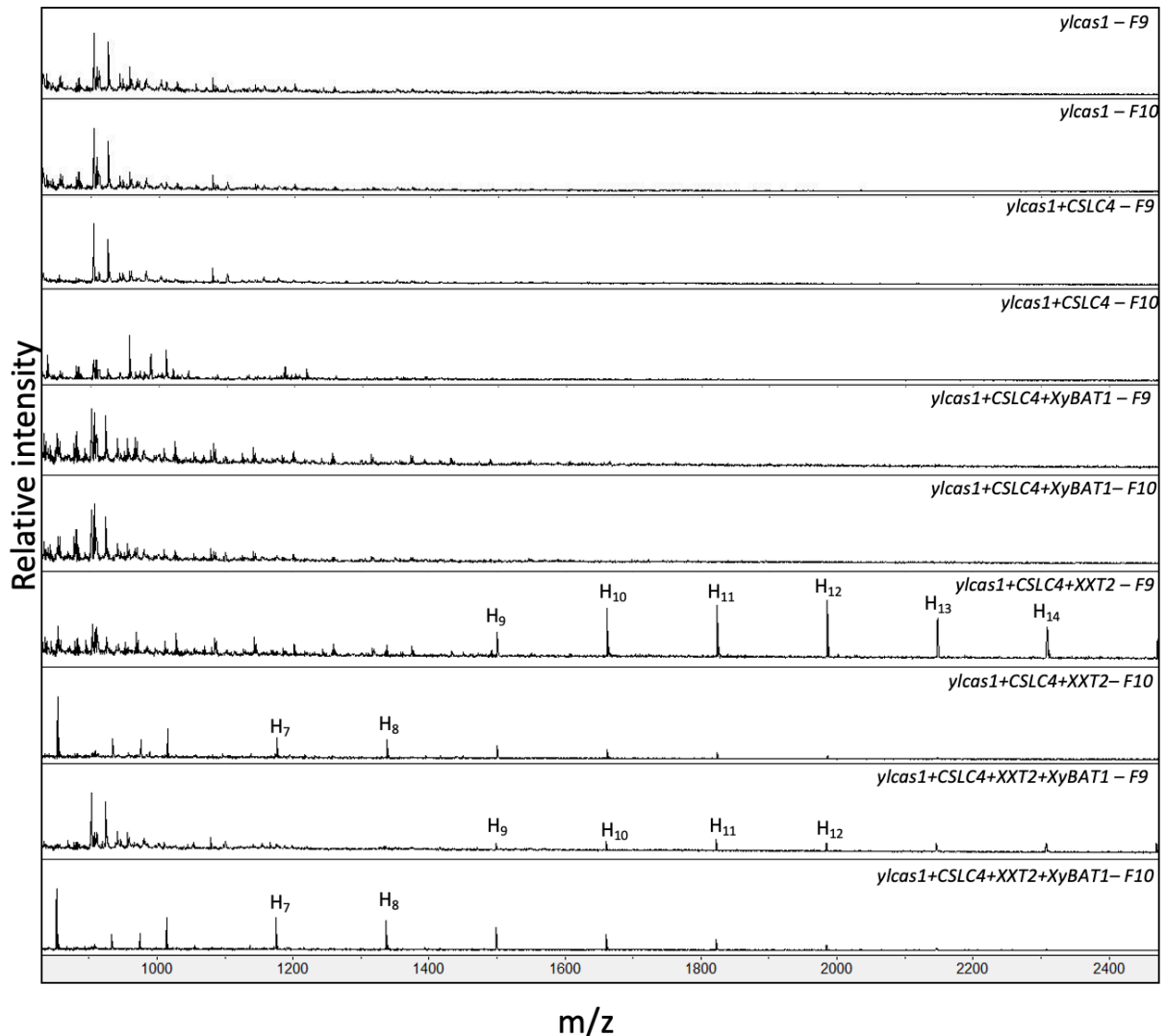


Figure 4-3. OLIMP spectra of fraction 9 and 10 obtained through SEC separation of E-CELBA digested transgenic *Y. lipolytica* AIR.

(A) OLIMP spectra of fraction 9 and 10 separated using SEC of E-CELBA hydrolyzed AIR from transgenic *Y. lipolytica* strains expressing *CSLC4*; *CLSC4* and *XXT2*; *CSLC4* and *XyBAT1*; *CSLC4*, *XXT2* and *XyBAT1* on a WT background. (B) OLIMP spectra of fraction 9 and 10 separated using SEC of E-CELBA hydrolyzed AIR from transgenic *Y. lipolytica* strains expressing *CSLC4*; *CLSC4* and *XXT2*; *CSLC4* and *XyBAT1*; *CSLC4*, *XXT2* and *XyBAT1* on *ylcas1* background. H_n - number of hexoses; Ac_n - number of *O*-acetyl substituents; F9 – Fraction 9; F10 – Fraction 10. The spectra show (Mass + Na⁺) adducts.

The monosaccharide compositional analysis of the E-CELBA digested AIR indicates that about 90% of the oligos in SEC-separated fractions 9 and 10 are primarily contained glucose, with only minor traces of glucosamine, galactose, and mannose (see Table 13A). There was no significant difference in glucose content between the WT or *ylcas1* strains and those expressing *CSLC4*, *XXT2*, and *XyBAT1*, or just *CSLC4* and *XXT2*, where both hexose and *O*-acetylated hexose ladders were observed in OLIMP (Table 13A and Figure 4-3). Glycosidic linkage analysis on these fractions revealed a notable increase of 4-glucose, about 5-6%, in the SEC fractions from strains co-expressing *CSLC4* and *XXT2*, or *CSLC4*, *XXT2*, and *XyBAT1*, compared to other strains (Figure 4-4). The control supernatant showed a significant amount of galactose, mannose, and glucosamine, indicating that the E-CELBA endo- β -1,4-glucanase also digests other nonspecific polymers (Table 13B). This is further supported by the substantial abundance of 3,6-glucose and 6-glucose observed in the glycosidic linkage analysis of the SEC separated fractions (Figure 4-4). These linkages are typically present in native *Y. lipolytica* wall. These results suggests that while the enzyme is somewhat unspecific, it is still capable of digesting β -1,4-glucans. Comparing the total sugars from SEC fractions, the supernatant, and the pellet, no substantial increase in glucose was observed in 1,4-glucan producing strains, suggesting that the transgenes did not significantly alter the overall sugar composition of the *Yarrowia* wall (Table 13D). This conclusion is corroborated by the lack of observed changes in the composition of undigested AIR (Table 13E). The reduced sugar content in some strains, as seen in the sum of sugars from SEC fractions, supernatant, and pellet, may be due to the loss of sugars in 13 SEC fractions not included in the analysis. Overall, these results confirm that the transgenic *Yarrowia* strains expressing *CSLC4*, *XXT2*, and *XyBAT1*, or *CSLC4* and *XXT2*, can produce a 4-glucan backbone. Combined with OLIMP analysis, this suggests that the *O*-acetylated hexose ladder observed in the WT strain co-expressing *CSLC4*, *XXT2*, and *XyBAT1* is likely composed of *O*-acetylated 1,4-glucan.

(A)

E-CELBA digested AIR supernatant SEC fractions 9 and 10 (monosaccharides in $\mu\text{g}/\text{mg}$ AIR)												
Strains	Gal			Glc			GlcAm			Man		
	Mean	SD	stats	Mean	SD	stats	Mean	SD	stats	Mean	SD	stats
WT	3.09	0.86	ab	196.25	43.32	ab	1.92	0.09	cd	10.01	1.45	c
WT+ <i>CSLC4</i>	4.76	0.49	ab	137.23	34.64	ab	0.92	0.56	d	12.82	0.01	c
WT+ <i>CSLC4</i> + <i>XyBAT1</i>	4.28	0.17	ab	172.42	1.68	ab	3.43	1.10	bcd	12.88	0.42	c
WT+ <i>CSLC4</i> + <i>XXT2</i>	5.13	0.30	ab	145.32	24.49	ab	4.88	1.12	abcd	16.92	0.42	bc
WT+ <i>CSLC4</i> + <i>XXT2</i> + <i>XyBAT1</i>	2.88	0.40	b	206.95	16.65	ab	12.55	5.43	a	21.51	2.48	abc
<i>ylcas1</i>	2.54	0.83	b	110.81	34.29	b	5.71	1.31	abcd	9.05	0.81	c
<i>ylcas1</i> + <i>CSLC4</i>	4.10	1.38	ab	131.27	27.97	ab	0.58	0.12	d	10.25	0.88	c
<i>ylcas1</i> + <i>CSLC4</i> + <i>XyBAT1</i>	3.60	0.68	ab	126.52	3.82	ab	6.70	2.84	abcd	11.83	0.62	c
<i>ylcas1</i> + <i>CSLC4</i> + <i>XXT2</i>	9.27	3.07	a	187.84	18.45	ab	9.91	1.78	abc	29.46	7.60	ab
<i>ylcas1</i> + <i>CSLC4</i> + <i>XXT2</i> + <i>XyBAT1</i>	8.39	3.42	ab	241.46	49.18	a	11.56	0.77	ab	36.67	10.00	a

(B)

E-CELBA digested AIR supernatant (monosaccharides in $\mu\text{g}/\text{mg}$ AIR)												
Strains	Gal			Glc			GlcAm			Man		
	Mean	SD	stats	Mean	SD	stats	Mean	SD	stats	Mean	SD	stats
WT	10.41	1.45	c	70.20	1.51	cd	5.29	0.03	ab	50.11	3.60	bc
WT+ <i>CSLC4</i>	15.98	1.60	c	55.85	1.25	d	8.44	0.44	ab	35.87	0.16	c
WT+ <i>CSLC4</i> + <i>XyBAT1</i>	15.37	1.11	c	55.08	8.62	d	8.53	1.72	ab	38.37	3.35	c
WT+ <i>CSLC4</i> + <i>XXT2</i>	30.08	2.82	ab	86.65	10.33	c	5.02	1.12	b	66.93	4.06	ab
WT+ <i>CSLC4</i> + <i>XXT2</i> + <i>XyBAT1</i>	26.16	1.84	b	97.09	11.72	c	7.99	0.42	ab	65.24	2.41	ab
<i>ylcas1</i>	15.46	1.07	c	99.71	3.87	bc	9.16	1.41	a	67.20	2.97	ab
<i>ylcas1</i> + <i>CSLC4</i>	15.51	3.35	c	89.39	13.05	c	7.98	1.79	ab	70.08	14.15	ab
<i>ylcas1</i> + <i>CSLC4</i> + <i>XyBAT1</i>	13.02	0.23	c	80.42	0.65	cd	7.04	0.37	ab	62.34	2.29	ab
<i>ylcas1</i> + <i>CSLC4</i> + <i>XXT2</i>	32.34	1.65	ab	128.75	9.08	ab	8.09	0.07	ab	76.50	7.39	a
<i>ylcas1</i> + <i>CSLC4</i> + <i>XXT2</i> + <i>XyBAT1</i>	34.43	2.34	a	133.45	0.31	a	9.01	0.63	ab	80.81	5.32	a

(C)

E-CELBA digested AIR pellet (monosaccharides in $\mu\text{g}/\text{mg}$ AIR)												
Strains	Gal			Glc			GlcAm			Man		
	Mean	SD	stats	Mean	SD	stats	Mean	SD	stats	Mean	SD	stats
WT	6.19	6.05	abc	100.08	71.30	a	31.45	22.34	a	38.34	21.99	a
WT+ <i>CSLC4</i>	9.90	2.32	abc	141.85	16.24	a	46.59	5.04	a	43.57	5.82	a
WT+ <i>CSLC4</i> + <i>XyBAT1</i>	8.56	2.56	abc	113.71	53.27	a	51.52	7.19	a	35.86	7.55	a
WT+ <i>CSLC4</i> + <i>XXT2</i>	21.36	1.93	a	176.94	11.67	a	77.71	4.01	a	64.47	7.54	a
WT+ <i>CSLC4</i> + <i>XXT2</i> + <i>XyBAT1</i>	20.07	3.61	ab	145.58	59.26	a	87.38	9.11	a	55.21	11.32	a
<i>ylcas1</i>	4.08	1.53	bc	209.25	19.68	a	71.93	6.80	a	22.26	2.69	a
<i>ylcas1</i> + <i>CSLC4</i>	8.49	6.86	abc	183.95	67.21	a	56.78	28.44	a	37.57	12.51	a
<i>ylcas1</i> + <i>CSLC4</i> + <i>XyBAT1</i>	3.26	2.54	c	128.29	40.04	a	57.27	12.43	a	25.87	4.66	a
<i>ylcas1</i> + <i>CSLC4</i> + <i>XXT2</i>	11.78	6.16	abc	185.19	55.99	a	77.77	23.42	a	50.99	14.15	a
<i>ylcas1</i> + <i>CSLC4</i> + <i>XXT2</i> + <i>XyBAT1</i>	8.05	4.22	abc	137.40	41.58	a	83.77	12.14	a	39.02	7.58	a

(D)

Sum of SEC Fraction 9 and 10 + Supernatant + Pellet (monosaccharides in $\mu\text{g}/\text{mg}$ AIR)													
Strains	Gal			Glc			GlcAm			Man			Sum of all sugars
	Mean	SD	stats	Mean	SD	stats	Mean	SD	stats	Mean	SD	stats	
WT	19.69	3.74	d	366.54	29.50	a	38.66	22.41	b	98.46	16.94	bc	523.34
WT+ <i>CSLC4</i>	30.65	3.43	bcd	334.93	52.13	a	55.95	4.92	ab	92.26	6.00	bc	513.78
WT+ <i>CSLC4</i> + <i>XyBAT1</i>	28.22	3.50	cd	341.21	63.57	a	63.48	7.81	ab	87.11	10.49	c	520.02
WT+ <i>CSLC4</i> + <i>XXT2</i>	56.58	0.59	a	408.90	25.82	a	87.61	4.01	ab	148.33	3.06	ab	701.42
WT+ <i>CSLC4</i> + <i>XXT2</i> + <i>XyBAT1</i>	49.10	5.85	abc	449.61	87.64	a	107.91	4.11	a	141.95	16.21	abc	748.58
<i>ylcas1</i>	22.07	3.43	d	419.77	57.84	a	86.80	6.90	ab	98.51	6.48	bc	627.15
<i>ylcas1</i> + <i>CSLC4</i>	28.09	11.59	cd	404.60	52.28	a	65.35	30.35	ab	117.90	27.55	abc	615.94
<i>ylcas1</i> + <i>CSLC4</i> + <i>XyBAT1</i>	19.89	2.09	d	335.23	35.57	a	71.01	9.22	ab	100.04	6.33	abc	526.17
<i>ylcas1</i> + <i>CSLC4</i> + <i>XXT2</i>	53.39	1.44	a	501.78	46.62	a	95.77	25.13	ab	156.95	0.84	a	807.89
<i>ylcas1</i> + <i>CSLC4</i> + <i>XXT2</i> + <i>XyBAT1</i>	50.86	9.98	ab	512.31	91.07	a	104.34	12.00	a	156.50	22.91	a	824.01

(E)

Undigested AIR (monosaccharides in µg/mg AIR)													
Strains	Gal			Glc			GlcAm			Man			Sum of all sugars
	Mean	SD	stats	Mean	SD	stats	Mean	SD	stats	Mean	SD	stats	
WT	55.60	17.09	a	291.02	102.02	a	60.46	26.49	ab	188.31	56.36	a	595.39
WT+ <i>CSLC4</i>	59.73	3.42	a	304.75	23.03	a	55.64	4.85	ab	210.36	13.49	a	630.47
WT+ <i>CSLC4</i> + <i>XyBAT1</i>	51.02	7.38	a	241.44	67.20	a	48.88	11.14	b	182.92	24.67	a	524.26
WT+ <i>CSLC4</i> + <i>XXT2</i>	49.40	0.43	a	267.90	6.01	a	65.51	1.52	ab	227.17	2.14	a	609.97
WT+ <i>CSLC4</i> + <i>XXT2</i> + <i>XyBAT1</i>	50.65	1.69	a	243.17	32.84	a	70.47	0.69	ab	230.57	5.81	a	594.85
<i>ylcas1</i>	56.12	2.83	a	364.36	4.36	a	88.42	1.66	ab	200.17	0.60	a	709.07
<i>ylcas1</i> + <i>CSLC4</i>	62.52	9.80	a	333.85	42.80	a	78.26	12.64	ab	226.69	35.67	a	701.32
<i>ylcas1</i> + <i>CSLC4</i> + <i>XyBAT1</i>	66.29	3.91	a	346.68	0.73	a	93.09	3.02	a	249.30	15.14	a	755.35
<i>ylcas1</i> + <i>CSLC4</i> + <i>XXT2</i>	45.64	7.83	a	302.26	2.89	a	77.58	2.95	ab	223.41	41.04	a	648.89
<i>ylcas1</i> + <i>CSLC4</i> + <i>XXT2</i> + <i>XyBAT1</i>	50.01	2.91	a	291.04	4.76	a	86.56	10.09	ab	252.35	17.59	a	679.96

Table 13. Monosaccharide compositional analysis of *Y. lipolytica* transgenic strains.

(A) Monosaccharide composition of E-CELBA digested AIR supernatant from transgenic *Y. lipolytica* strains. The samples were separated by SEC, and fractions 9 and 10 were specifically pooled and analyzed (B) Monosaccharide composition of E-CELBA digested AIR supernatant from transgenic *Y. lipolytica* strains without SEC separation. (C) Monosaccharide composition of E-CELBA digested AIR pellet left over after digestion. (D) Sum of monosaccharides from SEC fractions 9 and 10, the supernatant and the pellet. (E) Monosaccharide composition of undigested AIR from transgenic *Y. lipolytica* strains. The column “mean” indicates the average between 2 individual replicates of the same strain. “SD” indicates the standard deviation. The alphabets in the “stats” column indicate the statistically significant differences between the strains obtained through ANOVA and Tukey HSD. Abbreviations: Gal- Galactose; Glc- Glucose; GlcAm- Glucosamine; Man- Mannose.

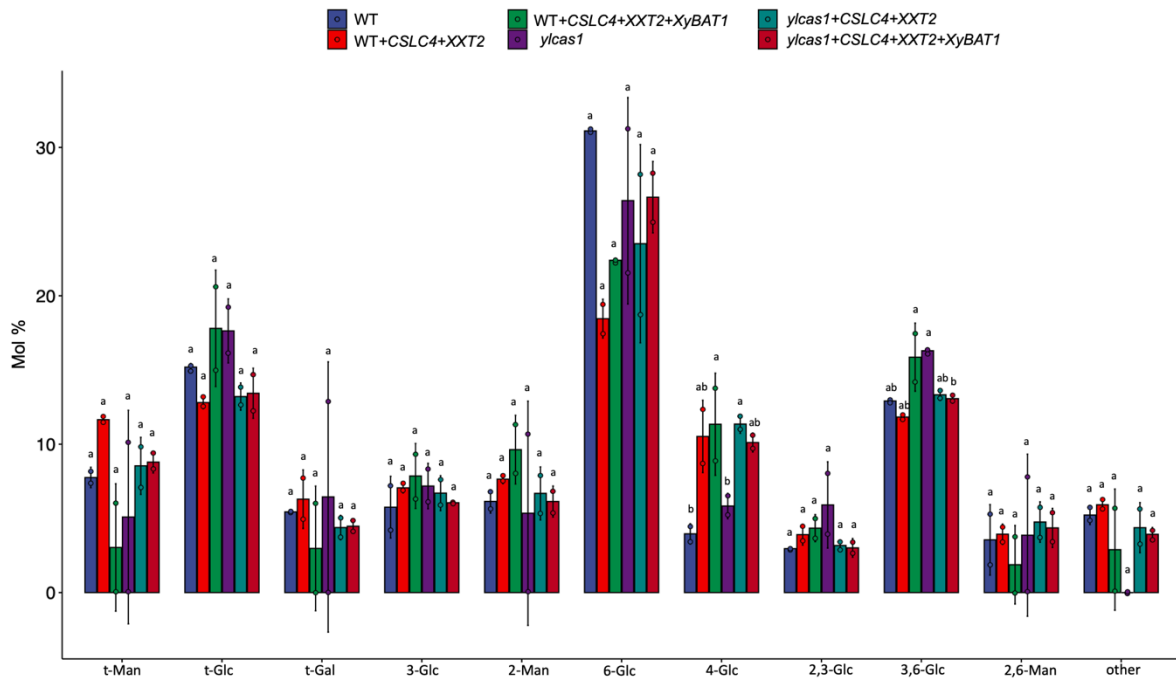


Figure 4-4. Glycosidic linkage analysis of transgenic *Y. lipolytica* strains.

Linkage analysis by gas chromatography was conducted on the E-CELBA digested AIR supernatant from transgenic *Y. lipolytica* strains expressing *CSLC4* and *XXT2*, as well as those expressing *CSLC4*, *XXT2*, and *XyBAT1*. The samples were separated by SEC, and fractions 9 and 10 were specifically pooled and analyzed. The major peaks from the chromatograms were integrated and identified based on retention times and fragment ion signatures, then expressed as mol percentages. The bars in the graph represent the average values with standard deviations between two individual replicates of the same strain. Statistically significant differences between the strains were determined using ANOVA followed by Tukey HSD, with different letters indicating significance. Abbreviations: t-terminal; Gal—Galactose; Glc—Glucose; Man—Mannose.

4.3 Discussion

4.3.1 *O*-acetylated glucan backbone production in *Y. lipolytica*

The process of elucidating the mechanisms involved in the synthesis of cell wall polysaccharides continues to pose significant challenges in plant biology. Even with the advancements brought by the genomics era, which have led to the identification of numerous genes involved in hemicellulose biosynthesis, many of these genes still require detailed functional characterization (Davis et al., 2010). Our study demonstrates the potential of employing synthetic biology tools in yeast to gain mechanistic insights into the *O*-acetylation pathway of the xyloglucan (XyG) backbone, a pathway that has proven difficult to study both in planta and in vitro. For example, expressing *OsXyBAT6* in wild-type *A. thaliana* plants resulted in severe growth defects, complicating further investigation (Zhong et al., 2020a). In this study, we successfully demonstrated the co-expression of *TmCSLC4* and *TmXXT2* in *Yarrowia lipolytica*, which are responsible for synthesizing the β -1,4-glucan backbone—a critical component of XyG. These findings are consistent with previous observations in *Pichia pastoris* (Cocuron et al., 2007). Notably, the addition of *BdXyBAT1* alongside *TmCSLC4* and *TmXXT2* in WT strains, as analyzed through OLIMP and glycosidic linkage analysis, confirmed the presence of an acetylated hexose, which is most likely an *O*-acetylated β -1,4-glucan. This suggests that *BdXyBAT1* was functional within the *Y. lipolytica* system, effectively transferring acetyl groups to the glucan backbone. The detection of this acetylated product indicates that the engineered pathway successfully produced an acetylated glucan, representing a significant achievement in reconstituting plant polysaccharide acetylation within a yeast system. To further verify the structure of the *O*-acetylated glucan, a ^1H NMR analysis of the enriched *O*-acetylated glucan could be conducted. An important observation was that the co-expression of these genes produced an *O*-acetylated glucan backbone, despite the fact that not all genes presumed to be involved in plant *O*-acetylation were expressed, such as *AXY9* and *RWAs* (Manabe et al., 2013, 2011; Schultink et al., 2015). The activity of *YICAS1* might be compensating for the missing factors, as it is thought to fulfil similar roles to *RWAs* and *TBLs*. For this compensation to occur, *BdXyBAT1* might interact with *YICAS1*, or the predicted transmembrane activity of *YICAS1* might lead to a pool of acetyl-donors in the Golgi lumen that *BdXyBAT1* can utilize. This hypothesis is further supported by the absence of *O*-acetylated oligos in the *ylcas1* knockout strain expressing the same genes, although an increase

in 4-glucose was observed. Further expressing *RWAs* and *AXY9* in the *ylcas1* strains producing 4-glucan backbone would help validate this hypothesis.

4.3.2 Functional interplay of CSLC4 and XXT2 in glucan chain production

The necessity for the expression of both *CSLC4* and *XXT2* for glucan chain production in *Y. lipolytica* suggests a potential interaction between these proteins, with *XXT2* likely playing a non-catalytic role in the process. This observation is consistent with previous findings that both *AtCSLC4* and *AtXXT2* are required for heterologous glucan synthase (GlcS) activity when expressed in *P. pastoris*, suggesting that these proteins form a complex, as demonstrated by bimolecular fluorescence complementation and co-immunoprecipitation (Chou et al., 2012; Cocuron et al., 2007). The requirement for *XXT2* alongside *CSLC4* for glucan chain production might serve as a mechanism to prevent *CSLC4* from generating a non-xylosylated glucan backbone, which could potentially aggregate within the endomembrane system in planta (Cocuron et al., 2007; Whistler and BeMiller, 1973). While multiple glycosyltransferases involved in xylan biosynthesis are known to interact (Zeng et al., 2010) the presence of *CSLA* alone is sufficient for mannan backbone formation and does not require the presence of a galactosyl transferase for its activity (Liepman et al., 2005). The topology of *CSLA* indicates its active site is in the Golgi lumen, while *CSLC*'s active site is proposed to be in the cytosol, allowing the enzyme to push the glucan chain through the membrane into the Golgi (Harholt et al., 2012). These distinctions highlight the functional variances in mannan and XyG biosynthesis processes, despite their shared evolutionary origin. Nevertheless, no xylosylated glucan polysaccharide was detected through glycosidic linkage analysis or OLIMP in *Y. lipolytica*, possibly due to the absence of other *XXT*s such as *XXT1* and *XXT5*. The proposed XyG synthase complex includes at least two glucan synthases, which are colocalized with their N and C termini in close proximity, two *XXT2* proteins that interact with each other via disulfide bonds, and *XXT5* and *XXT1*, which interact with *XXT2*-*XXT2* and *CSLC4*-*CSLC4* homocomplexes (Chou et al., 2012). *XXT2*, *XXT5*, and *XXT1* physically interact through their catalytic domains localized in the Golgi lumen (Chou et al., 2012). Additionally, *XXT1* and *XXT2* are responsible for synthesizing XXGG-type XyGs, while *XXT3*, *XXT4*, and *XXT5* collectively complete the synthesis of XXXG patterns (N. Zhang et al., 2023). Moreover, the limited information on nucleotide sugar donor substrates required for xylosyltransferase activity and the lack of understanding of nucleotide sugar transporters (NSTs) for these substrates in *Y. lipolytica* might also contribute to this phenomenon.

4.3.3 Improving the efficiency of heterologous *O*-acetylated glucan backbone production

The genotyping results indicated that the expression cassettes integrated randomly, rather than at the expected targeted D-1 locus. This unexpected outcome is likely due to either insufficient homology arms or reduced recombination efficiency, a known challenge in organisms like *Y. lipolytica*, which are prone to non-homologous recombination (Mattanovich et al., 2014). Random integration can result in variable gene expression levels due to position effects, where the integration site influences the transcriptional activity of the inserted gene (Dujon et al., 2004)). This variability could account for the inconsistent expression and potentially suboptimal functionality of the introduced genes. To verify the expression levels and assess the impact of random integration on gene expression, qRT-PCR could be performed on the transgenic strains. To improve the engineering of *O*-acetylation pathways in yeast, several strategies could be employed in future studies. As random integration is believed to occur through the non-homologous end joining (NHEJ) DNA repair pathway, it may be possible to increase the frequency of targeted integration by knocking out or conditionally repressing some of the known components of the NHEJ pathway, such as *Ku70* (Xia et al., 2019). One approach would be to enhance transformation efficiency and achieve targeted integration by using *Y. lipolytica* strains with a *Ku70* knockout. Additionally, the correct localization of the integrated proteins within the cell could be verified using fluorescent markers.

5. Conclusion and outlook

This study utilized a forward genetic approach (Chapter 3) to uncover independent pathways involved in suppression of growth and stress defects associated with cell wall hypoacetylation. The findings highlight the intricate nature of cell wall acetylation and its effects on plant growth and stress responses, revealing how specific genetic modifications can influence growth phenotypes, particularly in the *pAXY* line and its suppressor mutants. The loss of *O*-acetylation in the *A. thaliana axy9* mutant leads to severe developmental and stress-related defects (Schultink et al., 2015). However, the conditionally complemented *pAXY* line, maintaining reduced wall-bound acetate yet displaying stunted growth with normal fertility and xylem structure, has been crucial in identifying genetic suppressors that restore growth. The recovery of plant height in all nine suppressor mutants, despite continued reductions in wall *O*-acetylation, suggests that compensatory mechanisms may mitigate some adverse effects of *O*-acetylation loss (Figure 3-2). This indicates that reduced *O*-acetate levels do not directly cause developmental defects, hinting at alternative pathways that influence growth and stress responses. Analysis of cell wall composition in *pAXY* and its suppressor mutants shows a nuanced compensatory response to reduced crystalline cellulose, with increased levels of non-cellulosic cell wall sugars, such as altered pectic and hemicellulose monosaccharides (Section 3.2.5.2). This compensation varies among suppressor mutants, indicating that different genetic backgrounds may employ distinct strategies to compensate the loss of cellulose.

A significant finding is the role of brassinosteroid (BR) signaling in growth recovery. The key suppressor mutation in the *WD40* (AT3G15610) gene appears to affect BR signaling, potentially by influencing the degradation of the BR coreceptor BAK1 (Xi and Wang, 2022). The interaction between *WD40* and *UBQ3*, impacting BAK1 stability, suggests that enhanced BR signaling in *pAXY wd40* suppressor mutants could be crucial in mitigating growth and stress-related defects (Figures 3-20 and 3-21). Moreover, the involvement of HSP90 in BR signaling and possibly influenced by a mutation in the *PHOX3* gene (Figure 3-28), highlights the complexity of regulatory networks modulating plant growth and stress responses in the *pAXY* mutant. The loss of function of *KAKTUS* has been shown to alleviate stress-related defects in the xylan acetylation mutant *tbl29/esk1* (Bensussan et al., 2015). *KAKTUS* (KAK/UPL3) is involved in degrading the BZR1 transcription factor and acts as a negative regulator of BR signaling (Z. Zhang et al., 2023). This implies that BR signaling is crucial for

suppressing stress-related defects linked to hypoacetylation. To further investigate KAKTUS and BR signaling role in mitigating these defects, generating a *pAXY kak* mutant is necessary. Critical experiments are proposed to elucidate these findings in future. Complementation studies by overexpressing BAK1 and HSP90 independently in the *pAXY* background and generating knockouts for these proteins in the respective suppressor mutants will clarify their roles in BR signaling and growth recovery. Co-immunoprecipitation and yeast two-hybrid assays will provide insights into protein interactions, particularly between WD40, UBQ3 and BAK1. RNA-seq and qRT-PCR analyses will help identify changes in gene expression associated with these pathways, offering a detailed understanding of the molecular mechanisms driving growth recovery. Identifying that the loss of function of *AtKH26* suppress the *pAXY* phenotype, introduces a novel aspect of gene regulation. KH domain proteins, known for roles in RNA processing and stability, might influence growth by modulating the activity of ORRM2 (Figure 3-26), a gene implicated in cell size regulation. The loss of *AtKH26* potentially abolishes ORRM2 repression, enhancing growth through improved cell expansion (Karamat et al., 2021; Sun et al., 2012). This hypothesis opens new avenues for exploring how KH domain proteins regulate plant development at the molecular level. To validate this, analyzing cell size and growth in *atkh26-2* and *pAXY atkh26* mutants and conducting qRT-PCR for *ORRM2* and *CYCLIN-B2-1* are proposed. Further, Co-IP or Y2H assays could confirm ORRM2-AtKH26 interactions, while RNA-Seq could identify additional AtKH26 binding partners. Overall, this study provides new insights into the genetic and molecular mechanisms that enable plants to maintain growth and development despite cell wall acetylation defects. The discovery of multiple, independent pathways contributing to growth recovery underscores the resilience of plant biological systems, paving the way for future research to explore the broader implications of cell wall modifications and hormonal signaling in plant adaptation and stress tolerance. Understanding these complex interactions will be crucial for developing strategies to improve crop resilience and productivity under adverse environmental conditions.

There has been substantial advancement in identifying the molecular components responsible for plant cell wall polymer synthesis. However, the collaborative functioning of these components, particularly in determining polysaccharide length and decoration patterns, remains largely unexplored (Pauly et al., 2019). Chapter 4 of this thesis used synthetic biology approach to reconstruct the xyloglucan (XyG) backbone *O*-acetylation machinery in *Yarrowia lipolytica*, yielding valuable insights into plant cell wall polysaccharide biosynthesis. Co-expressing *TmCSLC4*, *TmXXT2*, and *BdXyBAT1* in this non-conventional yeast species

produced an *O*-acetylated 1,4-glucan backbone, demonstrating *BdXyBAT1*'s functionality in a heterologous system (Figures 4-2 and 4-4). This achievement represents a significant advancement in understanding the complex mechanisms of *O*-acetylation, which have been challenging to study in planta. Co-expressing these genes resulted in an *O*-acetylated 1,4-glucan backbone, despite the absence of key *O*-acetylation genes like *AXY9* and *RWAs*. *YlCAS1* may compensate for these missing factors by either interacting with *BdXyBAT1* or creating a pool of acetyl donors in the Golgi lumen for *BdXyBAT1* to utilize. Expressing *RWAs* and *AXY9* in *ylcas1* strains producing the 1,4-glucan backbone could help confirm this. Further to confirm the structure of produced *O*-acetylated 1,4-glucan, a ¹H NMR analysis of the enriched *O*-acetylated glucan could be performed in future. However, challenges such as random integration of expression cassettes and specificity of the E-CELBA suggest that further optimization is necessary. Future research should focus on enhancing targeted gene integration and engineering subcellular localization to better replicate plant cell conditions. This work not only deepens our understanding of plant cell wall but also opens new avenues for using *Y. lipolytica* in metabolic engineering to explore and harness plant biosynthetic pathways.

6. References

- Abbas, H.M.K., Askri, S.M.H., Ali, S., Fatima, A., Qamar, M.T.U., Xue, S.D., Muhammad, Z., Akram, W., Zhong, Y.J., 2022. Mechanism Associated with Brassinosteroids Crosstalk with Gibberellic Acid in Plants. *Brassinosteroids Signal. Interv. with Phytohormones their Relatsh. Plant Adapt. to Abiotic Stress*. 101–115. https://doi.org/10.1007/978-981-16-5743-6_6
- Albersheim, P., Darvill, A., Roberts, K., Sederoff, R., Stachelin, A., 2010. *Plant Cell Walls, Plant Cell Walls*. Garland Science. <https://doi.org/10.1201/9780203833476>
- Amos, R.A., Pattathil, S., Yang, J.-Y., Atmodjo, M.A., Urbanowicz, B.R., Moremen, K.W., Mohnen, D., 2018. A two-phase model for the non-processive biosynthesis of homogalacturonan polysaccharides by the GAUT1:GAUT7 complex. *J. Biol. Chem.* 293, 19047–19063. <https://doi.org/10.1074/jbc.RA118.004463>
- Anders, N., Wilkinson, M.D., Lovegrove, A., Freeman, J., Tryfona, T., Pellny, T.K., Weimar, T., Mortimer, J.C., Stott, K., Baker, J.M., Defoin-Platel, M., Shewry, P.R., Dupree, P., Mitchell, R.A.C., 2012. Glycosyl transferases in family 61 mediate arabinofuranosyl transfer onto xylan in grasses. *Proc. Natl. Acad. Sci. U. S. A.* 109, 989–993. <https://doi.org/10.1073/pnas.1115858109>
- Anthon, G.E., Barrett, D.M., 2010. Changes in tomato paste during storage and the effects of heating on consistency of reconstituted tomato paste. *J. Texture Stud.* 41, 262–278. <https://doi.org/10.1111/j.1745-4603.2010.00225.x>
- Arioli, T., Peng, L., Betzner, A.S., Burn, J., Wittke, W., Herth, W., Camilleri, C., Höfte, H., Plazinski, J., Birch, R., Cork, A., Glover, J., Redmond, J., Williamson, R.E., 1998. Molecular analysis of cellulose biosynthesis in *Arabidopsis*. *Science* (80-). 279, 717–720. <https://doi.org/10.1126/science.279.5351.717>
- Atmodjo, M.A., Hao, Z., Mohnen, D., 2013. Evolving views of pectin biosynthesis. *Annu. Rev. Plant Biol.* 64, 747–779. <https://doi.org/10.1146/annurev-arplant-042811-105534>
- Atmodjo, M.A., Sakuragi, Y., Zhu, X., Burrell, A.J., Mohanty, S.S., Atwood, J.A., Orlando, R., Scheller, H. V., Mohnen, D., 2011. Galacturonosyltransferase (GAUT)I and GAUT7 are the core of a plant cell wall pectin biosynthetic homogalacturonan:galacturonosyltransferase complex. *Proc. Natl. Acad. Sci. U. S. A.* 108, 20225–20230. <https://doi.org/10.1073/pnas.1112816108>
- Austin, R.S., Vidaurre, D., Stamatiou, G., Breit, R., Provart, N.J., Bonetta, D., Zhang, J., Fung, P., Gong, Y., Wang, P.W., McCourt, P., Guttman, D.S., 2011. Next-generation mapping of *Arabidopsis* genes. *Plant J.* 67, 715–725. <https://doi.org/10.1111/j.1365-313X.2011.04619.x>
- Baker, P., Ricer, T., Moynihan, P.J., Kitova, E.N., Walvoort, M.T.C., Little, D.J., Whitney, J.C., Dawson, K., Weadge, J.T., Robinson, H., Ohman, D.E., Codée, J.D.C., Klassen, J.S., Clarke, A.J., Howell, P.L., 2014. *P. aeruginosa* SGNH Hydrolase-Like Proteins AlgJ and AlgX Have Similar Topology but Separate and Distinct Roles in Alginate Acetylation. *PLOS Pathog.* 10, e1004334.
- Bar-Peled, M., O'Neill, M.A., 2011. Plant nucleotide sugar formation, interconversion, and salvage by sugar recycling. *Annu. Rev. Plant Biol.* 62, 127–155. <https://doi.org/10.1146/annurev-arplant-042110-103918>
- Barros, J., Serrani-Yarce, J.C., Chen, F., Baxter, D., Venables, B.J., Dixon, R.A., 2016. Role of bifunctional ammonia-lyase in grass cell wall biosynthesis. *Nat. plants* 2, 16050. <https://doi.org/10.1038/nplants.2016.50>
- Bashline, L., Li, S., Anderson, C.T., Lei, L., Gu, Y., 2013. The endocytosis of cellulose synthase in *Arabidopsis* is dependent on $\mu 2$, a clathrin-mediated endocytosis adaptin. *Plant Physiol.* 163, 150–160. <https://doi.org/10.1104/pp.113.221234>
- Bashline, L., Li, S., Zhu, X., Gu, Y., 2015. The TWD40-2 protein and the AP2 complex cooperate in the clathrin-mediated endocytosis of cellulose synthase to regulate cellulose biosynthesis. *Proc. Natl. Acad. Sci. U. S. A.* 112, 12870–12875. <https://doi.org/10.1073/pnas.1509292112>
- Bauer, S., Vasu, P., Persson, S., Mort, A.J., Somerville, C.R., 2006. Development and application of a suite of polysaccharide-degrading enzymes for analyzing plant cell walls. *Proc. Natl. Acad. Sci. U. S. A.* 103, 11417–11422. <https://doi.org/10.1073/pnas.0604632103>
- Bensussan, M., Lefebvre, V., Ducamp, A., Trouverie, J., Gineau, E., Fortabat, M.N., Guillebaux, A., Baldy, A., Naquin, D., Herbette, S., Lapiere, C., Mouille, G., Horlow, C., Durand-Tardif, M., 2015. Suppression of dwarf and Irregular Xylem phenotypes generates low-acetylated biomass lines in *arabidopsis*. *Plant Physiol.* 168, 452–463. <https://doi.org/10.1104/pp.15.00122>
- Berglund, J., Mikkelsen, D., Flanagan, B.M., Dhital, S., Gaunitz, S., Henriksson, G., Lindström, M.E., Yakubov, G.E., Gidley, M.J., Vilaplana, F., 2020. Wood hemicelluloses exert distinct biomechanical contributions to cellulose fibrillar networks. *Nat. Commun.* 11, 4692. <https://doi.org/10.1038/s41467-020-18390-z>
- Bischoff, V., Nita, S., Neumetzler, L., Schindelasch, D., Urbain, A., Eshed, R., Persson, S., Delmer, D., Scheible, W.R., 2010. TRICHOME BIREFRINGENCE and its homolog AT5G01360 encode plant-

- specific DUF231 proteins required for cellulose biosynthesis in arabidopsis. *Plant Physiol.* 153, 590–602. <https://doi.org/10.1104/pp.110.153320>
- Bolger, A.M., Lohse, M., Usadel, B., 2014. Trimmomatic: A flexible trimmer for Illumina sequence data. *Bioinformatics* 30, 2114–2120. <https://doi.org/10.1093/bioinformatics/btu170>
- Bosca, S., Barton, C.J., Taylor, N.G., Ryden, P., Neumetzler, L., Pauly, M., Roberts, K., Seifert, G.J., 2006. Interactions between MUR10/CesA7-dependent secondary cellulose biosynthesis and primary cell wall structure. *Plant Physiol.* 142, 1353–1363. <https://doi.org/10.1104/pp.106.087700>
- Bridgen, A.J., 2022. Identification and characterisation of fip37-4 suppressor mutants in *Arabidopsis thaliana*.
- Brown, D.M., Goubet, F., Wong, V.W., Goodacre, R., Stephens, E., Dupree, P., Turner, S.R., 2007. Comparison of five xylan synthesis mutants reveals new insight into the mechanisms of xylan synthesis. *Plant J.* 52, 1154–1168. <https://doi.org/10.1111/j.1365-313X.2007.03307.x>
- Brown, D.M., Zhang, Z., Stephens, E., Dupree, P., Turner, S.R., 2009. Characterization of IRX10 and IRX10-like reveals an essential role in glucuronoxylan biosynthesis in *Arabidopsis*. *Plant J.* 57, 732–746. <https://doi.org/10.1111/j.1365-313X.2008.03729.x>
- Broxterman, S.E., Schols, H.A., 2018. Characterisation of pectin-xylan complexes in tomato primary plant cell walls. *Carbohydr. Polym.* 197, 269–276. <https://doi.org/https://doi.org/10.1016/j.carbpol.2018.06.003>
- Buckeridge, M.S., 2010. Seed cell wall storage polysaccharides: Models to understand cell wall biosynthesis and degradation. *Plant Physiol.* 154, 1017–1023. <https://doi.org/10.1104/pp.110.158642>
- Burton, R.A., Wilson, S.M., Hrmova, M., Harvey, A.J., Shirley, N.J., Medhurst, A., Stone, B.A., Newbigin, E.J., Bacic, A., Fincher, G.B., 2006. Cellulose synthase-like CslF genes mediate the synthesis of cell wall (1,3;1,4)- β -D-glucans. *Science* (80-.). 311, 1940–1942. <https://doi.org/10.1126/science.1122975>
- Busse-Wicher, M., Gomes, T.C.F., Tryfona, T., Nikolovski, N., Stott, K., Grantham, N.J., Bolam, D.N., Skaf, M.S., Dupree, P., 2014. The pattern of xylan acetylation suggests xylan may interact with cellulose microfibrils as a twofold helical screw in the secondary plant cell wall of *Arabidopsis thaliana*. *Plant J.* 79, 492–506. <https://doi.org/10.1111/tpj.12575>
- Carpita, N.C., 1996. Structure and biogenesis of the cell walls of grasses. *Annu. Rev. Plant Physiol. Plant Mol. Biol.* 47, 445–476. <https://doi.org/10.1146/annurev.arplant.47.1.445>
- Carpita, N.C., Gibeaut, D.M., 1993. Structural models of primary cell walls in flowering plants: Consistency of molecular structure with the physical properties of the walls during growth. *Plant J.* 3, 1–30. <https://doi.org/10.1111/j.1365-313X.1993.tb00007.x>
- Carpita, N.C., McCann, M.C., 2002. The functions of cell wall polysaccharides in composition and architecture revealed through mutations. *Plant Soil* 247, 71–80. <https://doi.org/10.1023/A:1021115300942>
- Causier, B., Ashworth, M., Guo, W., Davies, B., 2012. The TOPLESS interactome: A framework for gene repression in *Arabidopsis*. *Plant Physiol.* 158, 423–438. <https://doi.org/10.1104/pp.111.186999>
- Cavalier, D.M., Keegstra, K., 2006. Two xyloglucan xylosyltransferases catalyze the addition of multiple xylosyl residues to cellohexaose. *J. Biol. Chem.* 281, 34197–34207. <https://doi.org/10.1074/jbc.M606379200>
- Cavalier, D.M., Lerouxel, O., Neumetzler, L., Yamauchi, K., Reinecke, A., Freshour, G., Zabortina, O.A., Hahn, M.G., Burgert, I., Pauly, M., Raikhel, N. V., Keegstra, K., 2008. Disrupting two *Arabidopsis thaliana* xylosyltransferase genes results in plants deficient in xyloglucan, a major primary cell wall component. *Plant Cell* 20, 1519–1537. <https://doi.org/10.1105/tpc.108.059873>
- Chaiwanon, J., Garcia, V.J., Cartwright, H., Sun, Y., Wang, Z.Y., 2016. Immunophilin-like FKBP42/TWISTED DWARF1 Interacts with the Receptor Kinase BRI1 to Regulate Brassinosteroid Signaling in *Arabidopsis*. *Mol. Plant* 9, 593–600. <https://doi.org/10.1016/j.molp.2016.01.008>
- Chen, T., Cui, P., Chen, H., Ali, S., Zhang, S., Xiong, L., 2013. A KH-Domain RNA-Binding Protein Interacts with FIERY2/CTD Phosphatase-Like 1 and Splicing Factors and Is Important for Pre-mRNA Splicing in *Arabidopsis*. *PLoS Genet.* 9, 1–14. <https://doi.org/10.1371/journal.pgen.1003875>
- Chen, X., Vega-Sánchez, M.E., Verhertbruggen, Y., Chiniqy, D., Canlas, P.E., Fagerström, A., Prak, L., Christensen, U., Oikawa, A., Chern, M., Zuo, S., Lin, F., Auer, M., Willats, W.G.T., Bartley, L., Harholt, J., Scheller, H. V., Ronald, P.C., 2013. Inactivation of OsIRX10 leads to decreased xylan content in rice culm cell walls and improved biomass saccharification. *Mol. Plant.* <https://doi.org/10.1093/mp/sss135>
- Cheng, Y., Kato, N., Wang, W., Li, J., Chen, X., 2003. Two RNA binding proteins, HEN4 and HUA1 act in the processing of AGAMOUS pre-mRNA in *Arabidopsis thaliana*. *Dev. Cell* 4, 53–66. [https://doi.org/10.1016/S1534-5807\(02\)00399-4](https://doi.org/10.1016/S1534-5807(02)00399-4)
- Chiniqy, D., Sharma, V., Schultink, A., Baidoo, E.E., Rautengarten, C., Cheng, K., Carroll, A., Ulvskov, P., Harholt, J., Keasling, J.D., Pauly, M., Scheller, H. V., Ronald, P.C., 2012. XAX1 from glycosyltransferase family 61 mediates xylosyltransfer to rice xylan. *Proc. Natl. Acad. Sci. U. S. A.* 109, 17117–17122. <https://doi.org/10.1073/pnas.1202079109>
- Chipuk, J.E., Bouchier-Hayes, L., Green, D.R., 2006. Mitochondrial outer membrane permeabilization during apoptosis: the innocent bystander scenario. *Cell Death Differ.* 13, 1396–1402.

- <https://doi.org/10.1038/sj.cdd.4401963>
- Chiu, W., Niwa, Y., Zeng, W., Hirano, T., Kobayashi, H., Sheen, J., 1996. Engineered GFP as a vital reporter in plants. *Curr. Biol.* 6, 325–330.
- Chou, Y.H., Pogorelko, G., Zabolina, O.A., 2012. Xyloglucan xylosyltransferases XXT1, XXT2, and XXT5 and the glucan synthase CSLC4 form Golgi-localized multiprotein complexes. *Plant Physiol.* 159, 1355–1366. <https://doi.org/10.1104/pp.112.199356>
- Chundawat, S.P.S., Beckham, G.T., Himmel, M.E., Dale, B.E., 2011. Deconstruction of lignocellulosic biomass to fuels and chemicals. *Annu. Rev. Chem. Biomol. Eng.* 2, 121–145. <https://doi.org/10.1146/annurev-chembioeng-061010-114205>
- Cingolani, P., Platts, A., Wang, L.L., Coon, M., Nguyen, T., Wang, L., Land, S.J., Lu, X., Ruden, D.M., 2012. A program for annotating and predicting the effects of single nucleotide polymorphisms, {SnpEff}. *Fly (Austin)*. 6, 80–92.
- Ciucanu, I., 2006. Per-O-methylation reaction for structural analysis of carbohydrates by mass spectrometry. *Anal. Chim. Acta* 576, 147–155. <https://doi.org/10.1016/j.aca.2006.06.009>
- Clough, S.J., Bent, A.F., 1998. Floral dip: A simplified method for *Agrobacterium*-mediated transformation of *Arabidopsis thaliana*. *Plant J.* 16, 735–743. <https://doi.org/10.1046/j.1365-313X.1998.00343.x>
- Cocuron, J.C., Lerouxel, O., Drakakaki, G., Alonso, A.P., Liepman, A.H., Keegstra, K., Raikhel, N., Wilkerson, C.G., 2007. A gene from the cellulose synthase-like C family encodes a β -1,4 glucan synthase. *Proc. Natl. Acad. Sci. U. S. A.* 104, 8550–8555. <https://doi.org/10.1073/pnas.0703133104>
- Cosgrove, D.J., 2005. Growth of the plant cell wall. *Nat. Rev. Mol. Cell Biol.* 6, 850–861. <https://doi.org/10.1038/nrm1746>
- Crombie, H.J., Chengappa, S., Hellyer, A., Grant Reid, J.S., 1998. A xyloglucan oligosaccharide-active, transglycosylating β -D-glucosidase from the cotyledons of nasturtium (*Tropaeolum majus* L) seedlings - Purification, properties and characterization of a cDNA clone. *Plant J.* 15, 27–38. <https://doi.org/10.1046/j.1365-313X.1998.00182.x>
- Curran, K.A., Morse, N.J., Markham, K.A., Wagman, A.M., Gupta, A., Alper, H.S., 2015. Short Synthetic Terminators for Improved Heterologous Gene Expression in Yeast. *ACS Synth. Biol.* 4, 824–832. <https://doi.org/10.1021/sb5003357>
- Dai, A., 2011. Drought under global warming: A review. *Wiley Interdiscip. Rev. Clim. Chang.* 2, 45–65. <https://doi.org/10.1002/wcc.81>
- Dal Santo, S., Stampfl, H., Krasensky, J., Kempa, S., Gibon, Y., Petutschnig, E., Rozhon, W., Heuck, A., Clausen, T., Jonaka, C., 2012. Stress-induced GSK3 regulates the redox stress response by phosphorylating glucose-6-phosphate dehydrogenase in *Arabidopsis*. *Plant Cell* 24, 3380–3392. <https://doi.org/10.1105/tpc.112.101279>
- Davis, J., Brandizzi, F., Liepman, A.H., Keegstra, K., 2010. *Arabidopsis* mannan synthase CSLA9 and glucan synthase CSLC4 have opposite orientations in the Golgi membrane. *Plant J.* 64, 1028–1037. <https://doi.org/10.1111/j.1365-313X.2010.04392.x>
- de Oliveira, D.M., Finger-Teixeira, A., Rodrigues Mota, T., Salvador, V.H., Moreira-Vilar, F.C., Correa Molinari, H.B., Craig Mitchell, R.A., Marchiosi, R., Ferrarese-Filho, O., Dantas dos Santos, W., 2015. Ferulic acid: A key component in grass lignocellulose recalcitrance to hydrolysis. *Plant Biotechnol. J.* 13, 1224–1232. <https://doi.org/10.1111/pbi.12292>
- de Souza, A., Hull, P.A., Gille, S., Pauly, M., 2014. Identification and functional characterization of the distinct plant pectin esterases PAE8 and PAE9 and their deletion mutants. *Planta* 240, 1123–1138. <https://doi.org/10.1007/s00425-014-2139-6>
- Delmer, D.P., 1999. Cellulose biosynthesis: Exciting times for a difficult field of study. *Annu. Rev. Plant Biol.* 50, 245–276. <https://doi.org/10.1146/annurev.arplant.50.1.245>
- Delmer, D.P., Amor, Y., 1995. Cellulose biosynthesis. *Plant Cell* 7, 987–1000. <https://doi.org/10.2307/3870052>
- Deng, J., Shi, Z.J., Li, X.Z., Liu, H.M., 2013. Soluble polysaccharides isolation and characterization from rabbiteye blueberry (*Vaccinium ashei*) fruits. *BioResources* 8, 405–419. <https://doi.org/10.15376/biores.8.1.405-419>
- Dhugga, K.S., Barreiro, R., Whitten, B., Stecca, K., Hazebroek, J., Randhawa, G.S., Dolan, M., Kinney, A.J., Tomes, D., Nichols, S., Anderson, P., 2004. Guar seed beta-mannan synthase is a member of the cellulose synthase super gene family. *Science* 303, 363–366. <https://doi.org/10.1126/science.1090908>
- Doblin, M.S., Pettolino, F.A., Wilson, S.M., Campbell, R., Burton, R.A., Fincher, G.B., Newbigin, E., Bacic, A., 2009. A barley cellulose synthase-like CSLH gene in transgenic *Arabidopsis*. *Pnas* 106, 5996–6001.
- Domozych, D.S., Ciancia, M., Fangel, J.U., Mikkelsen, M.D., Ulvskov, P., Willats, W.G.T., 2012. The Cell Walls of Green Algae: A Journey through Evolution and Diversity. *Front. Plant Sci.* 3, 82. <https://doi.org/10.3389/fpls.2012.00082>
- Dos Santos, H.P., Purgatto, E., Mercier, H., Buckeridge, M.S., 2004. The control of storage xyloglucan mobilization in cotyledons of *Hymenaea courbaril*. *Plant Physiol.* 135, 287–299.

- <https://doi.org/10.1104/pp.104.040220>
- Downes, B.P., Stupar, R.M., Gingerich, D.J., Vierstra, R.D., 2003. The HECT ubiquitin-protein ligase (UPL) family in Arabidopsis: UPL3 has a specific role in trichome development. *Plant J.* 35, 729–742. <https://doi.org/10.1046/j.1365-313X.2003.01844.x>
- Drake, J.W., Baltz, R.H., 1976. The biochemistry of mutagenesis. *Annu. Rev. Biochem.* 45, 11–37. <https://doi.org/10.1146/annurev.bi.45.070176.000303>
- Du, J., Kirui, A., Huang, S., Wang, L., Barnes, W.J., Kiemle, S.N., Zheng, Y., Rui, Y., Ruan, M., Qi, S., Kim, S.H., Wang, T., Cosgrove, D.J., Anderson, C.T., Xiao, C., 2020. Mutations in the Pectin Methyltransferase QUASIMODO2 Influence Cellulose Biosynthesis and Wall Integrity in Arabidopsis. *Plant Cell* 32, 3576–3597. <https://doi.org/10.1105/tpc.20.00252>
- Dujon, B., Sherman, D., Fischer, G., Durrens, P., Casaregola, S., Lafontaine, I., De Montigny, J., Marck, C., Neuvéglise, C., Talla, E., Goffard, N., Frangeul, L., Aigle, M., Anthouard, V., Babour, A., Barbe, V., Barnay, S., Blanchin, S., Beckerich, J.-M., Beyne, E., Bleykasten, C., Boisramé, A., Boyer, J., Cattolico, L., Confanioleri, F., De Daruvar, A., Despons, L., Fabre, E., Fairhead, C., Ferry-Dumazet, H., Groppi, A., Hantraye, F., Hennequin, C., Jauniaux, N., Joyet, P., Kachouri, R., Kerrest, A., Koszul, R., Lemaire, M., Lesur, I., Ma, L., Muller, H., Nicaud, J.-M., Nikolski, M., Oztas, S., Ozier-Kalogeropoulos, O., Pellenz, S., Potier, S., Richard, G.-F., Straub, M.-L., Suleau, A., Swennen, D., Tekaia, F., Wésolowski-Louvel, M., Westhof, E., Wirth, B., Zeniou-Meyer, M., Zivanovic, I., Bolotin-Fukuhara, M., Thierry, A., Bouchier, C., Caudron, B., Scarpelli, C., Gaillardin, C., Weissenbach, J., Wincker, P., Souciet, J.-L., 2004. Genome evolution in yeasts. *Nature* 430, 35–44. <https://doi.org/10.1038/nature02579>
- Dumont, M., Lehner, A., Bouton, S., Kiefer-Meyer, M.C., Voxeur, A., Pelloux, J., Lerouge, P., Mollet, J.C., 2014. The cell wall pectic polymer rhamnogalacturonan-II is required for proper pollen tube elongation: Implications of a putative sialyltransferase-like protein. *Ann. Bot.* 114, 1177–1188. <https://doi.org/10.1093/aob/mcu093>
- Edwards, M E, Dickson, C.A., Chengappa, S., Sidebottom, C., Gidley, M.J., Reid, J.S., 1999. Molecular characterisation of a membrane-bound galactosyltransferase of plant cell wall matrix polysaccharide biosynthesis. *Plant J.* 19, 691–697. <https://doi.org/10.1046/j.1365-313x.1999.00566.x>
- Edwards, Mary E., Dickson, C.A., Chengappa, S., Sidebottom, C., Gidley, M.J., Reid, J.S.G., 1999. Molecular characterisation of a membrane-bound galactosyltransferase of plant cell wall matrix polysaccharide biosynthesis. *Plant J.* 19, 691–697. <https://doi.org/10.1046/j.1365-313X.1999.00566.x>
- Egelund, J., Petersen, B.L., Motawia, M.S., Damager, I., Faik, A., Olsen, C.E., Ishii, T., Clausen, H., Ulvskov, P., Geshi, N., 2006. Arabidopsis thaliana RGXT1 and RGXT2 encode golgi-localized (1,3)- α -D-xylosyltransferases involved in the synthesis of pectic rhamnogalacturonan-II. *Plant Cell* 18, 2593–2607. <https://doi.org/10.1105/tpc.105.036566>
- El Refy, A., Perazza, D., Zekraoui, L., Valay, J.G., Bechtold, N., Brown, S., Hülskamp, M., Herzog, M., Bonneville, J.M., 2004. The Arabidopsis KAKTUS gene encodes a HECT protein and controls the number of endoreduplication cycles. *Mol. Genet. Genomics* 270, 403–414. <https://doi.org/10.1007/s00438-003-0932-1>
- Faik, A., 2010. Xylan biosynthesis: News from the grass. *Plant Physiol.* 153, 396–402. <https://doi.org/10.1104/pp.110.154237>
- Faik, A., Price, N.J., Raikhel, N. V., Keegstra, K., 2002. An Arabidopsis gene encoding an α -xylosyltransferase involved in xyloglucan biosynthesis. *Proc. Natl. Acad. Sci. U. S. A.* 99, 7797–7802. <https://doi.org/10.1073/pnas.102644799>
- Feng, R., Zhang, C., Ma, R., Cai, Z., Lin, Y., Yu, M., 2019. Identification and characterization of WD40 superfamily genes in peach. *Gene* 710, 291–306. <https://doi.org/10.1016/j.gene.2019.06.010>
- Formula, C., Values, O., Values, E., Seed, Y., Seed, G., 2021. The Chi-Square Test 4–5.
- Foster, C.E., Martin, T.M., Pauly, M., 2010. Comprehensive compositional analysis of plant cell walls (Lignocellulosic biomass) part I: Lignin. *J. Vis. Exp.* 5–8. <https://doi.org/10.3791/1745>
- Fry, S.C., York, W.S., Albersheim, P., Darvill, A., Hayashi, T., Joseleau, J. -P, Kato, Y., Lorences, E.P., Maclachlan, G.A., McNeil, M., Mort, A.J., Grant Reid, J.S., Seitz, H.U., Selvendran, R.R., Voragen, A.G.J., White, A.R., 1993. An unambiguous nomenclature for xyloglucan-derived oligosaccharides. *Physiol. Plant.* 89, 1–3. <https://doi.org/10.1111/j.1399-3054.1993.tb01778.x>
- Ganguly, A., Zhu, C., Chen, W., Dixit, R., 2020. FRA1 Kinesin Modulates the Lateral Stability of Cortical Microtubules through Cellulose Synthase-Microtubule Uncoupling Proteins. *Plant Cell* 32, 2508–2524. <https://doi.org/10.1105/tpc.19.00700>
- George, J., Stegmann, M., Monaghan, J., Bailey-Serres, J., Zipfel, C., 2023. Arabidopsis translation initiation factor binding protein CBE1 negatively regulates accumulation of the NADPH oxidase respiratory burst oxidase homolog D. *J. Biol. Chem.* 299, 105018. <https://doi.org/10.1016/j.jbc.2023.105018>
- Gerold Barth, Claude Gaillardin, 1997. Physiology and genetics of the dimorphic fungus *Yarrowia lipolytica*. *FEMS Microbiol. Rev.* 19, 219–237.

- Geshi, N., Johansen, J.N., Dilokpimol, A., Rolland, A., Belcram, K., Verger, S., Kotake, T., Tsumuraya, Y., Kaneko, S., Tryfona, T., Dupree, P., Scheller, H. V., Höfte, H., Mouille, G., 2013. A galactosyltransferase acting on arabinogalactan protein glycans is essential for embryo development in *Arabidopsis*. *Plant J.* 76, 128–137. <https://doi.org/10.1111/tpj.12281>
- Gibeaut, D.M., Pauly, M., Bacic, A., Fincher, G.B., 2005. Changes in cell wall polysaccharides in developing barley (*Hordeum vulgare*) coleoptiles. *Planta* 221, 729–738. <https://doi.org/10.1007/s00425-005-1481-0>
- Gibson, D.G., Young, L., Chuang, R.Y., Venter, J.C., Hutchison, C.A., Smith, H.O., 2009. Enzymatic assembly of DNA molecules up to several hundred kilobases. *Nat. Methods* 6, 343–345. <https://doi.org/10.1038/nmeth.1318>
- Gille, S., Cheng, K., Skinner, M.E., Liepman, A.H., Wilkerson, C.G., Pauly, M., 2011a. Deep sequencing of voodoo lily (*Amorphophallus konjac*): An approach to identify relevant genes involved in the synthesis of the hemicellulose glucomannan. *Planta* 234, 515–526. <https://doi.org/10.1007/s00425-011-1422-z>
- Gille, S., de Souza, A., Xiong, G., Benz, M., Cheng, K., Schultink, A., Reca, I.B., Pauly, M., 2011b. O-acetylation of *Arabidopsis* hemicellulose xyloglucan requires *AXY4* or *AXY4L*, proteins with a TBL an DUF231 domain. *Plant Cell* 23, 4041–4053. <https://doi.org/10.1105/tpc.111.091728>
- Gille, S., Hänsel, U., Ziemann, M., Pauly, M., 2009. Identification of plant cell wall mutants by means of a forward chemical genetic approach using hydrolases. *Proc. Natl. Acad. Sci. U. S. A.* 106, 14699–14704. <https://doi.org/10.1073/pnas.0905434106>
- Gille, S., Pauly, M., 2012. O-acetylation of plant cell wall polysaccharides. *Front. Plant Sci.* 3, 1–7. <https://doi.org/10.3389/fpls.2012.00012>
- Giovane, A., Servillo, L., Balestrieri, C., Raiola, A., D'Avino, R., Tamburrini, M., Ciardiello, M.A., Camardella, L., 2004. Pectin methylesterase inhibitor. *Biochim. Biophys. Acta* 1696, 245–252. <https://doi.org/10.1016/j.bbapap.2003.08.011>
- Gou, J.Y., Miller, L.M., Hou, G., Yu, X.H., Chen, X.Y., Liu, C.J., 2012. Acetylase-mediated deacetylation of pectin impairs cell elongation, pollen germination, and plant reproduction. *Plant Cell* 24, 50–65. <https://doi.org/10.1105/tpc.111.092411>
- Gou, M., Ran, X., Martin, D.W., Liu, C.-J., 2018. The scaffold proteins of lignin biosynthetic cytochrome P450 enzymes. *Nat. plants* 4, 299–310. <https://doi.org/10.1038/s41477-018-0142-9>
- Gou, X., Yin, H., He, K., Du, J., Yi, J., Xu, S., Lin, H., Clouse, S.D., Li, J., 2012. Genetic evidence for an indispensable role of somatic embryogenesis receptor kinases in brassinosteroid signaling. *PLoS Genet.* 8. <https://doi.org/10.1371/journal.pgen.1002452>
- Goubet, F., Barton, C.J., Mortimer, J.C., Yu, X., Zhang, Z., Miles, G.P., Richens, J., Liepman, A.H., Seffen, K., Dupree, P., 2009. Cell wall glucomannan in *Arabidopsis* is synthesised by CSLA glycosyltransferases, and influences the progression of embryogenesis. *Plant J.* 60, 527–538. <https://doi.org/10.1111/j.1365-313X.2009.03977.x>
- Goubet, F., Misrahi, A., Park, S.K., Zhang, Z., Twell, D., Dupree, P., 2003. AtCSLA7, a cellulose synthase-like putative glycosyltransferase, is important for pollen tube growth and embryogenesis in *Arabidopsis*. *Plant Physiol.* 131, 547–557. <https://doi.org/10.1104/pp.014555>
- Grantham, N.J., Wurman-Rodrich, J., Terrett, O.M., Lyczakowski, J.J., Stott, K., Iuga, D., Simmons, T.J., Durand-Tardif, M., Brown, S.P., Dupree, R., Busse-Wicher, M., Dupree, P., 2017. An even pattern of xylan substitution is critical for interaction with cellulose in plant cell walls. *Nat. plants* 3, 859–865. <https://doi.org/10.1038/s41477-017-0030-8>
- Gray, D., 2001. Overview of protein expression by mammalian cells. *Curr. Protoc. protein Sci.* Chapter 5, Unit5.9. <https://doi.org/10.1002/0471140864.ps0509s10>
- Gu, Y., Kaplinsky, N., Bringmann, M., Cobb, A., Carroll, A., Sampathkumar, A., Baskin, T.I., Persson, S., Somerville, C.R., 2010. Identification of a cellulose synthase-associated protein required for cellulose biosynthesis. *Proc. Natl. Acad. Sci. U. S. A.* 107, 12866–12871. <https://doi.org/10.1073/pnas.1007092107>
- Guerois, R., Nielsen, J.E., Serrano, L., 2002. Predicting changes in the stability of proteins and protein complexes: A study of more than 1000 mutations. *J. Mol. Biol.* 320, 369–387. [https://doi.org/10.1016/S0022-2836\(02\)00442-4](https://doi.org/10.1016/S0022-2836(02)00442-4)
- Günl, M., Neumetzler, L., Kraemer, F., de Souza, A., Schultink, A., Pena, M., York, W.S., Pauly, M., 2011. *AXY8* encodes an α -fucosidase, underscoring the importance of apoplastic metabolism on the fine structure of *Arabidopsis* cell wall polysaccharides. *Plant Cell* 23, 4025–4040. <https://doi.org/10.1105/tpc.111.089193>
- Günl, M., Pauly, M., 2011. *AXY3* encodes a α -xylosidase that impacts the structure and accessibility of the hemicellulose xyloglucan in *Arabidopsis* plant cell walls. *Planta* 233, 707–719. <https://doi.org/10.1007/s00425-010-1330-7>
- Harholt, J., Jensen, J.K., Verhertbruggen, Y., Søgaard, C., Bernard, S., Nafisi, M., Poulsen, C.P., Geshi, N., Sakuragi, Y., Driouch, A., Knox, J.P., Scheller, H.V., 2012. ARAD proteins associated with pectic Arabinan biosynthesis form complexes when transiently overexpressed in planta. *Planta* 236, 115–128.

- <https://doi.org/10.1007/s00425-012-1592-3>
- Harholt, J., Suttangkakul, A., Scheller, H.V., 2010. Biosynthesis of pectin. *Plant Physiol.* 153, 384–395. <https://doi.org/10.1104/pp.110.156588>
- Haron, S., Gong Wenfang, Mtawa, M., 2018. Genome-wide characterization, identification and expression analysis of WD40 proteins family in cotton 4–5.
- Hauser, M.T., Morikami, A., Benfey, P.N., 1995. Conditional root expansion mutants of *Arabidopsis*. *Development* 121, 1237–1252. <https://doi.org/10.1242/dev.121.4.1237>
- He, K., Xu, S., Li, J., 2013. BAK1 directly regulates brassinosteroid perception and BRI1 activation. *J. Integr. Plant Biol.* 55, 1264–1270. <https://doi.org/10.1111/jipb.12122>
- Helle, S., Cameron, D., Lam, J., White, B., Duff, S., 2003. Effect of inhibitory compounds found in biomass hydrolysates on growth and xylose fermentation by a genetically engineered strain of *S. cerevisiae*. *Enzyme Microb. Technol.* 33, 786–792. [https://doi.org/10.1016/S0141-0229\(03\)00214-X](https://doi.org/10.1016/S0141-0229(03)00214-X)
- Holkenbrink, C., Dam, M.I., Kildegaard, K.R., Beder, J., Dahlin, J., Doménech Belda, D., Borodina, I., 2018. EasyCloneYALI: CRISPR/Cas9-Based Synthetic Toolbox for Engineering of the Yeast *Yarrowia lipolytica*. *Biotechnol. J.* 13, 1–8. <https://doi.org/10.1002/biot.201700543>
- Huang, H., Weng, H., Sun, W., Qin, X., Shi, H., Zhao, B.S., Mesquita, A., Liu, C., Yuan, C.L., Hüttelmaier, S., Skibbe, J.R., Su, R., Deng, X., Dong, L., 2018. Recognition of RNA N6 -methyladenosine by IGF2BP Proteins Enhances mRNA Stability and Translation. *Nat. Cell Biol.* 20, 285–295. <https://doi.org/10.1038/s41556-018-0045-z>
- Huang, L., Takahashi, R., Kobayashi, S., Kawase, T., Nishinari, K., 2002. Gelation behavior of native and acetylated konjac glucomannan. *Biomacromolecules* 3, 1296–1303. <https://doi.org/10.1021/bm0255995>
- Immelmann, R., Gawenda, N., Ramírez, V., Pauly, M., 2023. Identification of a xyloglucan beta-xylopyranosyltransferase from *Vaccinium corymbosum*. *Plant Direct* 7, 1–13. <https://doi.org/10.1002/pld3.514>
- Jain, B.P., Pandey, S., 2018. WD40 Repeat Proteins: Signalling Scaffold with Diverse Functions. *Protein J.* 37, 391–406. <https://doi.org/10.1007/s10930-018-9785-7>
- Jankowicz-Cieslak, J., Till, B.J., 2016. Chemical Mutagenesis of Seed and Vegetatively Propagated Plants Using EMS. *Curr. Protoc. Plant Biol.* 1, 617–635. <https://doi.org/10.1002/cppb.20040>
- JARVIS, M.C., 1984. Structure and properties of pectin gels in plant cell walls. *Plant. Cell Environ.* 7, 153–164. <https://doi.org/10.1111/1365-3040.ep11614586>
- Jensen, J.K., Schultink, A., Keegstra, K., Wilkerson, C.G., Pauly, M., 2012. RNA-seq analysis of developing nasturtium seeds (*Tropaeolum majus*): Identification and characterization of an additional galactosyltransferase involved in xyloglucan biosynthesis. *Mol. Plant* 5, 984–992. <https://doi.org/10.1093/mp/sss032>
- Jensen, J.K., Sørensen, S.O., Harholt, J., Geshi, N., Sakuragi, Y., Møller, I., Zandleven, J., Bernal, A.J., Jensen, N.B., Sørensen, C., Pauly, M., Beldman, G., Willats, W.G.T., Scheller, H.V., 2008. Identification of a xylogalacturonan xylosyltransferase involved in pectin biosynthesis in *Arabidopsis*. *Plant Cell* 20, 1289–1302. <https://doi.org/10.1105/tpc.107.050906>
- Jobling, S.A., 2015. Membrane pore architecture of the CslF6 protein controls (1-3,1-4)- β -glucan structure. *Sci. Adv.* 1, e1500069. <https://doi.org/10.1126/sciadv.1500069>
- Johnson, A.M., Kim, H., Ralph, J., Mansfield, S.D., 2017. Natural acetylation impacts carbohydrate recovery during deconstruction of *Populus trichocarpa* wood. *Biotechnol. Biofuels* 10, 1–12. <https://doi.org/10.1186/s13068-017-0734-z>
- Jones, C.S., Anderson, A.C., Clarke, A.J., 2021. Mechanism of *Staphylococcus aureus* peptidoglycan O-acetyltransferase A as an O-acyltransferase. *Proc. Natl. Acad. Sci. U. S. A.* 118. <https://doi.org/10.1073/pnas.2103602118>
- Kabel, M.A., De Waard, P., Schols, H.A., Voragen, A.G.J., 2003. Location of O-acetyl substituents in xylo-oligosaccharides obtained from hydrothermally treated *Eucalyptus* wood. *Carbohydr. Res.* 338, 69–77. [https://doi.org/10.1016/S0008-6215\(02\)00351-8](https://doi.org/10.1016/S0008-6215(02)00351-8)
- KAMERLING Johannis, SCHAUER Roland, S.A., 1987. t' I. *Eur. J. Biochem.* 607, 601–607.
- Karamat, U., Sun, X., Li, N., Zhao, J., 2021. Genetic regulators of leaf size in Brassica crops. *Hortic. Res.* 8. <https://doi.org/10.1038/s41438-021-00526-x>
- Karlsson, P., Christie, M.D., Seymour, D.K., Wang, H., Wang, X., Hagmann, J., Kulcheski, F., Manavella, P.A., 2015. KH domain protein RCF3 is a tissue-biased regulator of the plant miRNA biogenesis cofactor HYL1. *Proc. Natl. Acad. Sci. U. S. A.* 112, 14096–14101. <https://doi.org/10.1073/pnas.1512865112>
- Keegstra, K., 2010. Plant cell walls. *Plant Physiol.* 154, 483–486. <https://doi.org/10.1104/pp.110.161240>
- Kerr, E.M., Fry, S.C., 2003. Pre-formed xyloglucans and xylans increase in molecular weight in three distinct compartments of a maize cell-suspension culture. *Planta* 217, 327–339. <https://doi.org/10.1007/s00425-003-1027-2>
- Kiefer, L.L., York, W.S., Darvill, A.G., Albersheim, P., 1989. Xyloglucan isolated from suspension-cultured

- sycamore cell walls is O-acetylated. *Phytochemistry* 28, 2105–2107. [https://doi.org/10.1016/S0031-9422\(00\)97928-7](https://doi.org/10.1016/S0031-9422(00)97928-7)
- Kim, D.Y., Scalf, M., Smith, L.M., Vierstra, R.D., 2013. Advanced proteomic analyses yield a deep catalog of ubiquitylation targets in Arabidopsis. *Plant Cell* 25, 1523–1540. <https://doi.org/10.1105/tpc.112.108613>
- Kim, S.J., Chandrasekar, B., Rea, A.C., Danhof, L., Zemelis-Durfee, S., Thrower, N., Shepard, Z.S., Pauly, M., Brandizzi, F., Keegstra, K., 2020. The synthesis of xyloglucan, an abundant plant cell wall polysaccharide, requires CSLC function. *Proc. Natl. Acad. Sci. U. S. A.* 117, 20316–20324. <https://doi.org/10.1073/PNAS.2007245117>
- Kim, T.W., Guan, S., Burlingame, A.L., Wang, Z.Y., 2011. The CDG1 Kinase Mediates Brassinosteroid Signal Transduction from BRI1 Receptor Kinase to BSU1 Phosphatase and GSK3-like Kinase BIN2. *Mol. Cell* 43, 561–571. <https://doi.org/10.1016/j.molcel.2011.05.037>
- Knox, J.P., 2008. Revealing the structural and functional diversity of plant cell walls. *Curr. Opin. Plant Biol.* 11, 308–313. <https://doi.org/10.1016/j.pbi.2008.03.001>
- Knox, J.P., Linstead, P.J., King, J., Cooper, C., Roberts, K., 1990. Pectin esterification is spatially regulated both within cell walls and between developing tissues of root apices. *Planta* 181, 512–521. <https://doi.org/10.1007/BF00193004>
- Kong, Y., Peña, M.J., Renna, L., Avci, U., Pattathil, S., Tuomivaara, S.T., Li, X., Reiter, W.D., Brandizzi, F., Hahn, M.G., Darvill, A.G., York, W.S., O’neill, M.A., 2015. Galactose-depleted xyloglucan is dysfunctional and leads to dwarfism in arabidopsis. *Plant Physiol.* 167, 1296–1306. <https://doi.org/10.1104/pp.114.255943>
- Kong, Y., Zhou, G., Abdeen, A.A., Schafhauser, J., Richardson, B., Atmodjo, M.A., Jung, J., Wicker, L., Mohnen, D., Western, T., Hahn, M.G., 2013. GALACTURONOSYLTRANSFERASE-LIKE5 Is Involved in the Production of Arabidopsis Seed Coat Mucilage. *Plant Physiol.* 163, 1203–1217. <https://doi.org/10.1104/pp.113.227041>
- Kooiman, P., 1971. Structures of the galactomannans from seeds of *Annona muricata*, *Arenga saccharifera*, *Cocos nucifera*, *Convolvulus tricolor*, and *Sophora japonica*. *Carbohydr. Res.* 20, 329–337. [https://doi.org/10.1016/S0008-6215\(00\)81387-7](https://doi.org/10.1016/S0008-6215(00)81387-7)
- Kretzschmar, A., Otto, C., Holz, M., Werner, S., Hübner, L., Barth, G., 2013. Increased homologous integration frequency in *Yarrowia lipolytica* strains defective in non-homologous end-joining. *Curr. Genet.* 59, 63–72. <https://doi.org/10.1007/s00294-013-0389-7>
- Laloum, T., De Mita, S., Gamas, P., Baudin, M., Niebel, A., 2013. CCAAT-box binding transcription factors in plants: Y so many? *Trends Plant Sci.* 18, 157–166. <https://doi.org/10.1016/j.tplants.2012.07.004>
- Langmead, B., Salzberg, S.L., 2012. Fast gapped-read alignment with Bowtie 2. *Nat. Methods* 9, 357–359. <https://doi.org/10.1038/nmeth.1923>
- Law, J.A., Jacobsen, S.E., 2011. Establishing, maintaining and modifying DNA methylation patterns in plants and animals 11, 204–220. <https://doi.org/10.1038/nrg2719>. Establishing
- Lee, C., Teng, Q., Zhong, R., Ye, Z.H., 2011. The Four Arabidopsis REDUCED WALL ACETYLATION Genes are expressed in secondary wall-containing cells and required for the acetylation of Xylan. *Plant Cell Physiol.* 52, 1289–1301. <https://doi.org/10.1093/pcp/pcr075>
- Lee, Y., Rubio, M.C., Alassimone, J., Geldner, N., 2013. A mechanism for localized lignin deposition in the endodermis. *Cell* 153, 402–412. <https://doi.org/10.1016/j.cell.2013.02.045>
- Lee, Y., Yoon, T.H., Lee, J., Jeon, S.Y., Lee, J.H., Lee, M.K., Chen, H., Yun, J., Oh, S.Y., Wen, X., Cho, H.K., Mang, H., Kwak, J.M., 2018. A Lignin Molecular Brace Controls Precision Processing of Cell Walls Critical for Surface Integrity in Arabidopsis. *Cell* 173, 1468–1480.e9. <https://doi.org/10.1016/j.cell.2018.03.060>
- Lemke, M.D., Woodson, J.D., 2023. A genetic screen for dominant chloroplast reactive oxygen species signaling mutants reveals life stage-specific singlet oxygen signaling networks. *Front. Plant Sci.* 14, 1–24. <https://doi.org/10.3389/fpls.2023.1331346>
- Lerouxel, O., Cavalier, D.M., Liepman, A.H., Keegstra, K., 2006. Biosynthesis of plant cell wall polysaccharides - a complex process. *Curr. Opin. Plant Biol.* 9, 621–630. <https://doi.org/10.1016/j.pbi.2006.09.009>
- Lerouxel, O., Siang Choo, T., Séveno, M., Usadel, B., Faye, L., Lerouge, P., Pauly, M., 2002. Rapid structural phenotyping of plant cell wall mutants by enzymatic oligosaccharide fingerprinting. *Plant Physiol.* 130, 1754–1763. <https://doi.org/10.1104/pp.011965>
- Li, C., Zhang, B., Chen, B., Ji, L., Yu, H., 2018. Site-specific phosphorylation of TRANSPARENT TESTA GLABRA1 mediates carbon partitioning in Arabidopsis seeds. *Nat. Commun.* 9. <https://doi.org/10.1038/s41467-018-03013-5>
- Li, J., Chory, J., 1997. A putative leucine-rich repeat receptor kinase involved in brassinosteroid signal transduction. *Cell* 90, 929–938. [https://doi.org/10.1016/s0092-8674\(00\)80357-8](https://doi.org/10.1016/s0092-8674(00)80357-8)
- Li, J., Jin, H., 2007. Regulation of brassinosteroid signaling. *Trends Plant Sci.* 12, 37–41.

- <https://doi.org/10.1016/j.tplants.2006.11.002>
- Li, Q.F., He, J.X., 2013. Mechanisms of signaling crosstalk between brassinosteroids and gibberellins. *Plant Signal. Behav.* 8. <https://doi.org/10.4161/psb.24686>
- Li, Q.F., Lu, J., Yu, J.W., Zhang, C.Q., He, J.X., Liu, Q.Q., 2018. The brassinosteroid-regulated transcription factors BZR1/BES1 function as a coordinator in multisignal-regulated plant growth. *Biochim. Biophys. Acta - Gene Regul. Mech.* 1861, 561–571. <https://doi.org/10.1016/j.bbagr.2018.04.003>
- Li, S., Lei, L., Somerville, C.R., Gu, Y., 2012. Cellulose synthase interactive protein 1 (CSI1) links microtubules and cellulose synthase complexes. *Proc. Natl. Acad. Sci. U. S. A.* 109, 185–190. <https://doi.org/10.1073/pnas.1118560109>
- Liepmann, A.H., Wilkerson, C.G., Keegstra, K., 2005. Expression of cellulose synthase-like (Csl) genes in insect cells reveals that CslA family members encode mannan synthases. *Proc. Natl. Acad. Sci. U. S. A.* 102, 2221–2226. <https://doi.org/10.1073/pnas.0409179102>
- Liu, J., Zuo, X., Peng, K., He, R., Yang, L., Liu, R., 2022. Biogas and Volatile Fatty Acid Production During Anaerobic Digestion of Straw, Cellulose, and Hemicellulose with Analysis of Microbial Communities and Functions. *Appl. Biochem. Biotechnol.* 194, 762–782. <https://doi.org/10.1007/s12010-021-03675-w>
- Liu, L., Hsia, M.M., Dama, M., Vogel, J., Pauly, M., 2016. A Xyloglucan Backbone 6-O-Acetyltransferase from *Brachypodium distachyon* Modulates Xyloglucan Xylosylation. *Mol. Plant* 9, 615–617. <https://doi.org/10.1016/j.molp.2015.11.004>
- Liu, L., Shang-Guan, K., Zhang, B., Liu, X., Yan, M., Zhang, L., Shi, Y., Zhang, M., Qian, Q., Li, J., Zhou, Y., 2013. Brittle Culm1, a COBRA-Like Protein, Functions in Cellulose Assembly through Binding Cellulose Microfibrils. *PLOS Genet.* 9, e1003704.
- Liu, S., Liu, Y., Liu, C., Zhang, F., Wei, J., Li, B., 2022. Genome-Wide Characterization and Expression Analysis of GeBP Family Genes in Soybean. *Plants* 11. <https://doi.org/10.3390/plants11141848>
- Liu, X.L., Liu, L., Niu, Q.K., Xia, C., Yang, K.Z., Li, R., Chen, L.Q., Zhang, X.Q., Zhou, Y., Ye, D., 2011. MALE GAMETOPHYTE DEFECTIVE 4 encodes a rhamnogalacturonan II xylosyltransferase and is important for growth of pollen tubes and roots in *Arabidopsis*. *Plant J.* 65, 647–660. <https://doi.org/10.1111/j.1365-313X.2010.04452.x>
- Liu, Z., Schneider, R., Kesten, C., Zhang, Yi, Somssich, M., Zhang, Youjun, Fernie, A.R., Persson, S., 2016. Cellulose-Microtubule Uncoupling Proteins Prevent Lateral Displacement of Microtubules during Cellulose Synthesis in *Arabidopsis*. *Dev. Cell* 38, 305–315. <https://doi.org/10.1016/j.devcel.2016.06.032>
- Liwanag, A.J.M., Ebert, B., Verhertbruggen, Y., Rennie, E.A., Rautengarten, C., Oikawa, A., Andersen, M.C.F., Clausen, M.H., Scheller, H.V., 2012. Pectin biosynthesis: GALS1 in *Arabidopsis thaliana* is a β -1,4-galactan β -1,4-galactosyltransferase. *Plant Cell* 24, 5024–5036. <https://doi.org/10.1105/tpc.112.106625>
- Lu, S., Li, Q., Wei, H., Chang, M.-J., Tunlaya-Anukit, S., Kim, H., Liu, J., Song, J., Sun, Y.-H., Yuan, L., Yeh, T.-F., Peszlen, I., Ralph, J., Sederoff, R.R., Chiang, V.L., 2013. Ptr-miR397a is a negative regulator of laccase genes affecting lignin content in *Populus trichocarpa*. *Proc. Natl. Acad. Sci. U. S. A.* 110, 10848–10853. <https://doi.org/10.1073/pnas.1308936110>
- Lunde, C., 2018. Small-scale DNA Extraction Method for Maize and Other Plants. *Bio-Protocol* 8, 1–6. <https://doi.org/10.21769/bioprotoc.2782>
- Lunin, V. V., Wang, H.-T., Bharadwaj, V.S., Alahuhta, M., Peña, M.J., Yang, J.-Y., Hartmann, A.A., Azadi, P., Himmel, M.E., Moremen, K.W., York, W.S., Bomble, Y.J., Urbanowicz, B.R., 2020. Full: Structure of the Xylan O-Acetyltransferase AtXOAT1 Reveals Molecular Insight into Polysaccharide Acetylation in Plants. *bioRxiv Prepr.* 21, 1–9. <https://doi.org/10.1101/2020.01.16.909127>
- Ma, J., Gu, Y., Marsafari, M., Xu, P., 2020. Synthetic biology, systems biology, and metabolic engineering of *Yarrowia lipolytica* toward a sustainable biorefinery platform. *J. Ind. Microbiol. Biotechnol.* 47, 845–862. <https://doi.org/10.1007/s10295-020-02290-8>
- Macknight, R., Bancroft, I., Page, T., Lister, C., Schmidt, R., Love, K., Westphal, L., Murphy, G., Sherson, S., Cobbett, C., Dean, C., 1997. FCA, a gene controlling flowering time in *Arabidopsis*, encodes a protein containing RNA-binding domains. *Cell* 89, 737–745. [https://doi.org/10.1016/S0092-8674\(00\)80256-1](https://doi.org/10.1016/S0092-8674(00)80256-1)
- Madson, M., Dunand, C., Li, X., Verma, R., Vanzin, G.F., Caplan, J., Shoue, D.A., Carpita, N.C., Reiter, W.D., 2003. The MUR3 gene of *Arabidopsis* encodes a xyloglucan galactosyltransferase that is evolutionarily related to animal exostosins. *Plant Cell* 15, 1662–1670. <https://doi.org/10.1105/tpc.009837>
- Madzak, C., Tréton, B., Blanchin-Roland, S., 2000. Strong hybrid promoters and integrative expression/secretion vectors for quasi-constitutive expression of heterologous proteins in the yeast *Yarrowia lipolytica*. *J. Mol. Microbiol. Biotechnol.* 2, 207–216.
- Maier, W., Moos, K., Seifert, M., Baumeister, R., 2014. MiModD - Mutation Identification in Model Organism Genomes.
- Manabe, Y., Nafisi, M., Verhertbruggen, Y., Orfila, C., Gille, S., Rautengarten, C., Cherk, C., Marcus, S.E., Somerville, S., Pauly, M., Paul Knox, J., Sakuragi, Y., Scheller, H.V., 2011. Loss-of-function mutation of REDUCED WALL ACETYLATION2 in *Arabidopsis* leads to reduced cell wall acetylation and increased

- resistance to *Botrytis cinerea*. *Plant Physiol.* 155, 1068–1078. <https://doi.org/10.1104/pp.110.168989>
- Manabe, Y., Verhertbruggen, Y., Gille, S., Harholt, J., Chong, S.L., Pawar, P.M.A., Mellerowicz, E.J., Tenkanen, M., Cheng, K., Pauly, M., Scheller, H.V., 2013. Reduced wall acetylation proteins play vital and distinct roles in cell wall O-acetylation in *Arabidopsis*. *Plant Physiol.* 163, 1107–1117. <https://doi.org/10.1104/pp.113.225193>
- Maruyama, K., Goto, C., Numata, M., Suzuki, T., Nakagawa, Y., Hoshino, T., Uchiyama, T., 1996. O-acetylated xyloglucan in extracellular polysaccharides from cell-suspension cultures of *Mentha*. *Phytochemistry* 41, 1309–1314. [https://doi.org/10.1016/0031-9422\(95\)00739-3](https://doi.org/10.1016/0031-9422(95)00739-3)
- Mattanovich, D., Jungo, C., Wenger, J., Dabros, M., Maurer, M., 2014. Yeast Suspension Culture, in: *Industrial Scale Suspension Culture of Living Cells*. pp. 94–129. <https://doi.org/https://doi.org/10.1002/9783527683321.ch02>
- McNeil, M., Darvill, A.G., Fry, S.C., Albersheim, P., 1984. Structure and function of the primary cell walls of plants. *Annu. Rev. Biochem.* 53, 625–663. <https://doi.org/10.1146/annurev.bi.53.070184.003205>
- Migliori, V., Mapelli, M., Guccione, E., 2012. On WD40 proteins propelling our knowledge of transcriptional control? *Epigenetics* 7, 815–822. <https://doi.org/10.4161/epi.21140>
- Mishra, A.K., Muthamilarasan, M., Khan, Y., Parida, S.K., Prasad, M., 2014. Genome-wide investigation and expression analyses of WD40 protein family in the model plant foxtail millet (*Setaria italica* L.). *PLoS One* 9, 1–13. <https://doi.org/10.1371/journal.pone.0086852>
- Mitchell, R.A.C., Dupree, P., Shewry, P.R., 2007. A novel bioinformatics approach identifies candidate genes for the synthesis and feruloylation of arabinoxylan. *Plant Physiol.* 144, 43–53. <https://doi.org/10.1104/pp.106.094995>
- Mittelsten Scheid, O., 2022. Mendelian and non-Mendelian genetics in model plants. *Plant Cell* 34, 2455–2461. <https://doi.org/10.1093/plcell/koac070>
- Mohnen, D., 2008. Pectin structure and biosynthesis. *Curr. Opin. Plant Biol.* 11, 266–277. <https://doi.org/10.1016/j.pbi.2008.03.006>
- Moreira, L.R.S., Filho, E.X.F., 2008. An overview of mannan structure and mannan-degrading enzyme systems. *Appl. Microbiol. Biotechnol.* 79, 165–178. <https://doi.org/10.1007/s00253-008-1423-4>
- Mortimer, J.C., Miles, G.P., Brown, D.M., Zhang, Z., Segura, M.P., Weimar, T., Yu, X., Seffen, K.A., Stephens, E., Turner, S.R., Dupree, P., 2010. Absence of branches from xylan in *Arabidopsis* gux mutants reveals potential for simplification of lignocellulosic biomass. *Proc. Natl. Acad. Sci. U. S. A.* 107, 17409–17414. <https://doi.org/10.1073/pnas.1005456107>
- Mottiar, Y., Vanholme, R., Boerjan, W., Ralph, J., Mansfield, S.D., 2016. Designer lignins: harnessing the plasticity of lignification. *Curr. Opin. Biotechnol.* 37, 190–200. <https://doi.org/10.1016/j.copbio.2015.10.009>
- Mueller, S.C., Brown, R.M.J., 1980. Evidence for an intramembrane component associated with a cellulose microfibril-synthesizing complex in higher plants. *J. Cell Biol.* 84, 315–326. <https://doi.org/10.1083/jcb.84.2.315>
- Müller, S., Bley, N., Glaß, M., Busch, B., Rousseau, V., Misiak, D., Fuchs, T., Lederer, M., Hüttelmaier, S., 2018. IGF2BP1 enhances an aggressive tumor cell phenotype by impairing miRNA-directed downregulation of oncogenic factors. *Nucleic Acids Res.* 46, 6285–6303. <https://doi.org/10.1093/nar/gky229>
- Müller, S., Sandal, T., Kamp-Hansen, P., Dalbøge, H., 1998. Comparison of expression systems in the yeasts *Saccharomyces cerevisiae*, *Hansenula polymorpha*, *Kluyveromyces lactis*, *Schizosaccharomyces pombe* and *Yarrowia lipolytica*. Cloning of two novel promoters from *Yarrowia lipolytica*. *Yeast* 14, 1267–1283. [https://doi.org/10.1002/\(SICI\)1097-0061\(1998100\)14:14<1267::AID-YEA327>3.0.CO;2-2](https://doi.org/10.1002/(SICI)1097-0061(1998100)14:14<1267::AID-YEA327>3.0.CO;2-2)
- Myers, Z.A., Kumimoto, R.W., Siriwardana, C.L., Gayler, K.K., Risinger, J.R., Pezzetta, D., Holt, B.F., 2016. NUCLEAR FACTOR Y, Subunit C (NF-YC) Transcription Factors Are Positive Regulators of Photomorphogenesis in *Arabidopsis thaliana*. *PLoS Genet.* 12, 1–30. <https://doi.org/10.1371/journal.pgen.1006333>
- Nazarov, I.B., Bakhmet, E.I., Tomilin, A.N., 2019. KH-Domain Poly(C)-Binding Proteins as Versatile Regulators of Multiple Biological Processes. *Biochem.* 84, 205–219. <https://doi.org/10.1134/S0006297919030039>
- Nicastro, G., Taylor, I.A., Ramos, A., 2015. KH-RNA interactions: Back in the groove. *Curr. Opin. Struct. Biol.* 30, 63–70. <https://doi.org/10.1016/j.sbi.2015.01.002>
- Nigg, E.A., 1993. Targets of cyclin-dependent protein kinases. *Curr. Opin. Cell Biol.* 5, 187–193. [https://doi.org/10.1016/0955-0674\(93\)90101-U](https://doi.org/10.1016/0955-0674(93)90101-U)
- Obel, N., Erben, V., Schwarz, T., Kühnel, S., Fodor, A., Pauly, M., 2009. Microanalysis of plant cell wall polysaccharides. *Mol. Plant* 2, 922–932. <https://doi.org/10.1093/mp/ssp046>
- Oehme, D.P., Shafee, T., Downton, M.T., Bacic, A., Doblin, M.S., 2019. Differences in protein structural regions that impact functional specificity in GT2 family β -glucan synthases. *PLoS One* 14, e0224442.

- Ogawa, M., Kay, P., Wilson, S., Swain, S.M., 2009. ARABIDOPSIS DEHISCENCE ZONE POLYGALACTURONASE1 (ADPG1), ADPG2, and QUARTET2 are Polygalacturonases required for cell separation during reproductive development in Arabidopsis. *Plant Cell* 21, 216–233. <https://doi.org/10.1105/tpc.108.063768>
- Oliver, D.J., Nikolau, B.J., Wurtele, E.S., 2009. Acetyl-CoA-Life at the metabolic nexus. *Plant Sci.* 176, 597–601. <https://doi.org/10.1016/j.plantsci.2009.02.005>
- Orfila, C., Degan, F.D., Jørgensen, B., Scheller, H.V., Ray, P.M., Ulvskov, P., 2012. Expression of mung bean pectin acetyl esterase in potato tubers: Effect on acetylation of cell wall polymers and tuber mechanical properties. *Planta* 236, 185–196. <https://doi.org/10.1007/s00425-012-1596-z>
- Ouyang, Y., Huang, X., Lu, Z., Yao, J., 2012. Genomic survey, expression profile and co-expression network analysis of OsWD40 family in rice. *BMC Genomics* 13. <https://doi.org/10.1186/1471-2164-13-100>
- Paredes, A.R., Somerville, C.R., Ehrhardt, D.W., 2006. Visualization of cellulose synthase demonstrates functional association with microtubules. *Science* 312, 1491–1495. <https://doi.org/10.1126/science.1126551>
- Park, Y.B., Lee, C.M., Kafle, K., Park, S., Cosgrove, D.J., Kim, S.H., 2014. Effects of Plant Cell Wall Matrix Polysaccharides on Bacterial Cellulose Structure Studied with Vibrational Sum Frequency Generation Spectroscopy and X-ray Diffraction. *Biomacromolecules* 15, 2718–2724. <https://doi.org/10.1021/bm500567v>
- Pauly, M., Albersheim, P., Darvill, A., York, W.S., 1999. Molecular domains of the cellulose/xyloglucan network in the cell walls of higher plants. *Plant J.* 20, 629–639. <https://doi.org/10.1046/j.1365-313X.1999.00630.x>
- Pauly, M., Gawenda, N., Wagner, C., Fischbach, P., Ramírez, V., Axmann, I.M., Voiniciuc, C., 2019. The suitability of orthogonal hosts to study plant cell wall biosynthesis. *Plants* 8, 1–18. <https://doi.org/10.3390/plants8110516>
- Pauly, M., Gille, S., Liu, L., Mansoori, N., de Souza, A., Schultink, A., Xiong, G., 2013. Hemicellulose biosynthesis. *Planta* 238, 627–642. <https://doi.org/10.1007/s00425-013-1921-1>
- Pauly, M., Keegstra, K., 2016. Biosynthesis of the Plant Cell Wall Matrix Polysaccharide Xyloglucan*. *Annu. Rev. Plant Biol.* 67, 235–259. <https://doi.org/10.1146/annurev-arplant-043015-112222>
- Pauly, M., Keegstra, K., 2008. Cell-wall carbohydrates and their modification as a resource for biofuels. *Plant J.* 54, 559–568. <https://doi.org/10.1111/j.1365-313X.2008.03463.x>
- Pauly, M., Ramírez, V., 2018. New insights into wall polysaccharide o-acetylation. *Front. Plant Sci.* 9, 1–12. <https://doi.org/10.3389/fpls.2018.01210>
- Pauly, M., Scheller, H.V., 2000. O-Acetylation of plant cell wall polysaccharides: identification and partial characterization of a rhamnogalacturonan O-acetyl-transferase from potato suspension-cultured cells.
- Pearl, L.H., Prodromou, C., 2006. Structure and mechanism of the Hsp90 molecular chaperone machinery. *Annu. Rev. Biochem.* 75, 271–294. <https://doi.org/10.1146/annurev.biochem.75.103004.142738>
- Pearl, L.H., Prodromou, C., Workman, P., 2008. The Hsp90 molecular chaperone: An open and shut case for treatment. *Biochem. J.* 410, 439–453. <https://doi.org/10.1042/BJ20071640>
- Peaucelle, A., Braybrook, S.A., Le Guillou, L., Bron, E., Kuhlemeier, C., Höfte, H., 2011. Pectin-induced changes in cell wall mechanics underlie organ initiation in Arabidopsis. *Curr. Biol.* 21, 1720–1726. <https://doi.org/10.1016/j.cub.2011.08.057>
- Peña, M.J., Kong, Y., York, W.S., O'Neill, M.A., 2012. A galacturonic acid-containing xyloglucan is involved in arabidopsis root hair tip growth. *Plant Cell* 24, 4511–4524. <https://doi.org/10.1105/tpc.112.103390>
- Peng, P., Zhao, J., Zhu, Y., Asami, T., Li, J., 2010. A direct docking mechanism for a plant GSK3-like kinase to phosphorylate its substrates. *J. Biol. Chem.* 285, 24646–24653. <https://doi.org/10.1074/jbc.M110.142547>
- Pérez, S., Rodríguez-Carvajal, M.A., Doco, T., 2003. A complex plant cell wall polysaccharide: Rhamnogalacturonan II. A structure in quest of a function. *Biochimie* 85, 109–121. [https://doi.org/10.1016/S0300-9084\(03\)00053-1](https://doi.org/10.1016/S0300-9084(03)00053-1)
- Perkins, M., Smith, R.A., Samuels, L., 2019. The transport of monomers during lignification in plants: anything goes but how? *Curr. Opin. Biotechnol.* 56, 69–74. <https://doi.org/10.1016/j.copbio.2018.09.011>
- Perrin, R.M., DeRocher, A.E., Bar-Peled, M., Zeng, W., Norambuena, L., Orellana, A., Raikhel, N. V., Keegstra, K., 1999. Xyloglucan fucosyltransferase, an enzyme involved in plant cell wall biosynthesis. *Science* (80-.). 284, 1976–1979. <https://doi.org/10.1126/science.284.5422.1976>
- Persson, S., Caffall, K.H., Freshour, G., Hilley, M.T., Bauer, S., Poindexter, P., Hahn, M.G., Mohnen, D., Somerville, C., 2007. The Arabidopsis irregular xylem8 mutant is deficient in glucuronoxylan and homogalacturonan, which are essential for secondary cell wall integrity. *Plant Cell* 19, 237–255. <https://doi.org/10.1105/tpc.106.047720>
- Pigne`de, G., Pigne`de, P., Wang, H.-J., Fudalej, F., Seman, M., Gaillardin, C., Nicaud, J.-M., 2000. Autocloning and Amplification of LIP2 in Yarrowia lipolytica. *Appl. Environ. Microbiol.* 66, 3283–3289.
- Popper, Z.A., Fry, S.C., 2003. Primary cell wall composition of bryophytes and charophytes. *Ann. Bot.* 91, 1–

12. <https://doi.org/10.1093/aob/mcg013>
- Popper, Z.A., Michel, G., Hervé, C., Domozych, D.S., Willats, W.G.T., Tuohy, M.G., Kloareg, B., Stengel, D.B., 2011. Evolution and diversity of plant cell walls: From algae to flowering plants. *Annu. Rev. Plant Biol.* 62, 567–590. <https://doi.org/10.1146/annurev-arplant-042110-103809>
- Prasad, B.D., Goel, S., Krishna, P., 2010. In Silico identification of carboxylate clamp type tetratricopeptide repeat proteins in Arabidopsis and rice as putative co-chaperones of Hsp90/Hsp70. *PLoS One* 5, 1–18. <https://doi.org/10.1371/journal.pone.0012761>
- Pratt, W.B., Galigniana, M.D., Harrell, J.M., DeFranco, D.B., 2004. Role of hsp90 and the hsp90-binding immunophilins in signalling protein movement. *Cell. Signal.* 16, 857–872. <https://doi.org/10.1016/j.cellsig.2004.02.004>
- Purushotham, P., Ho, R., Zimmer, J., 2020. Architecture of a catalytically active homotrimeric plant cellulose synthase complex. *Science* (80-.). 369, 1089–1094. <https://doi.org/10.1126/science.abb2978>
- Qi, W., Zhang, F., Sun, F., Huang, Y., Guan, R., Yang, J., Luo, X., 2012. Over-expression of a conserved RNA-binding motif (RRM) domain (csRRM2) improves components of Brassica napus yield by regulating cell size. *Plant Breed.* 131, 614–619. <https://doi.org/10.1111/j.1439-0523.2012.01998.x>
- Ramírez, V., Pauly, M., 2019. Genetic dissection of cell wall defects and the strigolactone pathway in Arabidopsis. *Plant Direct* 3, 1–11. <https://doi.org/10.1002/pld3.149>
- Ramírez, V., Xiong, G., Mashiguchi, K., Yamaguchi, S., Pauly, M., 2018. Growth- and stress-related defects associated with wall hypoacetylation are strigolactone-dependent. *Plant Direct* 2. <https://doi.org/10.1002/pld3.62>
- Reiter, W.D., Chapple, C., Somerville, C.R., 1997. Mutants of Arabidopsis thaliana with altered cell wall polysaccharide composition. *Plant J.* 12, 335–345. <https://doi.org/10.1046/j.1365-313X.1997.12020335.x>
- Ripoll, J.J., Rodríguez-Cazorla, E., González-Reig, S., Andújar, A., Alonso-Cantabrana, H., Perez-Amador, M.A., Carbonell, J., Martínez-Laborda, A., Vera, A., 2009. Antagonistic interactions between Arabidopsis K-homology domain genes uncover PEPPER as a positive regulator of the central floral repressor FLOWERING LOCUS C. *Dev. Biol.* 333, 251–262. <https://doi.org/10.1016/j.ydbio.2009.06.035>
- Robinson, J.T., Thorvaldsdóttir, H., Wenger, A.M., Zehir, A., Mesirov, J.P., 2017. Variant review with the integrative genomics viewer. *Cancer Res.* 77, e31–e34. <https://doi.org/10.1158/0008-5472.CAN-17-0337>
- Rodríguez-Gacio, M. del C., Iglesias-Fernández, R., Carbonero, P., Matilla, A.J., 2012. Softening-up mannan-rich cell walls. *J. Exp. Bot.* 63, 3976–3988. <https://doi.org/10.1093/jxb/ers096>
- Saez-Aguayo, S., Ralet, M.C., Berger, A., Botran, L., Ropartz, D., Marion-Poll, A., Northa, H.M., 2013. PECTIN METHYLESTERASE INHIBITOR6 promotes Arabidopsis mucilage release by limiting methylesterification of homogalacturonan in seed coat epidermal cells. *Plant Cell* 25, 308–323. <https://doi.org/10.1105/tpc.112.106575>
- Samakovli, D., Margaritopoulou, T., Prassinou, C., Milioni, D., Hatzopoulos, P., 2014. Brassinosteroid nuclear signaling recruits HSP90 activity. *New Phytol.* 203, 743–757. <https://doi.org/10.1111/nph.12843>
- Sampedro, J., Gianzo, C., Iglesias, N., Guitián, E., Revilla, G., Zarra, I., 2012. AtBGAL10 is the main xyloglucan β -galactosidase in Arabidopsis, and its absence results in unusual xyloglucan subunits and growth defects. *Plant Physiol.* 158, 1146–1157. <https://doi.org/10.1104/pp.111.192195>
- Samuels, A.L., Rensing, K.H., Douglas, C.J., Mansfield, S.D., Dharmawardhana, D.P., Ellis, B.E., 2002. Cellular machinery of wood production: Differentiation of secondary xylem in Pinus contorta var. latifolia. *Planta* 216, 72–82. <https://doi.org/10.1007/s00425-002-0884-4>
- Sánchez-Rodríguez, C., Bauer, S., Hématy, K., Saxe, F., Ibáñez, A.B., Vodermaier, V., Konlechner, C., Sampathkumar, A., Rüggeberg, M., Aichinger, E., Neumetzler, L., Burgert, I., Somerville, C., Hauser, M.-T., Persson, S., 2012. Chitinase-like1/pom-pom1 and its homolog CTL2 are glucan-interacting proteins important for cellulose biosynthesis in Arabidopsis. *Plant Cell* 24, 589–607. <https://doi.org/10.1105/tpc.111.094672>
- Sánchez-Rodríguez, C., Ketelaar, K.D., Schneider, R., Villalobos, J.A., Somerville, C.R., Persson, S., Wallace, I.S., 2017. BRASSINOSTEROID INSENSITIVE2 negatively regulates cellulose synthesis in Arabidopsis by phosphorylating cellulose synthase 1. *Proc. Natl. Acad. Sci. U. S. A.* 114, 3533–3538. <https://doi.org/10.1073/pnas.1615005114>
- Sandhu, A.P.S., Randhawa, G.S., Dhugga, K.S., 2009. Plant cell wall matrix polysaccharide biosynthesis. *Mol. Plant* 2, 840–850. <https://doi.org/10.1093/mp/ssp056>
- Scheller, H.V., Ulvskov, P., 2010. Hemicelluloses. *Annu. Rev. Plant Biol.* 61, 263–289. <https://doi.org/10.1146/annurev-arplant-042809-112315>
- Schultink, A., 2013. Identification and characterization of genes involved in the biosynthesis of the plant cell wall polysaccharide xyloglucan. PhD Thesis.
- Schultink, A., Liu, L., Zhu, L., Pauly, M., 2014. Structural diversity and function of xyloglucan sidechain substituents. *Plants* 3, 526–542. <https://doi.org/10.3390/plants3040526>
- Schultink, A., Naylor, D., Dama, M., Pauly, M., 2015. The role of the plant-specific altered xyloglucan9 protein

- in arabidopsis cell wall polysaccharide o-acetylation. *Plant Physiol.* 167, 1271–1283. <https://doi.org/10.1104/pp.114.256479>
- Seifert, G.J., 2004. Nucleotide sugar interconversions and cell wall biosynthesis: How to bring the inside to the outside. *Curr. Opin. Plant Biol.* 7, 277–284. <https://doi.org/10.1016/j.pbi.2004.03.004>
- Selig, M.J., Adney, W.S., Himmel, M.E., Decker, S.R., 2009. The impact of cell wall acetylation on corn stover hydrolysis by cellulolytic and xylanolytic enzymes. *Cellulose* 16, 711–722. <https://doi.org/10.1007/s10570-009-9322-0>
- Shigeta, T., Zaizen, Y., Sugimoto, Y., Nakamura, Y., Matsuo, T., Okamoto, S., 2015. Heat shock protein 90 acts in brassinosteroid signaling through interaction with BES1/BZR1 transcription factor. *J. Plant Physiol.* 178, 69–73. <https://doi.org/10.1016/j.jplph.2015.02.003>
- Shrawat, A.K., Lörz, H., 2006. Agrobacterium-mediated transformation of cereals: A promising approach crossing barriers. *Plant Biotechnol. J.* 4, 575–603. <https://doi.org/10.1111/j.1467-7652.2006.00209.x>
- Simmons, T.J., Mortimer, J.C., Bernardinelli, O.D., Pöppler, A.-C., Brown, S.P., deAzevedo, E.R., Dupree, R., Dupree, P., 2016. Folding of xylan onto cellulose fibrils in plant cell walls revealed by solid-state NMR. *Nat. Commun.* 7, 13902. <https://doi.org/10.1038/ncomms13902>
- Sims, I.M., Munro, S.L.A., Currie, G., Craik, D., Bacic, A., 1996. Structural characterisation of xyloglucan secreted by suspension-cultured cells of *Nicotiana plumbaginifolia*. *Carbohydr. Res.* 293, 147–172. [https://doi.org/10.1016/0008-6215\(96\)00142-5](https://doi.org/10.1016/0008-6215(96)00142-5)
- Sitaraman, J., Bui, M., Liu, Z., 2008. LEUNIG_Homolog and LEUNIG perform partially redundant functions during Arabidopsis embryo and floral development. *Plant Physiol.* 147, 672–681. <https://doi.org/10.1104/pp.108.115923>
- Smith-Jones, P.M., Solit, D.B., Akhurst, T., Afroze, F., Rosen, N., Larson, S.M., 2004. Imaging the pharmacodynamics of HER2 degradation in response to Hsp90 inhibitors. *Nat. Biotechnol.* 22, 701–706. <https://doi.org/10.1038/nbt968>
- Smith, P.J., Wang, H.-T., York, W.S., Peña, M.J., Urbanowicz, B.R., 2017. Designer biomass for next-generation biorefineries: leveraging recent insights into xylan structure and biosynthesis. *Biotechnol. Biofuels* 10, 286. <https://doi.org/10.1186/s13068-017-0973-z>
- Somerville, C., 2006. Cellulose synthesis in higher plants. *Annu. Rev. Cell Dev. Biol.* 22, 53–78. <https://doi.org/10.1146/annurev.cellbio.22.022206.160206>
- Somerville, C., Bauer, S., Brininstool, G., Facette, M., Hamann, T., Milne, J., Osborne, E., Paredez, A., Persson, S., Raab, T., Vorwerk, S., Youngs, H., 2004. Toward a systems approach to understanding plant cell walls. *Science* (80-.). 306, 2206–2211. <https://doi.org/10.1126/science.1102765>
- Sørensen, I., Pettolino, F.A., Wilson, S.M., Doblin, M.S., Johansen, B., Bacic, A., Willats, W.G.T., 2008. Mixed-linkage (1 → 3),(1 → 4)-β-D-glucan is not unique to the Poales and is an abundant component of *Equisetum arvense* cell walls. *Plant J.* 54, 510–521. <https://doi.org/10.1111/j.1365-313X.2008.03453.x>
- Sterling, J.D., Atmodjo, M.A., Inwood, S.E., Kolli, V.S.K., Quigley, H.F., Hahn, M.G., Mohnen, D., 2006. Functional identification of an Arabidopsis pectin biosynthetic homogalacturonan galacturonosyltransferase. *Proc. Natl. Acad. Sci. U. S. A.* 103, 5236–5241. <https://doi.org/10.1073/pnas.0600120103>
- Stirnemann, C.U., Petsalaki, E., Russell, R.B., Muller, C.W., 2010. WD40 proteins propel cellular networks. *Trends Biochem. Sci.* 35, 531–538. <https://doi.org/10.1016/j.tibs.2010.04.003>
- Sun, F., Liu, C., Zhang, C., Qi, W., Zhang, X., Wu, Z., Kong, D., Wang, Q., Shang, H., Qian, X., Li, F., Yang, J., 2012. A conserved RNA recognition motif (RRM) domain of *Brassica napus* FCA improves cotton fiber quality and yield by regulating cell size. *Mol. Breed.* 30, 93–101. <https://doi.org/10.1007/s11032-011-9601-y>
- Sun, T. ping, 2010. Gibberellin-GID1-DELLA: A pivotal regulatory module for plant growth and development. *Plant Physiol.* 154, 567–570. <https://doi.org/10.1104/pp.110.161554>
- Suzuki, S., Li, L., Sun, Y.-H., Chiang, V.L., 2006. The cellulose synthase gene superfamily and biochemical functions of xylem-specific cellulose synthase-like genes in *Populus trichocarpa*. *Plant Physiol.* 142, 1233–1245. <https://doi.org/10.1104/pp.106.086678>
- Takenaka, Y., Kato, K., Ogawa-Ohnishi, M., Tsuruhama, K., Kajijura, H., Yagyu, K., Takeda, A., Takeda, Y., Kunieda, T., Hara-Nishimura, I., Kuroha, T., Nishitani, K., Matsubayashi, Y., Ishimizu, T., 2018. Pectin RG-I rhamnosyltransferases represent a novel plant-specific glycosyltransferase family. *Nat. plants* 4, 669–676. <https://doi.org/10.1038/s41477-018-0217-7>
- Tamura, K., Shimada, T., Kondo, M., Nishimura, M., Hara-Nishimura, I., 2005. KATAMARI1/MURUS3 is a novel Golgi membrane protein that is required for endomembrane organization in Arabidopsis. *Plant Cell* 17, 1764–1776. <https://doi.org/10.1105/tpc.105.031930>
- Tan, L., Salih, H., Htet, N.N.W., Azeem, F., Zhan, R., 2021. Genomic analysis of WD40 protein family in the mango reveals a TTG1 protein enhances root growth and abiotic tolerance in Arabidopsis. *Sci. Rep.* 11, 1–10. <https://doi.org/10.1038/s41598-021-81969-z>

- Tanaka, K., Murata, K., Yamazaki, M., Onosato, K., Miyao, A., Hirochika, H., 2003. Three distinct rice cellulose synthase catalytic subunit genes required for cellulose synthesis in the secondary wall. *Plant Physiol.* 133, 73–83. <https://doi.org/10.1104/pp.103.022442>
- Taylor, N.G., Gardiner, J.C., Whiteman, R., Turner, S.R., 2004. Cellulose synthesis in the Arabidopsis secondary cell wall. *Cellulose* 11, 329–338. <https://doi.org/10.1023/b:cell.0000046405.11326.a8>
- Tedman-Jones, J.D., Lei, R., Jay, F., Fabro, G., Li, X., Reiter, W.D., Brearley, C., Jones, J.D.G., 2008. Characterization of Arabidopsis mur3 mutations that result in constitutive activation of defence in petioles, but not leaves. *Plant J.* 56, 691–703. <https://doi.org/10.1111/j.1365-313X.2008.03636.x>
- Terrett, O.M., Dupree, P., 2019. Covalent interactions between lignin and hemicelluloses in plant secondary cell walls. *Curr. Opin. Biotechnol.* 56, 97–104. <https://doi.org/10.1016/j.copbio.2018.10.010>
- Tian, C., Beeson, W.T., Iavarone, A.T., Sun, J., Marletta, M.A., Cate, J.H.D., Glass, N.L., 2009. Systems analysis of plant cell wall degradation by the model filamentous fungus *Neurospora crassa*. *Proc. Natl. Acad. Sci. U. S. A.* 106, 22157–22162. <https://doi.org/10.1073/pnas.0906810106>
- Tobimatsu, Y., Schuetz, M., 2019. Lignin polymerization: how do plants manage the chemistry so well? *Curr. Opin. Biotechnol.* 56, 75–81. <https://doi.org/10.1016/j.copbio.2018.10.001>
- Tokuriki, N., Tawfik, D.S., 2009. Stability effects of mutations and protein evolvability. *Curr. Opin. Struct. Biol.* 19, 596–604. <https://doi.org/10.1016/j.sbi.2009.08.003>
- Trassaert, M., Vandermies, M., Carly, F., Denies, O., Thomas, S., Fickers, P., Nicaud, J.M., 2017. New inducible promoter for gene expression and synthetic biology in *Yarrowia lipolytica*. *Microb. Cell Fact.* 16, 1–17. <https://doi.org/10.1186/s12934-017-0755-0>
- Tryfona, T., Bourdon, M., Delgado Marques, R., Busse-Wicher, M., Vilaplana, F., Stott, K., Dupree, P., 2023. Grass xylan structural variation suggests functional specialization and distinctive interaction with cellulose and lignin. *Plant J.* 113, 1004–1020. <https://doi.org/https://doi.org/10.1111/tpj.16096>
- Tsakraklides, V., Kamineni, A., Consiglio, A.L., MacEwen, K., Friedlander, J., Blitzblau, H.G., Hamilton, M.A., Crabtree, D. V., Su, A., Afshar, J., Sullivan, J.E., Latouf, W.G., South, C.R., Greenhagen, E.H., Shaw, A.J., Brevnova, E.E., 2018. High-oleate yeast oil without polyunsaturated fatty acids. *Biotechnol. Biofuels* 11, 1–11. <https://doi.org/10.1186/s13068-018-1131-y>
- Tuomivaara, S.T., Yaoi, K., O'Neill, M.A., York, W.S., 2015. Generation and structural validation of a library of diverse xyloglucan-derived oligosaccharides, including an update on xyloglucan nomenclature. *Carbohydr. Res.* 402, 56–66. <https://doi.org/10.1016/j.carres.2014.06.031>
- Urbanowicz, B.R., Peña, M.J., Moniz, H.A., Moremen, K.W., York, W.S., 2014. Two Arabidopsis proteins synthesize acetylated xylan in vitro. *Plant J.* 80, 197–206. <https://doi.org/10.1111/tpj.12643>
- Urbanowicz, B.R., Peña, M.J., Ratnaparkhe, S., Avci, U., Backe, J., Steet, H.F., Foston, M., Li, H., O'Neill, M.A., Ragauskas, A.J., Davill, A.G., Wyman, C., Gilbert, H.J., York, W.S., 2012. 4-O-methylation of glucuronic acid in Arabidopsis glucuronoxylan is catalyzed by a domain of unknown function family 579 protein. *Proc. Natl. Acad. Sci. U. S. A.* 109, 14253–14258. <https://doi.org/10.1073/pnas.1208097109>
- Vain, T., Crowell, E.F., Timpano, H., Biot, E., Desprez, T., Mansoori, N., Trindade, L.M., Pagant, S., Robert, S., Höfte, H., Gonneau, M., Vernhettes, S., 2014. The Cellulase KORRIGAN Is Part of the Cellulose Synthase Complex. *Plant Physiol.* 165, 1521–1532. <https://doi.org/10.1104/pp.114.241216>
- Valverde, R., Edwards, L., Regan, L., 2008. Structure and function of KH domains. *FEBS J.* 275, 2712–2726. <https://doi.org/10.1111/j.1742-4658.2008.06411.x>
- van Nocker, S., Ludwig, P., 2003. The WD-repeat protein superfamily in Arabidopsis: Conservation and divergence in structure and function. *BMC Genomics* 4, 1–11. <https://doi.org/10.1186/1471-2164-4-50>
- Vanholme, R., Cesarino, I., Rataj, K., Xiao, Y., Sundin, L., Goeminne, G., Kim, H., Cross, J., Morreel, K., Araujo, P., Welsh, L., Haustraete, J., McClellan, C., Vanholme, B., Ralph, J., Simpson, G.G., Halpin, C., Boerjan, W., 2013. Caffeoyl shikimate esterase (CSE) is an enzyme in the lignin biosynthetic pathway in Arabidopsis. *Science* 341, 1103–1106. <https://doi.org/10.1126/science.1241602>
- Vanholme, R., De Meester, B., Ralph, J., Boerjan, W., 2019. Lignin biosynthesis and its integration into metabolism. *Curr. Opin. Biotechnol.* 56, 230–239. <https://doi.org/10.1016/j.copbio.2019.02.018>
- Vanzin, G.F., Madson, M., Carpita, N.C., Raikhel, N. V., Keegstra, K., Reiter, W.D., 2002. The mur2 mutant of Arabidopsis thaliana lacks fucosylated xyloglucan because of a lesion in fucosyltransferase AtFUT1. *Proc. Natl. Acad. Sci. U. S. A.* 99, 3340–3345. <https://doi.org/10.1073/pnas.052450699>
- Vardhini, B. V., Anjum, N.A., 2015. Brassinosteroids make plant life easier under abiotic stresses mainly by modulating major components of antioxidant defense system. *Front. Environ. Sci.* 2, 1–16. <https://doi.org/10.3389/fenvs.2014.00067>
- Verherbruggen, Y., Yin, L., Oikawa, A., Scheller, H.V., 2011. Mannan synthase activity in the CSLD family. *Plant Signal. Behav.* 6, 1620–1623. <https://doi.org/10.4161/psb.6.10.17989>
- Vermaas, J. V., Dixon, R.A., Chen, F., Mansfield, S.D., Boerjan, W., Ralph, J., Crowley, M.F., Beckham, G.T., 2019. Passive membrane transport of lignin-related compounds. *Proc. Natl. Acad. Sci.* 116, 23117–23123. <https://doi.org/10.1073/pnas.1904643116>

- Vincken, J.P., York, W.S., Beldman, G., Voragen, A.G.J., 1997. Two general branching patterns of xyloglucan, XXXG and XXGG. *Plant Physiol.* 114, 9–13. <https://doi.org/10.1104/pp.114.1.9>
- Voet, D., Voet, J.G., Pratt, C.W., 2013. *Fundamentals Biochemistry*, 4th ed. John Wiley & Sons.
- Vogel, J.P., Raab, T.K., Somerville, C.R., Somerville, S.C., 2004. Mutations in PMR5 result in powdery mildew resistance and altered cell wall composition. *Plant J.* 40, 968–978. <https://doi.org/10.1111/j.1365-313X.2004.02264.x>
- Voiniciuc, C., Dama, M., Gawenda, N., Stritt, F., Pauly, M., 2019. Mechanistic insights from plant heteromannan synthesis in yeast. *Proc. Natl. Acad. Sci. U. S. A.* 116, 522–527. <https://doi.org/10.1073/pnas.1814003116>
- Vukelić, I., Radić, D., Pećinar, I., Lević, S., Djikanović, D., Radotić, K., Panković, D., 2024. Spectroscopic Investigation of Tomato Seed Germination Stimulated by *Trichoderma* spp. *Biology (Basel)*. <https://doi.org/10.3390/biology13050340>
- Vuttipongchaikij, S., Brocklehurst, D., Steele-King, C., Ashford, D.A., Gomez, L.D., Mcqueen-Mason, S.J., 2012. Arabidopsis GT34 family contains five xyloglucan α -1,6-xylosyltransferases. *New Phytol.* 195, 585–595. <https://doi.org/10.1111/j.1469-8137.2012.04196.x>
- Wagner, J.M., Liu, L., Yuan, S.F., Venkataraman, M. V., Abate, A.R., Alper, H.S., 2018. A comparative analysis of single cell and droplet-based FACS for improving production phenotypes: Riboflavin overproduction in *Yarrowia lipolytica*. *Metab. Eng.* 47, 346–356. <https://doi.org/10.1016/j.ymben.2018.04.015>
- Waters, M.T., Gutjahr, C., Bennett, T., Nelson, D.C., 2017. Strigolactone Signaling and Evolution. *Annu. Rev. Plant Biol.* 68, 291–322. <https://doi.org/10.1146/annurev-arplant-042916-040925>
- Weigel, D., Ahn, J.H., Blázquez, M.A., Borevitz, J.O., Christensen, S.K., Fankhauser, C., Ferrándiz, C., Kardailsky, I., Malancharuvil, E.J., Neff, M.M., Nguyen, J.T., Sato, S., Wang, Z.Y., Xia, Y., Dixon, R.A., Harrison, M.J., Lamb, C.J., Yanofsky, M.F., Chory, J., 2000. Activation tagging in Arabidopsis. *Plant Physiol.* 122, 1003–1013. <https://doi.org/10.1104/pp.122.4.1003>
- Whistler, R.L., BeMiller, J.N., 1973. *Industrial Gums, Polysaccharides and Their Derivatives*. Academic Press.
- Whitesell, L., Lindquist, S.L., 2005. HSP90 and the chaperoning of cancer. *Nat. Rev. Cancer* 5, 761–772. <https://doi.org/10.1038/nrc1716>
- Wilson, S.M., Ho, Y.Y., Lampugnani, E.R., Van de Meene, A.M.L., Bain, M.P., Bacic, A., Doblin, M.S., 2015. Determining the Subcellular Location of Synthesis and Assembly of the Cell Wall Polysaccharide (1,3; 1,4)- β -d-Glucan in Grasses. *Plant Cell* 27, 754–771. <https://doi.org/10.1105/tpc.114.135970>
- Winter, A., Andorfer, L., Herzele, S., Zimmermann, T., Saake, B., Edler, M., Griesser, T., Konnerth, J., Gindl-Altmutter, W., 2017. Reduced polarity and improved dispersion of microfibrillated cellulose in poly(lactic-acid) provided by residual lignin and hemicellulose. *J. Mater. Sci.* 52, 60–72. <https://doi.org/10.1007/s10853-016-0439-x>
- Winter, D., Vinegar, B., Nahal, H., Ammar, R., Wilson, G. V., Provart, N.J., 2007. An “electronic fluorescent pictograph” Browser for exploring and analyzing large-scale biological data sets. *PLoS One* 2, 1–12. <https://doi.org/10.1371/journal.pone.0000718>
- Wu, A.-M., Hörnblad, E., Voxeur, A., Gerber, L., Rihouey, C., Lerouge, P., Marchant, A., 2010. Analysis of the Arabidopsis IRX9/IRX9-L and IRX14/IRX14-L pairs of glycosyltransferase genes reveals critical contributions to biosynthesis of the hemicellulose glucuronoxylan. *Plant Physiol.* 153, 542–554. <https://doi.org/10.1104/pp.110.154971>
- Wu, A.-M., Rihouey, C., Seveno, M., Hörnblad, E., Singh, S.K., Matsunaga, T., Ishii, T., Lerouge, P., Marchant, A., 2009. The Arabidopsis IRX10 and IRX10-LIKE glycosyltransferases are critical for glucuronoxylan biosynthesis during secondary cell wall formation. *Plant J.* 57, 718–731. <https://doi.org/10.1111/j.1365-313X.2008.03724.x>
- Xi, D., Wang, Z., 2022. OsWDRP3, a WD-40 repeat protein interacts with OsBAK1 to control leaf angle by modulating BR signaling 1–28.
- Xia, W., Ci, S., Li, M., Wang, M., Dianov, G.L., Ma, Z., Li, L., Hua, K., Alagamuthu, K.K., Qing, L., Luo, L., Edick, A.M., Liu, L., Hu, Z., He, L., Pan, F., Guo, Z., 2019. Two-way crosstalk between BER and c-NHEJ repair pathway is mediated by Pol- β and Ku70. *FASEB J. Off. Publ. Fed. Am. Soc. Exp. Biol.* 33, 11668–11681. <https://doi.org/10.1096/fj.201900308R>
- Xiao, C., Somerville, C., Anderson, C.T., 2014. POLYGALACTURONASE INVOLVED IN EXPANSION1 functions in cell elongation and flower development in Arabidopsis. *Plant Cell* 26, 1018–1035. <https://doi.org/10.1105/tpc.114.123968>
- Xiong, G., Cheng, K., Pauly, M., 2013. Xylan O-acetylation impacts xylem development and enzymatic recalcitrance as indicated by the arabidopsis mutant tbl29. *Mol. Plant* 6, 1373–1375. <https://doi.org/10.1093/mp/sst014>
- Xiong, G., Li, R., Qian, Q., Song, X., Liu, X., Yu, Y., Zeng, D., Wan, J., Li, J., Zhou, Y., 2010. The rice dynamin-related protein DRP2B mediates membrane trafficking, and thereby plays a critical role in

- secondary cell wall cellulose biosynthesis. *Plant J.* 64, 56–70. <https://doi.org/10.1111/j.1365-313X.2010.04308.x>
- York, W.S., Darvill, A.G., McNeil, M., Stevenson, T.T., Albersheim, P., 1986. Isolation and characterization of plant cell walls and cell wall components. *Methods Enzymol.* 118, 3–40. [https://doi.org/10.1016/0076-6879\(86\)18062-1](https://doi.org/10.1016/0076-6879(86)18062-1)
- York, W.S., Kolli, V.S.K., Orlando, R., Albersheim, P., Darvill, A.G., 1996. The structures of arabinoxyloglucans produced by solanaceous plants. *Carbohydr. Res.* 285, 99–128. [https://doi.org/10.1016/0008-6215\(96\)00029-8](https://doi.org/10.1016/0008-6215(96)00029-8)
- Yu, X., Li, L., Zola, J., Aluru, M., Ye, H., Foudree, A., Guo, H., Anderson, S., Aluru, S., Liu, P., Rodermel, S., Yin, Y., 2011. A brassinosteroid transcriptional network revealed by genome-wide identification of BES1 target genes in *Arabidopsis thaliana*. *Plant J.* 65, 634–646. <https://doi.org/10.1111/j.1365-313X.2010.04449.x>
- Yuan, Y., Teng, Q., Zhong, R., Ye, Z.-H., 2016a. Roles of *Arabidopsis* TBL34 and TBL35 in xylan acetylation and plant growth. *Plant Sci.* 243, 120–130. <https://doi.org/https://doi.org/10.1016/j.plantsci.2015.12.007>
- Yuan, Y., Teng, Q., Zhong, R., Ye, Z.H., 2016b. TBL3 and TBL31, Two *Arabidopsis* DUF231 domain proteins, are required for 3-O-monoacetylation of xylan. *Plant Cell Physiol.* 57, 35–45. <https://doi.org/10.1093/pcp/pcv172>
- Zablackis, E., Huang, J., Müller, B., Darvill, A.G., Albersheim, P., 1995. Characterization of the cell-wall polysaccharides of *Arabidopsis thaliana* leaves. *Plant Physiol.* 107, 1129–1138. <https://doi.org/10.1104/pp.107.4.1129>
- Zabotina, O.A., Avci, U., Cavalier, D., Pattathil, S., Chou, Y.H., Eberhard, S., Danhof, L., Keegstra, K., Hahn, M.G., 2012. Mutations in multiple XXT genes of *Arabidopsis* reveal the complexity of xyloglucan biosynthesis. *Plant Physiol.* 159, 1367–1384. <https://doi.org/10.1104/pp.112.198119>
- Zeng, W., Jiang, N., Nadella, R., Killen, T.L., Nadella, V., Faik, A., 2010. A Glucurono(arabino)xylan synthase complex from wheat contains members of the GT43, GT47, and GT75 families and functions cooperatively. *Plant Physiol.* 154, 78–97. <https://doi.org/10.1104/pp.110.159749>
- Zeng, W., Lampugnani, E.R., Picard, K.L., Song, L., Wu, A.-M., Farion, I.M., Zhao, J., Ford, K., Doblin, M.S., Bacic, A., 2016. Asparagus IRX9, IRX10, and IRX14A Are Components of an Active Xylan Backbone Synthase Complex that Forms in the Golgi Apparatus. *Plant Physiol.* 171, 93–109. <https://doi.org/10.1104/pp.15.01919>
- Zhang, B., Deng, L., Qian, Q., Xiong, G., Zeng, D., Li, R., Guo, L., Li, J., Zhou, Y., 2009. A missense mutation in the transmembrane domain of CESA4 affects protein abundance in the plasma membrane and results in abnormal cell wall biosynthesis in rice. *Plant Mol. Biol.* 71, 509–524. <https://doi.org/10.1007/s11103-009-9536-4>
- Zhang, B., Gao, Y., Zhang, L., Zhou, Y., 2021. The plant cell wall: Biosynthesis, construction, and functions. *J. Integr. Plant Biol.* 63, 251–272. <https://doi.org/10.1111/jipb.13055>
- Zhang, B., Zhang, L., Li, F., Zhang, D., Liu, X., Wang, H., Xu, Z., Chu, C., Zhou, Y., 2017. Control of secondary cell wall patterning involves xylan deacetylation by a GDSL esterase. *Nat. Plants* 3, 1–9. <https://doi.org/10.1038/nplants.2017.17>
- Zhang, N., Julian, J.D., Yap, C.E., Swaminathan, S., Zabotina, O.A., 2023. The *Arabidopsis* xylosyltransferases, XXT3, XXT4, and XXT5, are essential to complete the fully xylosylated glucan backbone XXXG-type structure of xyloglucans. *New Phytol.* 238, 1986–1999. <https://doi.org/10.1111/nph.18851>
- Zhang, Z., Zhang, H., Gonzalez, E., Grismer, T., Zu, S.-L., Wang, Z.-Y., 2023. UPL3 Promotes BZR1 Degradation, Growth Arrest, and Seedling Survival under Starvation Stress in *Arabidopsis*. *bioRxiv Prepr.* 1–14. <https://doi.org/https://doi.org/10.1101/2023.10.18.562997>
- Zhao, B., Lv, M., Feng, Z., Campbell, T., Liscum, E., Li, J., 2016. TWISTED DWARF 1 Associates with BRASSINOSTEROID-INSENSITIVE 1 to Regulate Early Events of the Brassinosteroid Signaling Pathway. *Mol. Plant* 9, 582–592. <https://doi.org/10.1016/j.molp.2016.01.007>
- Zhong, R., Burk, D.H., Morrison, W.H. 3rd, Ye, Z.-H., 2002. A kinesin-like protein is essential for oriented deposition of cellulose microfibrils and cell wall strength. *Plant Cell* 14, 3101–3117. <https://doi.org/10.1105/tpc.005801>
- Zhong, R., Cui, D., Dasher, R.L., Ye, Z.-H., 2018a. Biochemical characterization of rice xylan O-acetyltransferases. *Planta* 247, 1489–1498. <https://doi.org/10.1007/s00425-018-2882-1>
- Zhong, R., Cui, D., Phillips, D.R., Richardson, E.A., Ye, Z.H., 2020a. A Group of O-Acetyltransferases Catalyze Xyloglucan Backbone Acetylation and Can Alter Xyloglucan Xylosylation Pattern and Plant Growth When Expressed in *Arabidopsis*. *Plant Cell Physiol.* 61, 1064–1079. <https://doi.org/10.1093/pcp/pcaa031>
- Zhong, R., Cui, D., Richardson, E.A., Phillips, D.R., Azadi, P., Lu, G., Ye, Z.H., 2020b. Cytosolic acetyl-CoA generated by ATP-citrate lyase is essential for acetylation of cell wall polysaccharides. *Plant Cell Physiol.* 61, 64–75. <https://doi.org/10.1093/pcp/pcz178>

- Zhong, R., Cui, D., Ye, Z.-H., 2018b. Members of the DUF231 Family are O-Acetyltransferases Catalyzing 2-O- and 3-O-Acetylation of Mannan. *Plant Cell Physiol.* 59, 2339–2349. <https://doi.org/10.1093/pcp/pcy159>
- Zhong, R., Cui, D., Ye, Z.H., 2018c. A group of *Populus trichocarpa* DUF231 proteins exhibit differential Oacetyltransferase activities toward xylan. *PLoS One* 13, 1–21. <https://doi.org/10.1371/journal.pone.0194532>
- Zhong, R., Cui, D., Ye, Z.H., 2017. Regiospecific acetylation of xylan is mediated by a group of DUF231-containing O-acetyltransferases. *Plant Cell Physiol.* 58, 2126–2138. <https://doi.org/10.1093/pcp/pcx147>

7. Appendix 1: Gene sequences

TmCSLC4

atggcccctaactccgtgtgtgtactatagaaaatcccaccagtattccgtgaaagagatgatgaaaaagagtgactcagaaagtctgt
 ttcagacaaacagaaaaagtcagatcttctaacagtttacttggtcctgctattgaaagcccacaaggctttaacgtgcttgcattgg
 ctggccatggcttcaaagtctttatgttcatctgtcaaaaagagagtgcctccagtacatctccgaagaggaaaggagcatccaaa
 gagtcgtgggaaattgatcgaattcatcaaagtgttttgcctatttctgtgttagcacttattgtcgagattatgcctattacatgaaatgga
 atttgggtcaatgatacaacctggggaatacaaggcttctgcactggctctatatggcttgggtgctttcagacttgattacattgcac
 cattggttggcctgctatctcagttctgtattgttattcatgattcaatcattggatcgtttgattttgtattggatgcttttgattaagtac
 aaaaactgaagccaaagatagatgagaatgcatacgcatacgaagataacagttccttccctatggttttagtccaaattcctatgtgcaa
 tgagcgagaagtctacgaacagctctatcggagctgtctgtcaattagattggccaaaagatagaatccttatccaagtttggatgactca
 gatgattcctctttacagttattgatcaaggaggaaagttcctcatggcgtcaaaaaggcgtaaacatcatctatcgtcatagattgattag
 gacaggggtataaggcagggaatatgaaatctgcaatgggatgtgattacgttaaagactatgagttcgtggctatctttgatgcagacttc
 caacctaatcccgacttttgaactgactatgccacattcaaagtgaccccgaagttggtctagtcaagctagatggctcctttgtcaa
 caaagatgagaacttgcttacaaggttgcaaacatcaatctttgtttcacttgaagtcgagcaacaggttaacgggtgtttccttaacttt
 ttcggttcaatggaaccgccggtgtttggagaatcaaggctcttgaggaaatccggaggctggctagagagaacaactgtcgaggaca
 tggatattgcagttagagcccacttgaatgggtggaagttgtcttttgaatgacgtaaaggttctatgcgaactgccagaatcttatgaa
 gcatacaaaaagcaacaacatagatggcatagtggtccaatgcagttgttctgtcttctgtccatctgtgctatcttccaagatatccgc
 ttggaaaaggtaacctgatcttttgttttcttttgaggaaattgatttggccttttactcttctcactcttttctgcatcctacctttgac
 aatgttcataccagaaactgaattaccttttgggtgatattacattcccataatcatgtcattccttaacattctgcctagtccaaaatcctt
 tcctttctgggtgccttattctattgttcgaaaacacatgagtgactaagtttaacgccatgattccggttgtttcagttgggttcagctta
 tgagtgggttgaacgaaaagaccggtagatcatctgaatctgacttactgccctggctgaaaaggaagagaagatattgagaagg
 aattcagaatcaggactggaaatgctgtcaaaagcttaaggaacaggaggagattgcacctctgaaaaggttaaccaagaagaagaaa
 aacaagatttccgaaaggaattagctcttgccttttgcctacttacggctgctggttagatcttactttctgctcagggtgtccacttctactt
 tttgctgtccaaggattaagtttctagtcgtaggattagacctaattggagaacaaatgtcttaaatcc

TmXXT2

tatgattgaacgatgccttggcgctcagcgatctagaaagatccagcgtgctttgagacattgcaaagttacggcactgtgtcttgcctta
 actgtggttgttctgcgtggactataggtgcaggaagtttgactccagagcaagattttgtagatattcgagatcatttctacagtag
 gaagagaagtgaaccacatagagtattggaagaggtgcaaacataacctccagttcctcatcttctgactcttcaaaatcatcagggga
 acaataacaactacgagcaattgatgtcaattccatattcgtacatgaaggcgaagatgataagcctgacccttcaaaccttacagttt

gggaccaaagatttccgattgggacgagcagaggtcacaatggcttaacaaaatccagatttccaaactttgccagccttctaaacc
cagagttctgttagtcaccgggtcatcccctaagccttgcgagaatccagtgaggagatcattacctttgaaatccatcaaaaacaagatt
gactattgtcgtgcatgggatcagattttctacaatatggcactactggatgctgaaatggccggattctgggcaaagtgccactta
ttcgaaaactattgttatctcacctgaagttgagttttgtggtggatggattctgacgctatgtttacagacatggctttgaactacctgg
gaaaggtacaaggatgtaaatctggtcatgcacggttgaacgaaatggtgatgacgagaaaaactggattggattgaatactggaa
gtttcctttgagaacactcaatgggcattagacttgttagatgtttgggctccaatgggacccaaaggaaaggtagggacgatgctg
gcaagatttaaccagagaattgaaaaacaggccagctttgaggccgatgatcaatctgctatggtctattgttggctaccaacgtg
agcaatggggtaacaaagttacttggagaatgcctactatctacacggttattggggtatcttagtagacagatatgaagagatgattga
aaactaccacctggctttggagatcacagatggcccttgggtactcacttcggtggatgtaaacctgtggaaagttcgggtgactacc
cgtcgaaagatgcttagacagatggacagagccttcaattcggagacaatcagattttgcaaatctatggttttacgcataagacatta
gcttccaaaagagttaagcgtgtagaaacgaaacatctatgccattggagggttaaagacgaaactgggtctgatacaccaccttcaag
gccgtaaagggtgtagtggttaaacc

BdXyBATI

atgaagctccatttcttgggtgaagctcttctcgggccgggtgccggtgacttctcggcgtggccatcctcatccttccaccaacgcgc
agtactcggcctggcggcgtggcggtgccgcacgccacgaagctggtgtcctcgacgccgggtgagcgtgatgaagtaactgc
gacatcttccggcgagtggtgggtgccggacacggagggcgcctactacaaccacaagacttgctacatgatccaggagcaccagaa
ctgctcaagtagcggccggccggacctgggcttctcaagtggcggtggaggccgtcgggctgcgagctgccgcgttcgacccg
gtgcagttctgcagttcggccccaagtcgctggcattctggtggggattcctggtcgcgaaccatattgcagttctgctctgcctc
ctctcacagtggtggtatcccaaggacatgtcggcgaaccggacggaccagaacaaggtgtactactacagagcatacaacttacc
atcaacatgttctggtcaccgttctggtccggggcggggagcccgaccacgacgaccggcgcacacgggccaactacagcctta
cctcgacgagccggacgacaagtgggtgtcccaggtgccccgcttcgactacgtctcgtctccgcccaactggttctcccgcc
ttccttcttacgagaagcggcgctcgtcggctgcagcttctgcagccggcagttacggcgtcccggacctgacgtctactactcc
cagcgcaaggcgtggcgctgtccctgcaggccatcaacgcccttcagggaaggtgaaggccgggtgatcgtgcggatgctgt
cgcccatgtcgcacttcgagaacgggacgtgggaccagggcggaactgcaagcgcacggagccgctccggagcaaccagacg
gtcatggaaggccgcacctgcagttctacacggcgcagatggaggagtaccgcggcgggagagaagacggccaaggcgaagg
ggtccggatgatgctatggacgccacggcggcgtgctgatgcggcccacgggacccgagccggtacgggactggcccaa
cgagaaggtgcagctctacaacgactgcatccactggtgcctgcccggccgatcgacatctggaacgacctccttccagatgatc
ctcgtctag

AtWD40

Atggagaagaagaaagtgcgactccgctagtgtccatggccattcgagacctgttggtgattgttctacagtccaatcactcctgat
 gggttcttctcatcagcgcgaagtaagattctcaaccaatgttgagaaatggggaaactggagattggattggtacattgaaggtcata
 aaggtgctgtgtggagtcttcttgataacaatgctttacgtgcagcttctgcatctgctgattttcagcgaagctttgggatgctttgac
 tggggatgtcttgacttttgagcacaagcatattgttcgagcatgcgccttctctcaggatacgaataatcacaacaggaggattg
 agaaaattctcgtgtttcacttgaatcgttggatgcacctcctacagaaattgataaatcctggttctatcagaacactaacatggc
 ttcacggtgatcaacaatattaagtcttgcactgatattggtggtgtgaggttatgggatgtgaggatggcaaaaatagtcaaaactct
 agaaaccaagtctcctgtcaccagtgtgaagtgagtcaagatggacggatataacaactgccgatgggtcaactgttaaatttggg
 atgcaaatcatttggactagtgaaggttacgacatgcctgcaatcgaatctgcatcgcttgagccaaaatctggcaacaaattcgt
 tctggtggagaagatgtgggttcgactcttatttccacaccggaaaggagattggatgcaacaagggacatcatggtccggctc
 actgtgtgagattgcaccaacaggtgagcttattgcttcagggtctgaagatggtacaatcagaattggcaaacctggaccggtgaatc
 ctgaagagatcagcaggtcaaagccgaagcagagtgtggatgaggttctcgtgaagattgaaggctttcacattaacaaggaaggaa
 aaaccgcagagaaacctctgatgctccaagaaaaagcgggaaggtg

AtDAAR2

Atgtgtgatggaagaaagaaaaaacataacttgcataaaaagatcgatcgagatatggggaagaagaaaggttcaagtactttg
 tggggatgcttctactgattcggcttcaaggggaatccagctgctgtttgtttctcaacgacgataacgagagagatgacacgtggct
 tcagtctctcgccgccgaattcaacatctccgaaactgttttctattccatcactggtttccaagctcgcttcagtctacgtggtttacc
 ccttagccgaggtggatctctgtggtcatgcaacttggcatctgctcattgtctcttcaaatggtttggttgattcagacatggttgatt
 tgcacaagatcagggttcttacagccaagcgtgttcagatactcagagctcagtgatggtgaagtgaagggaggaaccttttgat
 cgaattgaattccctgtggttacaactgtgatgtaatctcagtgatgatcctctctatgatccaagccttgaacggagctaccatt
 gttgatataaaagctactgcaacaaacaacatcctcgttgtgttccatctaaggaatctgactgaattgcaaccaagaatggatgat
 attgaaatgccctgtgatggcataattgtgacagctgctggttctacaggatcgtcctatgattttacagtcggtactttgctcctaagtc
 ggagttgatgaggacctgtttgtggaagtgcacattgtgcattggcacattactggagcatcaagatgaataagtttgatttcttagccta
 ccaagcttcgagtaggagtggaaacgataaggattcatctagacaaggagaagcagaggggttctcctgagaggcaaagccgttactgt
 gatggaaggccatgtcttggtc

AtSK11

atggcgtcagtggttatagctcctaactcctggagcaagagactctactggtgttgataaattgcctgaagaaatgaatgacatgaaaatt
 cgtgacgataaagaaatggaagcagcagtggttagatggaatggaacagagactggacatatcattgtgactactattggtgtagaa
 atggccaacaaaacagacaattagctacatggctgagcgtgtgtgtggtcacggatctttggtgtgtgtccaagcgaatgtcttga
 gacaggagaaactgttgcgataaagaaagtttacaagataggaggtacaagaaccgtgagcttcaacctgaggctacttgacct

cctaattgtgtctctgaaacattgtttcttcaaccactgaaaaagatgagctttacctaattctgttcttgagtacgtccagaaactgt
tcatcgtgttatcaaacactacaacaaactgaatcagagaatgcctcttatatactgcaaaccttacacttatcagatttttagagccttatctt
acattcaccgatgcattggtgtgtgcatcgtgacataaaacctcaaaactgttggtaaatccgcacactcatcaagtaaagctatgtgat
ttggaagtgcaaaagtattggtaaaaggagaaccaaacttctacatctgctcgaggtattacagagcacctgaactatTTTTGGAG
caaccgagtatacagagccattgatgtctggtctgcaggatgtgtctagctgaactattgcttgagagcccttgtccctggtgagag
cgggtgtgatcaactgtagagattatcaaggcttgggaacgcctactagagaagaaatcaagtgcataacccaaactacacggaat
tcaaattccctcagattaaagctcatcatggcacaagattttccaaaacgcatgcctccagaagctgtgatttggctcaagactcttc
aatactctcctaattctacgaagtgccgctctcgacacattagtcacccattctttgatgagtaaagagacccaaacgcacgtctaccta
ggagctttcctccaccgctttcaactcaagctcagagctgaaagggtaccattggagatggtagctaagtagtacctgagcatg
caaggaagcagtgctccttggctcggttg

AtUBQ3

Atgcaaattctcgtgaaaactcactggcaagactatcactctcgaggtgagagctctgacaccatcgacaatgtaaggcaaagat
tcaggacaaggaaggcattctccggatcagcaaagattaatattcccggtaaacagctagaagatggccgtaccttggccgattac
aacattcagaagaatcaaccctcatttggcttccggttaagaggtggtatgcaaatcttgtcaagactctgactggcaagaccattac
ttggaggtgagagctctgacactattgacaacgtcaaagcaaagatccaggacaaggaaggaatccctccggatcagcagagactt
atctttgccggttaagcagctgaagacggaagaactcttgcactacaacattcaaaaggagtcgaccttcatttggctctcgtctca
gaggtggtatgcaaatcttgtcaagacctcactggtaaaacaatcaccttgaggtgagagttcagacaccattgacaatgtcaaag
ctaagatccaagataaagagggaattcctccggatcagcagaggcttatctttgccggttaagcagctcgaagatggacgcaccttgc
agattacaacatccaaaaggagtcgacacttcatcttgcctcgtctccgtgggtggtatgcagatcttgtgaagaccttaccgaaag
accattactctggaggtgaaagctcagacaccatcgataatgtcaaggctaagattcaggacaaggaaggatcccaccagaccaa
cagagactcatctcgtgaaaacagcttgaggatggtcgcacactgcagattacaacatccagaaggagtcgactcttacttgggtt
cttcgtctcgtggtggaagct

8. Appendix 2: Vector maps

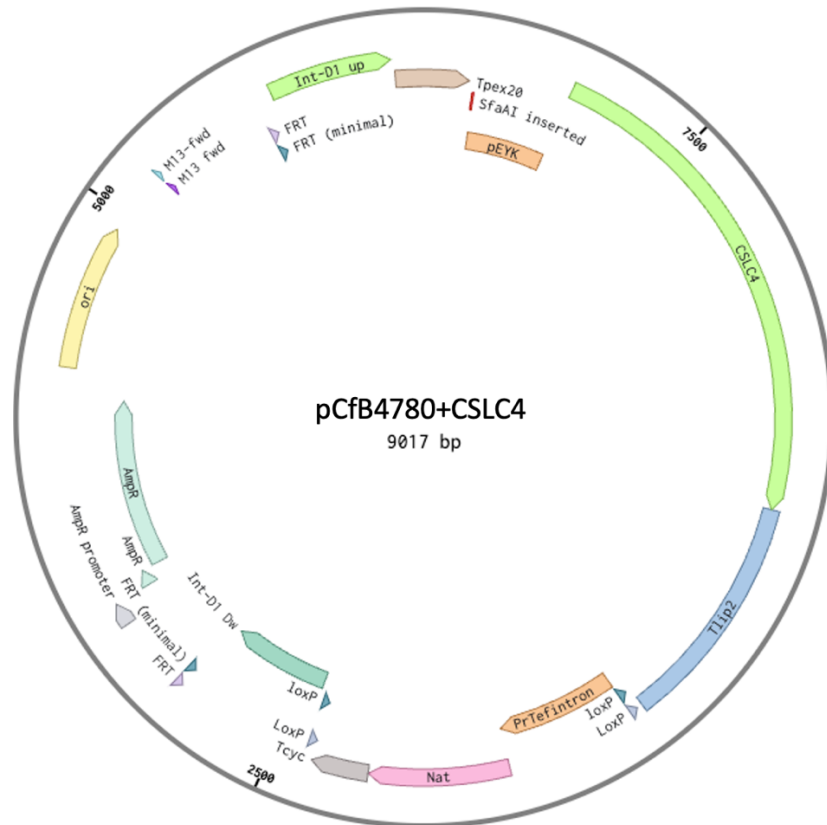


Figure 8-1. Vector map for *Y. lipolytica* constructs with *TmCSLC4* in expression cassette.

Vector was used for expression of *TmCSLC4* in *Y. lipolytica*. The selection markers are Amp for *E. coli* and Nat for *Y. lipolytica*. The expression cassette was excised using FD NotI restriction enzyme before transformation to *Y. lipolytica*. pEYK denotes the erythritol inducible promoter and TLip denotes the terminator. IntD-1 up and down are the homologous regions of recombination sites.



Figure 8-2. Vector map for *Y. lipolytica* constructs with *TmCSLC4* and *TmXXT2* in expression cassette.

Vector was used for expression of *TmCSLC4* and *TmXXT2* in *Y. lipolytica*. The selection markers are Amp for *E. coli* and Nat for *Y. lipolytica*. The expression cassette was excised using FD NotI restriction enzyme before transformation to *Y. lipolytica*. pEYK denotes the erythritol inducible promoter and TLip denotes the terminator. IntD-1 up and down are the homologous regions of recombination sites.

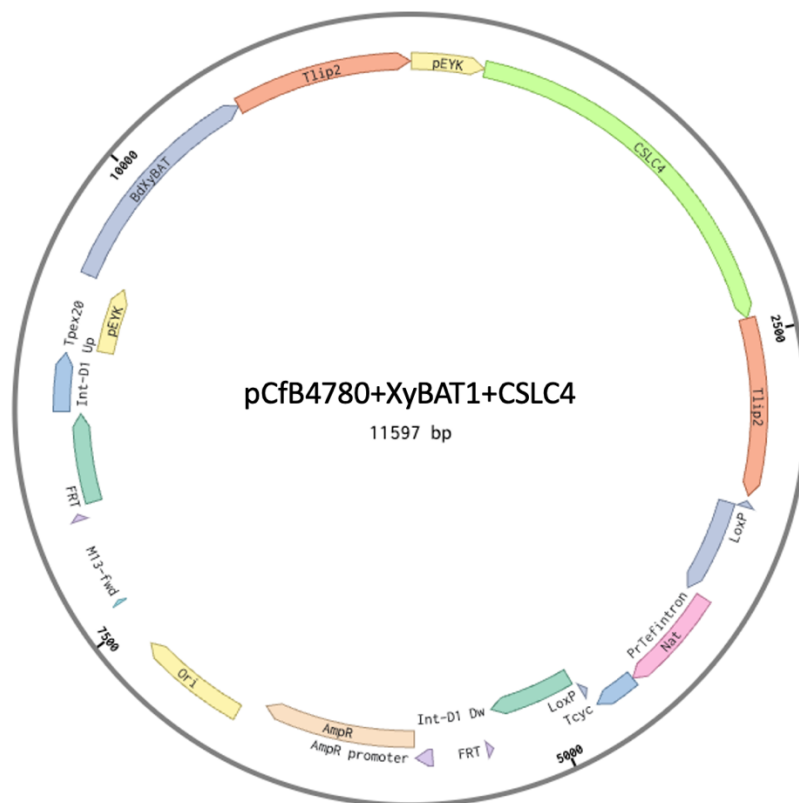


Figure 8-3. Vector map for *Y. lipolytica* constructs with *TmCSLC4* and *BdXyBAT1* in expression cassette.

Vector was used for expression of *TmCSLC4* and *BdXyBAT1* in *Y. lipolytica*. The selection markers are Amp for *E. coli* and Nat for *Y. lipolytica*. The expression cassette was excised using FD NotI restriction enzyme before transformation to *Y. lipolytica*. pEYK denotes the erythritol inducible promoter and TLip denotes the terminator. IntD-1 up and down are the homologous regions of recombination sites.

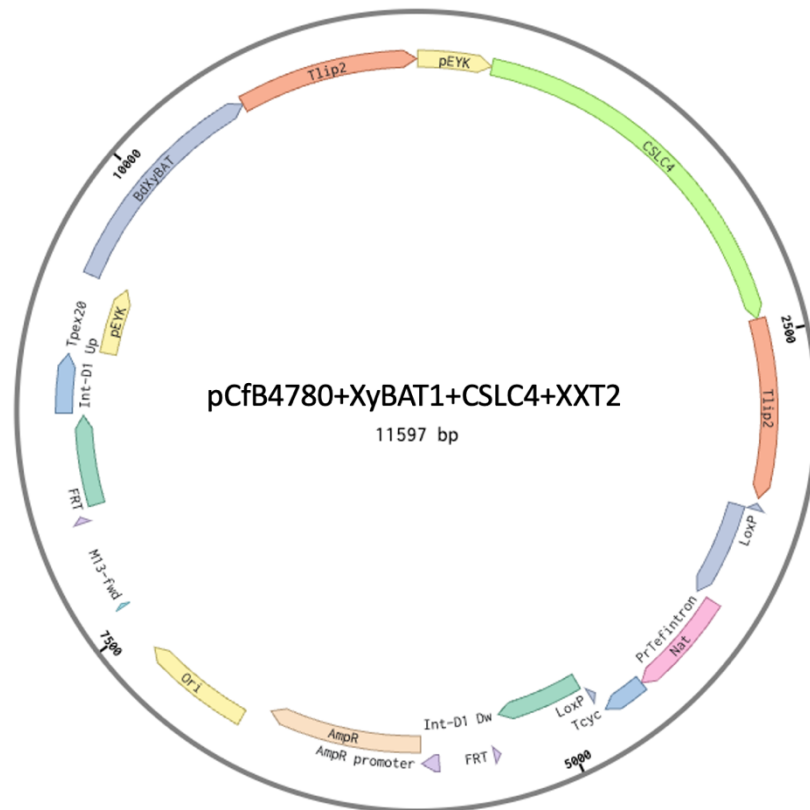


Figure 8-4. Vector map for *Y. lipolytica* constructs with *TmCSLC4*, *TmXXT2* and *BdXyBAT1* in expression cassette.

Vector was used for expression of *TmCSLC4*, *TmXXT2* and *BdXyBAT1* in *Y. lipolytica*. The selection markers are Amp for *E. coli* and Nat for *Y. lipolytica*. The expression cassette was excised using FD NotI restriction enzyme before transformation to *Y. lipolytica*. pEYK denotes the erythritol inducible promoter and TLip denotes the terminator. IntD-1 up and down are the homologous regions of recombination sites.

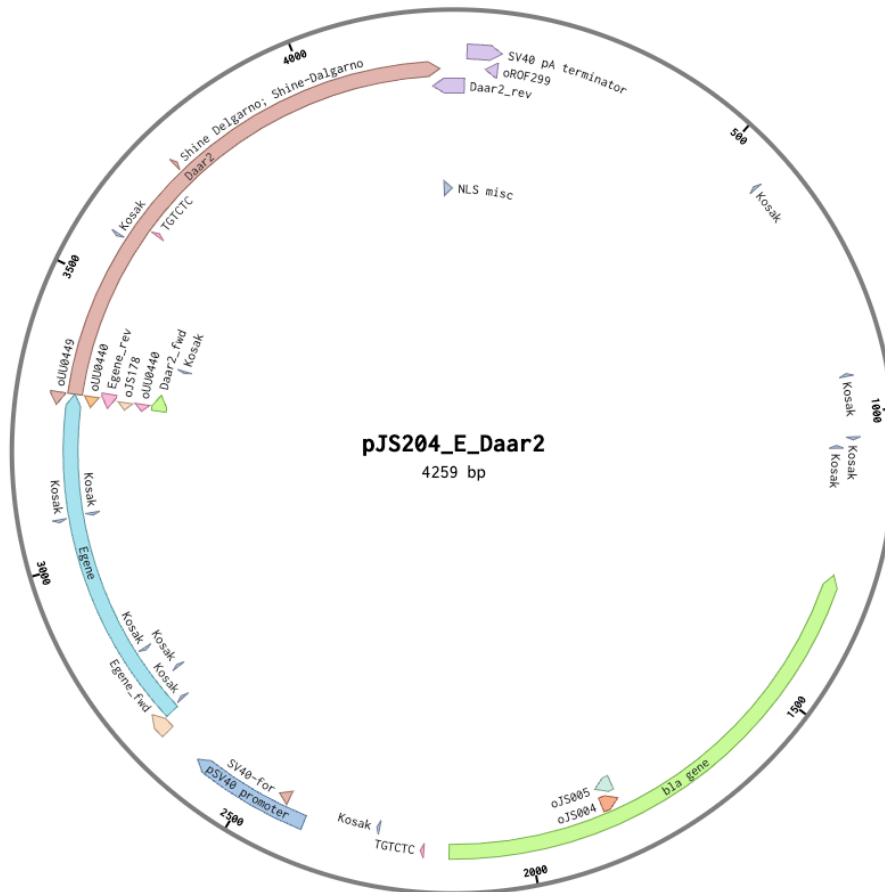


Figure 8-5. Vector map for mammalian 2 hybrid assay constructs with *AtDAAR2* attached to the C-terminus of *E gene* in expression cassette.

Vector was used for expression of *DAAR2* fused to the C-terminus of *E-gene* in CHO cell line. The selection markers are Amp for *E. coli*. SV40 denotes the constitutive promoter and SV40 pA denotes the terminator.

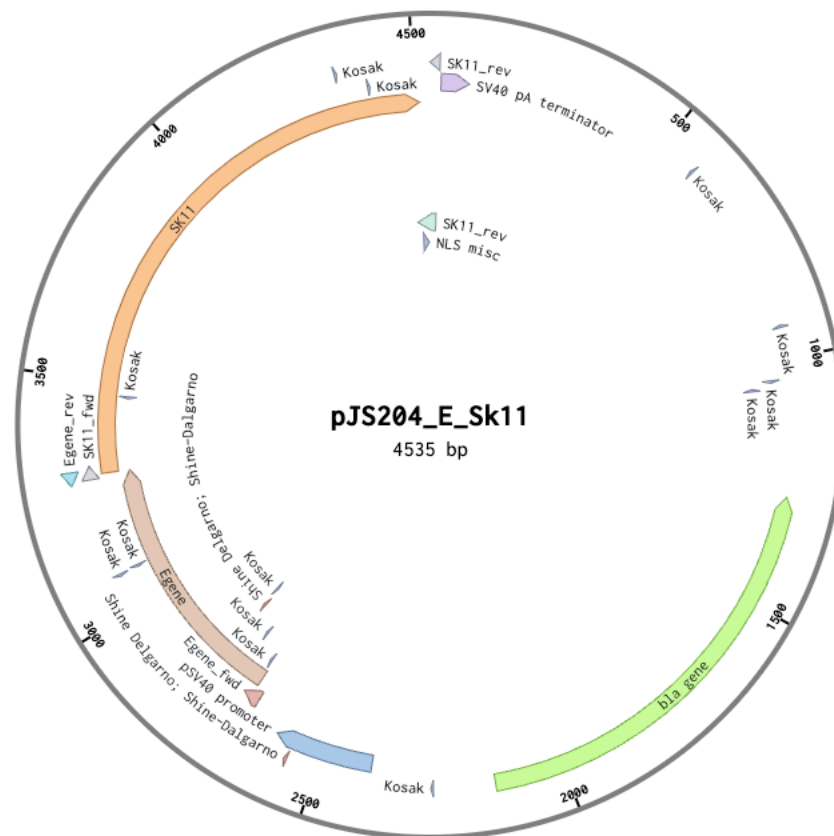


Figure 8-6. Vector map for mammalian 2 hybrid assay constructs with *AtSK11* attached to the C-terminus of *E gene* in expression cassette.

Vector was used for expression of *SK11* fused to the C-terminus of *E-gene* in CHO cell line. The selection markers are Amp for *E. coli*. SV40 denotes the constitutive promoter and SV40 pA denotes the terminator.

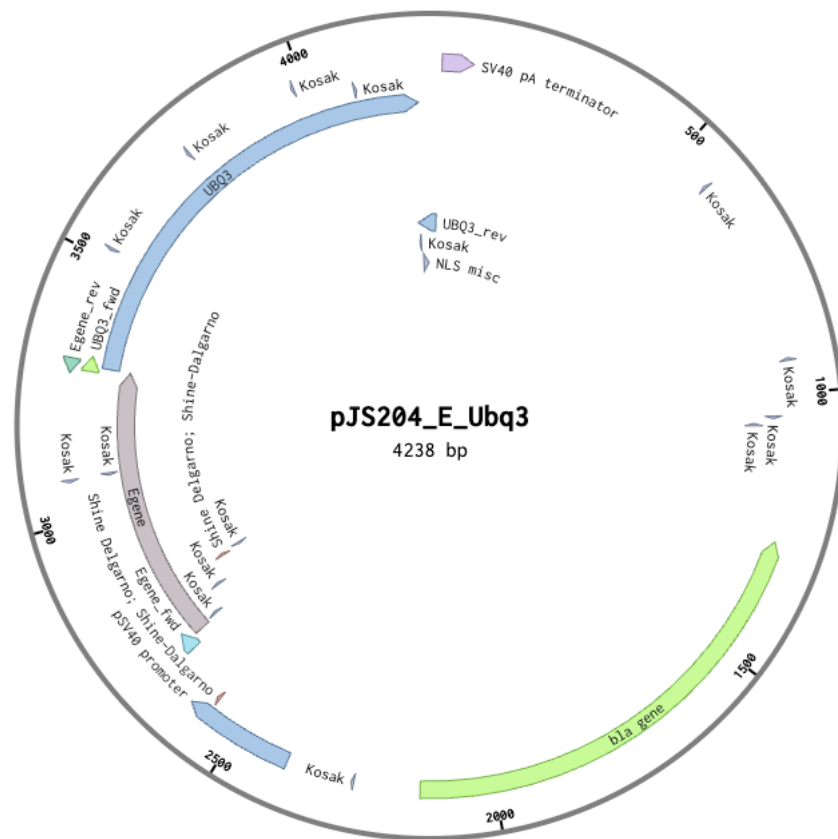


Figure 8-7. Vector map for mammalian 2 hybrid assay constructs with *AtUBQ3* attached to the C-terminus of *E gene* in expression cassette.

Vector was used for expression of *UBQ3* fused to the C-terminus of E-gene in CHO cell line. The selection markers are Amp for *E. coli*. SV40 denotes the constitutive promoter and SV40 pA denotes the terminator.

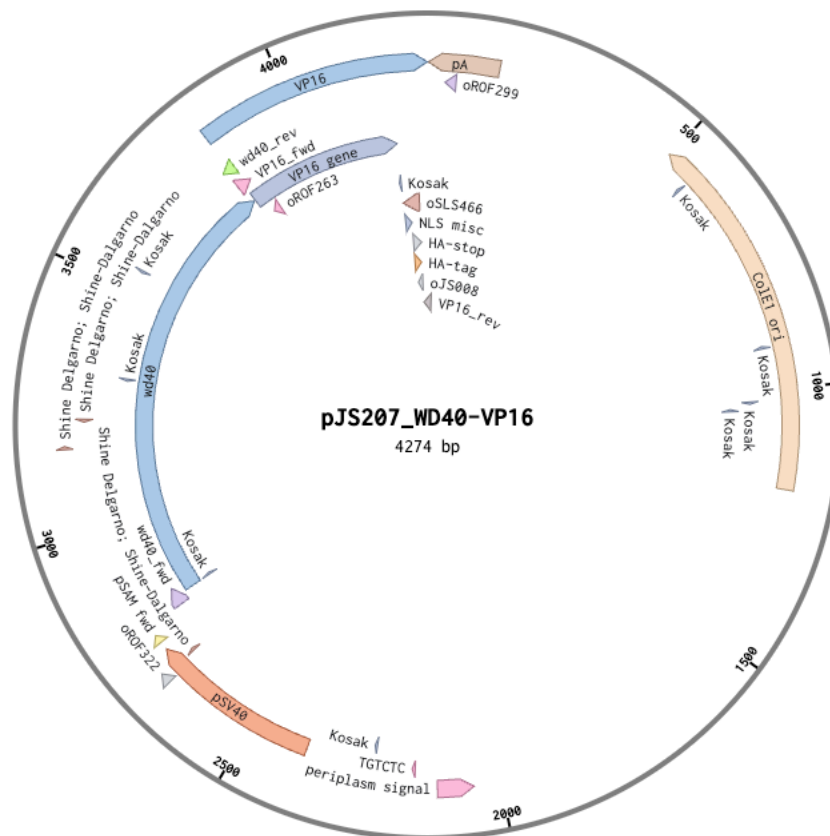


Figure 8-8. Vector map for mammalian 2 hybrid assay constructs with *VP16* domain attached to the C-terminus of *AtWD40* in expression cassette.

Vector was used for expression of *WD40* with C-terminus *VP16* fusion in CHO cell line. The selection markers are Amp for *E. coli*. SV40 denotes the constitutive promoter and SV40 pA denotes the terminator.

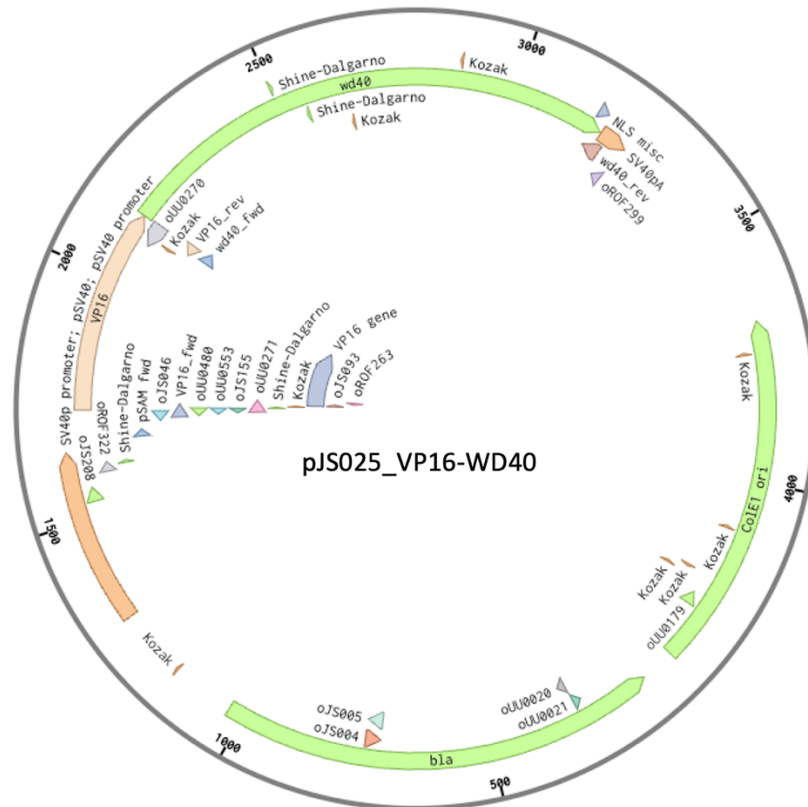


Figure 8-9. Vector map for mammalian 2 hybrid assay constructs with *VP16* domain attached to the N-terminus of *AtWD40* in expression cassette.

Vector was used for expression of *WD40* with N-terminus *VP16* fusion in CHO cell line. The selection markers are Amp for *E. coli*. SV40 denotes the constitutive promoter and SV40 pA denotes the terminator.

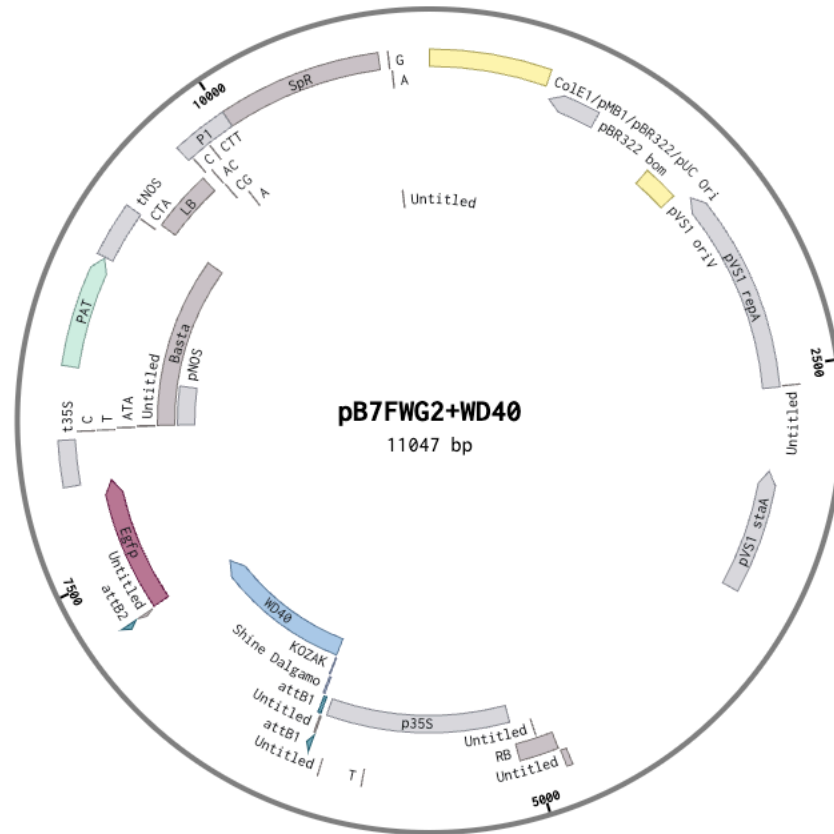


Figure 8-10. Vector map for subcellular localization of *AtWD40*-GFP in *N. benthamiana*.

Vector was used for expression of *AtWD40* with C-terminus GFP fusion. The selection markers are Amp for *E. coli* and Spc for *A. tumefaciens*. The construct was used for subcellular localization by transient expression of *AtWD40* in *N. benthamiana*.

9. Appendix 3: Miscellaneous data

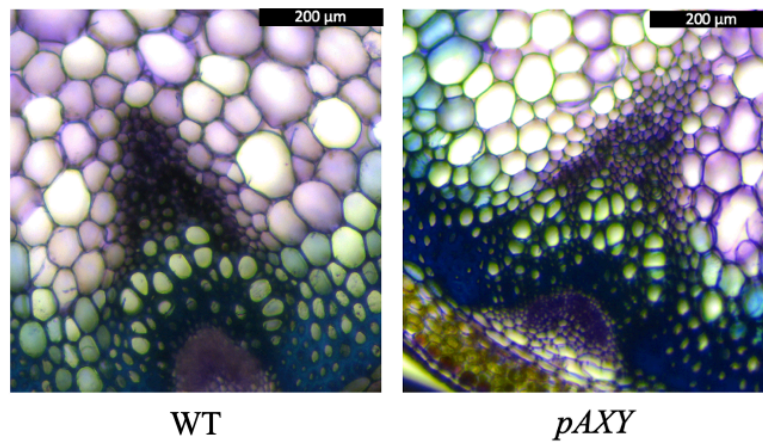


Figure 9-1. Stem cross sections of the WT and *pAXY* genotypes.

The cross sections of the stem tissues were stained with toluidine-O-blue and the results indicating no differences between the genotypes and a normal xylem.

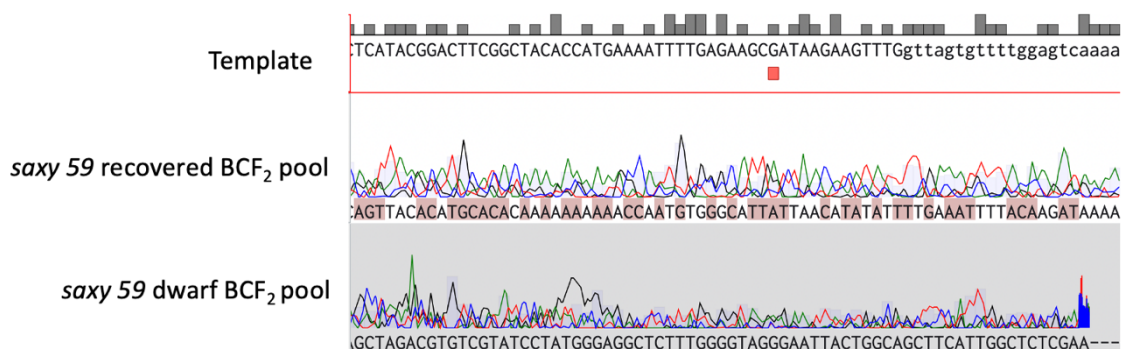


Figure 9-2. Sanger sequencing alignment of AT4G05612 amplicons from *saxy59* BCF₂ recovered and dwarf pool.

Sanger sequencing results for AT4G05612 did not provide any conclusive evidence for the presence of SNP due to the multiple repetitive sequences within the gene causing non-specific amplification and ambiguity in read alignment. The SNP position is highlighted in red color on template sequence.

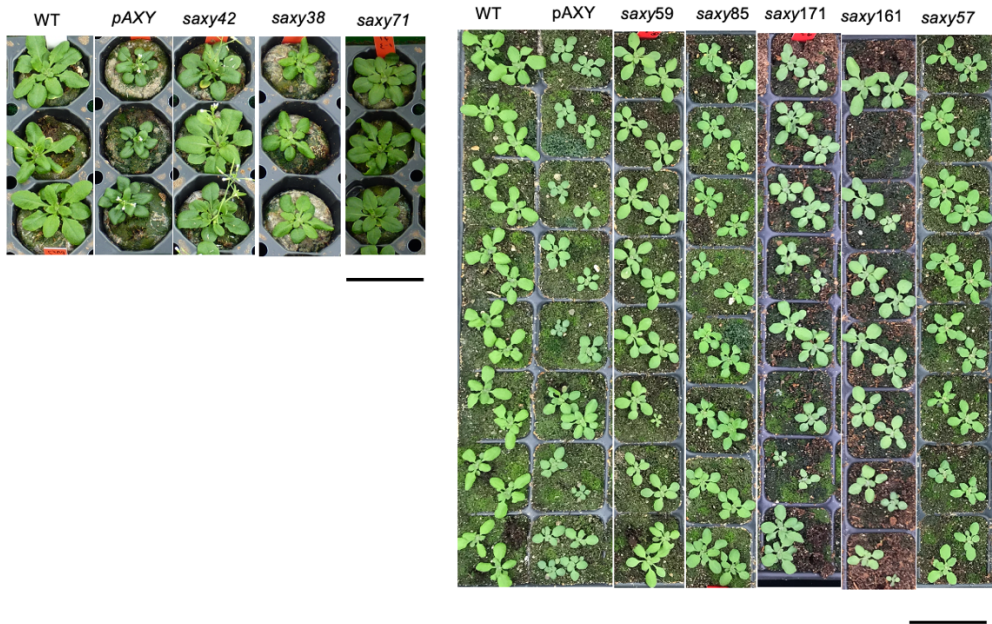
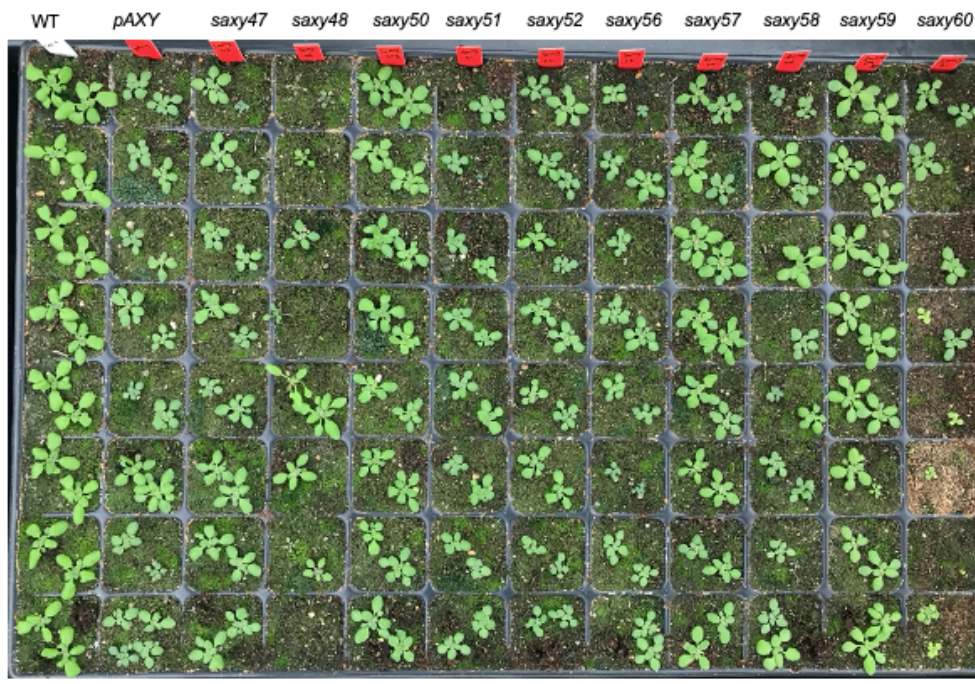


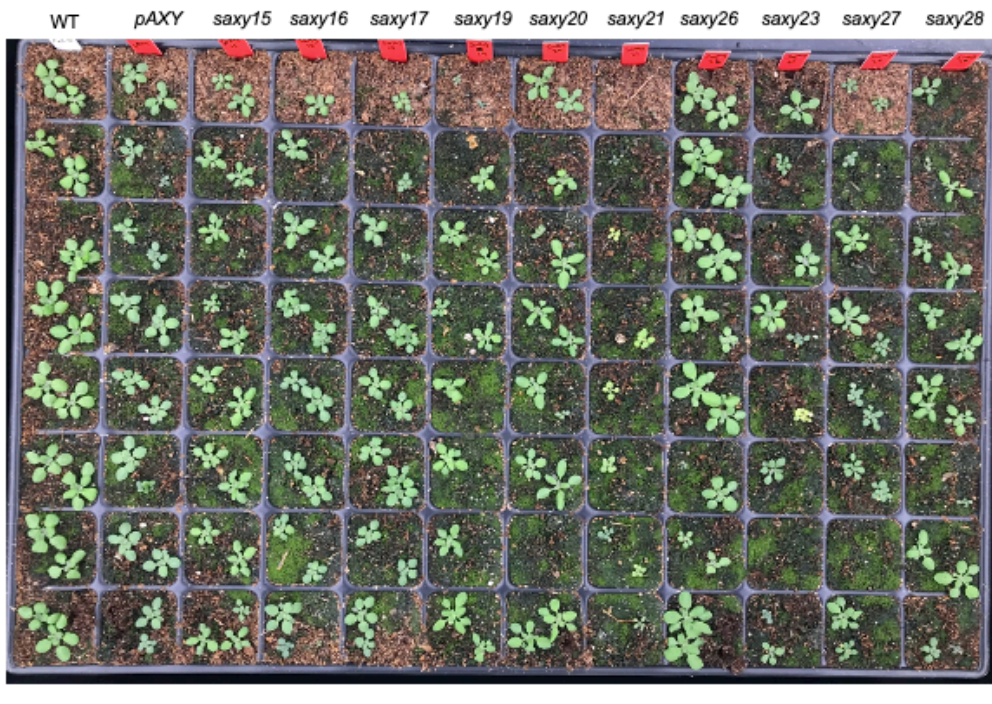
Figure 9-3. Growth phenotype of selected suppressor mutants.

Growth phenotype showing the rosette size of four-week-old, selected suppressor mutants for BSA analysis. The labels above each column represents the genotype of the plants. The black bar represents a scale of 5 cm.

(A)



(B)



(C)

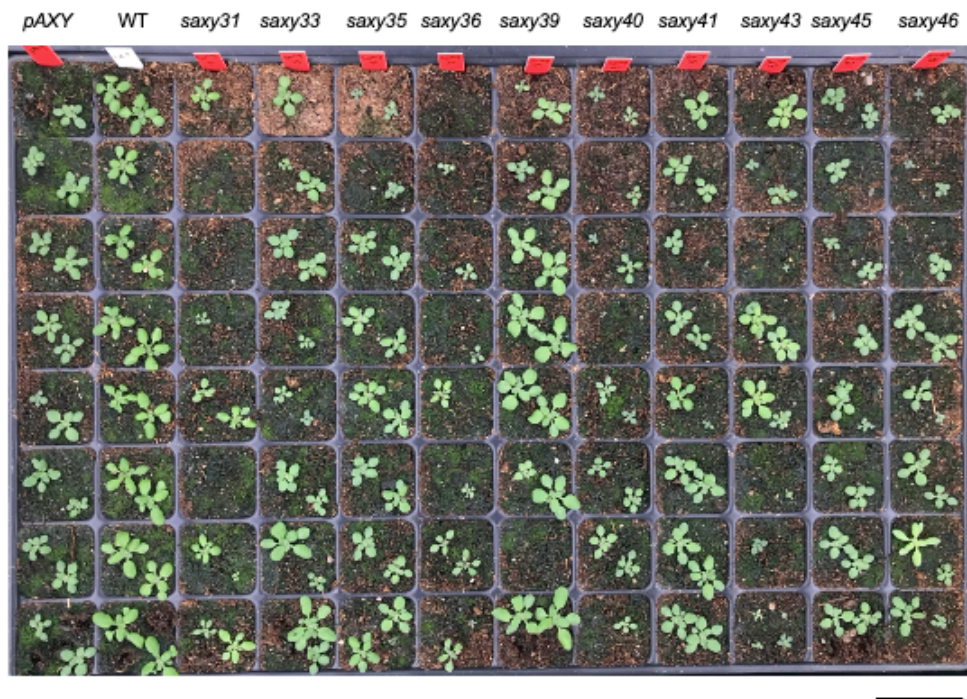


Figure 9-4. Growth phenotype of discarded suppressor mutants.

Growth phenotype showing the rosette size of four-week-old, discarded suppressor mutants. The labels above each column represents the genotype of the plants. The suppressors *saxy57* and *saxy59* were selected for further analysis and others were discarded because of uneven recovery. The black bar represents a scale of 5 cm.

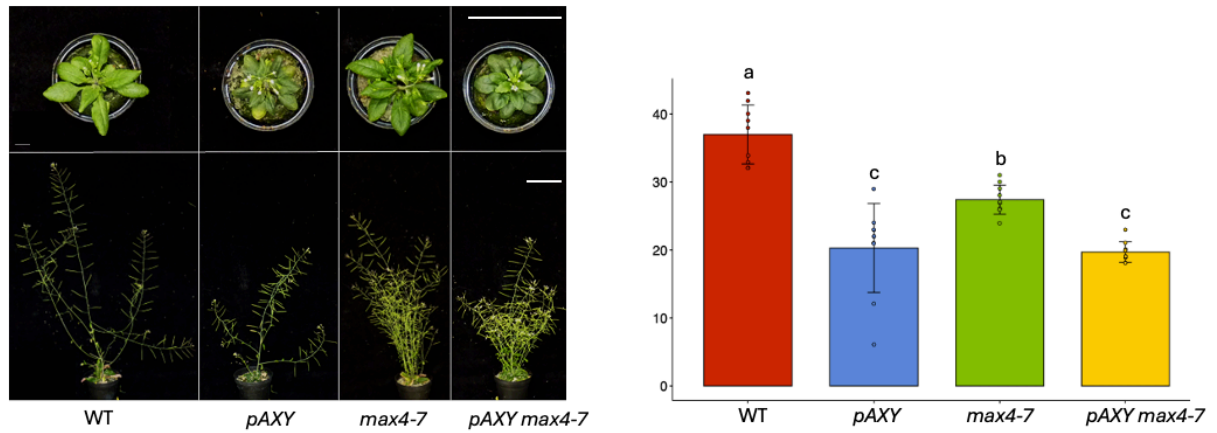


Figure 9-5. Growth phenotype of *pAXY max4-7* mutant.

(A) Growth phenotype showing the rosette size of four-week-old and stem height of six-week-old WT, *pAXY*, *max4-7*, and *pAXY max4-7*. The white bar represents a scale of 5 cm. (B) Height measurements of six-week-old WT, *pAXY*, *max4-7*, and *pAXY max4-7*. Error bars indicate standard deviation ($n = 10$), and the alphabets indicates the significant differences between the mean of genotypes (Tukey HSD, $p < 0.05$).

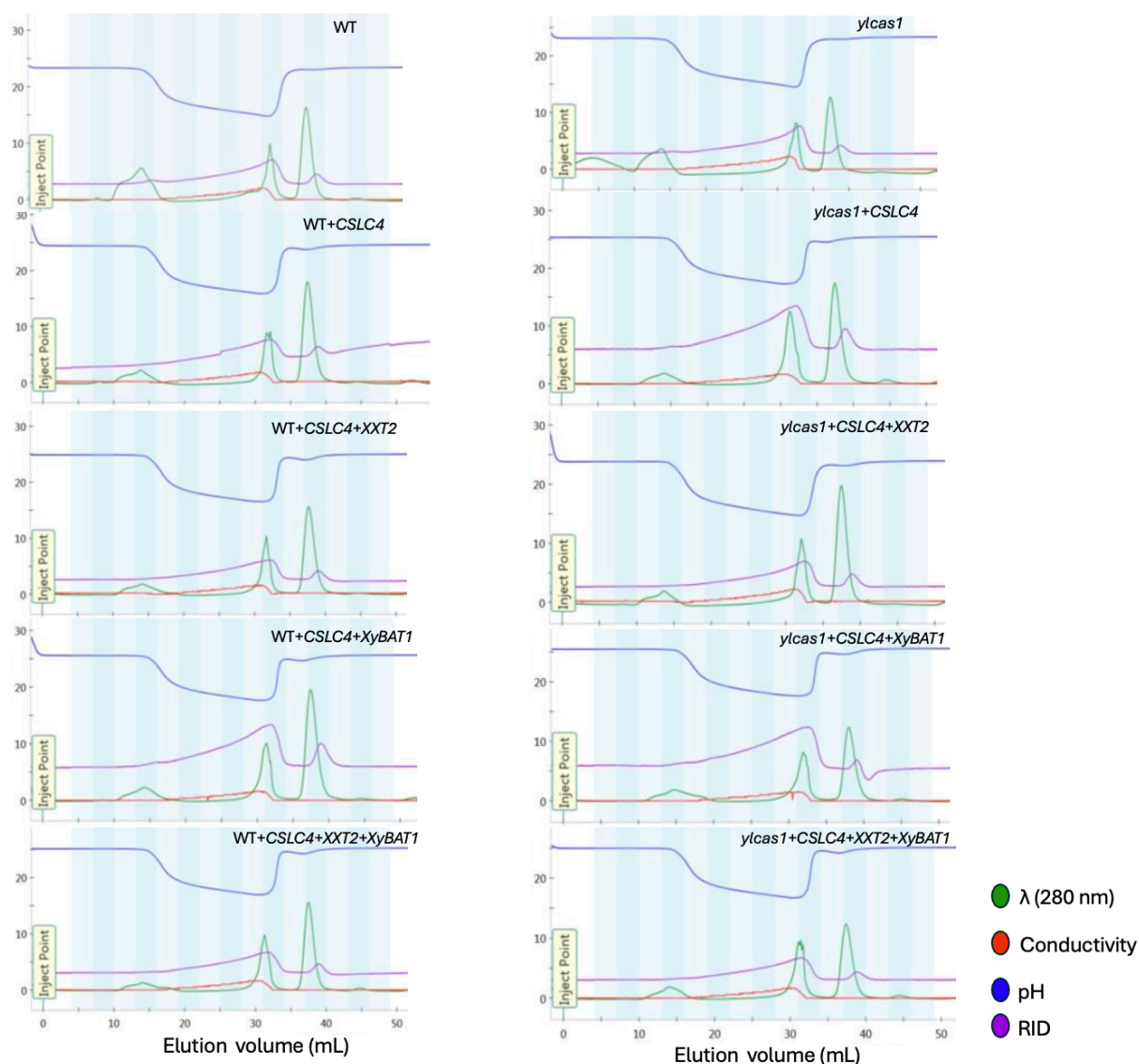
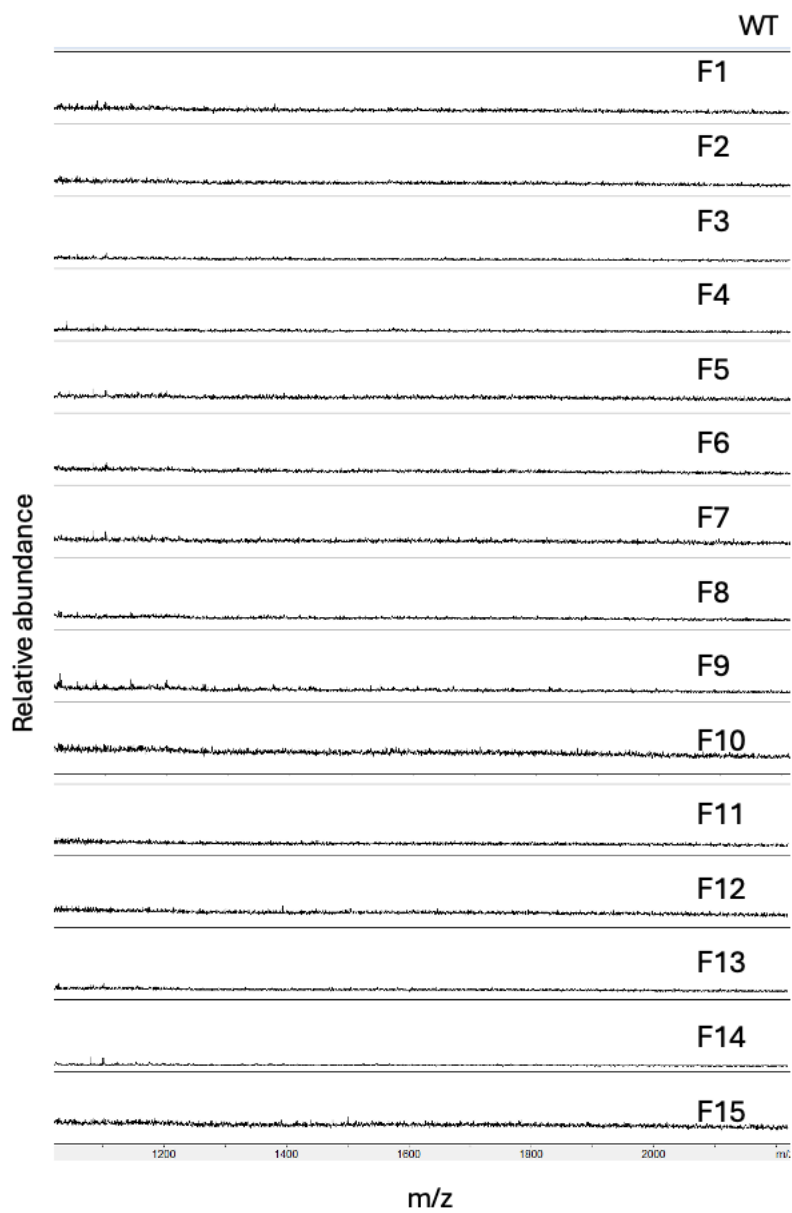


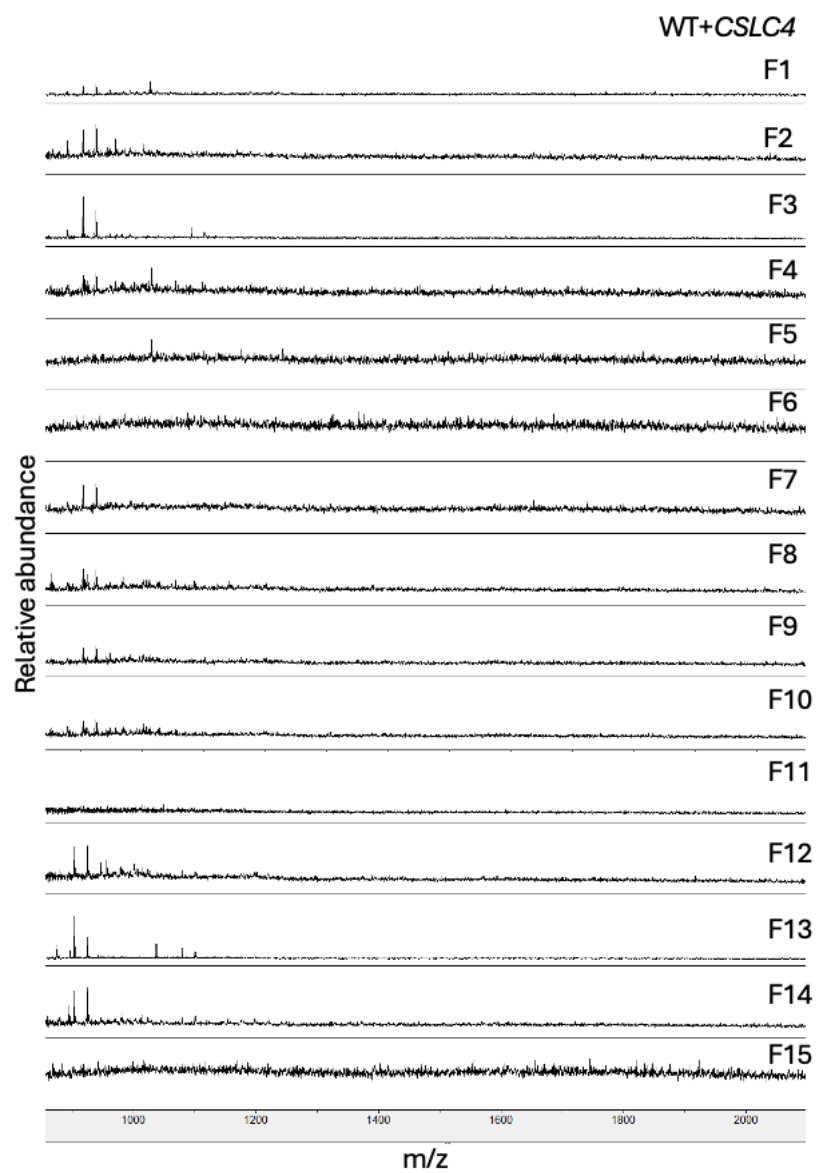
Figure 9-6. SEC Chromatograms of *Y. lipolytica* transgenic strains

Chromatograms for SEC runs of digested *Y. lipolytica* AIR samples. (λ (280 nm): absorption at 280 nm), RID: Refractive index, A total of 15 fractions were collected and the color theme behind chromatogram indicates each fraction collected (1.5 mL per minute). The fractions 9 and 10 at the elution volume of 30-35 mL was used for monosaccharide compositional analysis and glycosidic linkage analysis.

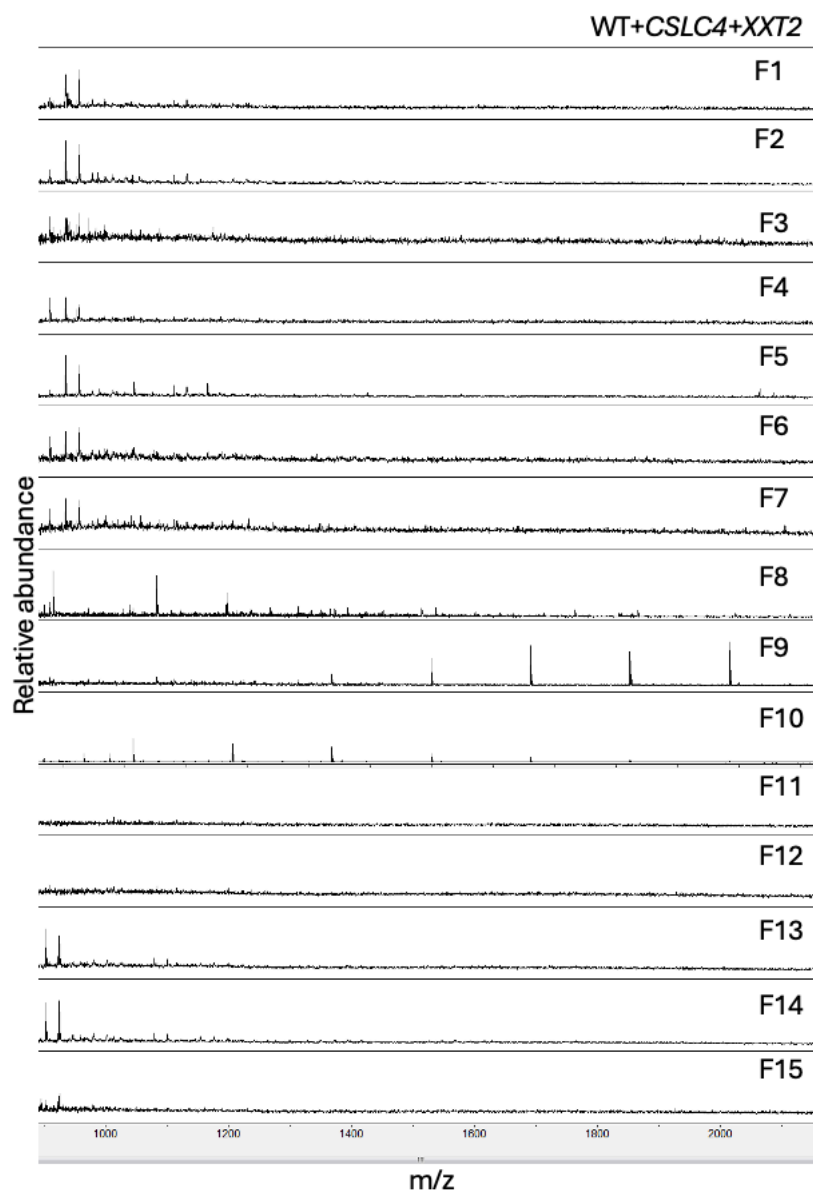
(A)



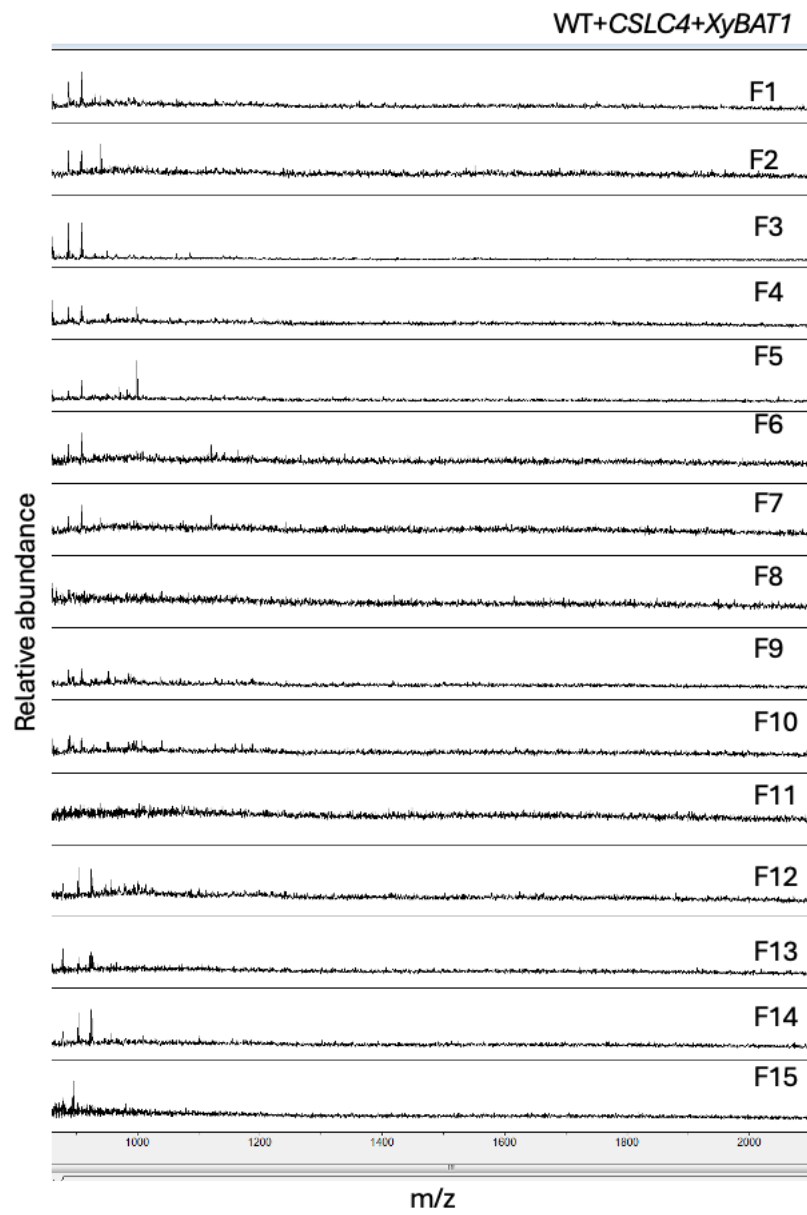
(B)



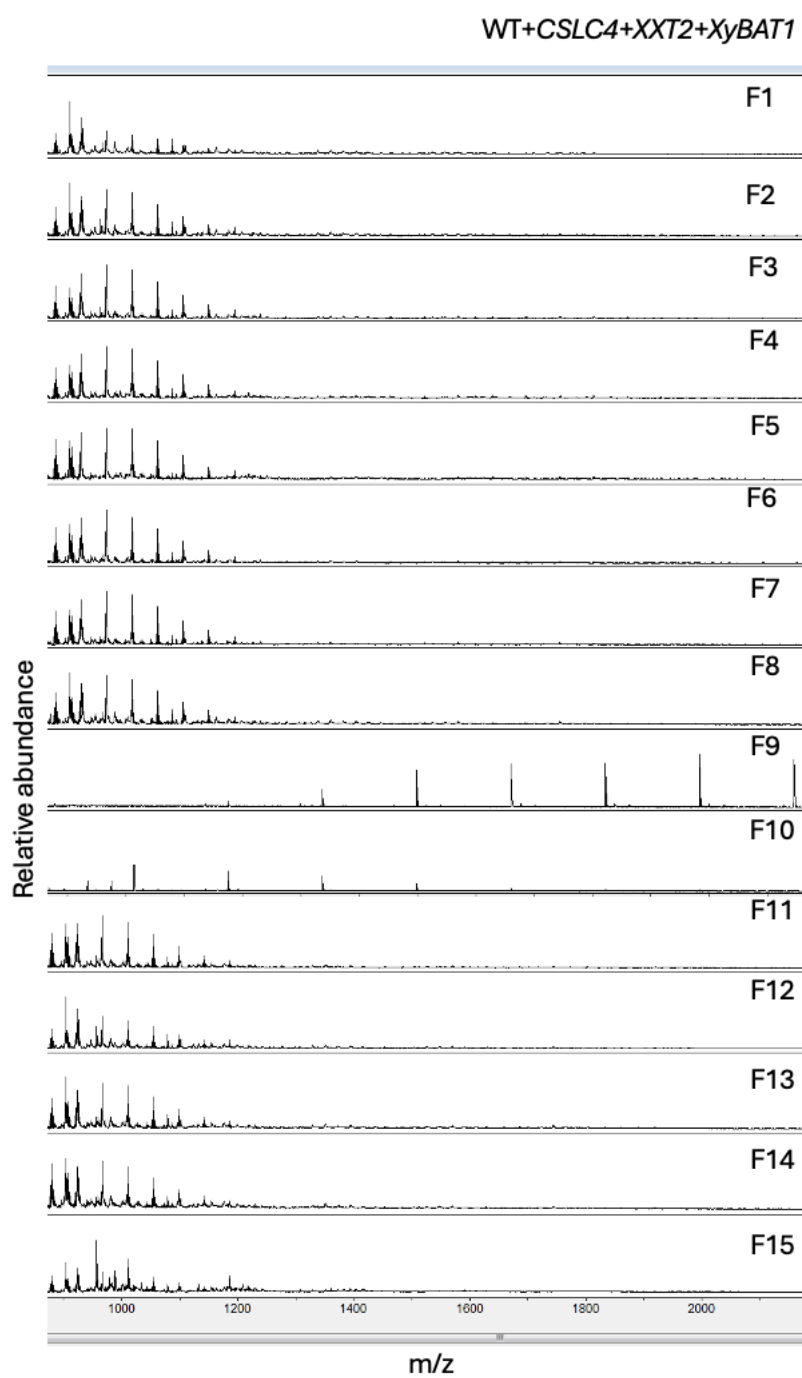
(C)



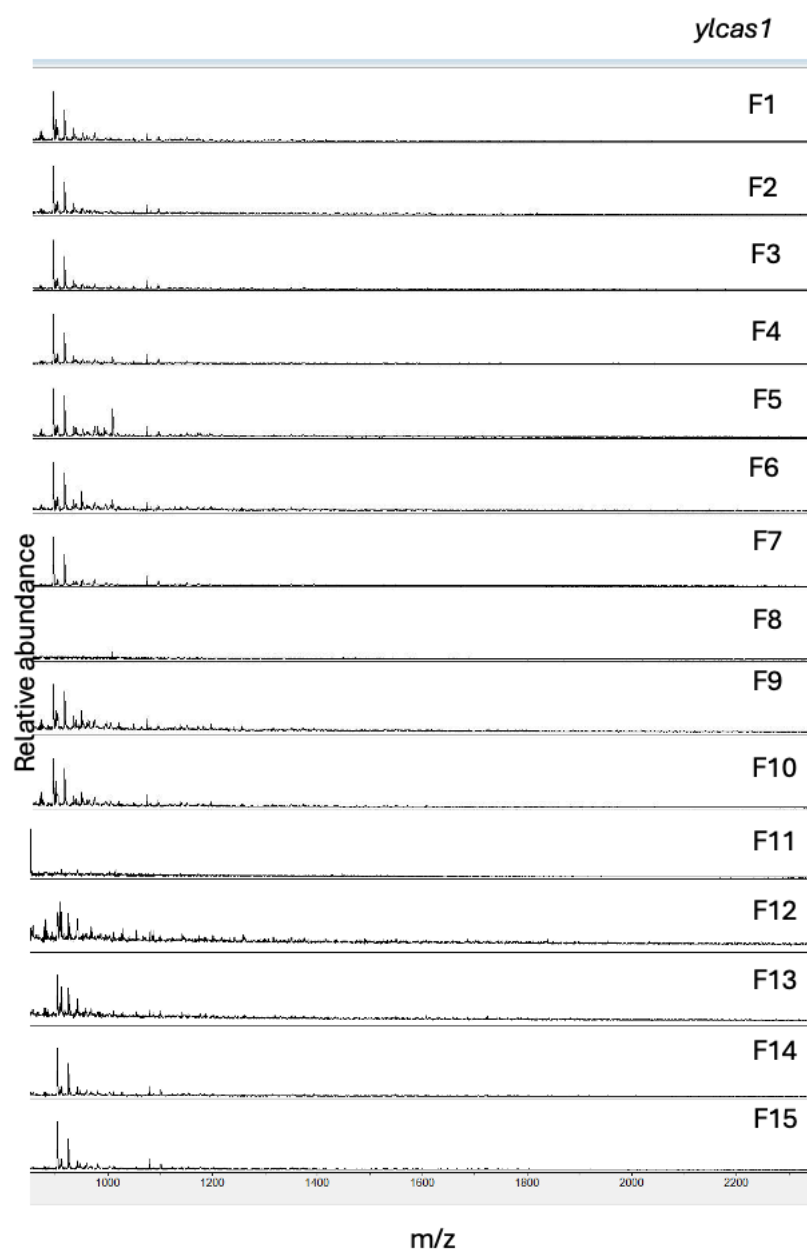
(D)



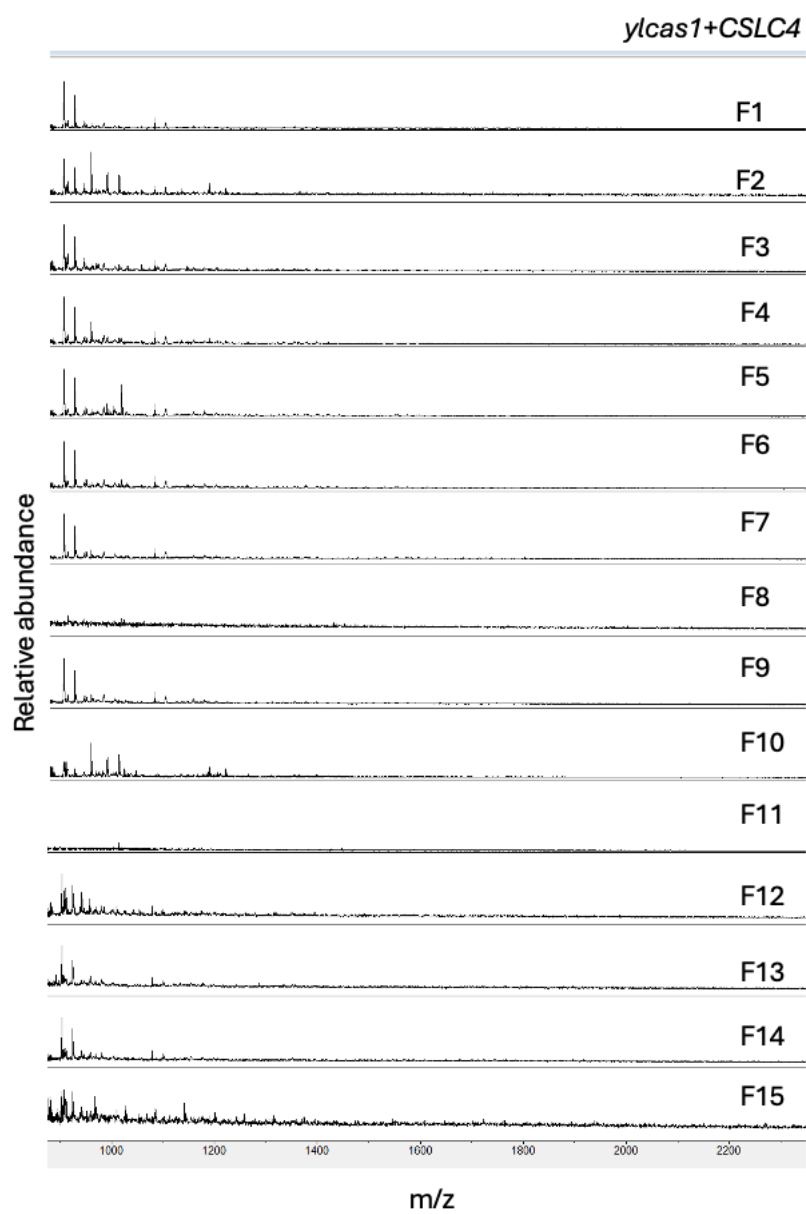
(E)



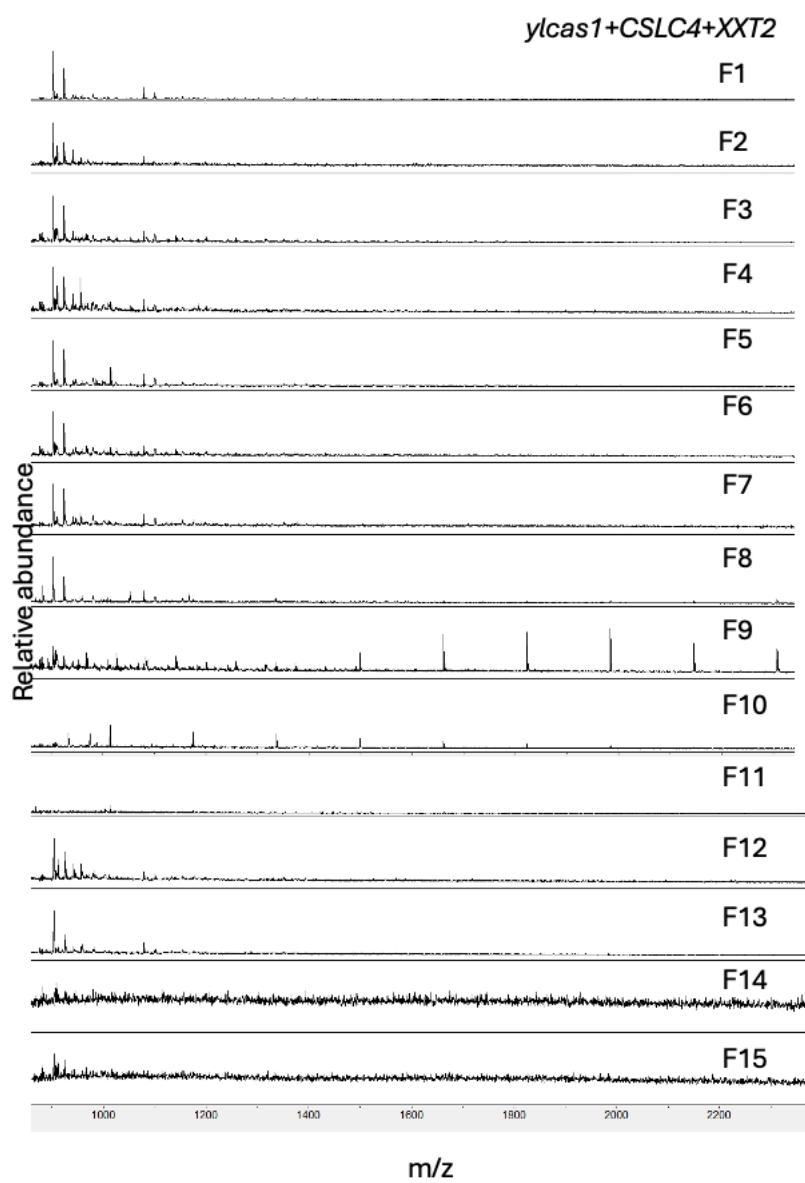
(F)



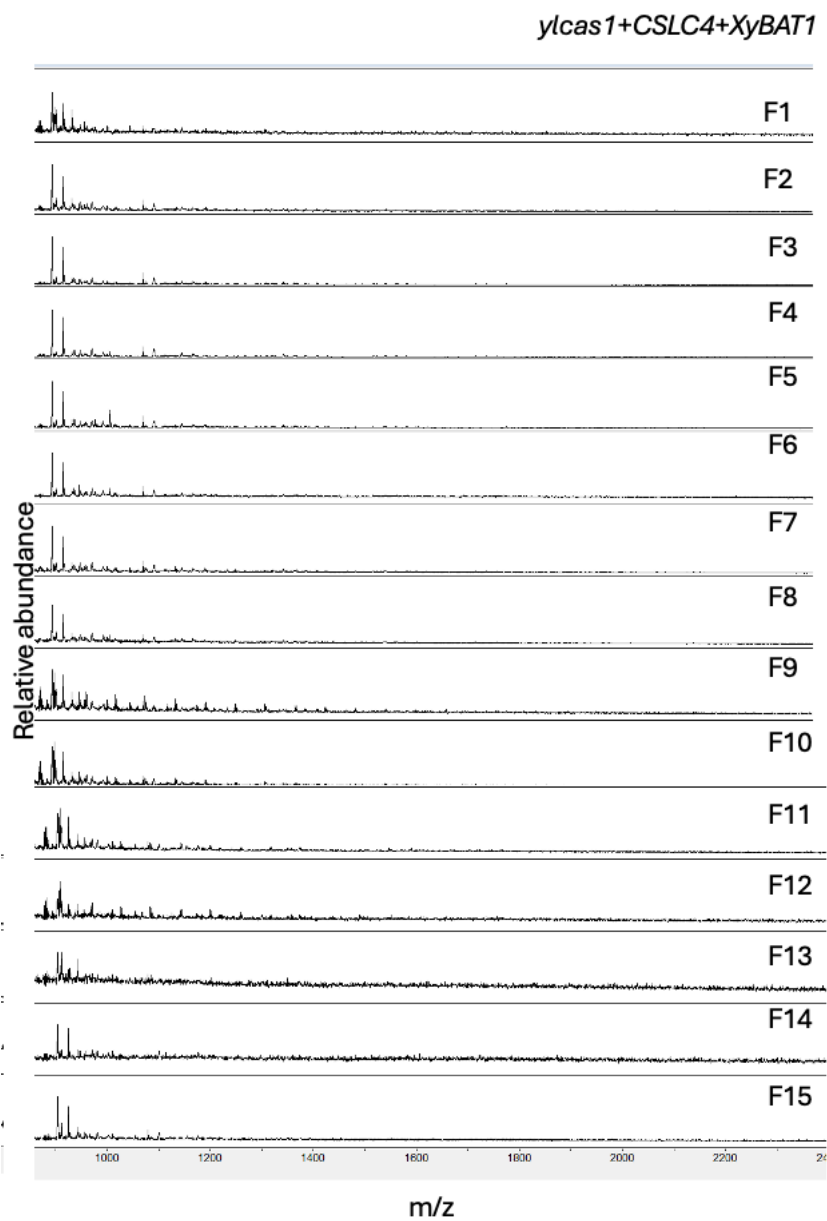
(G)



(H)



(I)



(J)

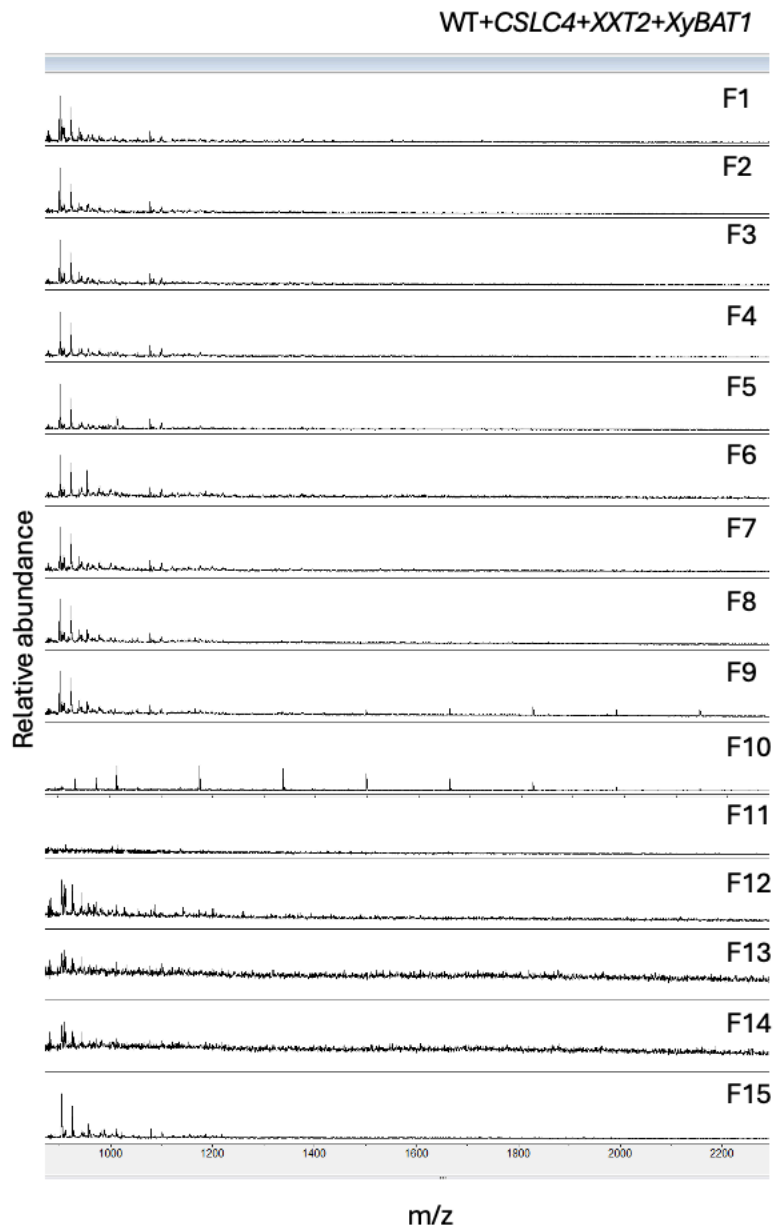


Figure 9-7. OLIMP spectra of SEC fractions of E-CELBA digested transgenic *Y. lipolytica* AIR.

OLIMP spectra of 15 SEC fractions of E-CELBA digested AIR from transgenic *Y. lipolytica* strains expressing *CSLC4*; *CLSC4* and *XXT2*; *CSLC4* and *XyBAT1*; *CSLC4*, *XXT2* and *XyBAT1* on WT and *ylcas1* background (A-J). The strain names are mentioned in each figure. H_n - number of hexoses; Ac_n - number of *O*-acetyl substituents; F- Fraction. The spectra show (Mass + Na⁺) adducts.

10. Acknowledgement

Foremost, I owe my highest gratitude to my Ph.D. supervisor Prof. Dr. Markus Pauly, for allowing me to pursue a Ph.D. in this intriguing topic. Even more for providing a friendly, motivating work environment, excellent guidance, constructive criticisms, support, and setting up high standards in research. My sincere thanks go to Dr. Vicente Ramírez, my co-supervisor, for introducing me to the projects, guiding me through all the experiments conducted in this thesis, proofreading, and correcting my thesis, and providing critical feedback.

I am also thankful to Prof. Dr. Björn Usadel for kindly agreeing to be my mentor and for his support and feedback throughout my research.

I would like to extend my sincere thanks to Prof. Dr. Matias Zurbriggen and Jonas Schön for their support with the mammalian 2-hybrid assay at the Institute of Synthetic Biology, HHU. Additionally, I am grateful to Dr. Sebastian Hänsch for his assistance with the confocal microscope at the Centre for Advanced Imaging, HHU.

Special thanks to my colleagues, Dr. Shaogan Wang and Marius Karbach, for their invaluable support and feedback during my thesis work and collaboration.

I am deeply appreciative of Katharina Grosche, Felix Roth, Barbara Schulten, and Josef Schoregge for their valuable technical support, ensuring that everything ran smoothly within the institute.

I am grateful to all the current and former members of the Institute for Plant Cell Biology and Biotechnology, HHU, for their unwavering support and for creating a friendly work environment enriched by shared social activities. A heartfelt thanks to the PlaCeBio²Tec community - Felix, Katharina, Barbara, Jutta, Vicente, Shaogan, Nicky, Niklas, Thomas, Merve, Xinhui, Yi, Sylwia, Allegra, Marius, Lucas, Ronja, Stefan, Benjamin, Gabriel, and Tim for their support and feedback on my projects at various stages.

I thank Dr. Sigrun Feldbrügge and Ms. Han dang Klein at JUNO, HHU, who made my life easier in Düsseldorf with their kind help and assistance with visa and official formalities at the city office.

This journey would not have been possible without the support of many individuals who helped, mentored, and guided me at different stages of my career. I am especially thankful to Dr. Iyappan Sellamuthu, who inspired me to pursue a career in plant sciences and guided me during my bachelor's studies in Chennai. My gratitude also goes to Prof. Dr. Dorothea Bartels for allowing me to undertake my bachelor's thesis at her institute and for her guidance during my master's studies at the University of Bonn. I also thank Prof. Dr. Franziska Turck for her guidance during my master's thesis and for introducing me to R programming.

I cherish the priceless memories created during my Ph.D. with my batchmates and friends in Düsseldorf - Senthil, Sainath, Srimeenakshi, Pavithran, Alex, and Mohan whose joyful company made the journey more enjoyable.

A special thanks to my dear friends Amrish, Adithya, Sagi, Bennet, Kiran, Delphine, Eyüp, Shyam, Mahalakshmi, Deepika, Veda, Florian, M Jay, and Selva, who supported, helped, and encouraged me during challenging times.

I would like to express my heartfelt gratitude to my sister Banupriya and her family for helping me settle in Germany when I first arrived, and for their unwavering love and support.

Finally, words cannot fully convey the depth of my gratitude to my cherished family - my parents, Natarajan and Kalaiselvi, and my little sister Priyadarshini. Their unwavering love, dedication, and support have been the cornerstone of my journey.